Université de Liège – University of Liège

Faculté des Sciences – Faculty of Sciences

PhD Thesis

Long-term study of the MHWs in the Mediterranean Sea and the Red Sea:

an assessment of their trends, drivers, and their early indicators

Manal Hamdeno

En vue de l’obtention du diplôme – Submitted in fulfilment of the requirements for

Doctorat en Océanographie – Doctor of Sciences in Oceanography

Années académiques – Academic years: 2021-2026

Promotrice – Supervisor: Aida Alvera-Azcárate
(GeoHydrodynamics and Environment Research, Liège, Belgium)

Cette thèse a débuté le 1er octobre 2021 et a été défendue le 21 avril 2026

This PhD Thesis started on October 1st, 2021, and finished on April 21st, 2026

Jury Members

Xavier Fettweis (President) – *University of Liège, Belgium*

Jean-Marie Beckers (Secretary) – *University of Liège, Belgium*

Aida Alvera-Azcárate – *University of Liège, Belgium*

Sylvie Gobert – *University of Liège, Belgium*

Ibrahim Hoteit – *University of Science and Technology (KAUST), Thuwal, Saudi Arabia*

Francisco Pastor – *Mediterranean Center for Environmental Studies, Valencia, Spain*

University of Liège

Faculty of Sciences

Department of Astrophysics, Geography and Oceanography

Abstract

PhD Thesis in Oceanography

Long-term study of the MHWs in the Mediterranean Sea and the Red Sea: an assessment of their trends, drivers, and their early indicators

By : Manal Hamdeno

MHWs have become one of the most significant manifestations of ocean warming, with profound implications for marine ecosystems, regional climate, and extreme weather events. This thesis provides a comprehensive analysis of MHW dynamics in two thermally sensitive semi-enclosed basins, the Mediterranean Sea and the Red Sea, by integrating surface and subsurface observations, atmospheric forcing, ecological responses, and interactions with compound and extreme events. The objective is to move beyond a surface-based description of MHWs and develop an integrated understanding of their physical drivers, vertical structure, and impacts within the coupled ocean–atmosphere system.

Using daily datasets spanning 1982–2024, MHWs were identified following the Hobday et al. (2016) framework, while additional atmospheric and oceanic variables were analyzed to characterize the mechanisms controlling their evolution. The results show a significant intensification of MHWs in both basins, with increasing frequency, duration, and cumulative intensity over recent decades, consistent with global trends. However, strong regional variability is observed. In the Mediterranean Sea, a west–east contrast emerges, with more intense and variable events in the western basin and more persistent events in the eastern basin. In the Red Sea, a pronounced north–south gradient reflects the influence of stratification and basin-scale circulation.

The contribution of long-term warming is found to be a key factor in MHW occurrence, with a substantial fraction of events directly attributable to the upward shift in background sea surface temperature. Nevertheless, detrended analyses reveal that internal variability remains essential, indicating that MHWs arise from the interaction between gradual warming and short-term atmospheric and oceanic processes. Atmospheric forcing is identified as the primary trigger of MHW development, with events consistently associated with positive air temperature anomalies, reduced wind speed, and enhanced surface heat fluxes. Strong air–sea coupling is confirmed by the high correlation between sea surface temperature and near-surface air temperature, particularly in the Mediterranean basin.

Beyond surface processes, this thesis demonstrates that MHWs exhibit a pronounced vertical structure. Subsurface temperature analyses reveal that MHWs extend well below the mixed layer, with anomalies penetrating to depths of several hundred meters. This vertical extent is modulated by stratification and mixed layer dynamics, which control the redistribution and retention of heat within the upper ocean. The presence of subsurface heat reservoirs provides a mechanism for ocean memory, allowing thermal anomalies to persist beyond the duration of atmospheric forcing and influencing the development of subsequent events.

The ecological impacts of MHWs are assessed through the analysis of mixed layer depth, chlorophyll-a, and nitrate concentrations. Results show that MHWs lead to enhanced stratification, reduced nutrient availability, and decreased primary productivity in both basins, with stronger effects in oligotrophic regions such as the eastern Mediterranean and the southern Red Sea. A compound stress framework further reveals that physical and biogeochemical anomalies frequently co-occur, amplifying ecosystem stress. Complementary laboratory experiments on zooplankton (*Acartia tonsa*) demonstrate that elevated temperatures significantly increase mortality rates, indicating direct biological impacts in addition to large-scale environmental changes.

The analysis of compound marine and atmospheric heatwaves shows that the most extreme events occur when MHWs and atmospheric heatwaves co-occur. These compound events are characterized by stronger intensity, longer duration, and enhanced spatial coherence, reflecting nonlinear amplification driven by coupled ocean–atmosphere feedbacks. Their frequency has increased over time, particularly during summer, when stratification and radiative forcing maximize air–sea interaction.

A novel aspect of this thesis is the investigation of interactions between MHWs and Mediterranean tropical-like cyclones (Medicanes). The results show that Medicanes preferentially develop over regions with positive sea surface temperature anomalies and elevated ocean heat content, suggesting that MHWs provide favorable conditions for storm intensification. In turn, Medicanes induce strong ocean feedbacks through vertical mixing and surface cooling, leading to the redistribution of heat within the water column. This bidirectional interaction highlights the role of MHWs within a broader system of coupled extreme events.

Overall, this thesis demonstrates that MHWs in the Mediterranean Sea and the Red Sea are not isolated surface phenomena but rather emerge from the interaction of atmospheric forcing, ocean stratification, and subsurface heat storage, with important implications for ecosystems and extreme weather processes. The results provide a unified framework for understanding MHW dynamics in semi-enclosed basins and highlight the growing importance of compound and vertically structured extremes under ongoing climate change.

Key words: MHW, Mediterranean Sea, Red Sea, Sea temperature, Climate change, MHW drivers, MHW Impacts, Atmospheric heatwaves, Medicanes.

Université de Liège

Faculté des Sciences

Département d'Astrophysique, de Géographie et d'Océanographie

Résumé

Doctorat en Océanographie

Etude à long terme des canicules marines en mer Méditerranée et en mer Rouge : une évaluation de leurs tendances, de leurs facteurs déterminants et de leurs premiers indicateurs

Par: Manal Hamdeno

Les vagues de chaleur marines (MHWs, MHWs) sont devenues l'une des manifestations les plus marquantes du réchauffement des océans, avec des implications majeures pour les écosystèmes marins, le climat régional et les événements météorologiques extrêmes. Cette thèse doctorale propose une analyse approfondie de la dynamique des MHWs dans deux bassins semi-fermés thermiquement sensibles, la mer Méditerranée et la mer Rouge, en intégrant des observations de surface et de subsurface, les forçages atmosphériques, les réponses écologiques, ainsi que les interactions avec des événements composés et extrêmes. L'objectif est de dépasser une description limitée à la surface des vagues de chaleur marines et de développer une compréhension intégrée de leurs mécanismes physiques, de leur structure verticale et de leurs impacts au sein du système couplé océan–atmosphère.

À partir de jeux de données journaliers couvrant la période 1982–2024, les MHWs ont été identifiées selon la méthodologie de Hobday et al. (2016), tandis que des variables atmosphériques et océaniques complémentaires ont été analysées afin de caractériser les mécanismes contrôlant leur évolution. Les résultats montrent une intensification significative des MHWs dans les deux bassins, avec une augmentation de leur fréquence, de leur durée et de leur intensité cumulée au cours des dernières décennies, en accord avec les tendances globales. Toutefois, une forte variabilité régionale est observée. En mer Méditerranée, un contraste ouest–est se dessine, avec des événements plus intenses et plus variables dans le bassin occidental, et des événements plus persistants dans le bassin oriental. En mer Rouge, un gradient nord–sud marqué reflète l'influence de la stratification et de la circulation à l'échelle du bassin.

La contribution du réchauffement à long terme apparaît comme un facteur clé dans l'occurrence des MHWs, une fraction importante des événements étant directement attribuable à l'élévation du niveau de base de la température de surface de la mer. Néanmoins, les analyses (après avoir enlevé la tendance) révèlent que la variabilité interne reste essentielle, indiquant que les MHWs résultent de l'interaction entre le réchauffement progressif et des processus atmosphériques et océaniques à court terme. Les forçages atmosphériques sont identifiés comme le principal déclencheur des MHWs, les événements étant systématiquement associés à des anomalies positives de température de l'air, à une diminution de la vitesse du vent et à une augmentation des flux de chaleur de surface. Un fort couplage air–mer est confirmé par la corrélation élevée

entre les anomalies de température de surface de la mer et celles de la température de l'air proche de la surface, en particulier en Méditerranée.

Au-delà des processus de surface, cette thèse montre que les MHWs présentent une structure verticale marquée. Les analyses de température de subsurface révèlent que les anomalies associées aux MHWs s'étendent bien en dessous de la couche de mélange, atteignant des profondeurs de plusieurs centaines de mètres. Cette extension verticale est modulée par la stratification et la dynamique de la couche de mélange, qui contrôlent la redistribution et la rétention de la chaleur dans l'océan supérieur. La présence de réservoirs de chaleur de subsurface constitue un mécanisme de mémoire océanique, permettant aux anomalies thermiques de persister au-delà de la durée du forçage atmosphérique et d'influencer le développement d'événements ultérieurs.

Les impacts écologiques des MHWs sont évalués à travers l'analyse de la profondeur de la couche de mélange, de la concentration en chlorophylle-a et de la disponibilité en nitrates. Les résultats montrent que les MHWs entraînent un renforcement de la stratification, une réduction de l'apport en nutriments et une diminution de la productivité primaire dans les deux bassins, avec des effets plus marqués dans les régions oligotrophes telles que la Méditerranée orientale et la mer Rouge méridionale. Une approche basée sur les événements composés met également en évidence la co-occurrence fréquente d'anomalies physiques et biogéochimiques, amplifiant le stress sur les écosystèmes. Des expériences en laboratoire sur le zooplancton (Acartia tonsa) montrent en outre que l'élévation de la température augmente significativement les taux de mortalité, indiquant des impacts biologiques directs en plus des modifications environnementales à grande échelle.

L'analyse des événements composés marins et atmosphériques montre que les conditions les plus extrêmes surviennent lorsque les MHWs et les vagues de chaleur atmosphériques coïncident. Ces événements composés se caractérisent par une intensité plus élevée, une durée plus longue et une cohérence spatiale accrue, traduisant une amplification non linéaire liée aux rétroactions couplées entre l'océan et l'atmosphère. Leur fréquence a augmenté au cours du temps, en particulier durant l'été, lorsque la stratification et le forçage radiatif maximisent les échanges air–mer.

Un aspect novateur de cette thèse réside dans l'étude des interactions entre les MHWs et les cyclones méditerranéens de type tropical (Medicanes). Les résultats montrent que les Medicanes se développent préférentiellement au-dessus de régions caractérisées par des anomalies positives de température de surface de la mer et un contenu thermique océanique élevé, suggérant que les MHWs fournissent des conditions favorables à l'intensification des tempêtes. En retour, les Medicanes induisent de fortes rétroactions océaniques par le biais du mélange vertical et du refroidissement de surface, entraînant une redistribution de la chaleur dans la colonne d'eau. Cette interaction bidirectionnelle met en évidence le rôle des MHWs dans un système plus large d'événements extrêmes couplés.

Dans l'ensemble, cette thèse démontre que les vagues de chaleur marines en mer Méditerranée et en mer Rouge ne sont pas des phénomènes limités à la surface, mais résultent de l'interaction entre les forçages atmosphériques, la stratification océanique et le stockage de chaleur en

subsurface, avec des implications importantes pour les écosystèmes et les processus météorologiques extrêmes. Les résultats proposent un cadre unifié pour comprendre la dynamique des MHWs dans les bassins semi-fermés et mettent en évidence l'importance croissante des événements extrêmes combinés et de leur structure verticale dans un contexte de changement climatique.

Mots-clés: Vague de chaleur marine, mer Méditerranée, mer Rouge, Température des océans, Changement climatique, Facteurs de vagues de chaleur marines, Impacts des vagues de chaleur marines, Vagues de chaleur atmosphériques, Medicanes.

جامعة لييج

كلية العلوم

قسم الفيزياء الفلكية والجغرافيا وعلم المحيطات

الملخص

أطروحة دكتوراه في علم المحيطات

دراسة طويلة الأمد لموجات الحر البحرية في البحر الأبيض المتوسط والبحر الأحمر

إعداد: منال حمدينه

تُعتبر موجات الحر البحرية من أهم مظاهر الاحترار المتزايد في المحيطات، لما لها من تأثيرات واضحة على النظم البيئية البحرية، والمناخ الإقليمي، والظواهر الجوية المتطرفة. تهدف هذه الأطروحة إلى دراسة ديناميكيات موجات الحر البحرية في حوضين شبه مغلقين يتميزان بحساسية عالية للتغيرات الحرارية، وهما البحر الأبيض المتوسط والبحر الأحمر، من خلال دمج بيانات سطحية وتحت سطحية، وتحليل التأثيرات الجوية، والاستجابات البيئية، بالإضافة إلى دراسة التفاعلات مع الظواهر المركبة والمتطرفة. ويسعى هذا العمل إلى تقديم فهم متكامل لهذه الظواهر، يتجاوز التركيز على السطح فقط ليشمل البنية الرأسية وآليات التأثير داخل النظام المتكامل بين المحيط والغلاف الجوي.

اعتمدت الدراسة على بيانات يومية تمتد من عام 1982 إلى عام 2024، حيث تم تحديد موجات الحر البحرية باستخدام منهجية معيارية تعتمد على تجاوز درجات حرارة سطح البحر لقيم مرجعية مناخية. كما تم تحليل عدد من المتغيرات الجوية والمحيطية لفهم العوامل التي تتحكم في نشأة هذه الظواهر وتطورها. وتُظهر النتائج وجود زيادة واضحة في شدة موجات الحر البحرية في كلا الحوضين، من حيث التكرار والمدة والشدة التراكمية، بما يتماشى مع الاتجاهات العالمية. ومع ذلك، يظهر تباين إقليمي ملحوظ؛ ففي البحر الأبيض المتوسط يوجد اختلاف واضح بين الحوض الغربي والشرقي، حيث تسود أحداث أكثر شدة وتغيراً في الغرب، مقابل أحداث أطول وأكثر استمرارية في الشرق. أما في البحر الأحمر، فيظهر تدرج من الشمال إلى الجنوب مرتبط بطبيعة التطبق المائي ودوران المياه داخل الحوض.

تشير النتائج إلى أن الاحترار طويل المدى يلعب دوراً أساسياً في زيادة حدوث موجات الحر البحرية، حيث يرتبط جزء كبير من هذه الظواهر بارتفاع درجات حرارة سطح البحر على المدى الطويل. ومع ذلك، فإن استمرار الأحداث بعد إزالة هذا الاتجاه العام يدل على أن التغيرات قصيرة المدى لا تزال مؤثرة، وأن هذه الظواهر تنتج عن تفاعل بين الاحترار التدريجي والعوامل الجوية والمحيطية. ويُعد الغلاف الجوي العامل الأساسي في بداية هذه الظواهر، حيث ترتبط موجات الحر البحرية بارتفاع درجات حرارة الهواء، وانخفاض سرعة الرياح، وزيادة تدفق الحرارة نحو سطح البحر. كما يظهر ارتباط قوي بين حرارة سطح البحر وحرارة الهواء، خاصة في البحر الأبيض المتوسط، مما يعكس قوة التفاعل بين المحيط والغلاف الجوي.

وتوضح هذه الدراسة أن موجات الحر البحرية لا تقتصر على الطبقة السطحية فقط بل تمتد إلى أعماق كبيرة داخل المياه. حيث أظهرت النتائج أن الشذوذات الحرارية قد تصل إلى مئات الأمتار تحت السطح، ويتحكم في ذلك كل من التطبق المائي وديناميكيات طبقة الخلط. كما أن وجود حرارة مخزنة تحت السطح يساهم في ما يُعرف بذاكرة المحيط، حيث تستمر هذه الشذوذات لفترة أطول حتى بعد انتهاء التأثيرات الجوية، وقد تؤثر على حدوث موجات حر لاحقة.

أما من ناحية التأثيرات البيئية، فقد تم تحليل التغيرات في عمق طبقة الخلط وتركيز الكلوروفيل، وتوفر المغذيات. وتُظهر النتائج أن موجات الحر البحرية تؤدي إلى زيادة التطبق، وتقليل وصول المغذيات إلى السطح، مما يؤدي إلى انخفاض الإنتاجية الأولية في كلا الحوضين، خاصة في المناطق الفقيرة بالمغذيات مثل شرق البحر الأبيض المتوسط وجنوب البحر الأحمر. كما يوضح تحليل الظواهر المركبة أن التغيرات الفيزيائية والبيئية تحدث في نفس الوقت بشكل متكرر، مما يزيد من الضغط على النظم البيئية. وتُظهر التجارب المعملية على العوالق الحيوانية أن ارتفاع درجات الحرارة يؤدي إلى زيادة معدلات النفوق، مما يشير إلى وجود تأثيرات مباشرة لهذه الظواهر على الكائنات البحرية.

كما يبين تحليل التفاعل بين موجات الحر البحرية والجوية أن أشد الحالات تحدث عند تزامنهما معاً، حيث تكون هذه الأحداث أكثر شدة وأطول مدة وأكثر انتشاراً، نتيجة تفاعل متبادل بين المحيط والغلاف الجوي. وقد لوحظ زيادة في تكرار هذه الحالات خلال السنوات الأخيرة، خاصة في فصل الصيف.

ومن الجوانب المهمة في هذه الدراسة تحليل العلاقة بين موجات الحر البحرية والأعاصير المتوسطية ذات الطابع المداري. حيث أظهرت النتائج أن هذه الأعاصير تتكون غالباً فوق مناطق ذات درجات حرارة مرتفعة ومخزون حراري كبير، مما يشير إلى أن موجات الحر البحرية تساعد على تهيئة الظروف المناسبة لزيادة شدة هذه العواصف. وفي المقابل، تؤثر هذه الأعاصير على المحيط من خلال زيادة الخلط وتبريد السطح، مما يؤدي إلى إعادة توزيع الحرارة داخل عمود الماء. ويعكس هذا التفاعل العلاقة المتبادلة بين الظواهر المتطرفة في المحيط والغلاف الجوي.

بشكل عام، توضح هذه الأطروحة أن موجات الحر البحرية في البحر الأبيض المتوسط والبحر الأحمر ليست مجرد ظواهر سطحية، بل ناتجة عن تفاعل معقد بين العوامل الجوية، والتطبق المائي، وتخزين الحرارة تحت السطح، مع تأثيرات واضحة على البيئة البحرية والظواهر الجوية المتطرفة. كما تقدم هذه الدراسة إطاراً متكاملاً لفهم هذه الظواهر في الأحواض شبه المغلقة، وتبرز أهمية دراسة الظواهر المركبة والبنية الرأسية في ظل التغير المناخي المستمر.

الكلمات المفتاحية: موجات الحر البحرية، البحر الأبيض المتوسط، البحر الأحمر، درجة حرارة البحر، تغير المناخ، آثار موجات الحر البحرية، موجات الحر الجوية، الأعاصير المتوسطية ذات الطابع المداري.

Acknowledgements

I would like to express my deepest gratitude to my supervisor, **Prof. Aida Alvera-Azcárate**, for her continuous support, guidance, and encouragement throughout this PhD. Her scientific insight, patience, and kindness have been invaluable, and I am especially grateful for her constant availability, friendly attitude, and the confidence she placed in me during this journey.

I would also like to warmly thank the entire **GHER group** for providing a stimulating, collaborative, and supportive research environment. It has been a privilege to be part of such a dynamic and inspiring team.

My sincere thanks go to my collaborators, **Prof. Ibrahim Hoteit, Dr. George Krokos, Dr. Tamer Hafez, Dr. Manu Soto, and Kene Uba**, for their valuable contributions, insightful discussions, and support throughout this work. I am also grateful to **KAUST University** and the **PiE group** for hosting me and providing the opportunity to conduct part of this research in such an enriching scientific environment.

I would like to thank all my friends for their support during this journey. A very special thanks goes to **Nourhan** ❤️ , for her unconditional love, support, and for being a true family away from home. **Mohamed, Kene, and Cécile** without your support and guides this work was not going to finish, Thank you for every single advise, I am grateful for having you in my life ❤️ .

I am also deeply grateful to my friends **Juan, Maria, Basile, and Mathurin**, whose friendship, encouragement, and support made this journey much easier and more enjoyable.

My deepest gratitude goes to my family, my **mother**, my **sisters**, and my **brothers**, for their endless love, support, and belief in me.

This work is dedicated to the **soul of my father**, who has always been my greatest motivation. His words have been a guiding light throughout this journey, and he continues to inspire me every day.

I would also like to thank the **University of Liège** for providing the academic environment in which this research was conducted.

Finally, this work benefited from financial support from the **F.R.S.-FNRS (Fonds de la Recherche Scientifique de Belgique, Communauté Française de Belgique)** through the funding of my *Aspirant* grant.

Contents

Figures:

Tables:

Chapter One: General Introduction

1.1 Introduction:

The global climate system is undergoing rapid transformation as a consequence of increasing atmospheric concentrations of greenhouse gases from human activities (IPCC, 2018, 2019, 2022). A key aspect of this change is the substantial uptake of excess heat by the world's oceans, which serve as the primary heat reservoir of Earth's climate system (von Schuckmann et al., 2020; IPCC, 2022). Observational estimates indicate that about 89% of the excess heat accumulated between 1960 and 2020 has been stored in the ocean, compared with approximately 6% in land systems, 1% in the atmosphere, and the remainder contributing to ice melt (Cheng et al., 2017; von Schuckmann et al., 2020; IPCC, 2022). This large heat uptake highlights the central role of the ocean in regulating the pace and spatial distribution of global climate change (Trenberth, 2020; Cheng et al., 2023).

Ocean warming has already caused widespread changes in the physical structure and dynamics of the marine environment (IPCC, 2022; Cheng et al., 2023). Rising sea surface temperatures (SST) have been observed across all ocean basins in recent decades, accompanied by increases in ocean heat content and significant modifications to the vertical stratification of the upper ocean (Cheng et al., 2017, 2023; von Schuckmann et al., 2020). Enhanced stratification reduces vertical mixing between surface and deeper waters, thereby influencing nutrient transport, oxygen distribution, and the exchange of heat between the ocean and atmosphere (Doney et al., 2012; IPCC, 2014). These physical changes are occurring alongside other climate-driven stressors, including ocean acidification, deoxygenation, and sea-level rise, which together alter marine biogeochemical cycles and ecosystem functioning (Doney et al., 2012; Breitburg et al., 2018).

Beyond gradual long-term warming, the accumulation of heat in the ocean also alters ocean temperature variability on shorter timescales. In particular, the increasing background temperature of the ocean raises the probability of extreme thermal events in marine environments (Frölicher et al., 2018; Oliver et al., 2018a; Sen Gupta et al., 2020). As mean ocean temperatures continue to rise, temperature anomalies that previously represented rare extremes are becoming increasingly common, leading to a fundamental shift in the frequency and magnitude of ocean temperature variability (Oliver et al., 2018a; Collins et al., 2019). Among the most prominent manifestations of these extreme temperature anomalies are marine heatwaves , which are prolonged periods of unusually warm ocean temperatures relative to the local seasonal climatology (Doney et al., 2012; Hobday et al., 2016; Frölicher et al., 2018; Oliver et al., 2018a). Over the past decade, MHWs have emerged as a major focus of climate research because of their increasing occurrence and their potential to disrupt marine ecosystems and socio-economic activities (Oliver et al., 2018a; Arafeh-Dalmau et al., 2019; Smale et al., 2019; Benedetti-Cecchi, 2021). Observational analyses show that the frequency, duration, and intensity of MHWs have increased significantly across the global ocean since the early twentieth century, largely due to long-term ocean warming superimposed on natural climate variability (Oliver et al., 2018a; Darmaraki et al., 2019a; Sen Gupta et al., 2020).

1.2 MHWs:

1.2.1 Definition and Conceptual Framing:

MHWs are episodic extreme events in which ocean temperatures become unusually warm relative to the local seasonal cycle. The most widely adopted and internationally accepted definition was introduced by Hobday et al., (2016), who proposed that an MHW occurs when SST exceeds a location-specific, seasonally varying 90th percentile threshold for at least five consecutive days, based on a long-term climatological reference period of typically 30 years or more. This percentile-based approach provides a robust and objective framework for detecting thermal extremes, as it accounts for the strong spatial and seasonal variability of ocean temperatures (Hobday et al., 2016). It enables consistent identification of MHWs across contrasting climatic regimes, from cold temperate seas to persistently warm tropical and subtropical basins (Hobday et al., 2016). Consequently, it offers a common basis for interregional comparison of marine heat extremes and their evolving characteristics under climate change.

Within this framework, MHWs are characterized using a standardized set of metrics that describe their temporal evolution and thermal intensity (Hobday et al., 2016; Fig.1). **Event duration** is the total number of consecutive days during which SST exceeds the local threshold, expressed in days. **Frequency** refers to the number of discrete MHW events occurring within a given period, typically reported as events per year. **Mean intensity** is the average temperature anomaly above the threshold over the event duration (°C), while **maximum intensity** is the largest instantaneous exceedance reached during the event (°C). To account for both magnitude and persistence, **cumulative intensity** is defined as the time-integrated temperature anomaly above the threshold over the full event duration, expressed in °C.days. The **rates of onset and decay** quantify how rapidly temperatures rise above or fall below the threshold, respectively, and are commonly reported in °C/day. Finally, the **spatial and vertical extents** describe the horizontal area (km^2) and vertical depth (m) affected by an MHW at a given time or over its lifetime.

Building on these metrics, Hobday et al., (2018) introduced a severity categorization scheme that classifies MHWs according to their intensity relative to local climatological variability (Fig. 1). In this framework, events are grouped into four categories (Moderate, Strong, Severe, and Extreme) based on how much the temperature anomaly exceeds the threshold, scaled by the difference between the climatological mean and the 90th percentile threshold. Importantly, the categorization is dynamic, so a single event may shift between categories as it strengthens or weakens over its lifetime. Such classification provides an intuitive measure of event magnitude and has proven valuable for communicating risk, comparing impacts across regions, and linking physical extremes to ecological responses (Hobday et al., 2018). Together, these standardized metrics and severity categories offer a comprehensive and flexible framework for monitoring MHWs, assessing their evolution under climate change, and interpreting their potential biological and biogeochemical consequences.

The detection of MHWs using a percentile-based approach depends critically on how the baseline climatology is defined. In practice, a fixed historical reference period is commonly used to characterize the local seasonal cycle and its variability, from which day-of-year thresholds are derived (Hobday et al., 2016). The selection of this baseline directly influences detection sensitivity and the interpretation of long-term trends under climate change. For instance, using a warmer or more recent baseline shifts percentile thresholds upward, which may reduce the number of detected events even as absolute temperatures continue to rise. In contrast, fixed historical baselines emphasize the extent to which current conditions deviate from past "normal" states and are therefore more suitable for highlighting long-term changes in extreme thermal exposure (Hobday et al., 2016; Holbrook et al., 2019; Fernández-Álvarez et al., 2025; Smith et al., 2025).

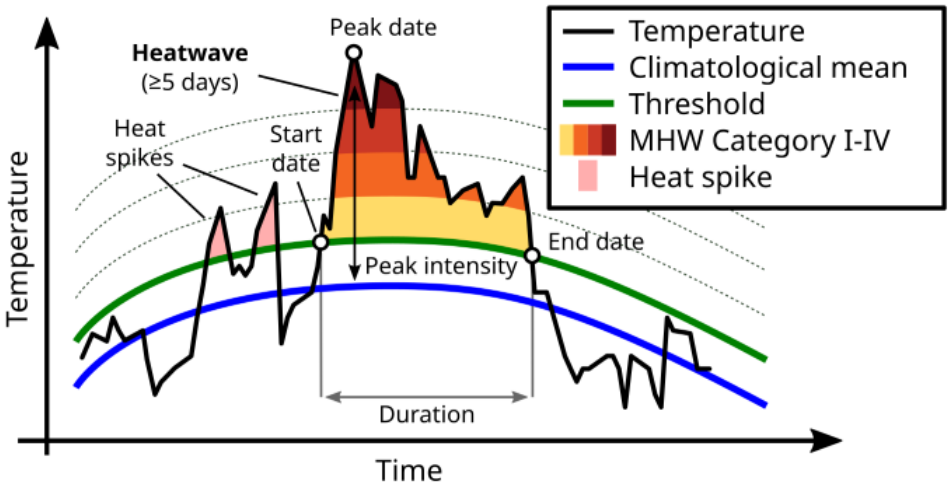

Figure 1. Conceptual representation of a MHW event following the detection framework proposed by Hobday et al. (2016,2018). A MHW occurs when SST exceeds a seasonally varying threshold (typically the 90th percentile) for at least five consecutive days. The figure highlights key event characteristics, including duration, start and end dates, and peak intensity relative to the climatological mean.

1.2.2 MHW Drivers:

MHWs arise from the interaction of multiple physical processes that regulate the accumulation, redistribution, and persistence of heat within the upper ocean (Holbrook et al., 2019; Sen Gupta et al., 2020). Unlike long-term ocean warming associated with gradual climate change, MHWs typically emerge from short-term anomalies in atmospheric and oceanic conditions that produce extreme temperature deviations relative to the local climatology (Hobday et al., 2016; Oliver et al., 2018a; Holbrook et al., 2019; Sen Gupta et al., 2020). Their development therefore reflects the combined influence of atmospheric forcing, ocean circulation, large-scale climate variability, and subsurface heat storage processes (Vogt et al., 2022; Bian et al., 2024; Gröger et al., 2024). These mechanisms often interact across multiple spatial and temporal scales, and their relative importance varies depending on regional oceanographic conditions. Understanding how these processes interact is essential for interpreting regional variability in MHW occurrence and for improving projections of future extreme warming events under continued climate change (Frölicher et al., 2018; Holbrook et al., 2019; Sen Gupta et al., 2020).

Atmospheric forcing frequently provides the initial conditions that trigger MHWs by altering the surface heat balance of the ocean (Bond et al., 2015; Holbrook et al., 2019; Sen Gupta et al., 2020; Vogt et al., 2022). Persistent atmospheric anomalies can modify wind patterns, radiative fluxes, and turbulent heat exchange at the air-sea interface, allowing heat to accumulate within the surface mixed layer (Bian et al., 2024; Gröger et al., 2024). Reduced wind speeds weaken vertical mixing between the mixed layer and deeper waters, limiting the upward transport of cooler subsurface water and enabling rapid SST increases (Benedetti-Cecchi, 2021; Vogt et al., 2022; Darmaraki et al., 2024). Atmospheric blocking events can further intensify this process by establishing quasi-stationary high-pressure systems that promote clear-sky conditions, enhanced shortwave radiation, and reduced heat loss from the ocean surface (Garrabou et al., 2009; Bond et al., 2015; Vogt et al., 2022; Darmaraki et al., 2024). Such conditions were observed during the 2013-2016 Northeast Pacific MHW, where a persistent atmospheric ridge suppressed mixing and allowed heat to accumulate in the upper ocean (Bond et al., 2015; Di Lorenzo and Mantua, 2016). The influence of atmospheric forcing can be particularly strong in semi-enclosed basins such as the Mediterranean, where tight coupling between regional atmospheric circulation and the ocean surface enhances the sensitivity of SST to atmospheric anomalies (Darmaraki et al., 2019a; Ibrahim et al., 2021; Pastor and Khodayar, 2023; Darmaraki et al., 2024; Artana et al., 2026).

Oceanic processes also play a crucial role by redistributing heat through horizontal transport and regional circulation changes (Oliver et al., 2017, 2021; Holbrook et al., 2019). Variability in ocean currents, mesoscale eddies, and frontal systems can advect warm water masses into new regions and generate prolonged temperature anomalies (Holbrook et al., 2019; Sen Gupta et al., 2020; Oliver et al., 2021; Vogt et al., 2022). Shifts in the strength or position of major boundary currents have been linked to MHW formation in several regions, as these currents transport large amounts of heat across the ocean (Oliver et al., 2018b, 2018a; Holbrook et al., 2019; Gröger et al., 2024). Mesoscale eddies and ocean fronts further contribute to regional temperature variability by trapping and transporting warm water over long distances, sometimes sustaining localized warming events for several months (Holbrook et al., 2019). Horizontal convergence of warm water masses can therefore lead to the accumulation of heat within a particular region, particularly when atmospheric conditions simultaneously favor surface warming. These circulation-driven processes are often reinforced by strong ocean stratification, which limits vertical mixing and allows heat anomalies to persist within the mixed layer (Oliver et al., 2021).

Large-scale climate variability can further modulate the background conditions that favor MHW development by altering atmospheric circulation patterns, wind systems, and air–sea heat fluxes across entire ocean basins (McPhaden et al., 2006; Holbrook et al., 2019). Among these modes, the El Niño–Southern Oscillation (ENSO) represents the dominant source of interannual climate variability and is characterized by alternating warm (El Niño) and cool (La Niña) SST anomalies in the equatorial Pacific, commonly monitored using the Oceanic Niño Index (ONI) based on SST anomalies in the Niño 3.4 region (Barnston and Livezey, 1987; McPhaden et al., 2006). Although ENSO originates in the tropical Pacific, its influence extends globally through atmospheric teleconnections that modify wind patterns and heat fluxes in distant regions, including the Indian Ocean and the Middle East (Bjerknes, 1969; McPhaden et al., 2006; Mohamed et al., 2021). In the North Atlantic sector, the Atlantic Multidecadal Oscillation (AMO) represents multidecadal basin-wide SST variability, while the North Atlantic Oscillation (NAO) describes fluctuations in the atmospheric pressure gradient between the Azores High and the Icelandic Low, which strongly influence wind patterns and regional climate across Europe and the Mediterranean (Hurrell et al., 2003; Zhang, 2007; Schneider et al., 2013). Additional teleconnection patterns such as the East Atlantic Pattern (EAP), the East Atlantic/West Russian pattern (EATL/WRUS), and the Indian Ocean Dipole (IOD; defined by SST differences between the western and eastern equatorial Indian Ocean) can further influence atmospheric circulation and regional heat fluxes (Barnston and Livezey, 1987; Behera et al., 2021; Cai et al., 2021). Through these mechanisms, large-scale climate modes shape the environmental conditions that can either favor or suppress MHW development across different regions.

Finally, subsurface ocean processes can play an important role in sustaining MHWs by storing heat beneath the surface mixed layer and modulating the vertical structure of temperature anomalies (Holbrook et al., 2020; Dayan et al., 2023). Although MHWs are typically identified using SST observations, recent studies have shown that warming events can extend well below the surface and persist longer at depth (Juza et al., 2022; Dayan et al., 2023; Darmaraki et al., 2024; Nadimpalli et al., 2025). Strong ocean stratification can trap warm water below the mixed layer, creating subsurface heat reservoirs that remain insulated from atmospheric cooling. Subsequent mixing events may then reintroduce this stored heat to the surface, prolonging the duration of surface warming. Variations in thermocline depth can also influence MHW development by bringing warmer subsurface water closer to the surface or reducing the upwelling of cooler water (Oliver et al., 2017; Holbrook et al., 2020; Dayan et al., 2023). These vertical processes are particularly important in stratified environments such as semi-enclosed seas and tropical basins, where limited vertical mixing allows heat anomalies to persist within the upper ocean for extended periods (Holbrook et al., 2020; Juza et al., 2022; Dayan et al., 2023; Gröger et al., 2024). Together with atmospheric forcing, ocean circulation, and climate variability, subsurface heat storage forms an integral component of the multi-scale processes that govern MHW evolution.

1.2.3 The Impacts of MHWs:

MHWs can have significant consequences for marine ecosystems because many marine organisms live close to their physiological thermal limits (Sen Gupta et al., 2020). Sudden or prolonged increases in ocean temperature can disrupt metabolic processes, alter species interactions, and trigger widespread ecological disturbances across different marine habitats (Smale et al., 2019; Oliver et al., 2021). As these extreme warming events become more frequent and intense under ongoing climate change, their ecological impacts are increasingly observed in both coastal and open-ocean ecosystems. Elevated temperatures can influence biological systems through both direct and indirect pathways, affecting organism physiology, reproduction, and survival, while also modifying nutrient availability, primary productivity, and trophic interactions within marine food webs (Doney et al., 2012; Smale et al., 2019; Sen Gupta et al., 2020). These combined effects can lead to shifts in species distribution, changes in ecosystem structure, and alterations in marine biodiversity.

One important pathway through which MHWs influence marine ecosystems is by modifying upper-ocean stratification and nutrient dynamics (Theodorou et al., 2025). Increased stratification during warming events often reduces vertical mixing between surface waters and deeper nutrient-rich layers, limiting the nutrient supply required for phytoplankton growth within the euphotic zone (Smale et al., 2019; Darmaraki et al., 2024; Theodorou et al., 2025). As a result, phytoplankton biomass and primary productivity may decline, particularly in oligotrophic regions where nutrient availability is already limited (Racault et al., 2012; Hayashida et al., 2020; Arteaga and Rousseaux, 2023; Theodorou et al., 2025). Changes in phytoplankton communities can propagate through the marine food web by affecting zooplankton populations and higher trophic levels. In some cases, MHWs may also favor the development of harmful algal blooms when warming and stratified conditions promote the growth of opportunistic phytoplankton species (Smale et al., 2019; Greenhough et al., 2025).

Benthic ecosystems are particularly vulnerable to MHWs because many benthic organisms have limited mobility and cannot easily escape unfavorable thermal conditions (Garrabou et al., 2009; Smale et al., 2019). Elevated temperatures can cause physiological stress and increased mortality among benthic species such as corals, sponges, and other invertebrates (Garrabou et al., 2009; Genevier et al., 2019; Darmaraki et al., 2025; Nadimpalli et al., 2025). These disturbances can alter community composition and reduce biodiversity, especially when habitat-forming organisms decline. In coral reef ecosystems, extreme warming can trigger coral bleaching, a process in which corals expel their symbiotic algae under thermal stress, potentially leading to coral mortality if elevated temperatures persist (Hughes et al., 2018). Although some coral populations, such as those in the Red Sea, exhibit relatively high thermal tolerance, prolonged MHWs may still pose risks if temperature thresholds are exceeded (Fine et al., 2013; Genevier et al., 2019; Darmaraki et al., 2025).

Beyond these direct ecological effects, MHWs can also drive broader ecosystem changes and socio-economic impacts. Temperature anomalies may force species to shift their geographic ranges toward cooler regions, altering community composition and regional biodiversity patterns (Smale et al., 2019; Fredston et al., 2023). Such changes can influence fisheries productivity by modifying the distribution and abundance of commercially important species, with potential consequences for coastal communities that depend on marine resources (Mills et al., 2013; Fredston et al., 2023).

1.2.4 Compound MHWs and Atmospheric Extremes:

MHWs are increasingly recognized as part of broader compound climate extremes rather than isolated oceanic events (Burger et al., 2022; Aboelkhair et al., 2023; Chen et al., 2023; Choi et al., 2024; Jangir et al., 2024; Paredes-Fortuny et al., 2025; Zhou et al., 2025; Russo et al., 2026). Compound extremes occur when two or more climate hazards occur simultaneously or sequentially, producing combined impacts that can exceed those associated with each event individually (AghaKouchak et al., 2020; Le Grix et al., 2021). In the ocean–atmosphere system, MHWs may interact with other extreme phenomena such as atmospheric heatwaves, droughts, or intense storm systems through coupled physical processes that modify surface heat fluxes, atmospheric circulation, and ocean dynamics (Aboelkhair et al., 2023; Choi et al., 2024; Jangir et al., 2024; Paredes-Fortuny et al., 2025; Zhou et al., 2025; Russo et al., 2026). These interactions can amplify thermal stress within the ocean and increase the persistence or intensity of warming events. Because MHWs are strongly influenced by air-sea heat exchanges, momentum, and moisture, the simultaneous occurrence of atmospheric and oceanic extremes can reinforce positive feedbacks that intensify both marine and atmospheric conditions.

Within this framework, particular attention has been given to the co-occurrence of marine and atmospheric heatwaves. Atmospheric heatwaves can significantly alter the ocean surface heat balance by increasing incoming solar radiation, weakening wind-driven mixing, and modifying turbulent heat exchange between the ocean and atmosphere (Aboelkhair et al., 2023; Russo et al., 2026). These processes favor the accumulation of heat within the surface mixed layer and can contribute to the initiation or intensification of MHWs. Observational and modeling studies have shown that the concurrence of atmospheric and MHWs can prolong warming events and enhance their magnitude through strong air-sea coupling (AghaKouchak et al., 2020; Aboelkhair et al., 2023; Paredes-Fortuny et al., 2025; Russo et al., 2026). Such compound temperature extremes illustrate how atmospheric variability can interact with ocean processes to generate persistent warm anomalies in the upper ocean.

In addition to atmospheric heatwaves, recent research has begun to examine how MHWs may interact with cyclonic systems, including tropical-like cyclones known as medicanes in the Mediterranean Sea (Choi et al., 2024; Jangir et al., 2024; Zhou et al., 2025). Although relatively rare, medicanes can produce intense winds, heavy precipitation, and significant coastal impacts across the basin (Romero and Emanuel, 2013; Miglietta and Rotunno, 2019; Jangir et al., 2024). Warm SSTs and elevated upper-ocean heat content associated with MHWs can enhance latent and sensible heat fluxes from the ocean to the atmosphere, potentially providing additional energy that supports cyclone development or intensification (Borzì et al., 2024). Case studies of recent medicanes such as Zorbas (2018), Ianos (2020), and Apollo (2021) suggest that cyclone intensification may occur in the presence of either basin-scale MHW conditions or localized warm-core ocean eddies that supply heat to the atmosphere (Borzì et al., 2024; Jangir et al., 2024). Despite these emerging findings, the interaction between MHWs and Mediterranean cyclogenesis remains less well understood than the coupling between atmospheric and MHWs, highlighting the need for further research on compound ocean-atmosphere extremes in the region.

1.2.5 MHWs Across the Global Ocean:

MHWs have been documented in all major ocean basins and marginal seas, demonstrating that extreme ocean temperature events are a widespread phenomenon rather than isolated regional anomalies (Frölicher et al., 2018; Oliver et al., 2018a; Holbrook et al., 2019; Smale et al., 2019; Sen Gupta et al., 2020; Benedetti-Cecchi, 2021). Under global warming, satellite SST records show a marked increase in the frequency, duration, and intensity of MHWs over recent decades (Oliver et al., 2018a; Holbrook et al., 2019). The global distribution of notable MHW events highlights the diverse environmental contexts in which they occur, ranging from open-ocean regions to coastal ecosystems and semi-enclosed seas (Fig. 2).

One of the most widely studied MHW events occurred in the Northeast Pacific Ocean between 2013 and 2016, commonly referred to as the "Blob." This event was characterized by exceptionally warm surface waters that persisted for several years across a large portion of the North Pacific (Bond et al., 2015; Di Lorenzo and Mantua, 2016). The event developed primarily due to persistent atmospheric high-pressure systems that suppressed wind-driven mixing and reduced heat loss from the ocean surface. As a result, heat accumulated in the upper ocean, producing temperature anomalies several degrees above the climatological mean (Bond et al., 2015). The Blob had widespread ecological consequences, including harmful algal blooms, disruptions in plankton communities, and increased mortality among marine mammals and seabirds (Di Lorenzo and Mantua, 2016; Smale et al., 2019).

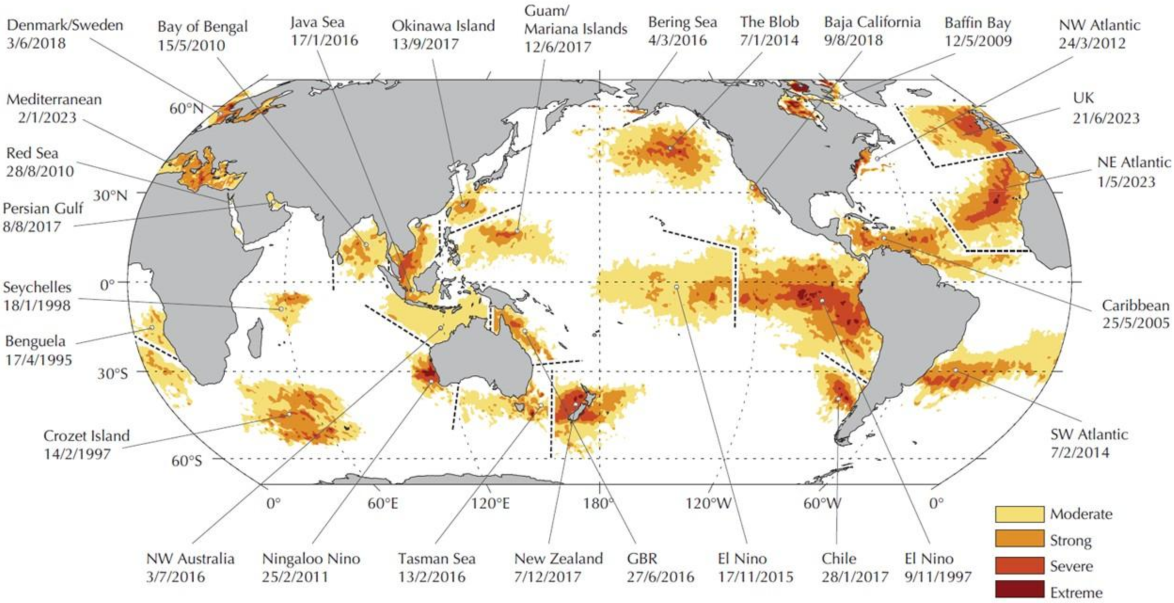

Figure 2. *Global distribution of notable MHW events recorded in recent decades. Colours indicate event severity categories, and labels highlight well-documented regional events (Smith et al., 2021).*

Another well-documented MHW occurred in the Northwest Atlantic during 2012, affecting the northeastern continental shelf of North America. This event developed rapidly and was linked to anomalous atmospheric circulation patterns and shifts in the jet stream position associated with the North Atlantic Oscillation (Mills et al., 2013; Holbrook et al., 2019). The resulting ocean warming produced SST anomalies that exceeded historical variability and caused significant ecological and economic impacts, including changes in fish distribution and fisheries management challenges (Mills et al., 2013; Oliver et al., 2018a).

Extreme MHWs have also been recorded in the Southern Hemisphere, particularly in the Tasman Sea between Australia and New Zealand (Oliver et al., 2018b). The 2015-2016 Tasman Sea MHW was driven by anomalously strong poleward transport of warm subtropical waters by the East Australian Current, combined with atmospheric heat flux anomalies (Oliver et al., 2017, 2018b). This event led to substantial ecosystem restructuring, including the loss of kelp forests and the poleward expansion of several warm-water species (Smale et al., 2019).

In tropical regions, MHWs are frequently associated with large-scale climate variability such as the El Niño–Southern Oscillation (ENSO). Strong El Niño events in 1998, 2010, and 2015-2017 generated prolonged warm anomalies across the Indo-Pacific, resulting in widespread coral bleaching across major reef systems, including the Great Barrier Reef (Hughes et al., 2018; Sen Gupta et al., 2020). Elevated SSTs, combined with weak winds and clear-sky conditions during these events, intensified thermal stress on coral ecosystems, leading to extensive coral mortality and long-term degradation of reef habitats (Hughes et al., 2018; Sen Gupta et al., 2020).

While MHWs occur in both open-ocean and coastal environments, semi-enclosed seas are often particularly susceptible to these events due to their restricted exchange with the open ocean and strong coupling with regional atmospheric conditions (Lionello et al., 2006; Darmaraki et al., 2019a, 2019b; Genevier et al., 2019; Mohamed et al., 2021, 2022a). In such basins, limited horizontal heat transport can allow thermal anomalies to persist for extended periods, while strong seasonal stratification can trap heat in the upper ocean and amplify surface warming. These physical characteristics can enhance the development and persistence of MHWs compared with more open-ocean environments (Darmaraki et al., 2019a; Pastor et al., 2020; Pastor and Khodayar, 2023).

Among semi-enclosed systems, the Mediterranean Sea and the Red Sea have received increasing scientific attention because of their rapid warming trends and their ecological and socio-economic importance. Both basins have experienced a marked increase in MHW occurrence in recent decades, with events affecting large portions of their surface area and causing significant ecological disturbances (Darmaraki et al., 2019a, 2019b; Genevier et al., 2019; Juza et al., 2022; Pastor and Khodayar, 2023). Understanding the occurrence and variability of MHWs across different ocean regions therefore requires considering both global climate drivers and regional oceanographic processes. Comparative analyses of semi-enclosed basins provide valuable insights into how local environmental conditions influence the development, persistence, and ecological consequences of extreme ocean warming events. The following sections therefore focus on the Mediterranean Sea and the Red Sea, two semi-enclosed basins where MHWs have intensified in recent decades.

1.3 The Mediterranean Sea:

1.3.1 Basin Geometry:

The Mediterranean Sea is a semi-enclosed basin located between Europe, Africa, and Asia, extending from the Strait of Gibraltar in the west to the Levantine Basin in the east. It covers an area of approximately 2.5 million km² and reaches depths exceeding 5,000 m in several locations, making it one of the largest semi-enclosed seas in the global ocean (Lionello et al., 2006; Tanhua et al., 2013; Pinardi et al., 2019). Although relatively small compared to major ocean basins, the Mediterranean Sea plays a significant role in regional climate dynamics, thermohaline circulation, and marine biodiversity (Tanhua et al., 2013; Pinardi et al., 2019; Allam et al., 2020; Pastor et al., 2020).

The Mediterranean basin is typically divided into two major sub-basins: the Western Mediterranean Basin (WMB) and the Eastern Mediterranean Basin (EMB). These sub-basins are separated by the Strait of Sicily, a shallow sill that restricts deep-water exchange between the western and eastern parts of the basin. The western basin includes the Alboran Sea, the Balearic Sea, and the Gulf of Lion, while the eastern basin comprises the Ionian Sea, the Adriatic Sea, the Aegean Sea, and the Levantine Basin. These regions vary in bathymetry, water mass properties, and circulation patterns, resulting in strong spatial variability in oceanographic conditions across the Mediterranean. The overall bathymetric structure and subdivision of the Mediterranean Sea are shown in Fig.3, which highlights the distinction between the western and eastern basins and the complex topography of the region.

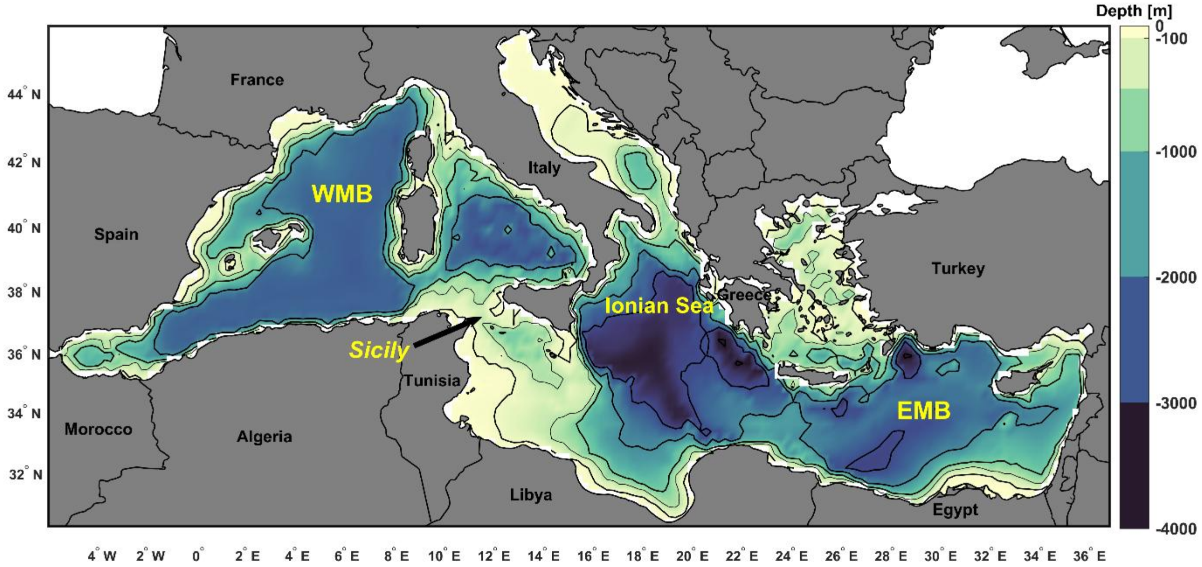

Figure 3. *Bathymetry of the Mediterranean Sea showing the Western Mediterranean Basin (WMB) and the Eastern Mediterranean Basin (EMB), separated by the Strait of Sicily. Bathymetry corresponds to the GEBCO bathymetry dataset (https://www.gebco.net).*

1.3.2 Mediterranean Circulation and Atmospheric Forcing:

Mediterranean circulation is typically described as an inverse estuarine system, where relatively fresh Atlantic Water enters the basin at the surface through the Strait of Gibraltar, while saltier Mediterranean waters exit at intermediate depths (Tanhua et al., 2013; Pinardi et al., 2019; Allam et al., 2020). This circulation is primarily driven by strong net evaporation, which exceeds precipitation and river runoff. As Atlantic Water flows eastward, it becomes progressively warmer and saltier due to intense evaporation and heat exchange with the atmosphere (Pinardi et al., 2019; Allam et al., 2020). This process leads to the formation of several characteristic Mediterranean water masses, including Levantine Intermediate Water (LIW), Western Mediterranean Deep Water (WMDW), and Eastern Mediterranean Deep Water (EMDW). These water masses play an essential role in the Mediterranean overturning circulation, which redistributes heat and salt throughout the basin and influences exchanges between the Mediterranean and the Atlantic Ocean (Pinardi et al., 2019). Mesoscale features such as eddies and fronts are especially important in the Mediterranean Sea and contribute significantly to its oceanographic variability (Brenner, 1993; Tanhua et al., 2013; Barcikowska et al., 2018; Allam et al., 2020; Pisano et al., 2020). These structures influence the horizontal transport of heat and salt, modify biological productivity, and shape the spatial distribution of marine ecosystems. Satellite observations and numerical modelling studies have shown that mesoscale variability plays a key role in controlling regional ocean circulation and mixing processes within the basin (Pisano et al., 2020).

Atmospheric forcing strongly influences Mediterranean ocean dynamics due to the basin's relatively small spatial scale and strong air-sea coupling. Seasonal variations in wind patterns, surface heat fluxes, and evaporation regulate the stratification and mixing of the upper ocean. In winter, intense cooling and evaporation in regions such as the Gulf of Lion, the Adriatic Sea, and the Aegean Sea can trigger deep convection events that contribute to deep-water formation and renewal of Mediterranean deep waters (Lionello et al., 2006; Tanhua et al., 2013). These deep-water formation processes are a critical component of the Mediterranean overturning circulation and play an important role in regulating the basin's heat and salt budgets (Pinardi et al., 2019). The Mediterranean region is also affected by several characteristic wind systems, including the Mistral, Bora, and Etesian winds, which can significantly impact surface circulation and vertical mixing (Tanhua et al., 2013; Allam et al., 2020). Variability in these atmospheric patterns can lead to substantial changes in upper-ocean stratification and temperature distribution, thereby influencing the development and persistence of extreme ocean temperature events. The complex interplay between basin geometry, water mass formation, and atmospheric forcing makes the Mediterranean Sea a dynamically active system despite its semi-enclosed nature.

1.3.3 Biodiversity and Ecosystem Vulnerability:

The Mediterranean Sea is recognized as one of the most biologically diverse marine regions on Earth. Although it represents less than 1% of the global ocean surface, the basin hosts an estimated 7–10% of the world's known marine species, many of which are endemic to the region (Diaz-Almela et al., 2007; Rivetti et al., 2014; Chefaoui et al., 2018). This high biodiversity reflects the Mediterranean's complex geological history, diverse habitats, and strong environmental gradients. A wide range of marine ecosystems are present within the basin, including seagrass meadows dominated by Posidonia oceanica, coralligenous assemblages, rocky reef communities, and pelagic ecosystems (Diaz-Almela et al., 2007; Garrabou et al., 2009; Katsanevakis et al., 2014; Guerrero-Meseguer et al., 2017, 2020; Mannino et al., 2017). These habitats support a rich variety of fish, invertebrates, and primary producers that contribute to the ecological functioning and productivity of Mediterranean marine ecosystems. The basin also sustains economically important fisheries and provides essential ecosystem services to surrounding coastal populations.

However, Mediterranean ecosystems are increasingly exposed to environmental stressors from both natural and anthropogenic pressures. Coastal development, pollution, overfishing, and the introduction of invasive species have already altered many marine habitats within the basin (Katsanevakis et al., 2014; Mannino et al., 2017). These pressures interact with climate-driven changes such as ocean warming, stratification, and changes in circulation patterns, increasing the vulnerability of Mediterranean ecosystems to extreme environmental events. MHWs are among the most significant emerging threats to Mediterranean marine ecosystems (Mannino et al., 2017). Elevated temperatures during these events can disrupt ecological processes, alter species interactions, and cause widespread mortality among temperature-sensitive organisms (Smale et al., 2019). Therefore, understanding the dynamics of MHWs in the Mediterranean Sea is essential for assessing future ecosystem risks under ongoing climate change.

1.3.4 MHWs in the Mediterranean Sea:

The Mediterranean Sea is widely recognized as a climate-change hotspot, with warming rates exceeding the global ocean average and extreme temperature events intensifying in recent decades (Darmaraki et al., 2019a; Pastor et al., 2020). Recent studies show that Mediterranean MHWs have become more frequent, longer, and more intense across various regions of the basin over the past several decades (Darmaraki et al., 2019a, 2024; Ibrahim et al., 2021; Pastor and Khodayar, 2023). One of the most well-documented MHW events occurred in the summer of 2003, when exceptionally high SSTs affected large areas of the northwestern Mediterranean (Garrabou et al., 2009). This event caused widespread mass mortality among benthic invertebrate communities, including sponges, corals, and gorgonians, highlighting the vulnerability of Mediterranean ecosystems to extreme thermal stress (Garrabou et al., 2009; Rivetti et al., 2014).

Recent studies show that MHWs in the Mediterranean often display strong spatial variability, reflecting the influence of basin-scale circulation and regional atmospheric forcing. Several extreme events, including those in 2015, 2017, 2018, and 2022, have affected large portions of the basin and have been linked to persistent anticyclonic conditions, weak winds, enhanced shortwave radiation, and strong stratification (Darmaraki et al., 2019a, 2019b, 2024; Juza et al., 2022). These events exhibit pronounced spatial heterogeneity, with the western Mediterranean typically experiencing more intense but shorter-lived events, whereas the eastern basin often shows longer-duration anomalies sustained by subsurface heat storage and circulation processes (Darmaraki et al., 2019a, 2024; Pisano et al., 2020; Juza et al., 2022). Recent studies have highlighted the importance of subsurface MHWs in the Mediterranean, showing that thermal anomalies can extend below the mixed layer and persist beyond periods of direct atmospheric forcing and this vertical extension can increases ecosystem exposure and reduces thermal refuges (Juza et al., 2022; Darmaraki et al., 2024; Denaxa et al., 2025; Artana et al., 2026).

The combination of rapid regional warming, complex ocean circulation, and high ecological sensitivity makes the Mediterranean Sea a particularly important region for investigating MHWs and their environmental consequences. Understanding the physical mechanisms driving these events and their ecological impacts is therefore essential for predicting future changes in Mediterranean marine ecosystems.

1.4 The Red Sea:

1.4.1 Basin geometry:

The Red Sea is a narrow, elongated basin located between northeastern Africa and the Arabian Peninsula. It extends approximately 2,000 km from the Gulf of Suez in the north to the Bab-el-Mandeb Strait in the south, covering about 438,000 km² and reaches depths over

2,000 m in its central trough (Sofianos et al., 2002; Carvalho et al., 2019). Unlike the Mediterranean Sea, which connects to the Atlantic Ocean through the Strait of Gibraltar, the Red Sea exchanges water with the Indian Ocean via the relatively narrow Bab-el-Mandeb Strait (Fig. 4). The Red Sea is characterized by high salinity and temperature, making it one of the warmest and most saline marine environments in the global ocean (Sofianos et al., 2002; Chaidez et al., 2017; Carvalho et al., 2019; Krokos et al., 2019). These conditions result primarily from intense evaporation and minimal freshwater input, as the basin receives little precipitation and lacks major river inflows, consequently, surface salinity values often exceed 40 PSU in many areas of the basin (Sofianos et al., 2002).

The basin is typically divided into northern and southern regions, which differ in bathymetry and hydrographic characteristics. The northern Red Sea, including the Gulfs of Suez and Aqaba, is generally deeper and more strongly stratified, while the southern Red Sea is influenced by seasonal exchanges with the Gulf of Aden through the Bab-el-Mandeb Strait (Carvalho et al., 2019; Liu and Yao, 2022). This connection allows relatively fresher water from the Gulf of Aden to enter the southern Red Sea, contributing to a meridional gradient in temperature and salinity across the basin (Sofianos et al., 2002; Krokos et al., 2021).

The combination of restricted exchange, intense evaporation, and strong meridional gradients creates a unique thermohaline structure that distinguishes the Red Sea from most other ocean basins. These characteristics strongly influence the basin's circulation patterns and its response to atmospheric variability.

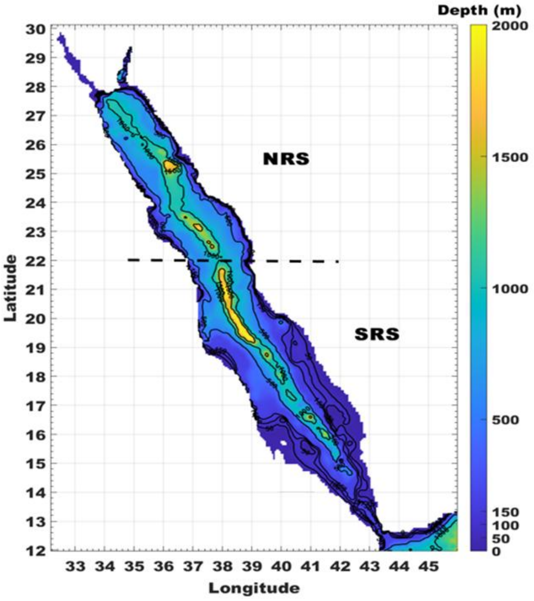

Figure 4. *Bathymetry map of the Red Sea. Bathymetry corresponds to the GEBCO bathymetry dataset (https://www.gebco.net).*

1.4.2 Circulation and Atmospheric Forcing:

Circulation in the Red Sea is largely determined by the interaction between basin geometry and seasonal atmospheric forcing (Sofianos et al., 2002; Rasul and Stewart, 2015; Krokos et al., 2021). Unlike the Mediterranean Sea, where circulation is dominated by an inverse estuarine system driven by evaporation, the Red Sea exhibits strong seasonal variability associated with the Indian Ocean monsoon system (Rasul and Stewart, 2015; Sofianos and Johns, 2015, 2017; Krokos et al., 2019). In winter, prevailing northerly winds drive a surface circulation in which relatively fresher water from the Gulf of Aden enters the southern Red Sea through the Bab-el-Mandeb Strait, while saltier Red Sea water exits at intermediate depths (Sofianos et al., 2002; Rasul and Stewart, 2015; Sofianos and Johns, 2015). In summer, the reversal of wind patterns associated with the southwest monsoon alters the exchange between the Red Sea and the Gulf of Aden, resulting in a more complex three-layer circulation system in the strait (Sofianos et al., 2002; Rasul and Stewart, 2015; Yao and Hoteit, 2018; Carvalho et al., 2019; Hoteit et al., 2021; Liu and Yao, 2022). This seasonal variability plays an important role in regulating the heat and salt budgets of the basin.

Mesoscale circulation features also contribute significantly to Red Sea ocean dynamics. Satellite observations and numerical models reveal numerous eddies and gyres that influence the transport of heat and nutrients throughout the basin (Sofianos et al., 2002; Zhan et al., 2016, 2018, 2019; Hoteit et al., 2021; Krokos et al., 2021). These mesoscale structures can persist for several months and play a key role in redistributing warm water masses and shaping regional oceanographic variability (Zhan et al., 2016, 2018, 2019). Atmospheric forcing strongly influences the thermal structure of the Red Sea (Rasul and Stewart, 2015; Sofianos and Johns, 2015; Carvalho et al., 2019; Krokos et al., 2019). Persistent northerly winds dominate much of the basin for most of the year, promoting strong evaporation and contributing to the formation of highly saline water masses (Sofianos and Johns, 2017; Alawad et al., 2020). Seasonal variations in wind patterns and heat fluxes can significantly affect upper-ocean stratification and temperature variability, thereby influencing the development and persistence of extreme warming events (Krokos et al., 2021).

1.4.3 Biodiversity, Coral Reef Ecosystems, and Environmental Vulnerability:

The Red Sea is characterized by strong stratification, extremely low riverine input, and chronically low nutrient concentrations in surface waters (Sofianos and Johns, 2015; Alawad et al., 2020; Hoteit et al., 2021). As a result, biological productivity in the basin is generally limited by the availability of nutrients in the euphotic layer, and physical processes controlling vertical mixing and circulation play a dominant role in regulating ecosystem variability (Raitsos et al., 2013; Alawad et al., 2020). Atmospheric forcing, particularly the regional wind regime, is one of the primary drivers of upper-ocean dynamics in the Red Sea and strongly influences the distribution of nutrients and phytoplankton biomass (Raitsos et al., 2013; Alawad et al., 2020; Hoteit et al., 2021). Surface winds are largely constrained by the steep topography of the surrounding Arabian and African mountain ranges, producing a predominantly north–south wind system aligned with the basin axis (Langodan et al., 2017b). In the northern Red Sea, winds typically blow from the northwest throughout the year, while the southern basin experiences seasonal reversals associated with the Indian monsoon system (Raitsos et al., 2013; Langodan et al., 2017b, 2017b; Alawad et al., 2020). These seasonal wind patterns modulate upper-ocean circulation, mixed layer depth, and thermocline structure, thereby influencing the vertical transport of nutrients into surface waters (Yao et al., 2014; Sofianos and Johns, 2015).

In addition to basin-scale winds, several localized atmospheric features exert strong control on Red Sea oceanography. Among these, the Tokar Gap wind jet, located along the Sudanese coast near approximately 19°N, represents one of the most intense and dynamically significant regional wind systems (Jiang et al., 2009; Davis et al., 2015). The Tokar jet forms when hot, low-pressure air over the Sudanese desert accelerates through the Tokar Gap toward the Red Sea, generating strong cross-basin winds that are most pronounced during the summer months (Jiang et al., 2009; Davis et al., 2015). The strong wind forcing associated with the Tokar jet induces intense surface stress, which enhances vertical mixing and drives Ekman transport across the basin. As a consequence, a dipolar system of mesoscale eddies frequently develops in the central Red Sea during Tokar wind events, significantly altering the regional circulation and vertical structure of the water column (Sofianos and Johns, 2003; Jiang et al., 2009; Davis et al., 2015).

Enhanced vertical mixing and eddy-induced upwelling associated nutrient-rich subsurface waters into the euphotic zone (Raitsos et al., 2013; Langodan et al., 2017b; Alawad et al., 2020). Such processes are particularly important in the central Red Sea, where Tokar wind events can temporarily weaken stratification and increase mixed layer depth, facilitating the upward transport of nitrate and other nutrients (Raitsos et al., 2013; Sofianos and Johns, 2015; Alawad et al., 2020; Krokos et al., 2021). The resulting increase in nutrient availability can stimulate phytoplankton growth and lead to localized increases in chlorophyll-a concentrations observed by satellite sensors (Racault et al., 2012; Raitsos et al., 2013; Alawad et al., 2020). Indeed, several studies have reported strong links between wind variability, mixed layer dynamics, and phytoplankton phenology across the Red Sea, highlighting the importance of atmospheric forcing in controlling primary productivity in this oligotrophic basin (Raitsos et al., 2013; Kheireddine et al., 2017; Allam et al., 2020).

The Red Sea is globally recognized for its extensive and diverse coral reef ecosystems, which extend along much of the basin's coastline (Al-Horani et al., 2006; Cochran et al., 2024; Cerutti et al., 2025). These reefs support high biodiversity and provide critical habitat for a wide range of marine organisms (Cochran et al., 2024; Gonzalez et al., 2024; Cerutti et al., 2025). Coral reefs in the Red Sea also play important roles in regional fisheries, coastal protection, and tourism. A remarkable feature of Red Sea coral reefs is their apparent tolerance to relatively high water temperatures compared with reefs in many other regions (Genevier et al., 2019). Some coral populations in the northern Red Sea have demonstrated resilience to thermal stress that would typically cause bleaching in other tropical reef systems (Fine et al., 2013; Genevier et al., 2019). This resilience has led to suggestions that parts of the northern Red Sea may serve as potential refugia for coral reefs under future climate warming (Fine et al., 2013). Despite this apparent thermal tolerance, Red Sea ecosystems remain vulnerable to environmental change (Genevier et al., 2019; Gonzalez et al., 2024; Cerutti et al., 2025). Rapid coastal development, pollution, and increasing SSTs pose growing threats to coral reef health (Genevier et al., 2019; Cerutti et al., 2025). Moreover, extreme warming events associated with MHWs can still induce coral bleaching and ecosystem disruption, particularly in regions where environmental conditions exceed the thermal limits of reef organisms (Genevier et al., 2019).

1.4.4 MHWs in the Red Sea:

Recent studies have documented significant warming trends across the Red Sea, with SSTs increasing steadily over recent decades (Chaidez et al., 2017; Krokos et al., 2019). These warming trends have been accompanied by a rising occurrence of MHWs that affect large portions of the basin (Genevier et al., 2019; Mohamed et al., 2021; Darmaraki et al., 2025; Nadimpalli et al., 2025; Theodorou et al., 2025). Observational analyses indicate that such events can persist for extended periods and may expose coral reef ecosystems to prolonged thermal stress (Genevier et al., 2019; Darmaraki et al., 2025). MHWs in the Red Sea often show pronounced spatial variability due to the basin's complex circulation and strong meridional gradients in temperature and salinity. A strong correlation is reported between the mean SST and the frequency of MHW (Mohamed et al., 2021). Because coral reefs are highly sensitive to temperature anomalies, prolonged MHWs can trigger coral bleaching events and disrupt reef ecosystem functioning. Although some Red Sea coral communities exhibit higher thermal tolerance compared with reefs in other tropical regions, the increasing frequency and intensity of MHWs may still pose significant risks to the long-term stability of these ecosystems (Fine et al., 2013; Genevier et al., 2019; Darmaraki et al., 2025).

The unique environmental conditions of the Red Sea therefore provide an important opportunity to investigate how marine ecosystems respond to extreme ocean warming in a highly saline and thermally variable environment. Comparing MHW dynamics between the Red Sea and other semi-enclosed basins, such as the Mediterranean Sea, can offer valuable insights into the physical and ecological processes governing extreme ocean temperature events.

1.5 Research Gaps and Motivation:

Despite the rapid growth of research on MHWs over the past decade, several uncertainties remain regarding their mechanisms, vertical structure, ecological implications, and interactions with other climate extremes in semi-enclosed seas. Numerous studies have documented the increasing frequency, duration, and spatial heterogeneity of MHWs in the Mediterranean Sea, confirming that the basin is experiencing a strong intensification of extreme ocean warming (Darmaraki et al., 2019a, 2024; Genevier et al., 2019; Ibrahim et al., 2021; Mohamed et al., 2021; Juza et al., 2022; Dayan et al., 2023; Pastor and Khodayar, 2023). However, much of the existing work has focused primarily on characterizing the occurrence and trends of surface events rather than providing a comprehensive basin-scale assessment of their underlying mechanisms and variability across different sub-regions.

A first limitation concerns the attribution of physical drivers. Several studies have identified atmospheric forcing, air-sea heat fluxes, stratification, and circulation anomalies as key factors contributing to Mediterranean MHWs. However, many analyses have focused on individual extreme events or short observational periods rather than systematically examining the combined influence and relative importance of atmospheric and oceanic processes across seasons and sub-basins. Consequently, the interplay between large-scale atmospheric forcing, regional circulation, and upper-ocean preconditioning in shaping MHW variability in semi-enclosed seas remains insufficiently quantified.

A second important gap relates to the vertical structure of MHWs. While most studies identify MHWs using SST observations, recent research indicates that warming anomalies often extend below the mixed layer and may persist at depth, producing subsurface MHWs with distinct temporal and spatial characteristics. Although several investigations have begun to document the subsurface expression of Mediterranean MHWs, vertically resolved analyses remain limited compared with surface-based assessments, constraining our understanding of the three-dimensional evolution and persistence of extreme warming events.

A third research gap concerns compound climate extremes involving MHWs. Increasing evidence shows that MHWs frequently co-occur with atmospheric heatwaves, and their simultaneous occurrence can amplify ocean warming through enhanced air–sea heat fluxes and reduced vertical mixing (Aboelkhair et al., 2023; Paredes-Fortuny et al., 2025). However, most studies have focused on the surface intensification of these compound events, while their potential influence on the vertical structure of MHWs and the penetration of heat into deeper ocean layers remains poorly understood.

Recent studies have also begun to examine the relationship between MHWs and Mediterranean tropical-like cyclones (medicanes). Elevated SSTs associated with MHWs may contribute to medicane formation or intensification (Miglietta and Rotunno, 2019; Jangir et al., 2024). Nevertheless, existing work has primarily explored how MHWs influence medicanes, often through individual case studies. In contrast, the potential impacts of medicanes on MHW evolution, such as their role in modifying ocean mixing or redistributing heat anomalies, remain largely unexplored.

1.6 Thesis Objectives:

The overall objective of this thesis is to advance the understanding of MHWs in semi-enclosed seas through a long-term, basin-scale, and vertically resolved analysis of their variability, physical drivers, ecological implications, and compound interactions in the Mediterranean Sea and the Red Sea. By integrating satellite observations, ocean reanalysis datasets, and statistical analyses, this research aims to provide a comprehensive assessment of the mechanisms controlling extreme ocean warming in these two rapidly warming regional seas. To achieve this goal, the thesis addresses the following specific scientific objectives:

I. Characterization of MHW variability

To characterize the long-term spatiotemporal variability of both surface and subsurface MHWs in the Mediterranean Sea and the Red Sea from 1982 to the present. Particular emphasis is placed on regional heterogeneity, vertical penetration, persistence, recurrence, and long-term trends.

II. Investigation of physical drivers

To investigate the physical mechanisms controlling MHW development by quantifying the relative contributions of atmospheric forcing and oceanic processes as well as their seasonal and regional differences within the Mediterranean and Red Seas.

III. Ecological implications

To assess the ecological implications of MHWs by examining their influence on surface primary productivity variability in both basins, providing insights into potential ecosystem responses to extreme ocean warming.

IV. Compound climate extremes

To examine compound climate extremes by quantifying the co-occurrence of MHWs with atmospheric heatwaves in the Mediterranean Sea and investigating the interaction between MHWs and Mediterranean tropical-like cyclones (medicanes). This objective aims to evaluate how compound events may amplify environmental exposure and influence the persistence and recovery of extreme ocean temperature anomalies.

Through these objectives, this thesis seeks to improve understanding of the processes governing MHW variability and compound extremes in semi-enclosed seas, thereby contributing to a more comprehensive assessment of how regional marine environments respond to increasing climate variability and ocean warming.

1.7 Thesis Structure:

This thesis is organized into ten chapters that progressively address the objectives outlined above and provide a comprehensive investigation of MHWs in the Mediterranean Sea and the Red Sea.

- **Chapter one:** introduces the scientific context of the thesis by reviewing the current understanding of MHWs, their physical drivers, ecological implications, and compound interactions, with particular emphasis on semi-enclosed seas and the Mediterranean and Red Sea basins.
- **Chapter two:** focuses on the long-term spatiotemporal variability of surface MHWs in the Mediterranean Sea. Based on a published study in Frontiers in Marine Science, this chapter examines the frequency, duration, intensity, and regional variability of surface MHWs in the basin and investigates their relationship with large-scale climate variability.
- **Chapter three:** investigates the long-term variability of surface MHWs in the Red Sea. Based on a published study in Ocean Science, this chapter characterizes the spatial and temporal evolution of MHWs in the basin, with emphasis on regional contrasts, trends, and links with large-scale climate patterns.
- **Chapter four:** extends the analysis from the surface to the subsurface by examining subsurface MHWs in the Mediterranean Sea and the Red Sea. This chapter addresses the vertical structure, penetration depth, persistence, and regional variability of extreme warming events below the ocean surface.
- **Chapter five:** investigates the physical drivers of MHWs in both basins, with particular attention to the relative roles of atmospheric forcing and oceanic processes, as well as their seasonal and regional differences.
- **Chapter six:** examines the impacts of MHWs on surface primary productivity in the Mediterranean Sea and the Red Sea. This chapter evaluates how extreme thermal events influence biological variability at the ocean surface and explores the implications of MHWs for ecosystem functioning in both basins.

- **Chapter seven:** focuses on compound extremes in the Mediterranean Sea, with emphasis on the co-occurrence of MHWs with atmospheric heatwaves and Mediterranean tropical-like cyclones (medicanes).
- **Chapter eight:** introduce the implementation of MarineHeatwaves.jl which is a high-performance framework for MHW detection in Julia.
- **Chapter nine:** provides a general discussion that synthesizes the main findings of the thesis across both basins and scientific themes. It also presents the implementation of the Julia-based code developed to calculate and analyze MHWs, highlighting its relevance for reproducible and efficient analysis of large oceanographic datasets.
- **Chapter ten:** presents the general conclusions of the thesis, summarizes the main scientific contributions, and outlines perspectives for future research on MHWs in semi-enclosed seas.

Chapter Two: Spatiotemporal Variability of Surface MHWs in the Mediterranean Sea

Foreword

This chapter examines the spatiotemporal variability of MHWs in the Mediterranean Sea during the satellite era. Although the Mediterranean is recognized as a climate-change hotspot, many previous studies have focused on specific events or limited regions of the basin. A basin-wide and long-term assessment is therefore useful for better understanding how MHWs develop across this semi-enclosed sea, which is characterized by strong spatial heterogeneity and distinct oceanographic conditions between the western and eastern Mediterranean.

The main objectives of this chapter are to quantify the variability of MHWs in the Mediterranean Sea since 1982, to examine regional differences between the western and eastern basins, and to explore the large-scale conditions associated with these events. Particular attention is given to MHW frequency, duration, cumulative intensity, persistence, and their long-term evolution. The analysis uses daily SST data from the NOAA Optimum Interpolation SST dataset (OISSTv2) with a spatial resolution of 0.25°. MHWs are identified using the threshold-based framework proposed by Hobday et al. (2016).

By describing when and where MHWs occur and examining their regional variability, this chapter provides a baseline for understanding MHW activity in the Mediterranean Sea. The results also support the subsequent chapters of this thesis, which investigate subsurface MHWs, compound extreme events, and potential ecosystem responses.

This chapter is based on the following publication:

Hamdeno, M., and Alvera-Azcárate, A. (2023). *MHWs characteristics in the Mediterranean Sea: Case study the 2019 heatwave events*. Frontiers in Marine Science, 10, 1093760. https://doi.org/10.3389/fmars.2023.1093760

2.1 Data and Methods:

2.1.1 Datasets:

Daily SST data from January 1982 to December 2020 were obtained from the National Oceanic and Atmospheric Administration Optimum Interpolation SST dataset (NOAA OISST; Reynolds et al., 2007). This dataset is an interpolation of SST remote sensing values from AVHRR imagery onto a regular 0.25° × 0.25° grid with daily temporal resolution. Mediterranean Sea data were extracted from the global dataset.

The European Centre for Medium-Range Weather Forecasts (ECMWF) ERA5 reanalysis was used to obtain atmospheric variables and heat flux components (Hersbach et al., 2020). The atmospheric variables used were winds at 10 m (U10 and V10), air temperature at 2 m, and mean sea level pressure. The total net heat flux at the sea surface was calculated using net shortwave radiation, net longwave radiation, latent heat flux, and sensible heat flux. The dataset has a spatial resolution of 0.25° × 0.25° and an hourly temporal resolution.

Daily mixed layer depth (MLD) and potential temperature at different water depths were obtained from the Copernicus Marine Service (CMEMS) Ocean Data product. The data used are from a physical reanalysis generated by a numerical system consisting of the Nucleus for European Modelling of the Ocean (NEMO) hydrodynamic model and a variational data assimilation procedure (OceanVAR) for vertical temperature profiles. The horizontal grid resolution of the model is 0.04° × 0.04° and it has a daily temporal resolution (Escudier et al., 2020).

Daily average chlorophyll-a concentrations were obtained from the Copernicus Marine Service (CMEMS). The dataset is a newly processed surface chlorophyll product derived from multiple satellite observations and daily climatology from SeaWiFS. The dataset has a spatial resolution of 0.04° × 0.04° and a daily temporal resolution (Garnesson et al., 2022).

Finally, the normalized time series of the East Atlantic Pattern (EAP) and the East Atlantic/West Russian Pattern (EATL/WRUS) were obtained from the NOAA Climate Prediction Center.

2.1.2 Methods of Analysis:

2.1.2.1 SST Variability and Trends:

Empirical orthogonal function (EOF) analysis (Thomson and Emery, 2014) was used to assess the predominant spatiotemporal characteristics of SST variability from 1982 to 2020, using the monthly de-seasonalized and detrended SST dataset to focus on non-seasonal variability. Before decomposing the EOFs, the seasonal cycle and linear trends were removed from the monthly mean SST anomalies at each grid cell, and each point time series was divided by its standard deviation to normalize SST (Fenoglio-Marc et al., 2012; Mohamed et al., 2019). The mean seasonal cycle was estimated by calculating the monthly mean values for each calendar month at each grid point.

The SST anomalies were calculated by removing the historical climatological mean (1982–2020) at each grid point from the SST values at the same location. The strong seasonal signal was removed from the SSTA data in each grid cell to obtain de-seasonalized maps and time series (Skliris et al., 2012). This was done by subtracting the climatological mean of each calendar month from the corresponding months in all years. The least squares method (Wilks, 2019) was used to estimate linear trends in the de-seasonalized monthly SSTA. The Modified Mann–Kendall test (MMK) (Hamed and Ramachandra Rao, 1998; Wang et al., 2020) was used to test the statistical significance of the trends. In this study, the significance level was set at $p \leq 0.05$ to ensure that all reported trends were statistically significant at least at the 95% confidence level.

2.1.2.2 MHW Calculations and Relation with the Other Variables:

In this work, the standard MHW definition of Hobday et al., (2016) was applied to daily SST data from January 1982 to December 2020 to identify MHWs at the surface throughout the study period (1982–2020) and below the surface between June and December 2019. According to Hobday et al., (2016), a MHW is an unusually warm water event that persists for at least five consecutive days and during which SST exceeds the seasonally varying 90th percentile threshold. The climatological mean and the 90th percentile threshold were calculated in each grid cell for each calendar day of the year using daily SST data over a 39-year period (1982–2020). Two consecutive MHW events separated by a gap of two days or less were considered a single event.

Each MHW event was described by the following set of metrics: **Duration** (days), defined as the time between the start and end dates of an event; **Frequency** (events), defined as the number of events occurring each year; **Mean Intensity** (°C), defined as the average SSTA during the duration of the event; **Maximum Intensity** (°C), defined as the highest SSTA during an event; **Cumulative Intensity** (°C·days), defined as the integrated SSTA over the duration of the event; and **Total Days** (days), defined as the sum of MHW days in each year (Hobday et al., 2016, 2018).

The MATLAB toolbox **M_MHW** was used to determine all MHW metrics (Zhao and Marin, 2019). Annual statistics and time series for MHW frequency and duration were calculated from 1982 to 2020 for each region (whole Mediterranean, EMB, and WMB). Linear trends in SSTA and MHW characteristics were estimated using the least squares method (Wilks, 2019), and their statistical significance was determined using the Modified Mann–Kendall test (MMK) at the 95% confidence level, which accounts for autocorrelation when assessing the significance of the trend (Hamed and Ramachandra Rao, 1998; Wang et al., 2020).

The annual temporal variations in these MHW characteristics were correlated with teleconnection patterns such as EAP, EATL/WRUS, and NAO in order to better understand the relationship between MHWs and atmosphere–ocean connections.

ERA5 data, including U10, V10, air temperature, mean sea level pressure, and heat flux components, were used to examine atmospheric conditions during the most intense MHW events that occurred between June and December 2019 in both the WMB and EMB. Daily mean values of atmospheric variables were calculated by averaging the hourly data. Atmospheric variable anomalies and MLD anomalies were constructed in the same manner as for SST based on a daily climatology from 1982 to 2020.

The surface net heat flux, Q_T, in W/m² from June to December 2019 was estimated according to Thomson and Emery, (2014) and as described in Pinardi et al., (2003), Nagy et al., (2017, 2021), as follows:

$$\boldsymbol{Q_T = Q_s + Q_b + Q_c + Q_e}$$

where Q_s is the amount of heat absorbed by the ocean from incident solar radiation (W/m²), Q_b is heat loss from back radiation (W/m²), Q_c is sensible heat loss from convection and conduction (W/m²), and Q_e is latent heat loss from evaporation at the ocean surface (W/m²).

The wind stress components in the eastward and northward directions (τ_{wx}, τ_{wy}) were calculated according to Hellerman and Rosenstein, (1983) and as described by Nagy et al., (2020), in N/m², as:

$$\boldsymbol{\tau = C_D\, \rho_a\, \mid W \mid\, W}$$

where $\rho_a = 1.2$kg/m³ is the density of air, C_D is the drag coefficient computed according to Hellerman and Rosenstein (1983), and W is the wind speed component (m/s), representing the magnitude of the wind vector and calculated as the square root of the sum of the squared wind components. Daily averages of atmospheric parameters were obtained by averaging hourly data.

Finally, the role of SSTA during MHW events in modulating surface productivity (Chl-a) was examined by calculating their correlation and comparing their time series between June and December 2019.

2.2 Results:

2.2.1 Mediterranean SST Variability and Trends (1982-2020):

The first three EOF modes of SSTA explain about 76.57% of the total deseasoned variance in the SST data, as shown in Supplementary Fig.1. The first mode explains 55.42% of the total deseasoned SST variance (Supplementary Fig.1a). The spatial pattern shows positive values throughout the Mediterranean Sea, indicating an in-phase oscillation of the entire basin around the steady-state mean. The highest SSTA variability was observed over the WMB and the Adriatic Sea. The lowest SSTA variability was observed in the EMB, with minimal amplitude in the Aegean Sea and Levantine Basin. This SST variability is due to two reasons: the first reason is the presence of strong and persistent winds such as Tramontane and Mistral in the northwestern Mediterranean Sea and the Etesian winds in the Levantine Basin (Pastor et al., 2018, 2020); the second reason is the input of external water masses, such as the cold water inflow from the Atlantic Ocean through the Strait of Gibraltar into the Alboran Sea and the cold water inflow from the Black Sea through the Strait of Dardanelles into the Aegean Sea (Skliris et al., 2011, 2012; Mohamed et al., 2019). In the corresponding PC1 time series, the highest positive peak of interannual variability was found in the summers of 2003 and 2017, which were the warmest summers during our period of record as shown in Fig. 5. The highest negative peak was observed in the winters of 1984 and 1996, the coldest winter during the study period (Supplementary Fig.1b). These results are in good agreement with Skliris et al., (2012) and Mohamed et al., (2019). The second mode of SSTA explains about 15.56% of the total deseasoned variance in the SST data (Supplementary Fig.1c). The spatial distribution is a dipole with opposite variations between the WMB and EMB sub-basins. Maximum variability was found in the WMB, while maximum variability of opposite sign was observed in the Levantine and Aegean basins in the EMB. The corresponding PC2 time series show an alternation of positive and negative trends during the 1982-2020 period (Supplementary Fig.1d). The highest positive peak of interannual variability was found in the summers of 1985 and 1988, while the highest negative peak was observed in December 1984 and 2020. The third SSTA mode explains about 5.59% of the total deseasoned variance (Supplementary Fig.1e). The spatial distribution of this mode shows an out-of-phase oscillation of the central and western/eastern parts of the Mediterranean Sea. The highest variability was observed in the WMB (i.e., Alboran Sea) and EMB, while the lowest variability was observed in the central Mediterranean in the Ionian and Adriatic Seas (Supplementary Fig.1f). These results are consistent with those of Mohamed et al., (2019) who studied the interannual variability and trends of SST from 1993 to 2017 and found the same pattern of distribution of the first three SST EOFs with different magnitudes.

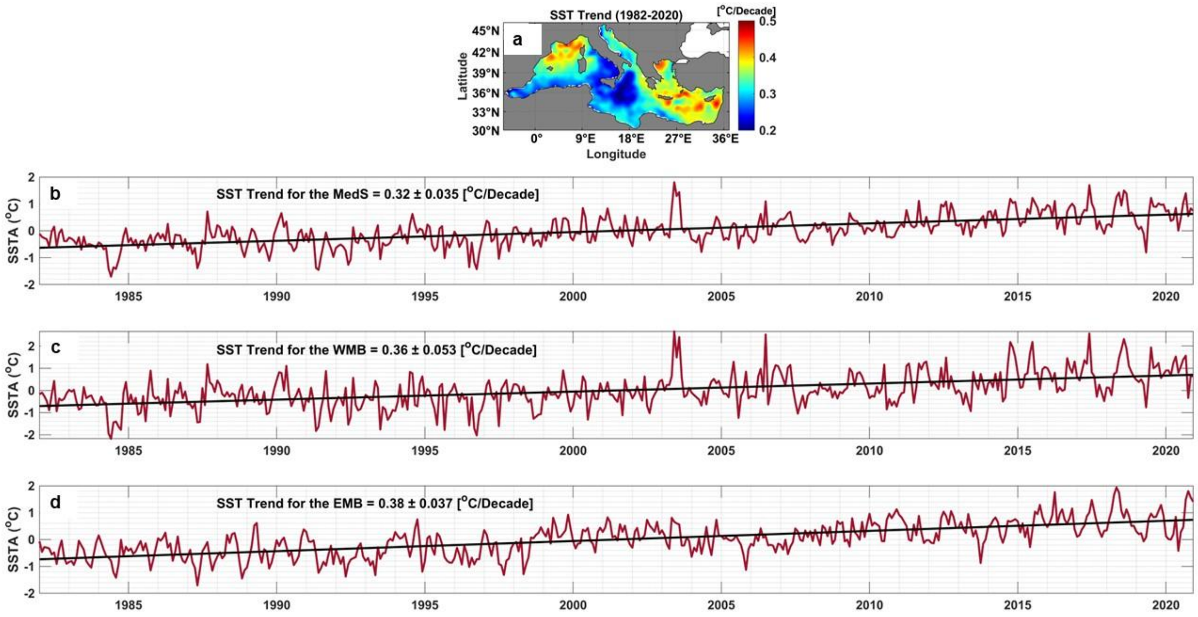

Figure 5. *The spatial and temporal trend of Mediterranean SST from 1982 to 2020. (a) The spatial trend map of deseasonalized SST in °C/decade and the temporal trend of monthly averaged SSTA for the whole Mediterranean Sea (b), WMB (c), and EMB (d). The SSTA trend is shown by the solid black line.*

Figure 5a shows the spatial trend map of deseasonalized SST from 1982 to 2020 in the Mediterranean Sea. A statistically significant ($p < 0.05$) trend was observed throughout the region with a 95% confidence interval. The linear trend in the Mediterranean Sea is not uniform, ranging from 0.2 to 0.5°C/decade. The WMB basin off the Gulf of Lions and the EMB basin in the Levantine Basin showed the strongest SST trends (> 0.45°C/decade). The lowest SST trends were observed in the Alboran and Ionian Seas (< 0.25°C/decade). Figures 5 b-d shows temporal trends in monthly SSTA in the Mediterranean Sea, WMB, and EMB from 1982 to 2020. The temporal SSTA trends in the entire Mediterranean Sea, WMB, and EMB were 0.32 ± 0.035°C/decade, 0.36 ± 0.053°C/decade, and 0.38 ± 0.037°C/decade, respectively. In the WMB, the highest SSTA values were observed in 2003, 2006, 2014, 2015, 2017, and 2018, while in the EMB, the highest SSTA values were recorded in 2016, 2017, 2018, and 2020.

2.2.2 MHWs in the Mediterranean Sea (1982 - 2020):

In this section, we discuss the interannual variability of MHWs in the Mediterranean Sea between 1982 and 2020 and compare their occurrence in the WMB and EMB. We also show all the mean characteristics of MHWs during the study period. Finally, this section also discusses the relationship between MHW frequency and the EAP and EATL/WRUS climate modes.

2.2.2.1 Mediterranean Sea MHWs Interannual Variability (1982-2020):

The temporal variability of the frequency and duration of MHWs and their relationship to annual SST in the Mediterranean Sea, WMB, and EMB during the study period are shown in Figures 6a-d. The annual MHW frequency in the Mediterranean Sea and its sub-basins varied from 0 to 7 events/year (Fig.6a). It can also be observed that the annual MHW frequency doubled during the last ten years of the study period. In the WMB, the highest annual MHW frequency (> 5 events/year) was recorded in 2006, 2011, 2012, and from 2015 to 2020, while in the EMB it was observed only in 2010 and 2016. A difference is observed between the variability of annual MHW duration in the WMB and EMB during the study period (Fig.6c). In the WMB, the annual MHW duration varied between 5 and 35 days/year, while in the EMB it varied between 5 and 47 days/year. The longest MHW duration (> 20 days/year) was recorded in the WMB in 2003, 2014, 2016, 2018, and 2020, while it was observed in the EMB in 2013 and from 2015 to 2020. During the study period (1982-2020), 96 MHW events occurred throughout the Mediterranean Sea, with a total of 1495 MHW days. More than half (54%) of the MHW events with 65.9% of the total MHW days have occurred in the last decade (2011-2020).

Throughout the study period, the correlation between the regional annual mean SST and the annual mean MHW frequency and duration was calculated for Mediterranean Sea, WMB, and EMB and shown in Figures 6b and d, respectively. The strongest relationship was found between SST and MHW frequency, with correlation coefficients of 0.96, 0.92, and 0.94 for Mediterranean Sea, WMB, and EMB, respectively.

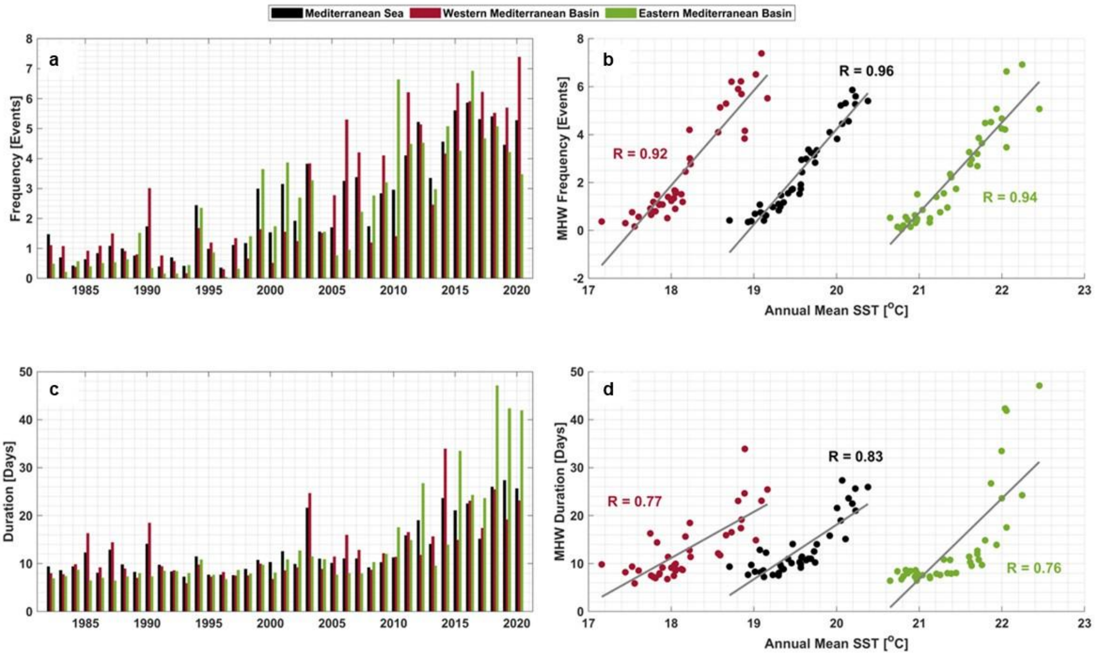

Figure 6. *Interannual variability of MHW metrics, (a) annual mean MHW frequency (events/year), (b) scatterplots of annual mean SST versus annual mean MHW frequency, (c) annual mean MHW duration (days/year), and (d) scatterplots of annual mean SST versus annual mean MHW duration. The colors black, red, and green represent the entire Mediterranean Sea, the WMB, and the EMB, respectively.*

2.2.2.2 Mediterranean Sea MHWs Characteristics (1982-2020):

Figures 7a-f shows the spatial distribution of annual mean MHW characteristics across the Mediterranean Sea from 1982 to 2020. The Mediterranean Sea exhibits high spatial variability in MHW properties. The mean annual MHW frequency varied between 1.5 and 3.5 events, with the highest mean frequency values recorded in the northern part of the WMB, the Adriatic Sea, and the Aegean Sea (Fig.7a). The mean MHW duration ranged from 10 to more than 25 days (Fig.7b), with the longest MHW duration observed in the southeastern part of the EMB (Levantine Basin).

The mean and maximum annual MHW intensities (Imean and Imax) showed the same pattern of spatial distribution with slightly different magnitudes (Fig. 7c,d). The most intense MHWs were observed in the northern part of the WMB and in the northern Adriatic Sea. Moreover, both the mean annual cumulative MHW intensity (Icum) and the total number of days showed the same pattern of spatial variability (Fig. 7e,f). Figure 7e shows that the mean annual MHW Icum varied between 15 and 35 °C. days, with the highest values (> 30 °C. days) found in the northern WMB, Adriatic Sea, and eastern part of the EMB. Mean annual MHW total days ranged from 25 to more than 50 days, with the highest values observed in the eastern Ionian Sea (Fig. 7e,f).

The linear trend of MHW metrics (frequency, duration, intensity, and total days) was calculated for the entire Mediterranean Sea from 1982 to 2020, and their significance was tested with a 95% confidence interval. A significant linear trend ($p < 0.05$) was found for all MHW metrics. The trend for the frequency of MHWs was 1.3 ± 0.246 events/decade and for the duration of MHWs the trend was estimated to be 3.6 ± 1.16 days/decade. For the mean and maximum intensity of MHWs, the trends were 0.06 ± 0.04 °C/decade and 0.12 ± 0.06°C/decade, respectively. Finally, the trend of the cumulative intensity of MHWs was 6.69 ± 2.18 °C. days/decade and it was 27.84 ± 6.33 days/decade for the total days of MHWs.

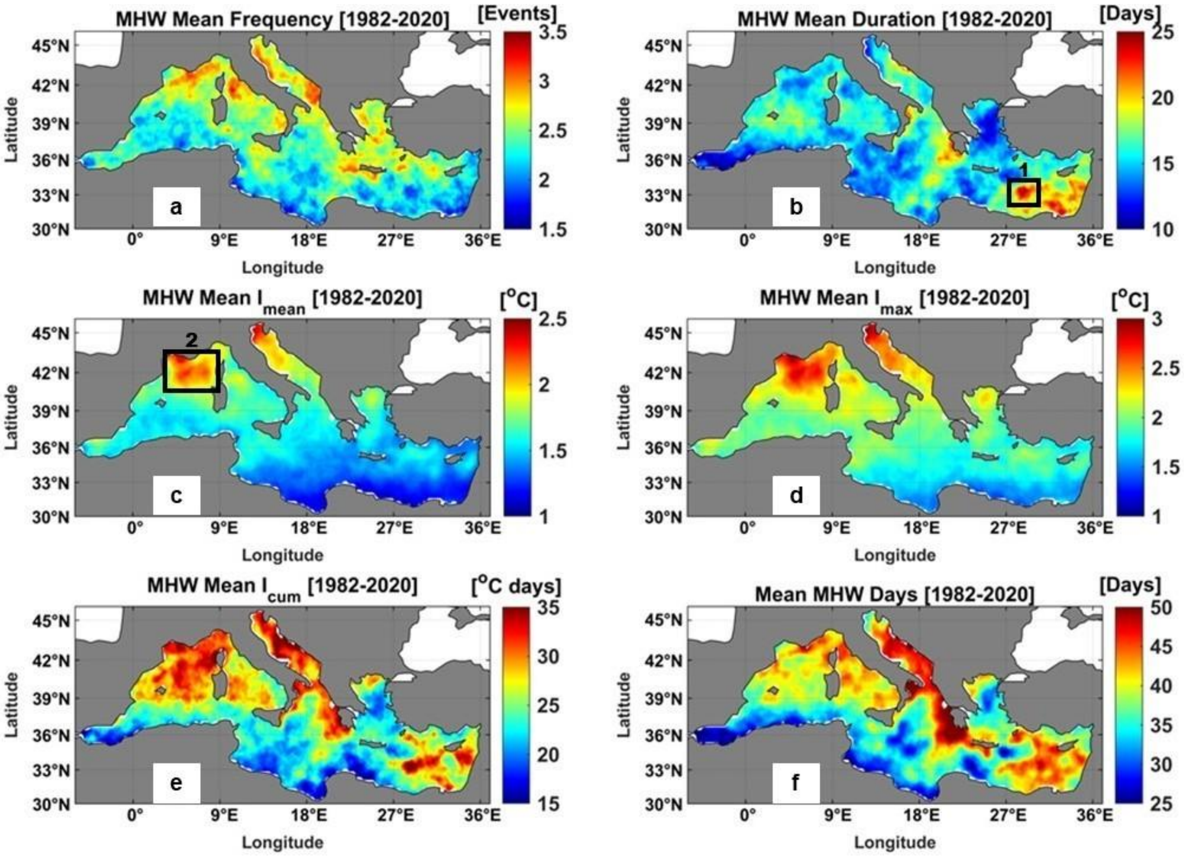

Figure 7. *Main characteristics of MHWs in the Mediterranean Sea during the study period (1982-2020), (a) mean MHW frequency (events), (b) MHW duration (days), (c) mean MHW intensity (°C), (d) maximum MHW intensity (°C), (e) MHW cumulative intensity (°C.days), and (f) MHW total days (days). The black rectangles on panel b and c is showing the selected study regions that represents the EMB and the WMB, respectively.*

2.2.2.3 Relationship Between MHW and Climate Indices:

Below, we examine the possible relationship between the climate indices (EAP and EATL/WRUS) and the annual frequency of MHW for the entire study area. Spatial correlation maps and linear correlations between the two climate indices and MHW frequency throughout the study area were calculated and plotted (Fig. 8a-d). A statistically significant high (> 0.65) positive correlation was observed between the EAP and MHW frequency in the Mediterranean Sea with a linear correlation of 0.74 (Fig. 8a,b). The highest correlation values were found in WMB, EMB, and the Adriatic Sea. The lowest spatial correlation was found in the Ionian Sea and Alboran Sea. The spatial correlation between EATL/WRUS and MHW frequency varied between -0.1 and -0.7 with a linear correlation of -0.44 (Fig. 8c,d). The highest negative (~ -0.6) correlation was observed in the EMB (Levantine Basin and Aegean Sea).

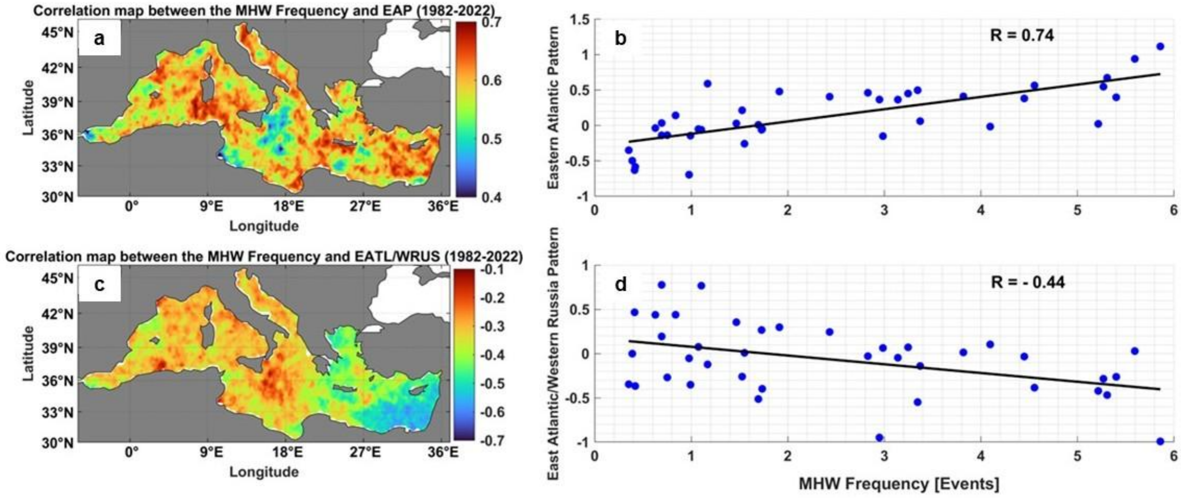

Figure 8. *The relationship between annual MHW frequency and teleconnection patterns over the Mediterranean Sea from 1982 to 2020. The correlation map between MHW frequency and Eastern Atlantic pattern (a) and the scatter plot between them (b). The correlation map between the MHW frequency and the East Atlantic/West Russian pattern (c) and the scatter plot between them (d).*

A comparison of the annual time series of MHW frequency (Fig. 6a) and the annual time series of EAP (Fig. 9a) also showed that both distributions were in very good agreement. Thus, between 1987 and 1994, the frequency of MHWs varied between 0 and 2 events/ year, and this low frequency was related to low SSTA values (negative anomalies or close to zero; see Fig. 5b) and the negative phase of the EAP. During the strong positive phase of the EAP (2012 - 2020), the frequency of MHWs was high, varying between 3 and 8 events/year, and the highest SSTA was observed during the study period in these years (Fig. 5b). The negative correlation between the EATL/WRUS and MHW frequency was also observed when comparing their annual time series between 1982 and 2020 (Fig. 6a, 9b).

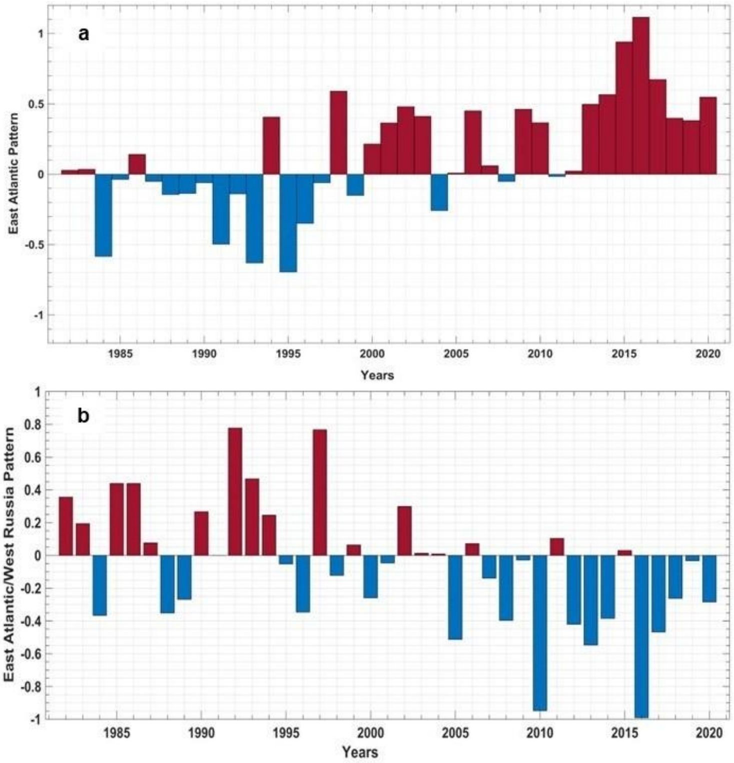

Figure 9. *The annual time series from 1982 to 2020 of (a) the Eastern Atlantic Pattern (EAP), and (b) the East Atlantic/West Russian Pattern (EATL/WRUS). The red and blue bars refer to the positive and negative phases of the climate indices, respectively.*

2.2.3 MHW Events in the Mediterranean Sea (June – December 2019):

To evaluate MHW events that occurred between June and December 2019 at the surface and subsurface in both the WMB and EMB, we selected a region representing each basin. As shown in Figure 7b, Region 1 represents the EMB, and this region suffers from the longest MHWs in the entire Mediterranean basin. Region 2, on the other hand, represents the WMB (Fig. 7c), and this region suffers from the strongest MHWs that occurred in the entire region. The vertical extent of the MHWs was calculated at different depth levels using the same method used to calculate the MHWs at the surface. The temperature threshold was calculated based on the climatological mean of the water temperature at each depth (at the surface and at different levels of the water column); the results are shown in Figures 10-12. The MHW events in each basin were categorized as moderate (when SST exceeds the threshold), strong (when SST exceeds the threshold by a factor of two), severe (when SST exceeds the threshold by a factor of three), or extreme (when SST exceeds the threshold by a factor of four) according to the categorization scheme of Hobday et al., (2018).

Figure 10a shows that six MHW events occurred in the WMB between June and December 2019. The Imean ranged from 1.81°C to 5.27°C, the Imax ranged from 2.25°C to 6.42°C, and the duration of the MHW events ranged from 5 to 20 days. Regarding the severity of the MHW events, three MHW events in the WMB were classified as strong (i.e., the SST exceeded twice the 90th percentile difference) and the remaining events were classified as moderate. The first strong event in the WMB basin lasted 15 days (26/06 to 10/07), and the Imean and Imax values associated with this event were the highest intensity values measured in the WMB basin during the study period. The second strong event in the WMB lasted 6 days (22/07 to 27/07) with an Imean and Imax of 4.14 and 4.8°C, respectively. Finally, the third strong MHW event in the WMB lasted 11 days (24/08 to 3/09) with an Imean and Imax of 4.18°C and 5.38°C, respectively. During the same period, there were only two MHW events in the EMB basin (Fig. 10b). Comparing the EMB MHW events with the WMB events, these two events are characterized by low intensity (~ 2°C) and long duration (21 days for the first event and 159 days for the second), and both were classified as strong events in the EMB (Fig. 10b).

To evaluate at what depth the effect of the defined MHW events reached, subsurface MHW was calculated for both the WMB and EMB at the different depth levels from June to December 2019, as shown in Figures 11-12. In the WMB, only the three strong categorized events extended to 15 m depth in the water column (Fig. 11a-c), and the effect of these events ended at 20 m depth (Fig. 11d). In the EMB, the effect of the MHW extended deeper than in the WMB, reaching to depths of 50 m. As in the WMB, the MHW in the EMB reached the subsurface only in the areas where the SST exceeded twice the threshold (Fig. 12).

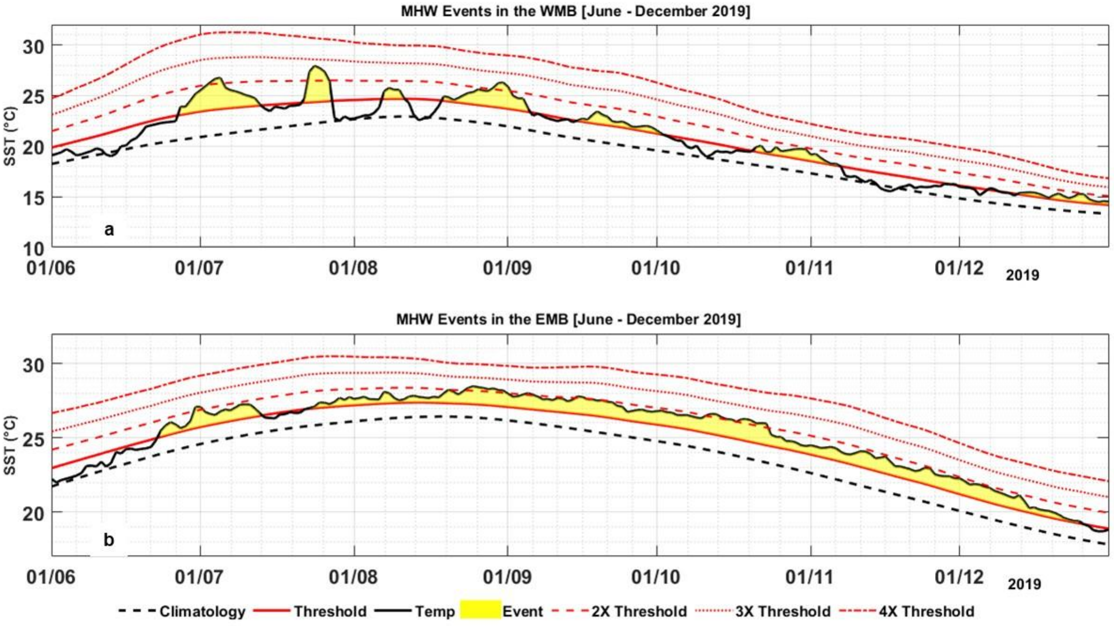

Figure 10. *MHW events between June and December 2019 in (a) WMB and (b) EMB. The yellow shaded area refers to the MHW event. The black solid line represents the SST, the black dotted line represents the climatology, the red solid line represents the threshold, and the red dotted lines define the MHW categories. The MHW categories are moderate (when SST exceeds the threshold), strong (when SST exceeds 2X threshold), severe (when SST exceeds 3X threshold), or extreme (when SST exceeds 4X threshold).*

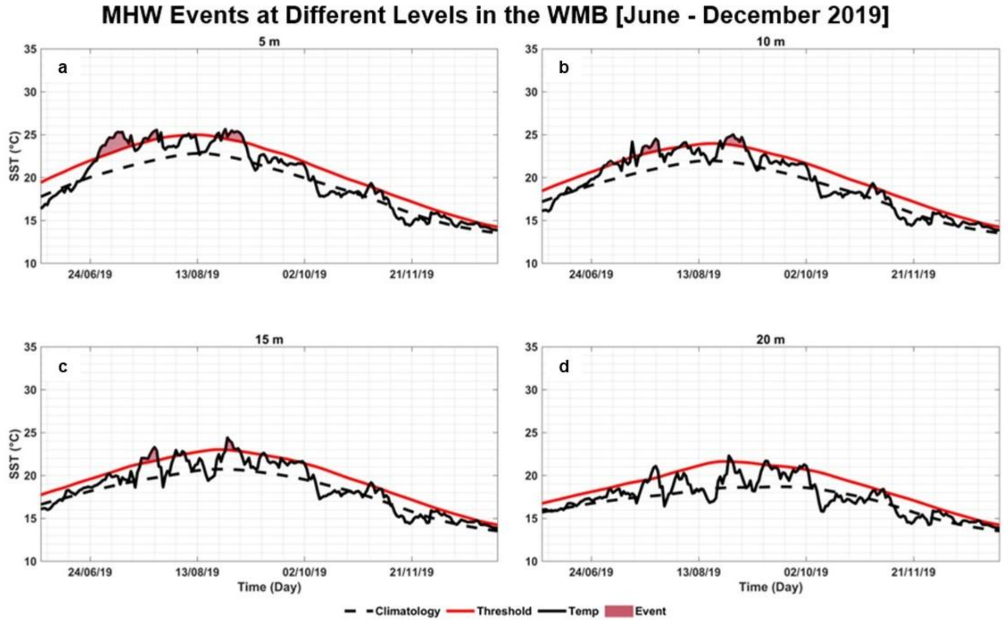

Figure 11. *The penetration of MHW events into the water column in the WMB at different depths (a) 5m, (b) 10m, (c) 15m, and (d) 20m. The red shaded area refers to the MHW event. The black solid line represents the water temperature, the black dotted line represents the climatology, and the red solid line represents the threshold.*

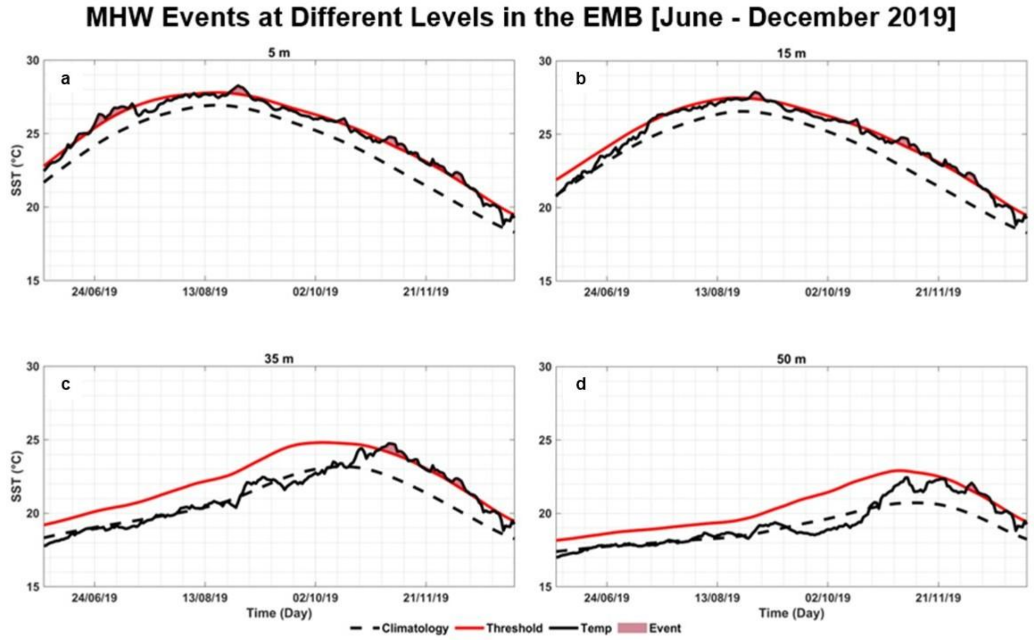

Figure 12. *The penetration of MHW events into the water column in the EMB at different depths (a) 5m, (b) 15m, (c) 35m, and (d) 50m. The red shaded area refers to the MHW event. The black solid line represents the water temperature, the black dotted line represents the climatology, and the red solid line represents the threshold.*

2.2.3.1 Atmospheric Conditions Associated With the 2019 MHWs in the Mediterranean Sea:

In this section, we examine the link between atmospheric conditions (e.g., heat flux, air temperature, mean sea level pressure, and wind stress) and MHW events that occurred in the WMB and EMB between June and December 2019. We focus here on those events that are classified as strong events (i.e., SST exceeded twice the threshold) and had the ability to penetrate deep into the water column. For both WMB and EMB, the atmospheric variable anomalies were compared to the SSTA during the duration of the MHW events (Figures 13, 14, and Supplementary Figures 2-4).

In the WMB, during the first MHW event (26/06/2019 to 10/07/2019), it was observed that the areas of the WMB that suffered from high SSTA (> 4°C) also suffered from high QT anomaly (> 50 W/m2), high positive anomaly (> 30 W/m2) of latent heat flux, high positive anomaly of air temperature (> 3.5°C), negative MSLP anomaly (< -50 hPa), and close to the mean value of wind stress (i.e., Wind stress anomaly ~ 0 N/m2), as shown in Figure 13. During the second strong event that occurred in the WMB between 22-27 July 2019, areas with high SSTA (> 4°C) had positive anomalies in total heat flux (> 20 W/m2), latent heat (> 20 W/m2), air temperature (> 2.5°C), and MSLP (~ 10 hPa), while the wind stress anomaly was below average (see Supplementary Fig. 2). During the last strong MHW event (Aug. 24, 2019, to Sept. 03, 2019) that occurred in the WMB, the high SSTA was combined with the same atmospheric conditions as the second event, but on a larger scale (see Supplementary Fig. 3).

Atmospheric conditions associated with the 2019 MHW events were different in the EMB than in the WMB. During the first event, which occurred between 23/06/2019 and 13/07/2019 in the EMB, the high SSTA was accompanied by a negative anomaly of the total heat flux (> 20 W/m2) and latent heat (> 15 W/m2), as well as a high temperature anomaly (> 1.5°C), a low MSLP system (~50 hPa below average), and slightly above average wind stress (Figure 14). In addition, during the second MHW event, which occurred in the EMB between July 22 and December 27, 2019, the same atmospheric conditions were associated with the high SSTA as during the first event, but with higher values (see Supplementary Fig. 4).

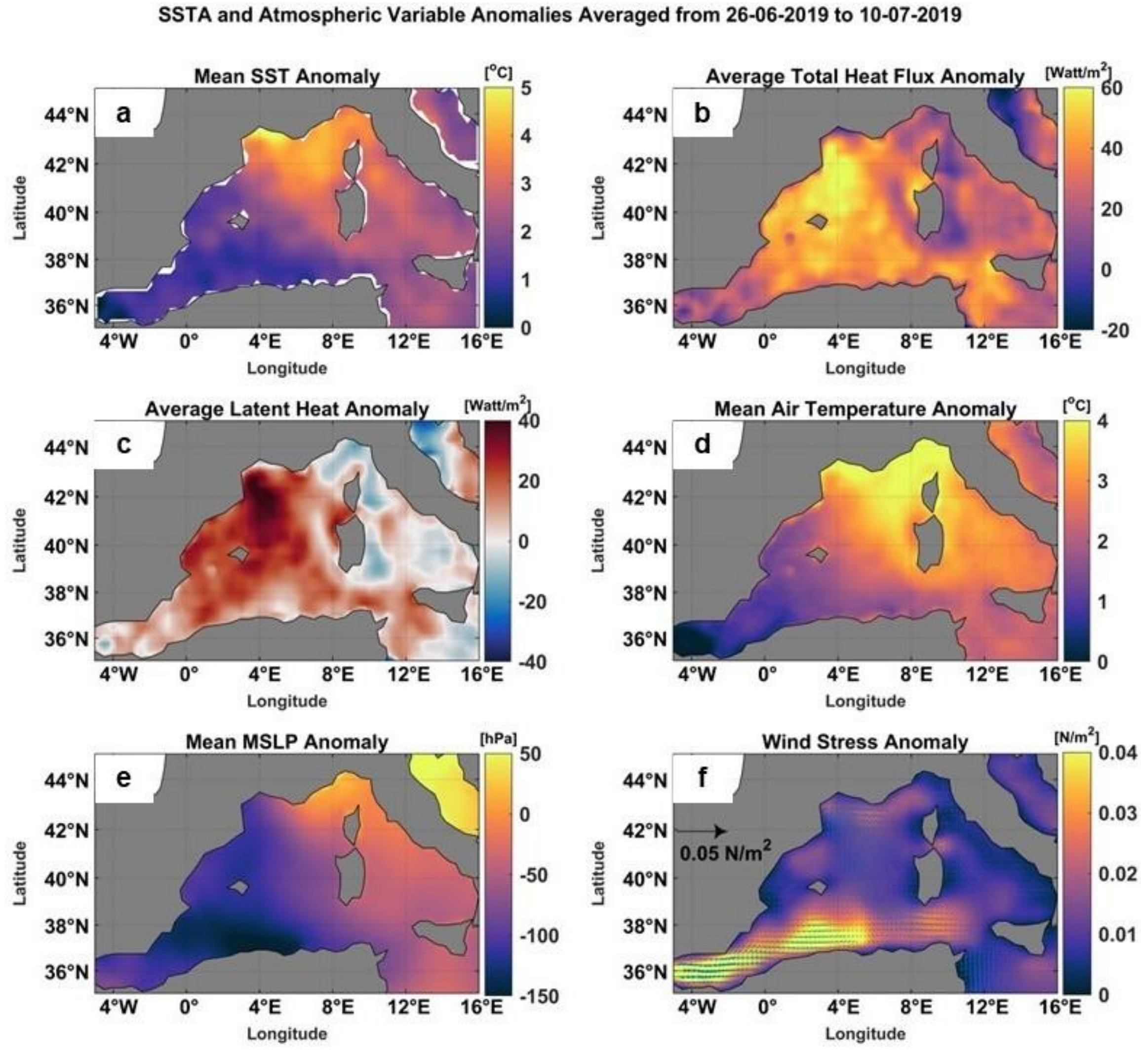
SSTA and Atmospheric Variable Anomalies Averaged from 26-06-2019 to 10-07-2019

__Figure 13.__ The mean (a) SST anomaly [°C], (b) total heat flux anomaly [W/m²], (c) latent heat flux anomaly [W/m²], (d) air temperature anomaly [°C], (e) mean sea level pressure anomaly [hPa], and (f) wind stress anomaly [N/m²] during the MHW event (26 June-10 July 2019) in the WMB. Note that the anomalies were calculated based on 1982-2020 climatology from ERA5 hourly data.

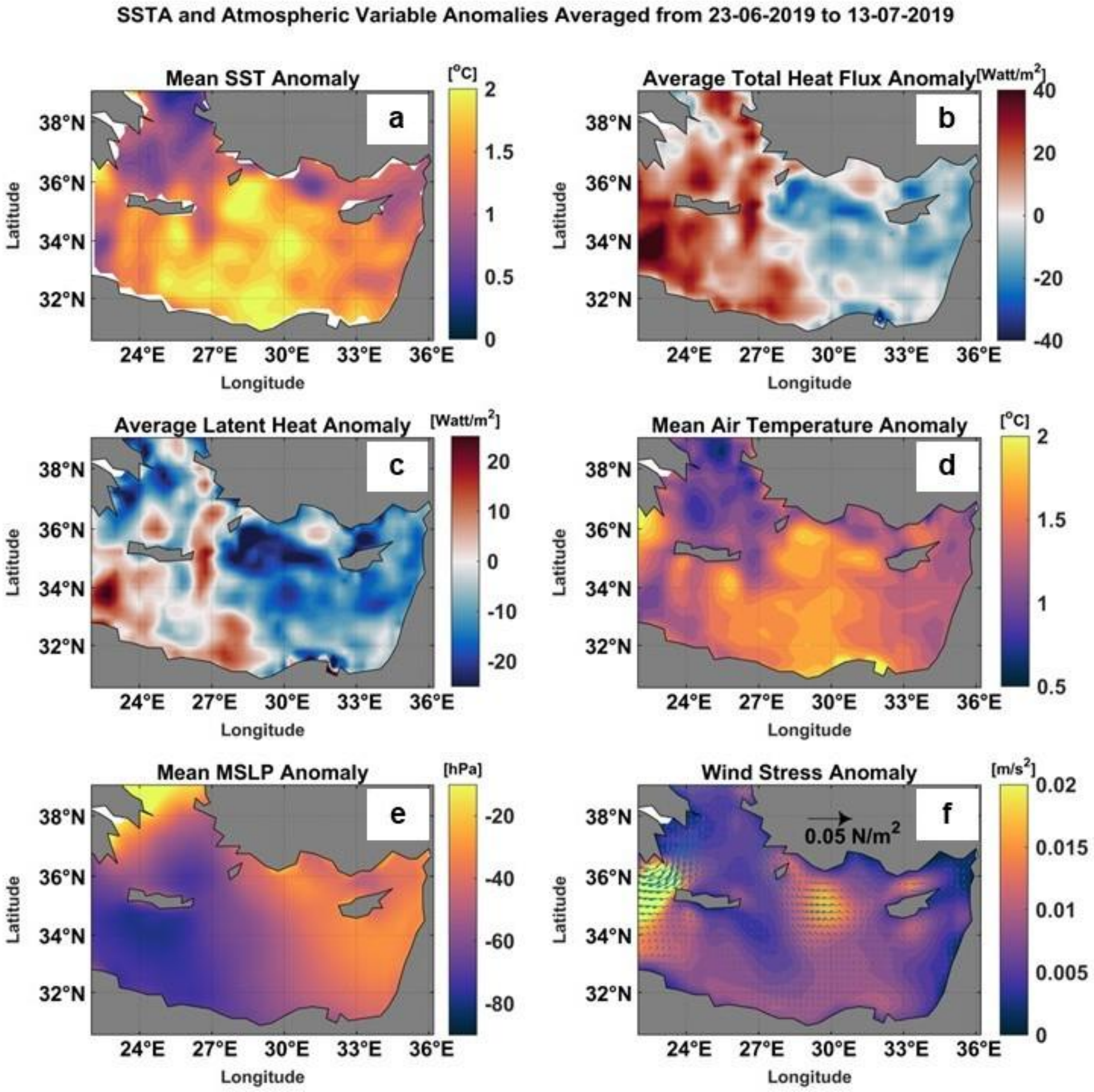

__Figure 14.__ The mean (a) SST anomaly [°C], (b) total heat flux anomaly [W/m²], (c) latent heat flux anomaly [W/m²], (d) air temperature anomaly [°C], (e) mean sea level pressure anomaly [hPa], and (f) wind stress anomaly [N/m²] during the MHW event (23 June-13 July 2019) in the EMB. Note that the anomalies were calculated based on 1982-2020 climatology from ERA5 hourly data.

2.2.3.2 The 2019 Mediterranean MHWs and the Depth of the Mixed Layer:

The temporal variability of the SSTA and MLD anomaly in Mediterranean Sea between June and December 2019 is shown in Figure 15. Here we aim to find out the relationship between MLD variability and the occurrence of MHWs. In both Mediterranean basins, a decrease in mixing layer thickness was observed during MHW events. In the WMB, MLD decreased by 2 to 10 m below average during high SSTA associated with MHW events (Fig. 15a). In the EMB, MLD decreased 2 to 18 m below the mean during MHW events (Fig. 15b). The time lag between MLDa and SSTA variability was calculated from June to December 2019 for the WMB and EMB. In the WMB, a time lag of 2 days was observed between the MLDa and the SSTA, meaning that the MLD shoaled 2 days before the SSTA increased, whereas in the EMB, the time lag between the MLDa and the SSTA was 1 day.

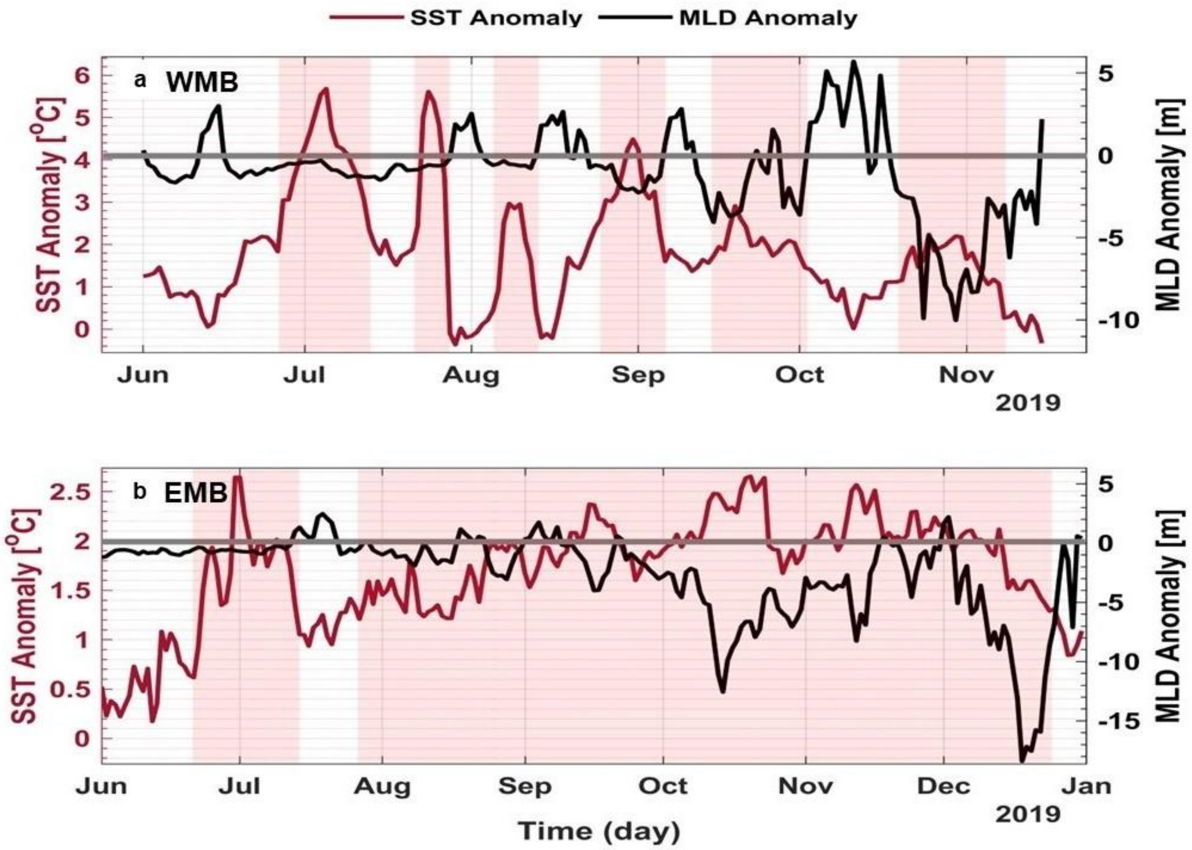

Figure 15. *Time series of SSTA (red line) and mixed layer depth anomaly (black line) for (a) the WMB and (b) the EMB between June and December 2019. The red shaded areas represent the MHW periods.*

2.2.3.3 The Role of 2019 MHWs in Modulating Surface Productivity in Mediterranean Sea:

Figures 16a-c shows the temporal variation of SSTA versus log Chl-a concentration in the WMB (Gulf of Lion) during the three strong MHW events that occurred between June and December 2019. During the first and second events (Fig. 16a-b), an inverse relationship between SSTA and Chl-a concentration is observed, with a decrease in Chl-a concentration occurred during the MHW events. During the third event (Fig. 16c), there is no clear evidence of the influence of the MHW event on the surface Chl-a variability. In the EMB (Levantine basin), the same comparison was made between the SSTA and log Chl-a concentrations (Fig. 17a-b). During the first event, which occurred from late June to mid-July 2019, a decrease in Chl-a concentration was observed during the MHW event, while there was no clear relationship between SSTA and Chl-a concentration during the second event. In addition, the correlation between SSTA and Chl-a was calculated over the same period (June to December 2019) in both Mediterranean basins. A negative correlation (R = - 0.49) was found between the SSTA and the Chl-a in the WMB (Fig. 18a). While the correlation between SSTA and Chl-a in the EMB was low and insignificant (Fig. 18b).

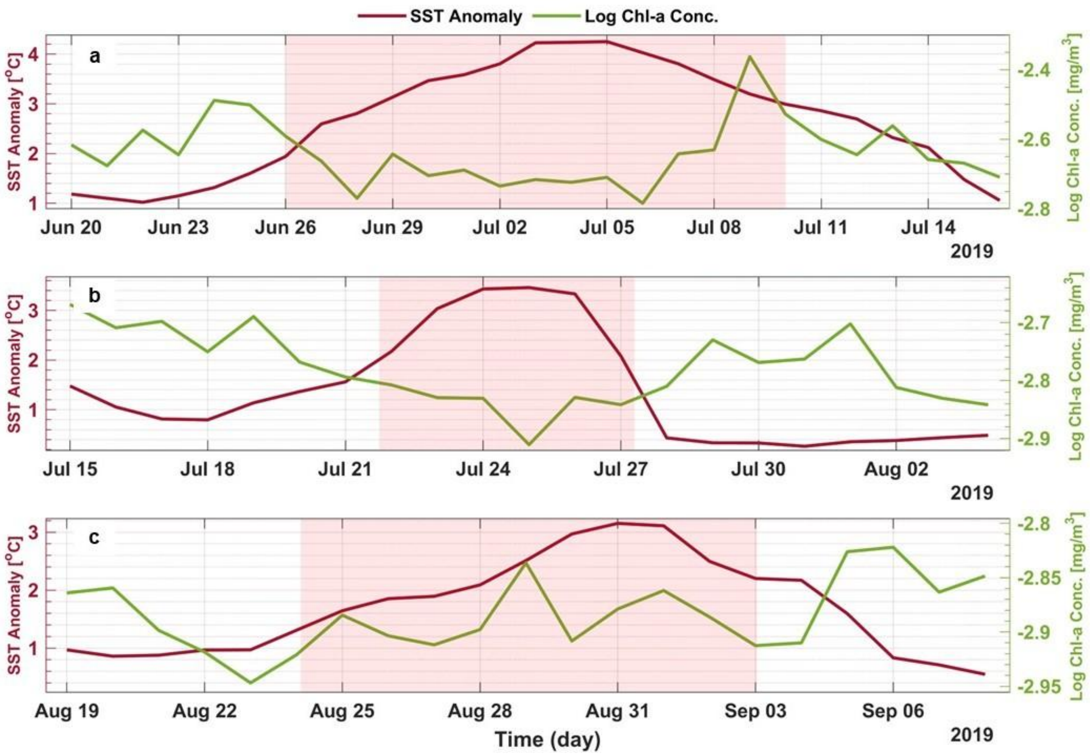

Figure 16. *Time series of SSTA (red line) and log Chl-a concentration (green line) in the WMB during the three strong MHW events between June and September 2019. (a) shows the first event, (b) shows the second event, and (c) shows the third event. The red shaded areas are the duration of the MHW events.*

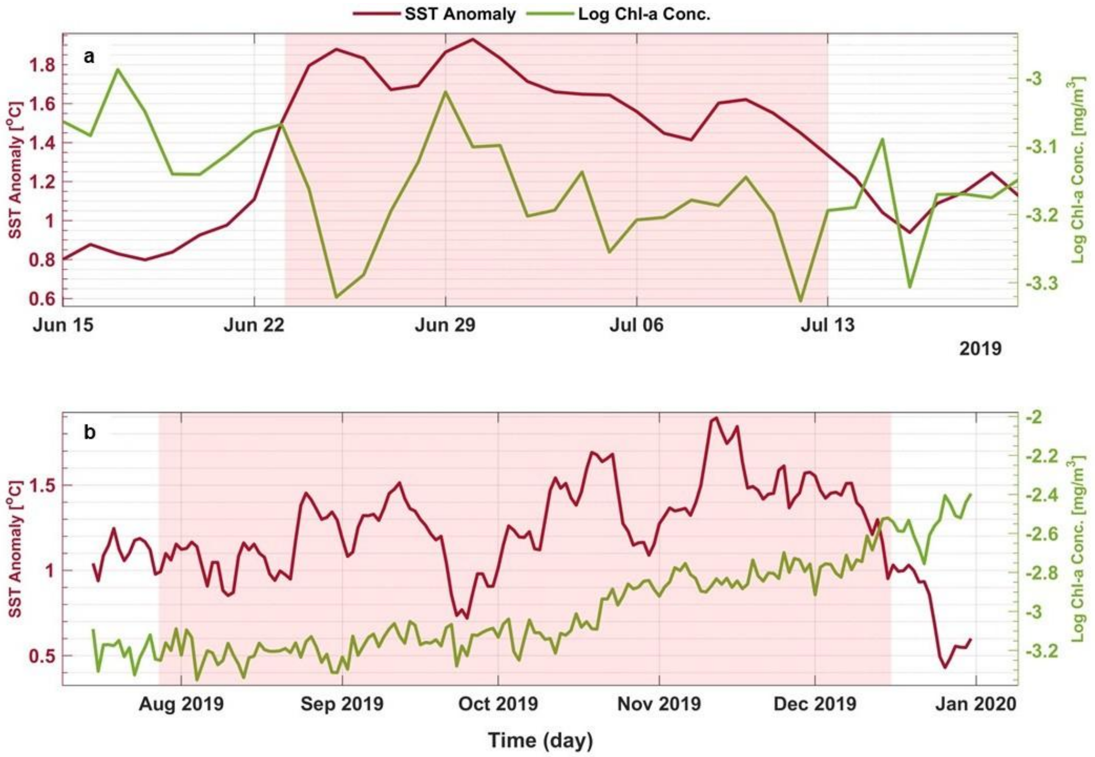

Figure 17. *Time series of SSTA (red line) and log Chl-a concentration (green line) in the EMB during MHW events between June and December 2019. (a) shows the first event and (b) shows the second event. The red shaded areas are the duration of the MHW events.*

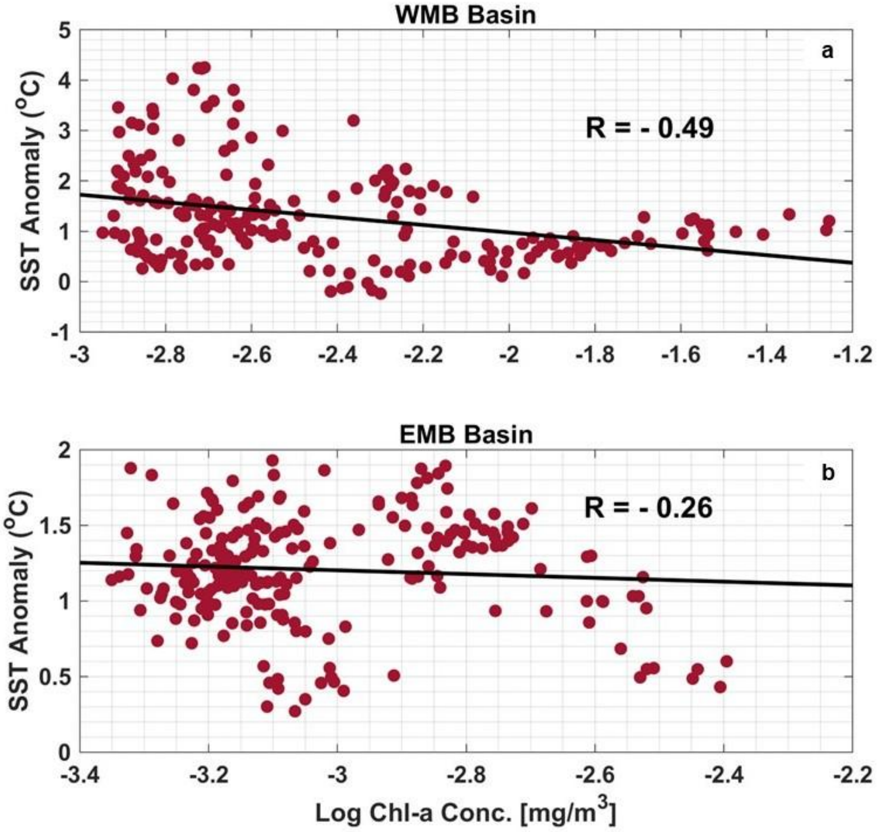

Figure 18. *Scatter plots of daily mean SST versus log Chl-a concentration for (a) WMB and (b) EMB between June and December 2019, with the black line representing the best-fit linear curve.*

2.3 Discussion:

In the last decade, the number of MHW has increased in the Mediterranean Sea, especially off the Gulf of Lion and the Tyrrhenian Sea in the WMB and the Levantine Basin in the EMB. During the study period (1982-2020), 96 MHW events occurred throughout the Mediterranean Sea, with a total of 1495 MHW days. During the last decade (2011-2020), more than half (54%) of the events occurred with 65.9% of the total MHW days. Our results also revealed that MHWs were more frequent and intense in the WMB than in the EMB, while the duration of MHWs was longer in the EMB. The 2019 MHW events occurred in the WMB and EMB along with other extreme events such as atmospheric heatwave and a Medicane (Mediterranean Hurricane). Detailed descriptions of the main results are provided in the following discussion sections.

2.3.1 The Trends of the SST and MHWs (1982-2020):

The spatiotemporal variability of the monthly SSTA was estimated using the EOF analysis. The spatial EOF pattern of the first mode that explained 55.42% of the SSTA variance showed an in-phase oscillation of the whole Mediterranean Sea. This can indicate an in-phase heating or cooling (gain or loss of heat) of the whole Mediterranean water volume. The highest SSTA variability was observed over the western part of the Mediterranean Sea with maximum amplitude off the Gulf of Lion, the Tyrrhenian Sea, and the Adriatic Sea (Supplementary Fig.1). Our SSTA trend analysis for the period from 1982 to 2020 showed high spatial variability of the linear SSTA throughout the Mediterranean Sea (Fig. 5a). The linear trend analysis showed a nonuniform SSTA trend of 0.2 to 0.5°C/decade throughout the Mediterranean Sea. The strongest trend was observed in the WMB basin off the Gulf of Lions and in the EMB basin in the Levantine Basin. The long-term trends of SST are in good agreement with what was observed from Skliris et al., (2012), Pastor et al., (2020), and Ibrahim et al., (2021). From 1985 to 2008, Skliris et al., (2012) found an average warming rate of about 0.37 °C/decade for the Mediterranean Sea and 0.26 °C/decade and 0.42 °C/decade for the WMB and EMB, respectively. Recent studies that have conducted long SST trend analyses, such as Pastor et al., (2020), have estimated a warming of 0.35 °C/decade over the Mediterranean Sea from 1982 to 2019. Ibrahim et al., (2021) calculated that the average rate of warming of the EMB between 1982 and 2020 was 0.33 ± 0.04 °C/decade. The areas that recognized by high SSTA variability and trends were characterized by the highest occurrence of MHWs. In the WMB, MHWs were characterized by their high frequency and intensity, whereas in the EMB, MHWs were characterized by their long duration (Figures 6, 7). Furthermore, for the entire Mediterranean Sea, the increasing trend in SSTA (0.32 ± 0.035 °C/decade) from 1982 to 2020 was combined with a trend of 1.3 ± 0.246 events/decade for the frequency of MHWs and a trend of 3.6 ± 1.16 days/decade for the MHWs duration. The estimated MHW trends are consistent with the results of Juza et al., (2022), who estimated trends in MHW frequency and duration between 2012 and 2020 to be 1.1-1.8 events/decade and 1.23-3.82 days/decade, respectively.

2.3.2 MHWs Frequency and Climate Indices (1982-2020):

To date, no study has compared the relative effects of large-scale climate modes variability on the occurrence of MHWs in the Mediterranean Sea. In the present work, we investigated the relationship between MHW frequency and the two climate indices EAP and EATL/WRUS in the Mediterranean during the study period (1982-2020). Our results showed a strong positive correlation between the EAP and MHW frequency in the Mediterranean region with a linear correlation of 0.74 (Fig. 8a-b), and the spatial correlation maps between the EAP and MHW frequency showed high correlation values over the entire Mediterranean Sea. A comparison of the annual time series of MHW frequency (Fig. 6a) and the annual time series of EAP (Fig. 9a) also showed that both distributions were in very good agreement. Thus, between 1987 and 1994, the frequency of MHWs varied between 0 and 2 events/year, and this low frequency was related to low SSTA values (negative anomalies or close to zero; see Fig. 5b) and the negative phase of the EAP. During the strong positive phase of the EAP (2012 - 2020), the frequency of MHWs was high, varying between 3 and 8 events/year, and the highest SSTA was observed during the study period in these years (Fig. 5b). The above results agree well with those of Skliris et al., (2012), who found that the long-term warming trend in the Mediterranean was strongly correlated with the EAP between 1985 and 2008.

A negative correlation was found between EATL/WRUS and MHW frequency in the Mediterranean Sea with a linear correlation of -0.44 (Fig. 8c-d), and the spatial correlation maps showed the highest negative correlation in the Levantine Basin and the Aegean Sea. This high correlation is due to the fact that the main surface temperature anomalies associated with the positive phase of the EATL/WRUS pattern reflect below-average temperatures over much of western Russia and northeastern Africa, so they mainly affect the EMB. The negative correlation between the EATL/WRUS and MHW frequency was also observed when comparing the annual time series of both values between 1982 and 2020 (Fig. 6a, 9b).

The relationship between MHW frequency and the NAO (The North Atlantic Oscillation) was also studied for the entire Mediterranean region during the study period, but the correlation between them was low and insignificant.

2.3.3 2019 MHWs in the Mediterranean Sea:

As a case study for MHWs in the Mediterranean region, we focused on events that occurred between June and December 2019. After identifying the 2019 MHW events in both the WMB and EMB, we investigated their link with atmospheric forcings and MLD variability, as well as their impact on Chl-a concentrations. The characteristics of the MHW events (Imean, Imax, and duration) that occurred in each Mediterranean basin and their corresponding MHW-onset, MHW-peak, and MHW-end dates and category are shown in Table 1.

Between June and December 2019, six MHW events were detected in the WMB, three of which were classified as strong events, while only two events were detected in the EMB during the same period, both of which were classified as strong events (Fig. 10). The vertical extent of these MHW events was calculated to know how deep they could propagate (Fig. 11-12). The results showed that only the strong events (i.e., when SST exceeded twice the climatological threshold) extended deep into the water column. In the WMB, MHW events extended to a depth of 20 m, whereas in the EMB they extended deeper than 50 m. The extent of MHW in the Mediterranean Sea was also investigated by Juza et al., (2022), who studied subregional MHW in the Mediterranean Sea between 2012 and 2020. Juza et al., (2022) concluded that the potential temperature associated with MHWs reaches a deeper layer in the EMB than in the WMB, which is consistent with our results. However, they found that the 2012-2020 distributions of potential temperature were positive up to 50-150 m in the WMB and up to 400 m in the EMB. This difference between our results and theirs could be due to the fact that they used in situ data for their analysis and averaged them over the 2012-2020 period while looking for the extent of the positive potential temperature anomaly. We, on the other hand, used a physical reanalysis of potential temperature generated by NEMO, and we calculated MHWs at different depths using the definition of Hobday et al., (2016) and focused our analysis on MHW events that occurred between June and December 2019. Moreover, we noticed that the subsurface MHWs that occurred in the autumn months (October to December) penetrates to the deeper water (35m and 50m depth; Fig. 12c-d) than the ones that occurred in the summer months (August and September) especially in the EMB. This could be attributed to the strong vertical mixing that occurs in the autumn and winter, which contributing to the higher propagation of the MHWs in these months while the strong stratification of the water column during the summer is decreasing the propagation of the surface MHWs to the deeper water layers. These results are consistent with Juza et al., (2022).

The link between atmospheric forcing anomalies (i.e., total heat flux, latent heat flux, air temperature, mean sea level pressure, and wind stress) and SSTA during MHW events at both WMB and EMB between June and December 2019 was examined (Fig. 13-14, and Supplementary Fig. 2-4). The relationship between atmospheric variable anomalies and SSTA during MHW events differed from the WMB and EMB, and the association of these MHW events with other extreme events (e.g., atmospheric heatwaves and medicanes) was also different in the two basins. In the WMB, during the events between June and December 2019, we found that the high anomaly of SST was associated with a high anomaly of total heat flux, latent heat flux, and air temperature, while the MSLP anomaly was below the climatological average during the first event and significantly higher during the other two events; moreover, the wind stress anomaly was close to zero during the three events. In the EMB, during the same period, the SSTA of the two MHW events that occurred during this period was associated with a negative anomaly in total heat flux, latent heat, and MSLP, while the air temperature anomaly was positive and wind stress was slightly above average. In both basins, the MHW events were associated with a shallow MLD (shallower than the average; Fig. 15), and cross-correlation showed a 2-day lag between the MLDa and SSTA in the WMD and 1 day in the EMB. A shallower mixing layer is associated with a lower heat capacity, which could further enhance SST warming and contribute to the formation of MHWs. The lag of a day or two between the shallow MLD and the increase in SSTA cannot be alone the cause of an MHW event. However, in MHWs, there is a combination of factors that can interact to cause an MHW, such as high heat fluxes and low wind speeds. These factors, when combined with the shallow MLD, can lead to an increase in temperature in the surface layer of the ocean. And for such extreme events as MHWs, a one- or two-day change in a variable can lead to an anomalous increase in SST, and thus an MHW. In addition, the long-term reduction in mean mixed layer depth also has important implications for the magnitude of SST extremes (Amaya et al., 2020, 2021).

We also investigated the possible interactions between the 2019 MHW events in both basins with other extreme events such as atmospheric heatwaves and medicanes. Our study found that the WMB MHW events that occurred between June and July 2019 coincided with the atmospheric heatwaves that hit Western Europe during the same period (Vautard et al., 2020). This observation is consistent with the results we obtained when studying the atmospheric conditions during the WMB MHW events. Therefore, it is believed that the MHW events that occurred in the WMB during the summer of 2019 were mainly due to the atmospheric heatwaves that struck Europe. The abrupt increase in air temperature during these heatwaves resulted in a strong heat transfer from the atmosphere to the ocean, which in turn led to an anomalous increase in SST and then MHW. On the other hand, a Medicane named Scott occurred in the EMB on October 25 and 26, 2019. According to news reports, Medicane Scott hit the Sinai Peninsula, the Palestinian territories, and parts of Israel and Egypt, bringing rough seas, strong tropical winds, and up to 200 mm of rain to the affected regions. Such storms are unusual this far east in the Mediterranean, and the driving force reported is the exceptionally warm water temperatures at this location (2-4°C warmer than normal for this time of year; https://modis.gsfc.nasa.gov/gallery/individual.php?db_date=2019-10-26). The occurrence of the longest MHW event in the EMB (July 22-December 27, 2019) coincided with the occurrence of Medicane Scott. The peak day of this MHW event was October 23, 2019, with an intensity of 2.69 °C (Table 1), and this event caused anomalously high heat loss from the ocean to the atmosphere and high latent heat flux (Supplementary Fig.3). According to our results on the EMB MHW event and the reports on Medicane Scott, the MHW event that occurred between July and December 2019 in the EMB might be contributed to the formation of Medicane Scott.

Finally, the role of MHWs in modulating the Chl-a concentrations in both basins was studied (Fig. 16-18). The SSTA associated with MHW events is inversely proportional to Chl-a concentration in both the WMB and EMB basins only during the events with the highest MHW intensity (Fig.16-17). This suggests that the MHWs must be intense and long enough to cause a significant response in chlorophyll concentration. For example, the first two MHW events in the WMB resulted in a decrease in Chl-a concentration at the surface, while the last event did not have a clear significant effect on Chl-a, which could be because the intensity of this event was lower than the other two events. In addition, the first MHW event in the EMB had an impact on Chl-a, while the second event had no impact on Chl-a, which could be due to the very long duration (158 days) of this event and that it also occurred from late July to late December, so the impact of the MHW event on Chl-a could be mitigated by the SST drop in November and December, the beginning of the winter season in our study region.

Table 1. *MHW events characteristics in the WMB and EMB between June and December 2019.*

Basin	Event no.	Onset Day	Peak Day	End Day	Duration (days)	Max. Intensity (°C)	Mean Intensity (°C)	MHW Category
WMB	1	26-06-2019	03-07-2019	10-07-2019	15	6.42	5.27	II Strong
	2	22-07-2019	25-07-2019	27-07-2019	6	4.80	4.14	II Strong
	3	08-08-2019	10-08-2019	12-08-2019	5	3.29	2.85	I Moderate
	4	24-08-2019	31-08-2019	03-09-2019	11	5.38	4.18	II Strong
	5	15-09-2019	19-09-2019	02-10-2019	18	3.26	2.64	I Moderate
	6	19-10-2019	31-10-2019	07-11-2019	20	2.25	1.81	I Moderate
EMB	1	23-06-2019	30-06-2019	13-07-2019	21	2.68	1.96	II Strong
	2	22-07-2019	23-10-2019	27-12-2019	159	2.69	1.91	II Strong

2.4 Conclusions and Suggestions for Future Studies:

Our main objective was to identify the main spatiotemporal characteristics of MHWs in the Mediterranean Sea using a 39-year (1982–2020) analysis of high-resolution satellite-based SST data. Moreover, in this study we focused on the 2019 MHW events that occurred in the Mediterranean sub-basins (WMB and EMB), their vertical extent, interactions with atmospheric forcings and their impact on surface Chl-a concentrations.

Our main findings in this study are summarized as follows:

- The pattern of SSTA trend between 1982 and 2020 showed high spatial variability over the Mediterranean Sea with trend values between 0.2 and 0.5°C/decade and high values recorded in the WMB basin off the Gulf of Lions and in the EMB basin in the Levantine Basin, which are the same areas distinguished by frequent, intense, and prolonged MHWs during the study period.
- The spatial maps of MHW characteristics between 1982 and 2020 showed a high spatial variability of MHWs over the Mediterranean basins. Thus, the most

frequent and intense MHWs were observed in the WMB and the longest MHWs were found in the EMB. The trend in the frequency and duration of MHWs between 1982 and 2020 was estimated to be 1.3 ± 0.246 events/decade and 3.6 ± 1.16 days/decade, respectively.

- More than half (54%) of the MHW events that occurred across the Mediterranean, with 66% of the total MHW days, occurred in the last decade (2011-2020).
- MHW frequency correlated with climate modes during the study period. A strong positive correlation ($R = 0.74$) was found between the EAP and MHW frequency throughout the Mediterranean, while MHW frequency was negatively correlated with the EATL/WRUS, with a correlation of -0.44.
- Between June and December 2019, six MHWs were detected in the WMB, three of which were classified as strong events, while two events occurred in the EMB, both of which fell into the strong MHWs category.
- The results showed that only the strong events (i.e., when SST exceeded twice the climatological threshold) extended deep into the water column. In the WMB, MHW events extended to a depth of 20 m, whereas in the EMB they extended deeper than 50 m.
- The propagation of the MHWs in the autumn and early winter months (October, November, and December) were higher than their propagation in the summer months (August and September) especially in the EMB.
- The WMB MHW events were associated with a large flux of heat from the atmosphere to the ocean and a decrease in MLD. Moreover, the first two events in the western Mediterranean were synchronized with the occurrence of a strong atmospheric heatwaves that hit Western Europe between June and July 2019. Therefore, we believe that these atmospheric heatwaves and the large heat flux absorbed by the ocean surface, along with the shallow MLD, were the driving forces behind the WMB MHW events between June and December 2019.
- The events of EMB MHW were associated with heat loss from the ocean to the atmosphere. Therefore, we assume that the air-sea flux did not cause the increase in SSTA, but that the high SSTA during the MHWs caused the anomalous upward net heat flux, consistent with the reports of Miyama et al. (2021). Moreover, this anomalously high heat flux absorbed by the atmosphere might be contributed to the formation of Medicane Scott, which occurred between October 25 and 26, 2019.
- Finally, a negative relationship was found between SSTA and surface Chl-a concentrations, and this negative influence of MHWs on Chl-a was more evident in the WMB than in the EMB.

To the best of our knowledge, this study attempted to determine the link between MHW and atmospheric forcings and their interactions with other extreme events during the study period. This could be considered as a first step to better understand that the severity of MHWs is not only directly caused by their occurrence, but also by their interactions with other atmospheric conditions that may lead to other catastrophic extreme events. Therefore, for future work, we propose to investigate the combination between MHWs and other extreme events in the region such as storms, atmospheric heatwaves, low chlorophyll-a events, and extreme nutrient and oxygen depletion events which is also suggested by (Leonard et al., 2014; Le Grix et al., 2021; Hamdeno et al., 2022). Due to the rapid increase in the frequency, days, and intensity of MHW, it is also necessary to quantify their potential impacts on the overall ecological components, structures, functioning, and overall health of the Mediterranean Sea. Therefore, for better regional ocean management, further studies should focus on ecosystem services and assess the socioeconomic impacts of MHWs.

Chapter Three: Spatiotemporal Variability of Surface MHWs in the Red Sea

Foreword

This chapter presents a basin-scale analysis of MHWs in the Red Sea over the period 1982-2021, focusing on their long-term variability and their links with large-scale climate modes. The Red Sea is a semi-enclosed marginal basin characterized by strong evaporation, restricted exchange with the open ocean, and slow water renewal. These characteristics make the basin particularly sensitive to thermal variability and extreme warming events. Despite this sensitivity, the variability and climatic drivers of Red Sea MHWs remain less well documented than in many other ocean regions.

The objectives of this chapter are to quantify the spatiotemporal variability of MHW frequency, duration, and intensity across the Red Sea, to examine differences between the northern and southern sub-basins, and to evaluate relationships between MHW variability and large-scale climate indices. The analysis focuses on the Atlantic Multidecadal Oscillation (AMO), Indian Ocean Dipole (IOD), East Atlantic/West Russia (EATL/WRUS) pattern, North Atlantic Oscillation (NAO), and Oceanic Niño Index (ONI).

Using daily SST anomaly data from 1982 to 2021, this study reveals a significant long-term warming trend across the basin, accompanied by pronounced meridional differences in MHW characteristics. The northern Red Sea tends to experience longer and more intense events, whereas the southern basin shows higher event frequency. A detailed case study of the 2010 northern Red Sea MHW further illustrates how combined atmospheric forcing and oceanic conditions can sustain extreme warming.

This work was published in Ocean Science in 2024.

Hamdeno, M., Alvera-Azcárate, A., Krokos, G., & Hoteit, I. (2024). Investigating the long-term variability of the Red Sea MHWs and their relationship to different climate modes: focus on 2010 events in the northern basin. Ocean Science, 20, 1087–1107. https://doi.org/10.5194/os-20-1087-2024

3.1 Data and Methods of Analysis:

3.1.1 Datasets:

To analyze the spatial and temporal variability of SST and MHWs in the RS and examine their interactions with different climate modes, focusing on the 2010 MHW events as a case study, various available data sources are used:

i- RS bathymetry was obtained from GEBCO's current bathymetric dataset. This is a global terrain model for ocean and land that provides elevation data in meters on a grid with an interval of 15 arc-seconds (Schenke, 2013). The bathymetry of the RS was extracted from the global bathymetry map.

ii- Daily high-resolution SST data from January 1, 1982 to December 31, 2021 obtained from the Copernicus Marine Environment Monitoring Service (CMEMS) website. The CMEMS Operational SST and Ice Analysis (OSTIA) reprocessed analysis product is based on an SST satellite and in situ observation (Good et al., 2020). The SST dataset consists of daily, gapless maps of SST and ice concentration (referred to as the L4 product) with a horizontal grid resolution of 0.05° × 0.05°.

iii- Hourly mixed layer depth (MLD) and water column temperature are obtained from a regionally tuned simulation of the MIT general circulation model (MITgcm; Marshall et al., 1997) with a horizontal resolution of 1 km and 50 vertical layers (Krokos et al., 2021). The model domain covers the entire RS, including the two Gulfs (Suez and Aqaba) at the northern end, with an open boundary in the Gulf of Aden. The topography of the model is based on the General Bathymetric Map of the Ocean (Weatherall et al., 2015) updated with available regional data. The model is driven with hourly, high-resolution (~5km) atmospheric downscaled WRF fields (Viswanadhapalli et al., 2017). The results of the MITgcm model for the RS have been extensively validated against different data sets and in different environments and applications, as described in Hoteit et al., (2021) and Krokos et al., (2021).

iv- The normalized monthly oceanic El Niño-Southern Oscillation Index (ONI), East Atlantic/West Russian Pattern (EATL/WRUS), Atlantic Multidecadal Oscillation (AMO), and North Atlantic Oscillation (NAO) time series from 1982 to 2021 were obtained from the National Oceanic and Atmospheric Administration (NOAA) (https://psl.noaa.gov/data/climateindices/list/). The Indian Ocean Dipole (IOD) was downloaded from the Japan Agency for Marine-Earth Science and Technology (JAMSTEC) for the aforementioned period.

v- Hourly atmospheric data is used to examine the variability of atmospheric conditions in relation to the variability of the SSTA over the entire study period, and used to examine the drivers of the 2010 MHW events, are from the European Center for Medium-Range Weather Forecasts (ECMWF) ERA5 (Hersbach et al., 2020). The dataset has a spatial resolution of 0.25°× 0.25°. The atmospheric fields include the wind components at 10 m altitude (U10 and V10), air temperature at 2 m altitude (Tair), dew point temperature at 2 m altitude (d2m), mean sea level pressure (MSLP), shortwave surface net radiation (Q_s), longwave surface net radiation (Q_b), sensible surface heat flux (Q_h), and latent surface heat flux (Q_e). Daily mean values of atmospheric variables were calculated by averaging the hourly data.

3.1.2 Methods of Analysis:

MHWs can be characterized by different methods, each of them has its advantages and disadvantages. These methods include the use of fixed thresholds, relative thresholds, and seasonally varying thresholds (Hobday et al., 2016; Mohamed et al., 2022b). In this work, the approach of Hobday et al. (2016, 2018) was used to define and categorize the RS surface MHWs (between 1982 and 2021) and subsurface MHWs (for the February-March 2010 MHW event in the northern region as a case study). Hobday et al. (2016) defined a MHW as an event of unusually high water temperature lasting five consecutive days or longer. During the MHW, water temperature exceeds the 90th percentile climatological threshold. The climatological mean and threshold are calculated in each grid cell for each calendar day of the year using daily water temperature data (at the surface and subsurface levels of the water column) over a 40-years period (1982-2021). MHWs can be described with a number of metrics, which are their duration (in day), which refers to the period between the start and end dates of a MHW event, frequency (in events) indicates the number of MHW events that have occurred within a given year or period, mean intensity (°C) is the average value of the temperature anomaly during the duration of a MHW event, maximum intensity (°C) is the highest value of the temperature anomaly recorded during a MHW event, cumulative intensity (°C.day) is the integrated temperature anomaly over the entire duration of a MHW event and is a measure of the overall intensity of the event, and total MHW days (MHWDs, in day) refers to the total number of MHW days that have occurred in a given year/period (Hobday et al., 2016, 2018). The MATLAB toolbox M_MHW was used to define the MHW metrics (Zhao and Marin, 2019). To provide a more comprehensive and detailed description of MHWs in the RS, we have divided the RS into two regions: the Northern Red Sea (NRS) and the Southern Red Sea (SRS). The NRS extends from 22°N to 30°N, while the SRS extends from 22°N to 12.5°N. This division was based on the north-south spatial thermal gradient in the RS, which shows different characteristics of SST and MHWs between the two sub-basins.

The winter and summer SST in the RS was calculated and averaged over the study period (1982-2021) at each grid point. The winter season was represented by the months of January, February, and March, while the summer season was represented by the months of July, August, and September. The selection of winter and summer months was based on the seasonal cycle of SST, with the three months of the lowest SSTs representing the winter season and the three months of the highest SSTs representing the summer season. We focused on these two seasons as it was observed that the most intense RS MHWs occurred predominantly during winters and summers. SSTA were calculated by removing the historical climatological mean (1982-2021) at each grid point from the SST values at the same location. The strong seasonal signal was removed from the SSTA data at each grid cell to obtain its deseasonalized map and time series (Skliris et al., 2012). Linear trends in SSTA and MHW metrics are estimated using the least squares method (Wilks, 2019) and their statistical significance is determined using the Modified Mann-Kendall test (MMK) at the 95% confidence level, which takes autocorrelation into account when assessing the significance of the trend (Hamed and Ramachandra Rao, 1998; Wang et al., 2020).

We further investigated the characteristics of MHWs during 'warm' or 'cold' years. Specifically, we define warm years as those that exhibit a pronounced positive SSTA compared to the long-term average, while cold years are characterized by a pronounced negative SSTA. The definition of "cold" and "warm" years is relative to the SSTA variability and does not necessarily imply that the SSTA in those years was unusual or extreme. Once the warm or cold years are identified, we calculate the average SSTA for those years by averaging the SSTA values over the entire years for each grid cell. Similarly, we calculate the MHWDs for the warm or cold years by averaging the MHWDs over those years for each grid cell. This gives us an indication of the overall spatial variability of the SSTA/MHWDs during the warm or cold years in our study period.

To gain a deeper understanding of the relationship between the different climate modes and the occurrence of MHWs over the last four decades in the RS, spatial correlations were examined. The correlation maps were calculated using the Pearson correlation coefficient (r), a widely used method for measuring linear correlations between two variables (Kirch, 2008; Patten and Newhart, 2017). The Pearson correlation coefficient ranges from -1 to 1, where -1 stands for a perfect negative correlation, 1 indicates a perfect positive correlation and 0 for no correlation. In this study, we calculated the correlation maps between the annual time series of each climate mode and the annual MHWs (in particular frequency, duration and total days) and SSTA in the RS. The results showed a similar spatial correlation pattern between the climate modes and the different MHW metrics, with only slight variations in the correlation coefficient values. For the sake of brevity, we present only the correlation results with MHW frequency and SSTA in our results. The MHW frequency was chosen for presentation because it had the higher correlations with climate modes compared to MHW duration and total days. To test the significance of the correlations, a two-tailed t-test was used (Patten and Newhart, 2017). The t-test is a statistical hypothesis test that compares the means of two samples and determines whether they differ significantly from each other. Finally, we also compared the time series between different climate modes and the frequency of MHWs in the RS and its sub-basins.

In this study, we have selected MHW events that occurred in 2010 for detailed analysis, focusing particularly on the most intense and longest winter event occurred in that year. The MHW events were identified using the methodology described by Hobday et al., (2016) and then categorized into four intensity levels based on the multiple of the local difference between the climatological mean and the climatological 90th percentile, which serves as a threshold for identifying MHW. The magnitude of the scale descriptors was defined as follows: moderate (1-2×, category I), strong (2-3×, category II), severe (3-4×, category III) and extreme (>4×, category IV) (Hobday et al. 2018). The intense event (category three MHW) that occurred between February and March 2010 was studied in detail, including its vertical extent and potential atmospheric drivers. The vertical extent of MHW was then defined by the first depth without MHWs. We also investigated the atmospheric conditions associated with these MHW events by using the ERA-5 atmospheric data to better understand the potential triggers for this event. Following the work of Thomson and Emery (2014) and the description of Nagy et al. (2017, 2021), the net surface heat flux (Q_T) in W/m^2 was calculated as expressed in Eq.1:

$$\mathbf{Q_T = Q_s + Q_b + Q_c + Q_e}, \qquad \mathbf{(1)}$$

where Q_s is the heat absorbed by the ocean from incident solar radiation in W/m^2, Q_b is the heat loss from back radiation in W/m^2, Q_c is the sensible heat loss from convection and conduction in W/m^2, and Q_e is the heat loss from evaporation (latent heat) at the ocean surface in W/m^2.

According to Alduchov and Eskridge, (1996) and as described in Bawadekji et al., (2022), the relative humidity (RH) were calculated from ERA5 air temperature (Tair) and dew point temperature (d2m) as expressed in Eq.2:

$$\boldsymbol{RH} = \frac{100 * \exp\left(\frac{17.625 * d2m(°C)}{243.04 + d2m(°C)}\right)}{\exp\left(\frac{17.625 * Tair(°C)}{243.04 + Tair(°C)}\right)}, \qquad \mathbf{(2)}$$

3.2 Results and Discussion:

3.2.1 SST and MHWs Characteristics and Trends in the Red Sea (1982 – 2021):

The spatial maps of average SST over the entire study period (1982-2021), winter months (January, February and March) and summer months (July, August and September) in the RS are shown in Figure 19. The average SST in the RS was between 23 and 28 °C throughout the study period, with a meridional gradient from north to south (Fig. 19a). The highest temperatures observed in the SRS and the lowest in the NRS and the Gulfs of Suez and Aqaba (Fig. 19a). In the winter (JFM), the average SST fluctuated between 18 and 27 °C (Fig. 19b), while in the summer (JAS) it fluctuated between 26 and 32 °C (Fig. 19c).

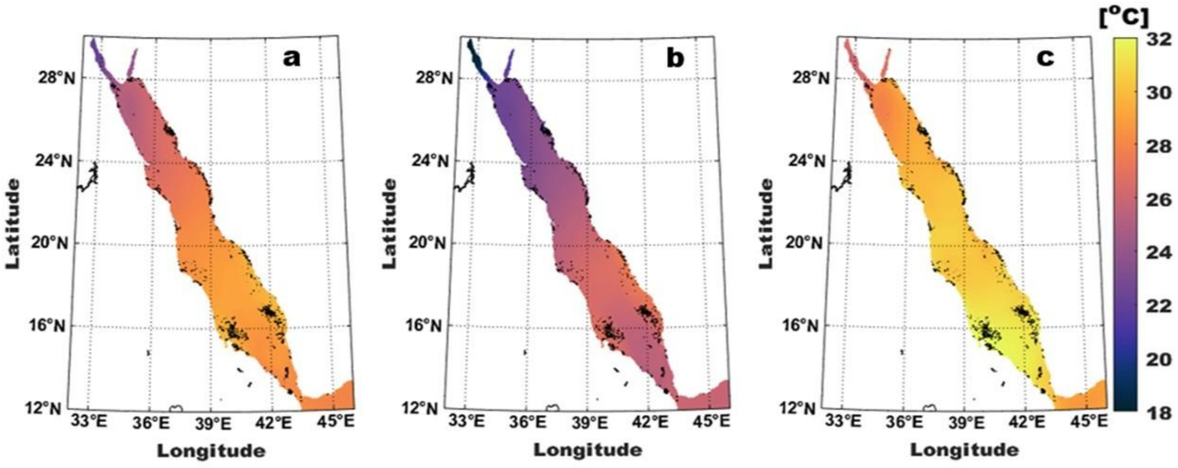

Figure 19. *The spatial distribution of average Red Sea SST (in °C) from 1982–2021 (a) over the entire study period, (b) during winter (January, February, and March), and (c) during summer (July, August, and September).*

The marine environment is influenced by both natural variability and global warming trends. Over time, the difference between a fixed baseline and current temperatures can widen, leading to an increasing number of detected MHWs. This temporal shift can complicate long-term studies of MHW trends and their impacts on marine ecosystems. However, using a fixed baseline simplifies the methodology for detecting MHWs and avoids the complexity that could arise from periodically updating the baseline, which could introduce variability and reduce the clarity of the detection process. A fixed baseline provides a standardized reference period that ensures consistency of MHW detection and analysis across different studies and time periods (e.g. (Genevier et al., 2019; Cheng et al., 2023)). This consistency allows for straightforward comparison between MHW events detected using the same criteria. In addition, a fixed baseline serves as a historical benchmark against which current and future MHW events can be measured. This allows an assessment of how current conditions deviate from a known historical norm. To account for SST variability during the study period and to emphasize the impact of external forcing on marine ecosystems, we calculated MHW characteristics in the RS based on 40-years of climatology (1982-2021).

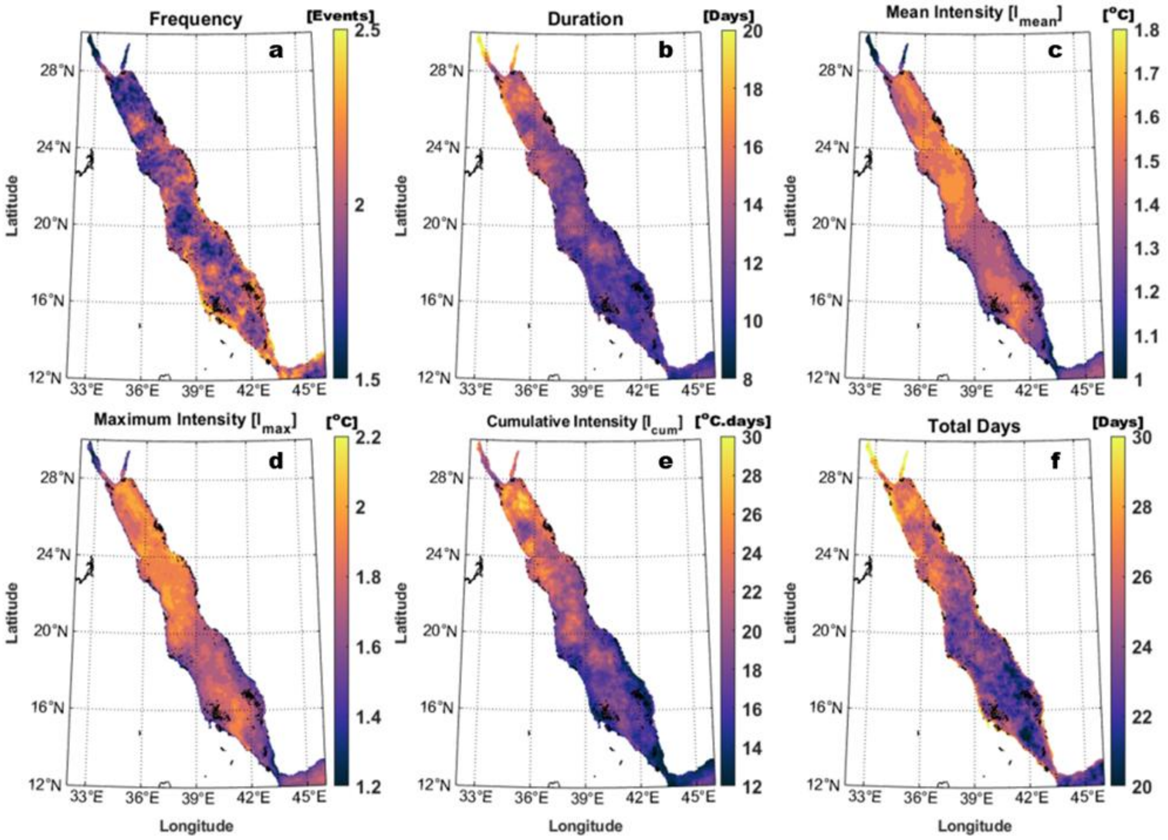

__Figure 20.__ The spatial distribution of average MHW characteristics in the RS between 1982 and 2021. The average MHW frequency (a), duration (b), mean intensity (c), maximum intensity (d), cumulative intensity (e), and total days (f).

The RS exhibits a high spatial variability of MHW characteristics. The mean annual MHW frequency varied between 1.5 and 2.5 events, with the highest mean frequency values recorded in the coastal areas of the SRS and the Strait of Bab El-Mandab (Fig. 20a). The mean duration of the MHW ranged from 8 to more than 20 days (Fig. 20b), with longer MHW durations observed in the NRS and the Gulfs of Suez and Aqaba. The mean and maximum annual MHW intensities (I_{mean} and I_{max}) showed the same pattern of spatial distribution with slightly different magnitudes (Fig. 20c, d). The most intense MHWs were observed in the NRS and in the western part of the SRS around Dahlak Kebir Island. Furthermore, the mean cumulative MHW intensity (I_{cum}) and the total number of heat days exhibited a north-south gradient, with higher values in the NRS region (Fig. 20e, f). Figure 3e shows that the mean MHW cumulative intensity varied between 10 and 35 °C.days, with the highest values (> 30 °C. days) found in the NRS and the lowest in the SRS and the Strait of Bab El-Mandab. The mean total MHW days ranged from 20 to over 30 days, with the highest values found in the Gulfs of Suez and Aqaba, the NRS and the coastal areas of the SRS (Fig. 20f). In general, the MHWs in the RS showed different characteristics between the northern and southern basins. The MHWs of the NRS were longer and more intense than those of the SRS, while the MHWs of the SRS were characterized by their frequent occurrence. The same pattern of MHW distribution was also observed by (Bawadekji et al., 2021 and Mohamed et al., 2021), even though different data sets and baselines were used for MHW detection.

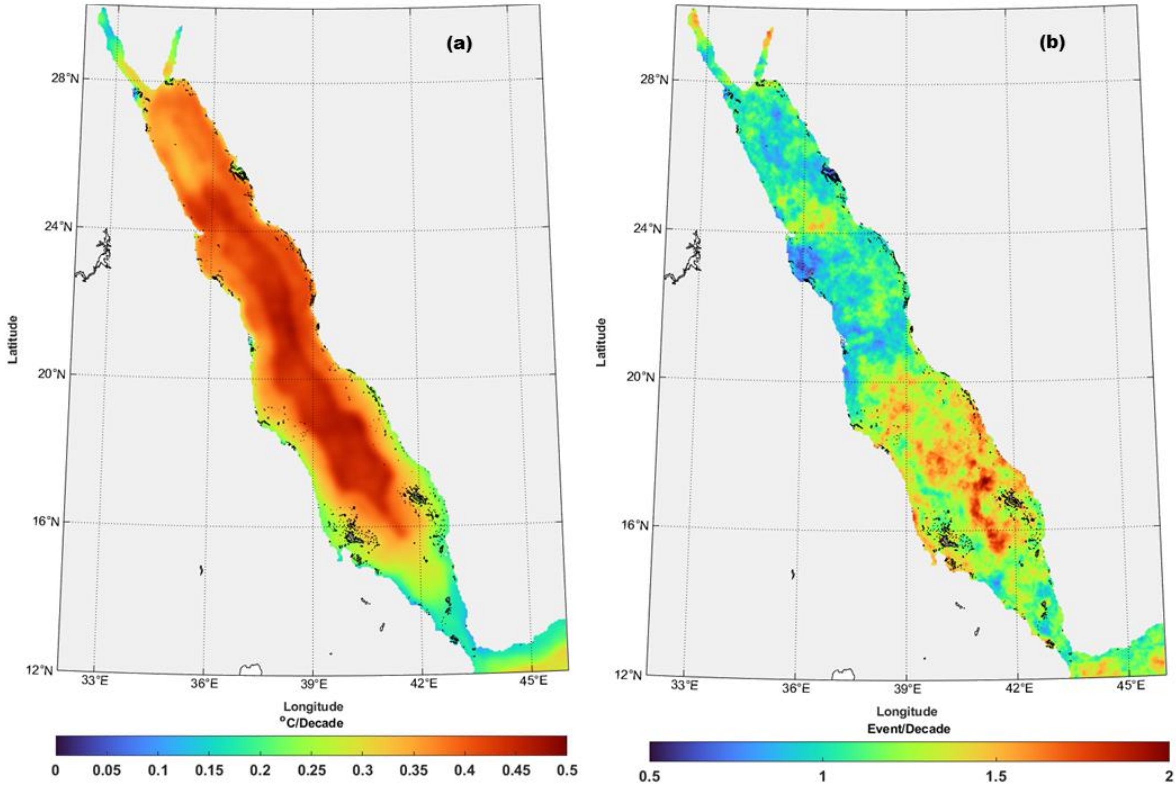

Figure 21. Trends in (a) SST (°C per decade) and (b) MHW frequency (events per decade) in the Red Sea from 1982–2021.

Spatial trend maps of deseasonalized SST and MHW frequency from 1982 to 2021 in RS are shown in Figure 21. A statistically significant ($p < 0.05$) trend with a 95% confidence interval was observed across the region. The trends of SST and MHW frequency in the RS are not uniform and range between 0.1 to 0.5°C/decade for SST and 0.5 to 2 events/decade for MHW frequency as shown in Figure 21. The NRS experienced high SST trends, with a maximum of about 0.4°C/decade between 25°N and 28°N. However, the highest SST trends were observed between 16°N and 25°N, with a gradient that increased towards offshore waters and exceeded 0.45°C/decade. The Strait of Bab El-Mandab and the Gulfs of Suez and Aqaba, on the other hand, showed the lowest SST trends, with trends below 0.15°C/decade. The MHW frequency trends were found to be highest in the SRS and the Gulfs of Suez and Aqaba, with a rate of over 1.5 events/decade, while the lowest trends were observed in the NRS and the Strait of Bab El-Mandab, with a rate of less than 1 event/decade. Furthermore, the trends in MHW duration and total days also displayed high spatial variability in the RS (Supplementary Fig. 5). The spatial trend of the MHW duration fluctuated between 2 to more than 10 days per decade, with an average temporal trend of 2.8 ± 1.25 days/decade (Supplementary Fig. 5a-b). The highest MHW duration trends were observed in the central RS, some parts of the NRS, and the northern part of the Suez and Aqaba Gulfs. The spatial trend of the MHW total days ranged between 15 to more than 30 days per decade, with an average temporal trend of 20.04 ± 6.88 days/decade (Supplementary Fig. 5c-d). The highest trends were observed in the SRS, some parts of the NRS, and the northern part of the Suez and Aqaba Gulfs. Notably, for all the MHW metrics (frequency, duration, and total days), there is an accelerated positive trend that is more pronounced in the last decade.

3.2.2 SST and MHWs Interannual Variability:

The temporal SSTA trends over the study period were 0.33 ± 0.02 °C/decade, 0.34 ± 0.04 °C/decade and 0.32 ± 0.03 °C/decade for the entire RS, NRS and SRS, respectively (Fig. 22). The observed SST trends from our study are in good agreement with (Raitsos et al., 2011; Barros et al., 2014; Chaidez et al., 2017; Liu and Yao, 2022). The analysis of the SSTA between 1982 and 2021 revealed three distinct phases of variability in the RS and its sub-basins (Fig. 22). The first phase, from 1982 to 1992, was characterized by negative SSTA on average. The second phase, between 1993 and 2015, showed a slow warming trend, but the SSTA fluctuated around zero, suggesting a relatively stable period with increased inter-annual variability. The third phase, from 2016 to 2021, was marked by a rapid increase in SSTA, with the anomaly consistently remaining positive. Moreover, the monthly SSTA data for the RS and its sub-basins show a clear warming trend that began in 1994, with an initial SSTA of approximately 0.5°C. The SSTA remained relatively stable for a few years, but then increased rapidly after 2016, reaching an SSTA of 1.5°C or higher (Supplementary Fig. 6a-c). This finding is consistent with the results of Raitsos et al. (2011) who studied RS temperatures from 1985 to 2007 and found an evidence of a pronounced warming trend that began in the mid-1990s.

It was also observed that during years when the RS experienced cold SSTs, the NRS was warmer than the SRS, especially during the winter and autumn months (Supplementary Fig. 6d). Conversely, during years when the RS experienced warm SSTs, the SRS was warmer than the NRS (Supplementary Fig. 6d). The year 2010 was one of the warmest years in the RS, but it was particularly warm in the NRS, with an SSTA difference between the NRS and SRS of over 1°C (Supplementary Fig. 6d). Further analysis revealed a decadal variability in the SSTA trends between the RS northern and southern basins (Supplementary Fig. 7-8). Between 1982 and 1991, the highest trends were observed in the NRS, with an average trend of 0.56°C/Decade, while the average trend in the SRS was 0.26°C/Decade. From 1992 to 2001, the spatial pattern of the SSTA trend was altered, with the highest trends observed in the SRS, with an average trend of 0.57°C/Decade, and lower trends in the NRS, with an average trend of 0.30°C/Decade. From 2002 to 2011, the highest trends were again observed in the NRS, with an average trend of 0.45°C/Decade, while the SRS experienced no trend in the SSTA during this period. Finally, over the last decade of the study period (2012-2021), the SRS had higher trends in the SSTA than the NRS, with an average trend of 1.35°C/Decade for the SRS and 0.89°C/Decade for the NRS.

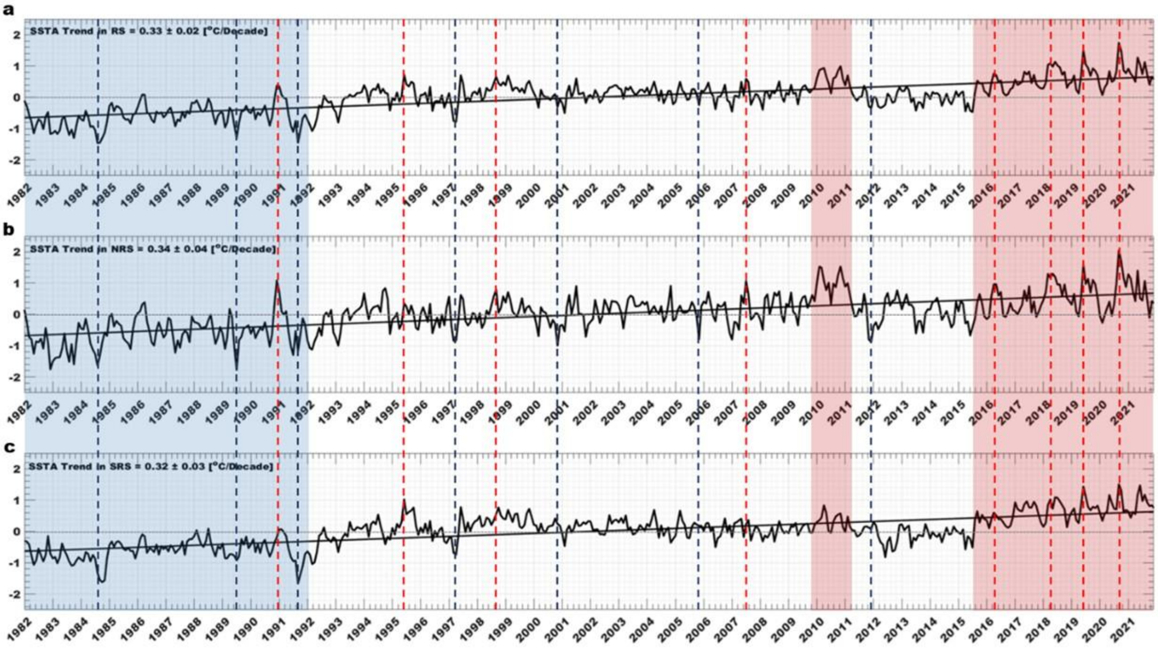

Figure 22. *Temporal evolution and trend in SST anomalies (°C) in the entire Red Sea (a), the Northern Red Sea (b), and the Southern Red Sea (c) from 1982–2021. The blue and red shaded areas represent the cold and warm periods, respectively. The blue and red dotted lines represent the coldest and warmest years, respectively.*

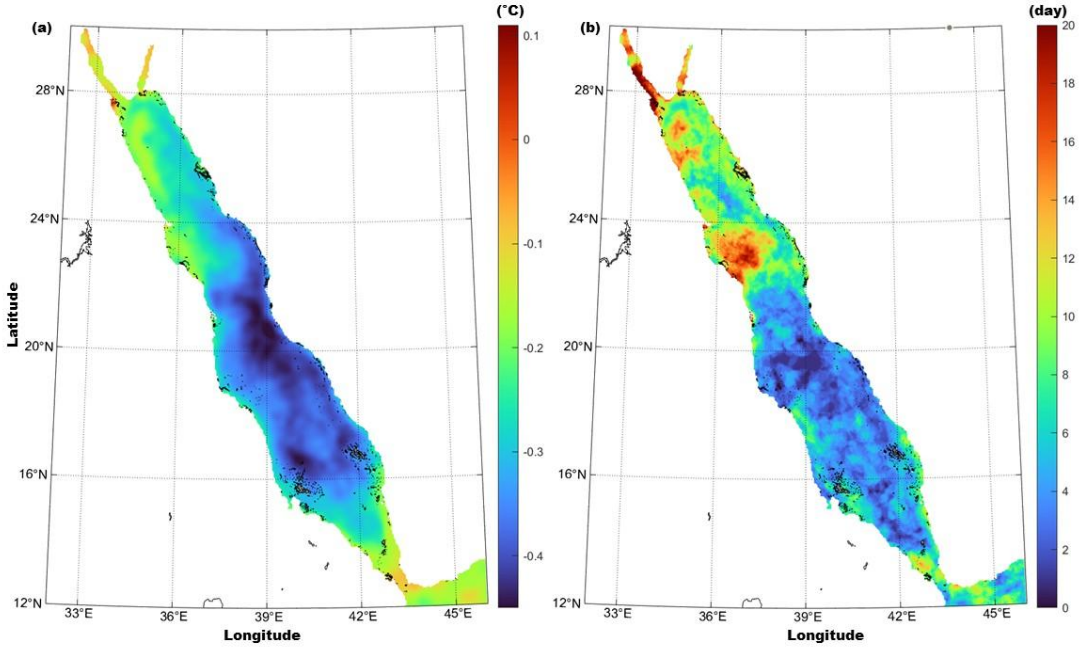

Figure 23. *Spatial distribution of the average (a) SST anomaly (°C) and (b) MHW days (days) in the Red Sea during the coldest years of the study period (1982–2021).*

Over the study period, there were years that were notably colder or warmer than the average for that period. The cold years were 1985, 1990, 1992, 1993, 1997, 2012 and 2013, while the warm years were 1991, 1995, 2010 and the last six years of the study period (2016-2021). During both the warm and cold years, the spatial distribution of the average SSTA and MHWDs was analyzed, as shown in Figures 23-25. In the cold years, the NRS and the Strait of Bab El-Mandab had the highest SSTA and MHWDs (Fig. 23). However, in the warm years, the SRS had the highest SSTA, and the SRS and the northern regions of the Gulfs of Suez and Aqaba had the highest number of MHWDs (Fig. 24). The year 2010 was an exception among the warm years, with a distinct spatial distribution of SSTA and MHWDs. In 2010, the NRS and the Gulfs of Suez and Aqaba had the highest SSTA and MHWDs (Fig. 25).

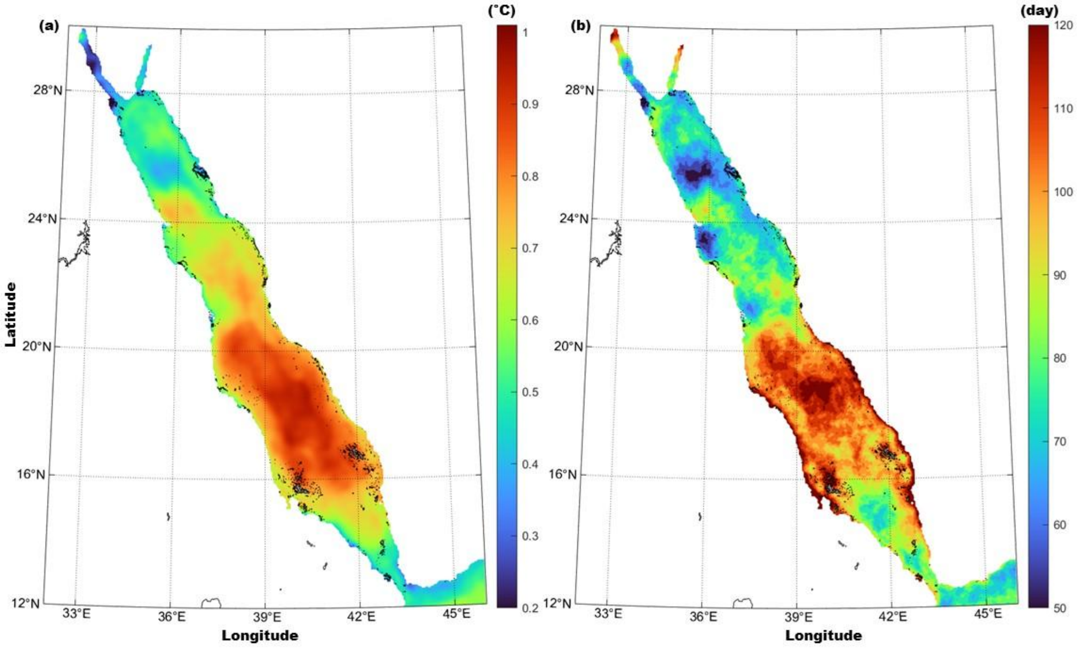

__Figure 24.__ Spatial distribution of the average (a) SST anomaly (°C) and (b) MHW days (days) in the Red Sea during the warmest years of the study period (1982–2021).

The inter-annual variations of MHWs frequency in the RS and its sub-basins during the study period are shown in Figure 26. The threshold for determining the years with the highest MHW frequency was set at one standard deviation above the mean of the annual MHW frequency. Based on this criterion, any year with more than four MHW events was classified as having a high MHW frequency. In the entire RS, the year 2010 and the last five years of the study period (2017-2021) had the highest annual MHW frequency (Fig. 26a). The NRS experienced the highest annual MHW frequency in the years 2010, 2018, 2019, and 2021 (Fig. 26b), while in the SRS, the year 1998 and the last five years of the study period had the highest annual MHW frequency (Fig. 26c). A total of 78 MHW events were recorded in the RS over the last four decades (1982-2021), with 36 of these events (46%) occurring in the last 10 years of the study period. Furthermore, a total of 1016 heat days were observed in the RS between 1982 and 2021, with 590 of these days (58%) occurring in the last decade. The findings of this study suggest that the recent rapid increase in SST in the RS has led to a positive trend in the occurrence of MHWs in the region. These findings are consistent with those of previous studies, such as Bawadekji et al., (2021) and Mohamed et al., (2021), which have also documented the increasing trend of MHWs in the RS. This trend is expected to continue in the future, as global warming is projected to cause further increases in SSTs, both in the RS and in other regions around the world.

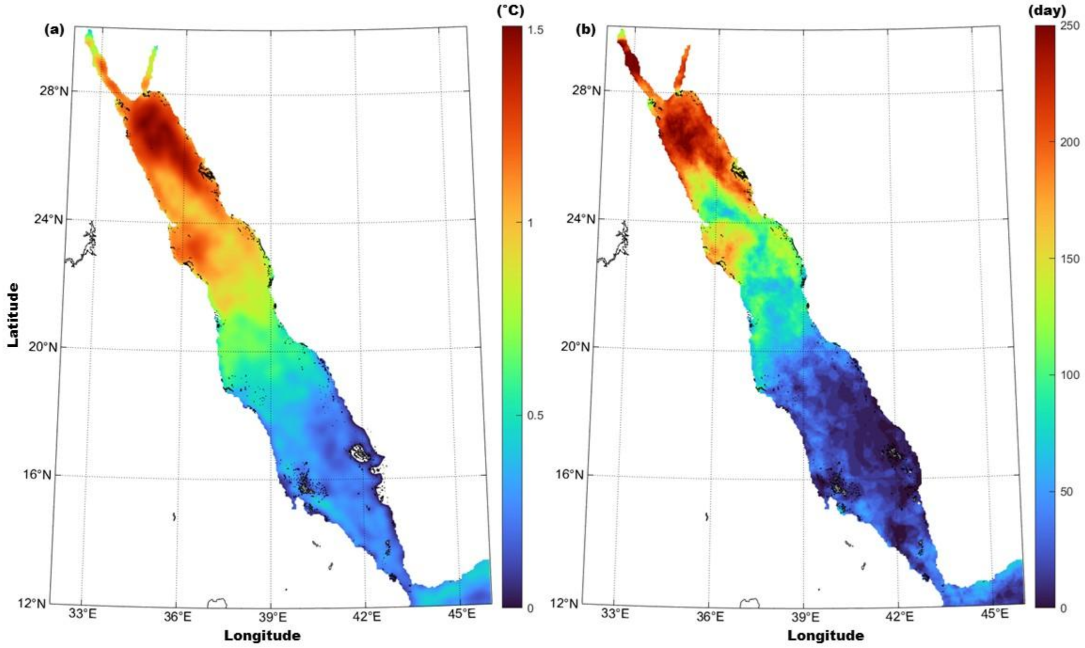

Figure 25. *Spatial distribution of the average (a) SST anomaly (°C) and (b) MHW days (days) in the Red Sea during the year 2010.*

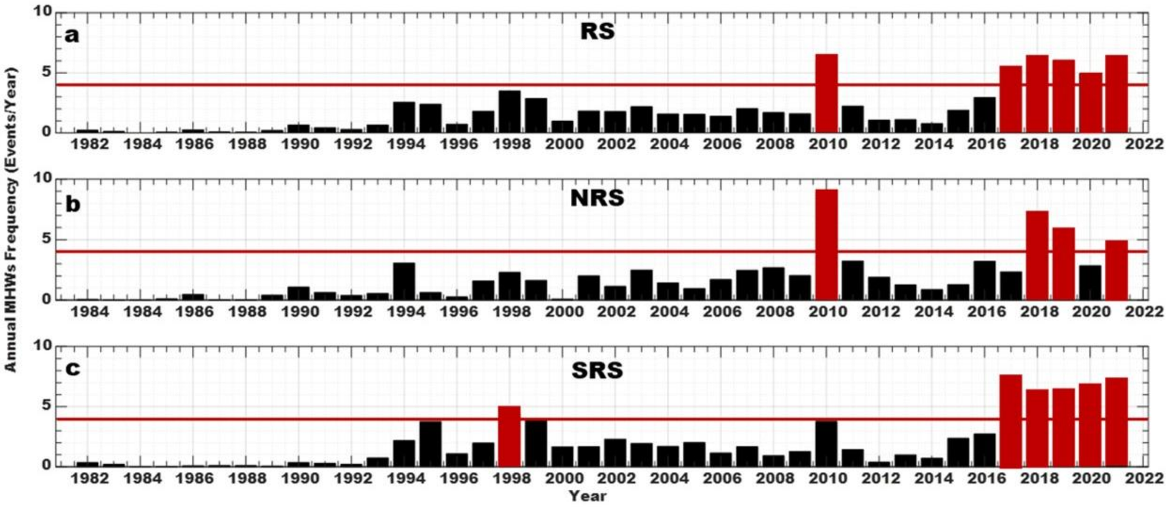

Figure 26. *Interannual variability in MHW frequency in the entire Red Sea (a), the Northern Red Sea (b), and the Southern Red Sea (c) from 1982–2021. The red bars represent the years with the highest frequency in each basin.*

To gain a better understanding of the atmospheric conditions associated with the years with the highest frequency of MHWs in the RS and its subregions, we compared the atmospheric variables with the annual MHW frequency. The anomalies of wind Speed (Ws), atmospheric temperature (Tair) and Qt are shown in Supplementary Figures 9-11. It was noticed that the years with a high MHW frequency were characterized by a specific set of atmospheric conditions such as reduced wind Ws, high Tair and high Qt which may have contributed to the frequent occurrence of MHWs in the RS during these years.

3.2.3 Climate Modes and MHWs in the Red Sea:

To investigate the potential relationship between climate indices, annual sea SSTA, and MHW metrics (i.e., frequency, duration, and total days) in the RS over the past four decades, a correlation analysis was conducted between different climate modes and SSTA/MHW metrics. It was observed that the correlation between climate modes and MHW frequency, duration, and total days displayed similar spatial patterns with slightly different correlation values that were not significantly different. To avoid repetition of figures and text, this section presents the correlation of climate modes with MHW frequency only. The significance of the correlations was tested with a 95% confidence interval. The analysis focused on the NOAA modes that showed a significant correlation ($p < 0.05$) with the SSTA and/or MHW frequency, as presented in Figure 27.

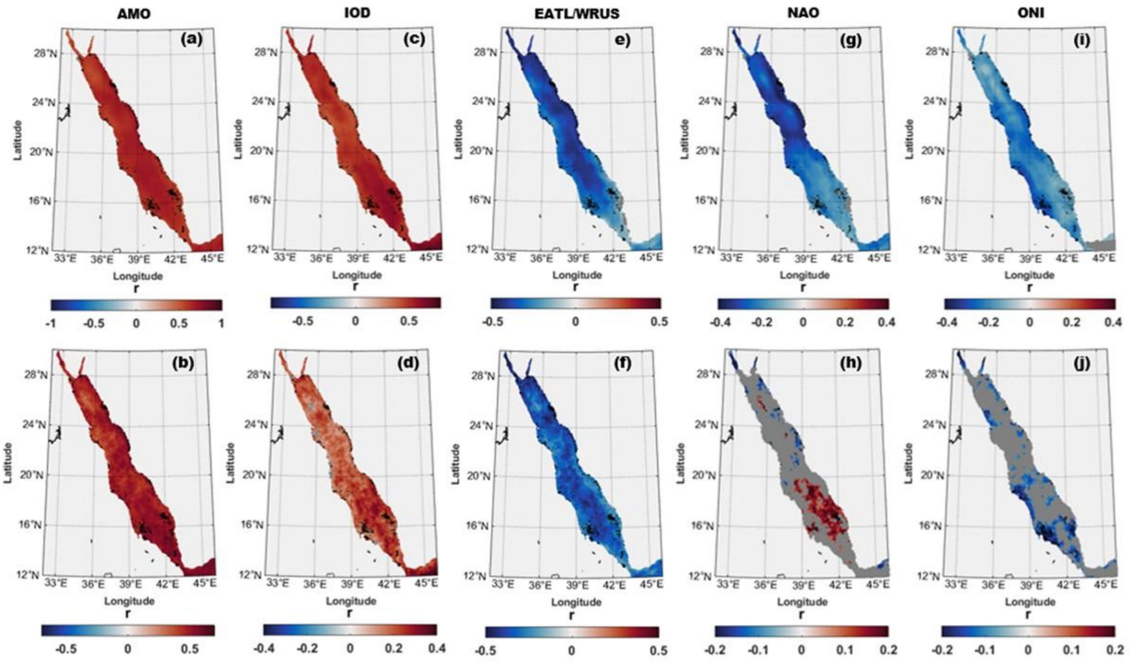

__Figure 27.__ Correlation maps of the SST anomaly (upper panels) and MHW frequency (lower panels) in the Red Sea with different climate modes from 1982–2020. Correlations are shown with the AMO index (a, b), IOD pattern (c, d), EATL/WRUS index (e, f), NAO index (g, h), and ONI index (i, j). Grey shading indicates areas where the correlation is not significant (p-value > 0.05).

The AMO index showed a highly significant positive correlation with both SSTA and MHW frequency across the whole RS, with a correlation coefficient of greater than 0.7 for SSTA and greater than 0.5 for MHW frequency (Fig. 27a-b). This finding is consistent with a previous study by Krokos et al. (2019), who reported that long-term AMO oscillations modulate SST trends in RS. The IOD index also showed a positive correlation with both SSTA and MHW frequency in RS, with a correlation coefficient of greater than 0.5 for SSTA and ranging between 0.2 and 0.4 for MHW frequency (Fig. 27c-d). The influence of the IOD on SSTA and MHW frequency was stronger in the SRS than in the NRS. A strong negative correlation was observed between the EATL/WRUS index and both SSTA and MHW frequency in the RS, with a correlation coefficient of approximately -0.5 for SSTA and between -0.3 and -0.5 for MHW frequency (Fig. 27e-f). This correlation was strongest in the NRS and in the offshore areas of the central and southern RS. To our knowledge, no previous study has examined the relationship between the EATL/WRUS index and SSTA or MHW frequency in the RS. However, a recent study by Hamdeno and Alvera-Azcaráte (2023) reported a negative correlation between the EATL/WRUS index and SSTA in the eastern Mediterranean region, which is geographically close to the RS and is frequently affected by systems of Mediterranean origin (Langodan et al., 2017a, 2017b). The NAO index showed a negative correlation with the SSTA in the RS, with a correlation coefficient of less than -0.3 (Fig. 27g). The influence of the NAO on the SSTA was stronger in the NRS than in the SRS. The correlation between the NAO index and MHW frequency was not significant, except in the SRS, where a positive correlation of 0.2 was observed, and in the Gulfs of Suez and Aqaba, where a negative correlation of -0.2 was observed (Fig. 27h). The ONI showed a negative correlation with the SSTA in the RS, which was more pronounced in the coastal areas of the central and southern RS (Fig. 27i). The correlation between the ONI and MHW frequency was not significant, except for a correlation of about -0.2 on the western coast of the SRS (Fig. 27j). Overall, the AMO and IOD indices showed the strongest and most consistent correlations with SSTA and MHW frequency in the RS, while the EATL/WRUS index showed a strong negative correlation with both SSTA and MHW frequency, particularly in the NRS. The NAO and ONI indices showed weaker and less significant correlations with SSTA and MHW frequency in the RS.

The time series of various climate modes were compared with the annual frequency of MHWs in the RS as presented in Figure 28. The results revealed a positive correlation between the AMO and the annual frequency of MHWs in the RS. The years with the lowest MHW frequency, from 1982 to 1994, were found to align with the negative phase of the AMO. Conversely, the years with the highest MHW frequency corresponded with the positive phase of the AMO, as shown in Figure 28a. Furthermore, IOD was also found to have a significant relationship with the annual frequency of MHWs in the RS. From 1982 to 1993, the IOD had on average negative phase, and the frequency of MHWs was the lowest. In contrast, the last seven years of the study period, from 2015 to 2021, had high MHW frequencies, which corresponded with the positive phase of the IOD, as depicted in Figure 28b. The analysis also revealed a negative correlation between the EATL/WRUS index and the frequency of MHWs in the RS. The years with low MHW frequency were found to correspond with the positive phase of the EATL/WRUS index, while the years with high MHW frequency corresponded with the negative phase of the index, as shown in Figure 28c. However, the comparison between the NAO and the ONI with the annual time series of MHW frequency did not suggest a clear relationship between their occurrence Figure 28d-e. The correlation maps in Figures 27e-h also support this finding, as the correlation was not significant in most parts of the RS. In conclusion, these results suggest that the AMO and IOD are the primary climate modes that align with the interannual variability of the MHWs frequency in the RS. The EATL/WRUS index also has a significant relationship with the annual MHW frequency, while the NAO and ONI do not appear to have a substantial relationship.

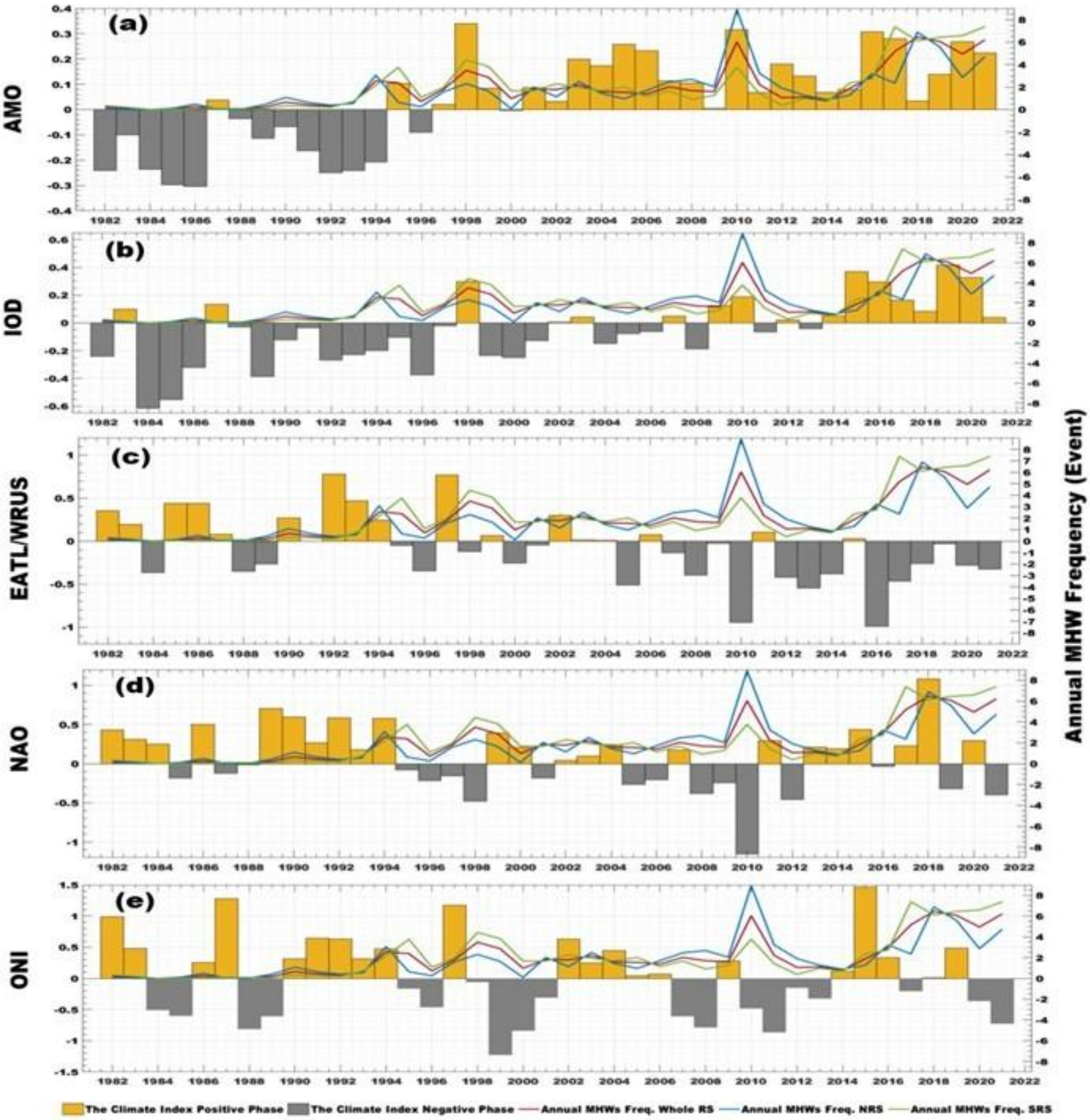

Figure 28. *Annual time series of normalized climate indices and MHW frequency in the Red Sea. The (a) AMO index, (b) IOD index, (c) EATL/WRUS pattern, (d) NAO index, and (e) ONI index are shown with annual MHW frequency in the entire Red Sea (red line), the Northern Red Sea (blue line), and the Southern Red Sea (green line). Yellow and grey bars indicate the positive and negative phases of the climate indices, respectively.*

In the last four decades, the year 2010 showed the highest MHW frequency particularly in the NRS, and in the same year had one of the strongest positive AMO phases (i.e. the AMO is positively correlated with the MHW frequency), while at the same time EATL/ WRUS and NAO had their strongest negative phases during the entire study period.

3.2.4 Case Study: 2010 MHWs in the Northern Red Sea:

The selection of 2010 as a case study for MHWs in the northern RS is based on several reasons. Firstly, 2010 was one of the warmest years on record, with a high frequency of MHWs in the region. Secondly, the spatial distribution of SSTAs and MHWDs in 2010 was found to be different from that of other warm years. Thirdly, although the SRS is known to be warmer than the NRS throughout the year (Fig. 19), in 2010 the SSTA of the NRS was higher by more than 1°C than the SRS (Supplementary Fig. 6d). Therefore, this section aims to provide a detailed description of the spatial and vertical extent as well as the potential atmospheric drivers of the intense MHW event that occurred in the NRS in 2010.

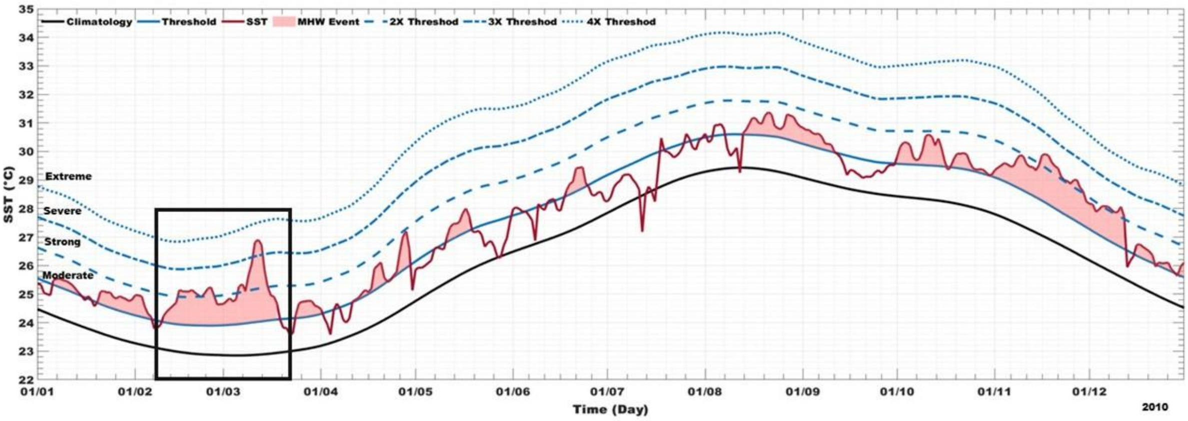

Figure 29. *MHW events in the Northern Red Sea in 2010. The shaded red area indicates the duration of the event. The solid red line represents the SST, the solid black line represents the climatology, the solid blue line represents the threshold, and the dotted blue lines represent the multiples of the threshold (defining the MHW categories).*

During both winter and summer of 2010, the NRS experienced ten MHW events (Fig. 29). These included one severe event in February and March (Category III), one strong event between October and December (Category II), and several moderate events (Category I). In this section, we will provide a detailed analysis of the most intense and longest winter MHW event that occurred in the NRS. This event occurred between February and March with an SSTA of about 4°C above the climatological average, peaking on March 12, 2010 (Fig. 29). This event was categorized as severe (i.e. the temperature exceeded 3X the threshold).

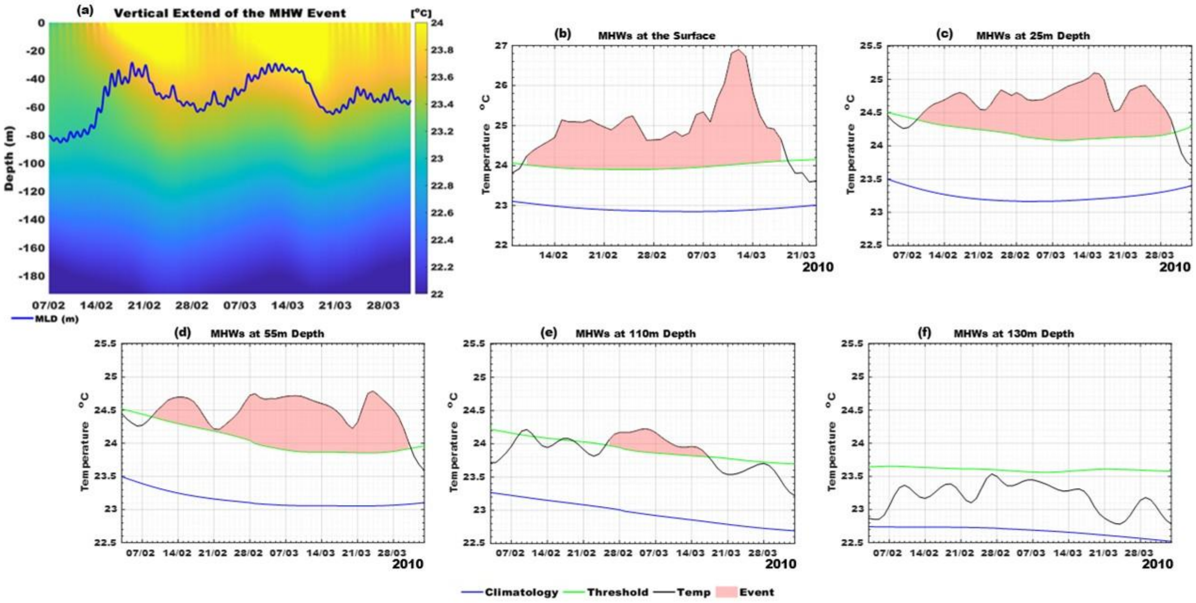

Figure 30. *The MHW event in the NRS between February and March 2010. (a) The vertical extent of the MHW, with the blue line representing the mixed-layer depth (MLD). (b–f) The MHW at different water column depths (surface, 25, 55, 110, and 130 m), with the shaded red area indicating the MHW event, the solid black line*

representing the SST (SST), the solid blue line representing the climatology mean, and the solid green line representing the 90th-percentile threshold.

To better understand the dynamics of the event, the anomaly of water column temperature compared to the mixed layer depth (MLD) and time series of the MHW at different depth levels (surface, 25 m, 55 m, 110 m and 130 m) was calculated, as shown in Figure 30. The results showed that the regular diurnal cycle of water temperature, characterized by high temperatures during the day and low temperatures during the night, gradually disappeared during the days of the MHW and was completely absent during the peak days of the event. This suggests that the ocean temperature reached a threshold where the usual nighttime cooling was insufficient to lower the high SSTA and the heat was stored in the water column for the duration of the event. In addition, the results revealed a strong negative relationship between upper layer temperature and MLD, with a thin mixed layer aligned with the days of the higher water temperature. The time lag between the drop in MLD and the high water temperature was approximately four days, indicating that the sharp drop in MLD may have contributed to the rise of the water temperatures (Fig. 30a). The results also showed that the temperature anomaly extended vertically into the water column, reaching a depth of approximately 120 m during the MHW event (Fig. 30b-f). The duration of the MHW event varied from the surface to the subsurface, with the surface event (February 9 to March 18) being shorter than the events at 25 m and 55 m depth (February 9 to March 31), meaning that the heat from the MHW event was stored longer in the middle layer than at the surface. At 110 m depth, the duration of the MHW was shortest compared to the upper layers (February 26 to March 17) and occurred around the peak day of the surface event (March 12).

To better understand how atmospheric forcings may have contributed to the development of this MHW event, the spatial averages of atmospheric variables before (February 3 to 7), during and after (March 10 to 15) the event were calculated and presented in Figure 31. Additionally, the time series of atmospheric variables averaged over the NRS (24° - 28° N and 34° - 39° E) during the event are presented in Supplementary Figure 12. Prior to the MHW event, the average SSTA in the NRS was about 1°C above average, while it was negative in the SRS and in the Strait of Bab El-Mandab. During the MHW event, the SSTA increased in the NRS and reached a local maximum of 4°C above the climatological average (Fig. 31a-c). The spatial distribution of the average Tair showed higher values in the west (over Egypt, Eritrea and Ethiopia) than in the east (over Saudi Arabia) (Fig. 31d-f). Over the NRS, the Tair increased by approximately 8°C compared to before the event. After the MHW, the Tair decreased but did not return to pre-MHW values (Fig. 31d-f and Supplementary Fig. 12b). The MSLP maps showed an opposite distribution to Tair, with areas of high Tair having low MSLP and vice versa (Fig. 31j-l). In addition, the average MSLP over the NRS decreased during the MHW event compared to before the event (Supplementary Fig. 12c). Before the MHW event, the winds blew from the eastern region and mainly flowed towards the SRS. During this event, the winds blew from the south and shifted to the west before reaching the NRS region, which experienced very low winds (Fig. 31m-o and Supplementary Fig. 12d). Furthermore, the relative humidity rose by 10% over the NRS during the MHW period (Supplementary Fig. 12e).

In the RS, the latent heat flux (LHF) shares a similar spatial and temporal distribution with the Qt (Nagy et al., 2021). The majority of the net surface heat exchange variability in the NRS is known to depend on the turbulent components of the surface flux, primarily the LHF (Papadopoulos et al., 2013). In our case study, before the MHW event, the LHF ranged from -140 to -60 W/m², and the Qt ranged from -150 to -20 W/m², indicating that the ocean was losing heat to the atmosphere (Fig. 31g-i and Supplementary Fig. 12f). During the MHW, the combined effect of increased Tair, humidity and reduced winds led to a strong decrease in the ocean latent heat loss, signifying reduced heat loss to the atmosphere. Particularly during the days of the MHW onset and peak, the LHF fluctuated between -20 and -10 W/m². This decrease coincided with a slight increase in net solar radiation from 180 W/m² before the MHW to more than 200 W/m² during the MHW (Supplementary Fig. 12f). Accordingly, the heat exchange between the air and ocean reversed, causing a prolonged ocean heat gain, with Qt reaching up to 100 W/m², ultimately driving the MHW (Fig. 31g-i).

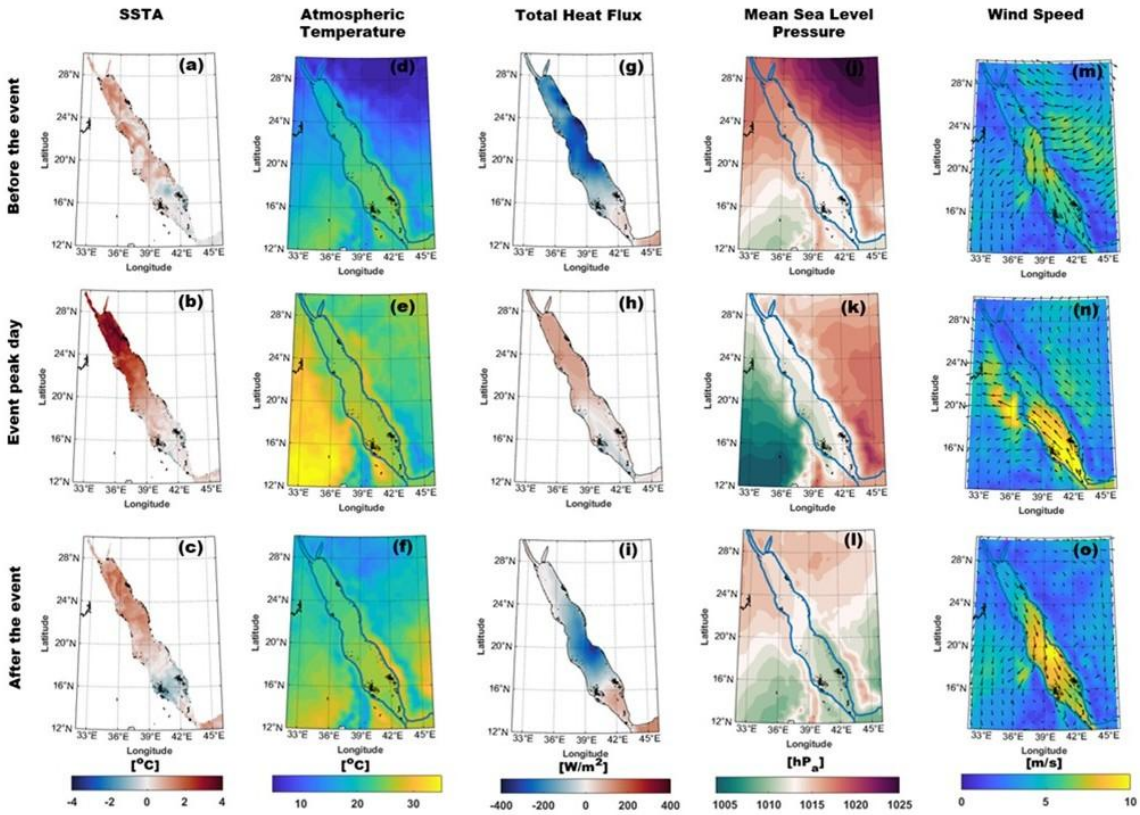

Figure 31. *The average spatial distribution of atmospheric variables before, during, and after the MHW event in the NRS. The upper panels show the period before the MHW event (3 to 7 February), the middle panels show the period during the MHW event (10 to 15 March), and the lower panels show the period after the MHW event (20 to 25 March). Panels (a)–(c) represent SST anomaly (SSTA; in °C), panels (d)–(f) represent atmospheric temperature (in °C), panels (g)–(i) represent total heat flux (in W m−2), panels (j)–(l) represent mean sea level pressure (in hPa), and panels (m)–(o) represent wind speed (in m s−1) and wind direction.*

In summary, our findings indicate that the late winter MHW event in the NRS was primarily driven by atmospheric forcing, specifically an increase in Tair and humidity, possibly linked to reduced winds. These atmospheric conditions collectively resulted in reduced LHF and a strong ocean heat gain, creating favourable conditions for MHW occurrence.

3.3 Conclusions:

This study aimed to analyse the characteristics and trends of SST and MHWs in the RS and investigate their relationship with climate modes. Over the past four decades, the RS has experienced a significant increase in SST and MHWs, with a notable acceleration in the past decade. The spatial distribution of MHWs showed high variability, with the highest frequency in the coastal areas of the southern region and the Strait of Bab El-Mandab. The mean duration of MHWs was longer in the northern region and the Gulfs of Suez and Aqaba, while the most intense MHWs were observed in the northern region and the western part of the southern region. The study revealed a warming trend in the RS since the mid-1990s, with a notable increase after 2016. A total of 78 MHW events and 1016 MHWDs were identified in the RS over the past four decades, with 46% of these events and 58% of the days occurring in the last decade. Considering the results of this study and the observed trends of MHWs in the region, it is recommended that future work considers an analysis of MHW trends based on different baselines. This comparison is particularly important when it comes to projecting future MHWs under different global warming scenarios, as the selection of an appropriate baseline is of utmost importance for the detection of future MHWs and the calculation of their trends.

The analysis of SSTA trends revealed a decadal variability with high trends alternating between the NRS and SRS. From 1982 to 1991, the highest trends were observed in the NRS, with an average trend of 0.56°C/Decade. However, from 1992 to 2001, the spatial pattern of the SSTA trend was altered, with the highest trends observed in the SRS, with an average trend of 0.57°C/Decade, and lower trends in the NRS, with an average trend of 0.30°C/Decade. From 2002 to 2011, the highest trends were again observed in the NRS, with an average trend of 0.45°C/Decade, while the SRS experienced no trend in the SSTA during this period. Finally, over the last decade of the study period (2012-2021), the SRS had higher trends in the SSTA than the NRS, with an average trend of 1.35°C/Decade for the SRS and 0.89°C/Decade for the NRS. The spatial distribution of average SSTA and MHWDs was analysed in both warm and cold years. In cold years, the NRS and the Strait of Bab El-Mandab had the highest SSTA and MHWDs. However, in warm years, the SRS had the highest SSTA values, and the SRS and the northern regions of the Gulfs of Suez and Aqaba had the highest number of MHWDs the year of 2010 an exception among the warm years, with the northern region having the highest SSTA and MHWDs.

Investigating the relationship between climate modes and SSTA and MHW frequency, it was found that the AMO and the IOD indices had high positive correlations with SST and MHW frequency in the RS. Meanwhile, the EATL/WRUS index showed a negative correlation with both SST and MHW frequency, particularly in the northern region. The NAO and the ONI indices showed weaker and less significant correlations with SST and MHW frequency in the RS. The study further examined the intense MHW event that occurred in the northern region between February and March of 2010. This MHW has extended to 120 m depth and was associated with a combination of atmospheric conditions, specifically an increase in Tair and humidity which were possibly linked to the reduced winds and resulted in reduced LHF and a strong ocean heat gain, creating favourable conditions for MHW occurrence. Interestingly, the AMO and the IOD were in a robust positive phase in 2010, while the EATL/WRUS and the

NAO were in their most pronounced negative phase. These climate indices have been shown to be correlated with SSTs and MHWs in the RS, and their combination in 2010 may have contributed to the increased occurrence of MHWs in that year.

In conclusion, this study has provided valuable insights into the characteristics and trends of SST and MHWs in the RS and their relationship with climate modes. The findings of this study can be useful for the management and conservation of marine ecosystems in the RS, as well as for the prediction and mitigation of the impacts of MHWs on these ecosystems. This research on MHWs in the RS region will also enable the generation of new scientific knowledge and help to fill gaps in the existing literature and advance marine science. For future work, the compound between MHWs and other extreme events will be investigated, and their impact on the RS ecosystem will also be studied.

Chapter Four: Subsurface MHWs in Semi-Enclosed Basins

Foreword

This chapter investigates the subsurface structure and long-term evolution of MHWs in two semi-enclosed basins: the Mediterranean Sea and the Red Sea. While previous studies have extensively documented surface MHWs, the vertical extent and persistence of subsurface thermal anomalies remain less well understood, particularly in marginal seas characterized by complex circulation and stratification dynamics. Understanding the depth-dependent evolution of MHWs is essential because subsurface heat anomalies may persist longer than surface signals and can expose deeper ecosystems to prolonged thermal stress.

The primary objective of this chapter is to quantify the vertical structure and long-term variability of MHWs in both basins using a consistent depth-resolved framework. By analysing temperature fields from the upper ocean to depths exceeding 1000 m, this study evaluates how MHW occurrence, intensity, and vertical penetration vary across different depth layers and seasons. Particular attention is given to the role of mixed-layer variability and regional oceanographic processes in modulating the vertical propagation of extreme warming events.

The chapter further provides the first systematic comparison of subsurface MHWs between the Mediterranean Sea and the Red Sea. These basins present contrasting oceanographic regimes: the Mediterranean exhibits active intermediate and deep-water formation that can redistribute heat vertically, whereas the Red Sea is characterized by strong stratification and more spatially confined deep-water renewal. Comparing these environments provides new insights into how basin-scale physical structure influences the vertical expression of marine heat extremes under ongoing climate warming.

This work contributes to the broader objectives of the thesis by extending the analysis of MHWs beyond the surface layer and by examining the mechanisms governing their vertical evolution. The study highlights the importance of incorporating subsurface dynamics when assessing MHW impacts and ecosystem vulnerability in semi-enclosed seas.

This research is currently being **prepared for submission to a peer-reviewed journal**.

4.1 Data and Methods:

4.1.1 Data:

Subsurface temperature and mixed-layer depth (MLD) fields were obtained from the Copernicus Marine Service Global Ocean Reanalysis product GLORYS12V1 (Jean-Michel et al., 2021). GLORYS12V1 is based on the NEMO ocean circulation model with assimilation of satellite and in situ observations, providing dynamically consistent three-dimensional ocean fields at 1/12° (~8 km) horizontal resolution and daily temporal frequency. The vertical grid consists of 50 z-levels extending to the deep ocean; in this study, the upper 1100 m were analysed, corresponding to 36 depth levels ranging from approximately 0.5 m to 1062 m.

Daily SST fields were derived from the Copernicus Marine Environment Monitoring Service (CMEMS) Operational SST and Sea Ice Analysis (OSTIA) Level-4 reprocessed product (Good et al., 2020), which provides gap-free daily SST maps at 0.05° × 0.05° spatial resolution from 1 January 1993 to 31 December 2024. To ensure spatial consistency between surface and subsurface variables, all oceanic fields were interpolated to a common 0.08° × 0.08° grid before analysis. The analysis period covers 1993-2024. A climatological baseline period of 1993-2022 was used to compute thresholds and anomalies.

To examine spatial variability within each basin, three representative subregions were defined using fixed longitude-latitude boxes (Fig. 32). In the MedS, the regions are the Northwestern Mediterranean (3°-11°E, 41.5°-43°N; representing WMB), the North Central Mediterranean (17°-20°E, 36°-39°N; representing CMB), and the Eastern Mediterranean (27°-32°E, 31.5°-35°N; representing EMB). In the RS, the regions are the Northern Red Sea (34°-36°E, 26°-27.8°N; representing NRS), the Central Red Sea (36°-40°E, 20°-23°N; representing CRS), and the Southern Red Sea (39°-43°E, 15°-18°N; representing SRS). Regional time series were computed as arithmetic means of all grid cells within each box. Basin-mean metrics were calculated as the simple mean of the three subregions within each basin.

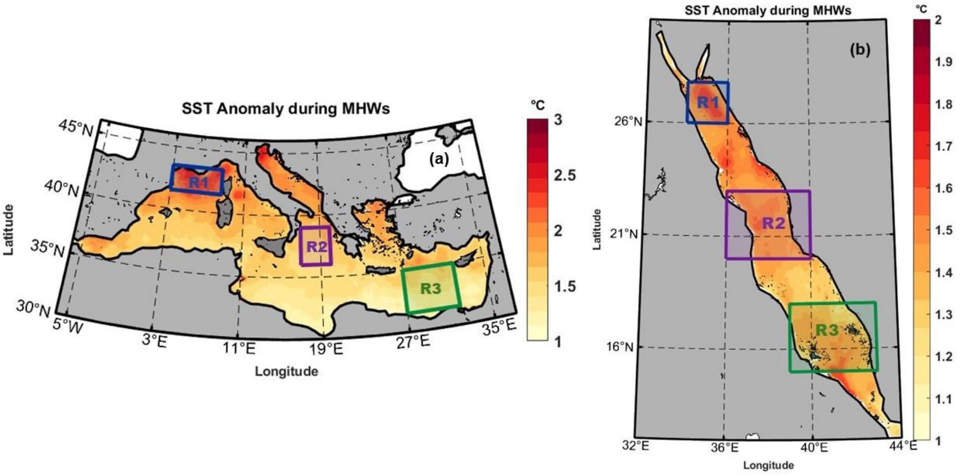

Figure 32. *Composite spatial distribution of SST anomalies (°C) during detected MHW days (1993 - 2024) in (a) the Mediterranean Sea and (b) the Red Sea. Colored boxes indicate the subregions analyzed in this study.*

4.1.2 Methods of Analysis:

MHWs were detected following the hierarchical framework of Hobday et al., (2016). For each grid cell, a seasonally varying climatology and threshold were defined using the 1993-2022 baseline period. The threshold corresponds to the 90th percentile of daily temperature, calculated with an 11-day moving window (± 5 days) centred on each calendar day to account for seasonal variability. The resulting climatology and percentile threshold were smoothed with a 31-day running mean. At the surface, an event was classified as a MHW when daily temperature exceeded the local threshold for at least five consecutive days. Interruptions of up to two days below the threshold were merged into a single event, consistent with Hobday et al., (2016).

To calculate the contribution of background warming to MHW characteristics, the linear temperature trend was removed from the raw daily SST time series at each grid cell, producing a detrended SST dataset representing internal climate variability. MHWs were then detected independently in the original (raw) SST dataset and the detrended SST dataset, using the same percentile-based definition (Hobday et al., 2016). For each metric (frequency, total MHW days, duration, maximum intensity, and cumulative intensity), the contribution of long-term warming was quantified as the difference between the raw and detrended datasets. The remaining component was attributed to internal variability. This framework follows established approaches used to separate background warming from short-term variability in climate extreme analyses (e.g., Oliver et al., 2018a; Holbrook et al., 2019; Laufkötter et al., 2020).

Subsurface MHWs were defined as surface-anchored events. First, surface MHWs were identified at each grid point. Then, for each surface MHW day, exceedances of the depth-dependent 90th percentile threshold were evaluated independently at all subsurface levels. A subsurface MHW was therefore defined as a positive temperature anomaly exceeding its local threshold at depth during an ongoing surface MHW event. This ensures that subsurface events represent the vertical extension of surface extremes rather than isolated deep anomalies. Depth-specific thresholds were computed independently at each vertical level, preserving the local thermal structure of the water column.

The vertical structure of MHWs was analysed across the full depth range and aggregated into four depth layers for trend analysis: 0-50 m, 50-200 m, 200-500 m, and 500-1100 m. Within each layer, annual MHW days were defined as the number of days during which at least one depth within that layer exceeded its local threshold during a surface-anchored event. Daily penetration depth (Zext) was defined as the average depth at which temperature exceeded its threshold during a surface MHW event. Annual maximum penetration depth (Zmax) was calculated as the average of the maximum Zext during a surface MHW event within each calendar year. Seasonal penetration depth was computed as the seasonal mean of Zext.

Seasons were defined climatologically as:

- Winter: January–March (JFM),
- Spring: April–June (AMJ),
- Summer: July–September (JAS),

- Autumn: October–December (OND).

Mixed layer depth (MLD) anomalies are analysed relative to MHW onset, and conditional probabilities are calculated to determine whether periods of anomalously shallow mixed layers tend to occur prior to MHW onset or whether MHW events are followed by subsequent adjustments in MLD. This assessment is conducted separately for each season in order to account for the pronounced seasonal variability in air-sea interactions and stratification dynamics in both the Mediterranean and the Red Sea.

Long-term trends in subsurface MHW metrics were estimated using Sen's slope estimator and evaluated for statistical significance with the non-parametric Mann–Kendall test (Sen, 1968; Hamed and Ramachandra Rao, 1998; Wilks, 2019). Trends are reported per decade, and statistical significance was assessed at the 95% confidence level.

4.2 Results:

4.2.1 SST Seasonality and Surface MHWs:

Seasonal mean SST shows spatial gradients in both the Mediterranean (MedS) and the Red Sea (RS) (Fig. 33-34). In the MedS (Fig. 33), winter (January–March) SST ranges from approximately 12-14 °C in the northwestern basin to 16-18 °C in the southeastern part (Levantine Basin). During spring (April–June), basin-wide warming increases SST to 16-20 °C. Summer (July–September) temperatures exceed 24 °C throughout most of the basin and reach above 28 °C in the EMB. Autumn (October–December) shows progressive cooling, with SST ranging from approximately 18-24 °C. A persistent west-east gradient is evident across all seasons, with consistently warmer conditions in the eastern basin relative to the western Mediterranean. In the RS (Fig. 34), SST displays a strong meridional gradient throughout the year. Winter temperatures range from about 20-23 °C in the NRS to about 24-26 °C in the SRS. Spring warming increases SST to 24-28 °C across the basin. During summer, SST exceeds 30 °C in the central and southern regions, while remaining near 28-29 °C in the north. Autumn SST remains elevated, particularly in the southern basin, where temperatures frequently exceed 28 °C. The RS consistently exhibits higher absolute SST values than the Mediterranean in all seasons.

The decadal evolution of surface MHW characteristics from 1982 to 2024 shows a progressive amplification in both basins (Fig. 35-36). In the Mediterranean (Fig. 35), MHW frequency, total MHW days, mean duration, maximum intensity, and cumulative intensity all increase from the first decade (1982-1991) to the most recent period (2012-2024). The strongest increases occur in total MHW days and cumulative intensity during the last decade. Subregional analysis reveals that the WMB (R1) experiences comparatively larger increases in maximum intensity, while the EMB (R3) shows stronger increases in duration and cumulative intensity. The CMB (R2) displays intermediate behaviour compared with the other basins. In the RS (Fig. 36), surface MHW frequency and total MHW days also increase across decades, with pronounced amplification after 2012. The SRS (R3) records the largest increases in the frequency and total days, while the NRS (R1) shows stronger increases in cumulative intensity. The CRS (R2) shows intermediate characteristics between the NRS and the SRS.

The decomposition analysis separating background warming from internal variability shows that long-term warming accounts for a substantial portion of the increase in total MHW frequency, total days, duration, and cumulative intensity in both basins (Fig. 35-36). While internal variability remains evident in the decadal variability, it does not fully explain the magnitude of the significant increase in MHW metrics specially in the last decade. The warming-driven component increases progressively and contributes to the MedS MHWs in the last 2 decades and the RS after 2012.

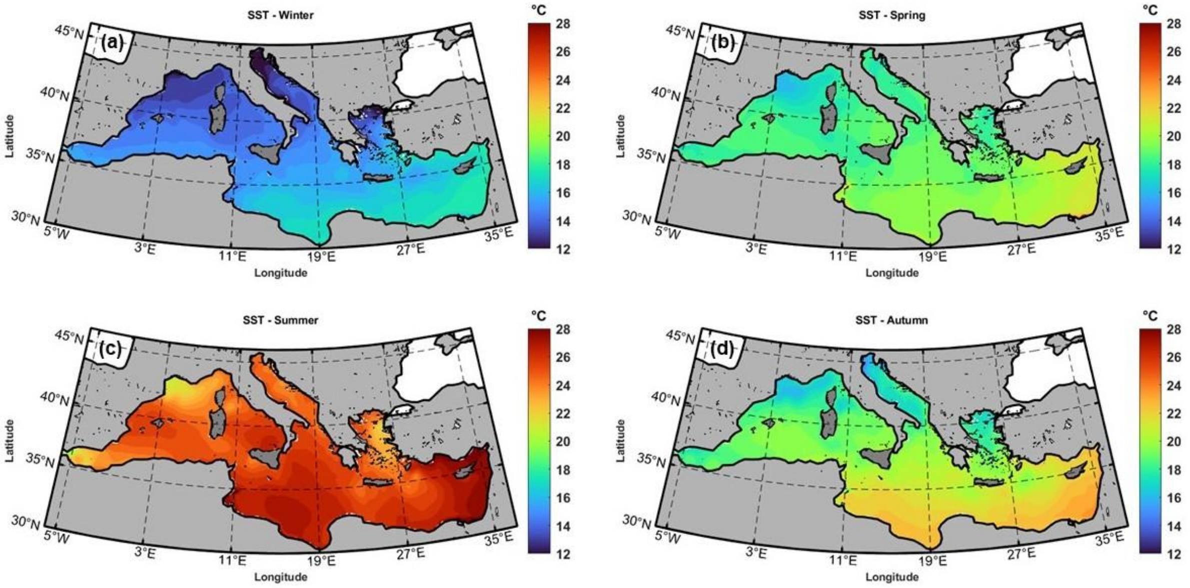

Figure 33. *Spatial distribution of seasonal mean SST (°C) averaged over 1993–2022 for (a) Winter (January–March), (b) Spring (April–June), (c) Summer (July–September), and (d) Autumn (October–December). The maps highlight the pronounced west–east thermal gradient and the strong summer amplification, particularly in the eastern Mediterranean.*

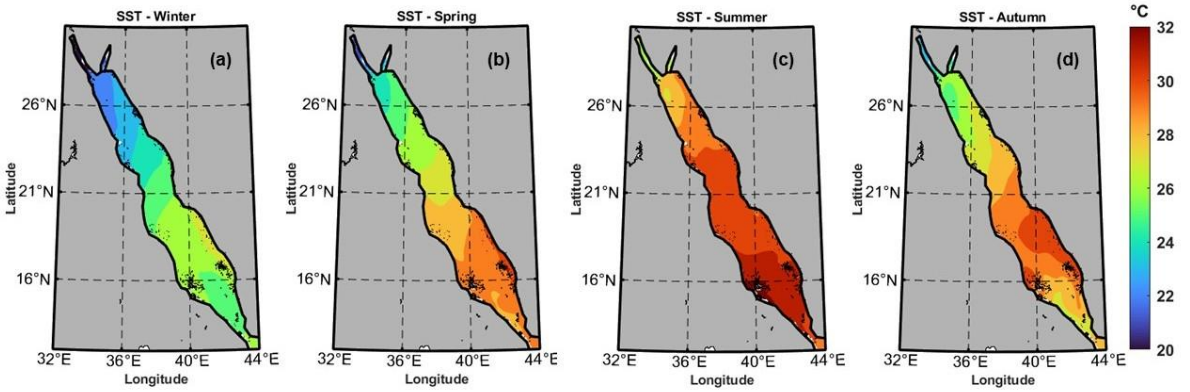

Figure 34. *Spatial distribution of seasonal mean SST (°C) averaged over 1993–2022 for (a) Winter (January–March), (b) Spring (April–June), (c) Summer (July–September), and (d) Autumn (October–December). The basin exhibits a persistent north–south thermal gradient with extreme summer warming in the central and southern sectors.*

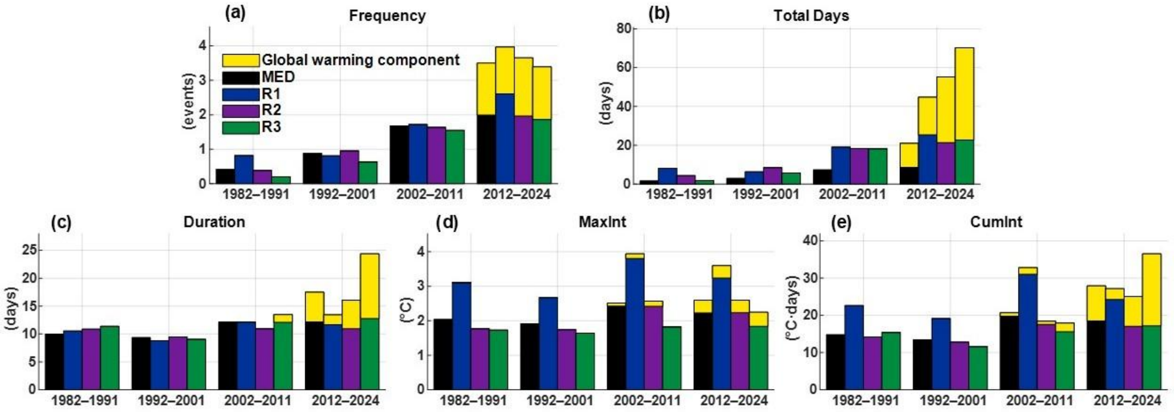

Figure 35. *Decadal averages (1982–1991, 1992–2001, 2002–2011, 2012–2024) of (a) MHW frequency (events/decade), (b) total MHW days (days/decade), (c) duration (days/decade), (d) maximum intensity (°C/decade), and (e) cumulative intensity (°C·days.decade^{-1}) for the entire Mediterranean basin (MED) and its subregions (R1: WMB, R2: CMB, R3: EMB). Yellow bars indicate the estimated contribution of the long-term background warming component to MHW frequency and cumulative metrics.*

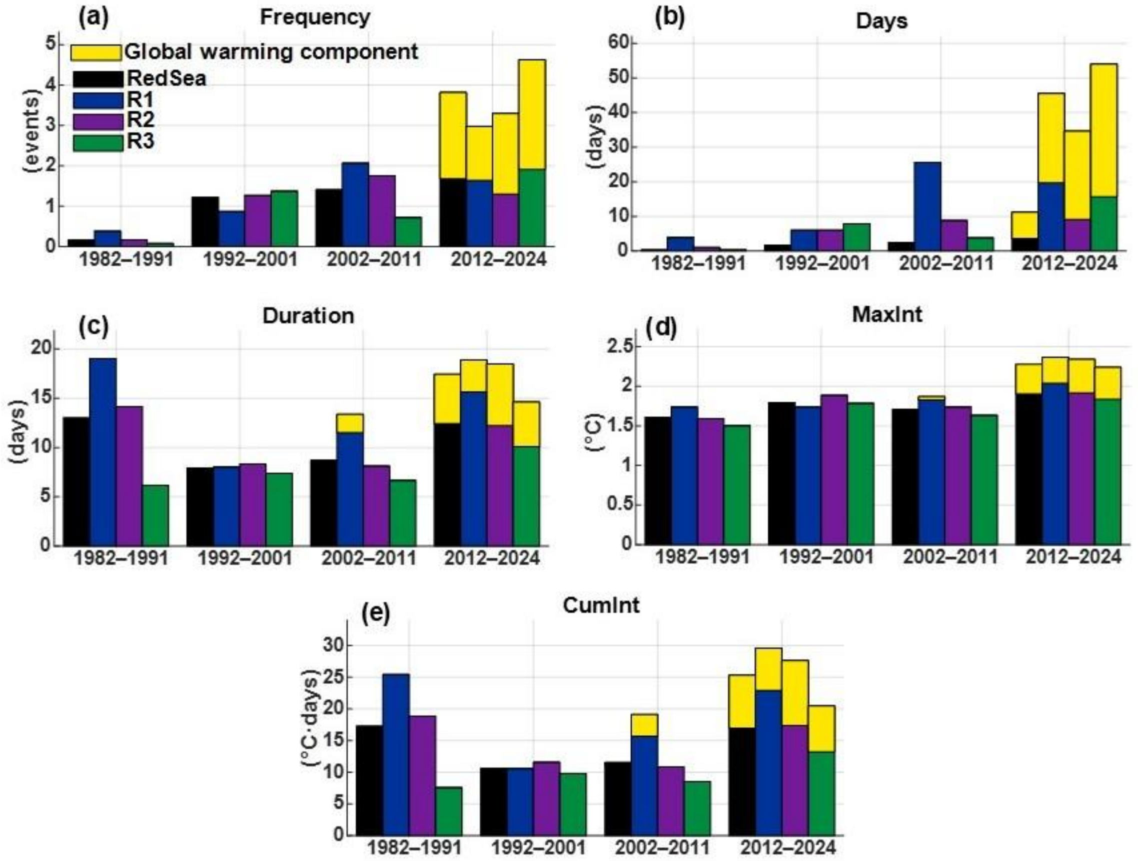

Figure 36. *Decadal averages (1982–1991, 1992–2001, 2002–2011, 2012–2024) of (a) MHW frequency (events/decade), (b) total MHW days (days/decade), (c) duration (days/decade), (d) maximum intensity (°C/decade), and (e) cumulative intensity (°C·days.decade^{-1}) for the entire Red Sea basin and its subregions (R1: NRS, R2: CRS, R3: SRS). Yellow bars represent the contribution of background warming to surface MHW amplification.*

4.2.2 Subsurface MHWs in the Mediterranean Sea:

The vertical structure and temporal evolution of subsurface MHWs in the MedS reveal a strongly surface-intensified system with progressively increasing vertical involvement over time (Fig. 37). Across all three subregions, MHW activity during the 1990s and early 2000s is mainly stronger in the upper 400 m, with limited penetration into deeper layers.

In the WMB (Fig. 37a-c), the subsurface MHW penetrates up to 600 m, and after 2014, the MHW signature was observed to reach depths of 900 m. A marked intensification occurs after 2011, when total MHW days increase sharply within the upper layer and occasionally reach depths of approximately 900 m, especially after 2017 (Fig. 37a). Mean MHW intensity in the surface layer (50-200 m) frequently exceeds 1.0 °C, while intermediate depths (200-500 m) typically show mean intensities of 0.3-0.8 °C, and deep layers (> 500 m) rarely exceed about 0.5 °C (Fig. 37b). Maximum MHW intensity is strongly amplified at the surface, often exceeding 2-3 °C in the upper 20 m during extreme years, especially in the last decade, while values at 200-500 m generally range between 1-2 °C and remain lower at greater depths (Fig. 37c). This pattern indicates both surface intensification and episodic deep vertical propagation during the most recent decade. Subsurface MHWs in the CMB exhibit a similar but more moderate evolution (Fig. 37d-f). During the early record, MHWs are mainly confined to the upper 300-500 m, with little sustained activity below 500 m. Between 2005 and 2014, enhanced activity becomes evident (i.e., more MHW days, higher intensities, and deeper positive anomaly extent), and several years after 2015 show penetration beyond 800 m. Overall, the CMB displays progressive vertical expansion of MHW activity during the last decade, though with fewer days and lower temperature anomalies than the WMB.

The EMB MHWs present a vertical structure characterized by a deeper MHW signature than in the WMB and CMB (Fig. 37g-i). The early years (i.e., 1990s) show a moderate MHW activity, less MHW days and lower intensities, compared with the other two basins. After around 2008 the EMB subsurface MHWs exhibits repeated multi-year high activity. Several events during the mid-to-late 2010s extend to 700-1000 m with longer durations and higher intensities, indicating deeper heat storage relative to the western and central basins. In the surface layer, mean intensity commonly ranges between 0.7-1.3 °C during strong years, while intermediate depths frequently reach up to 1 °C. Below 500 m, mean intensities remain modest (< 0.6 °C), but deep-reaching events occur more frequently than in WMB. Maximum intensities again exceed 2–3 °C near the surface and remain detectable (> 1 °C) at intermediate depths during major events.

When organized by layer, the Mediterranean subsurface MHW structure is dominated by the 0.5-400 m layer, which shows the largest increase in total MHW days and the strongest intensity amplification, especially after 2010. The 400-800 m layer exhibits progressive involvement during strong events across all subregions, with R3 showing the most sustained intermediate-depth engagement. Penetration below 800 m remains episodic and event-dependent, with substantially reduced intensity compared to upper layers. Overall, these results indicate that while Mediterranean MHWs are fundamentally surface-driven phenomena, the past decade has seen enhanced vertical expansion and increased intermediate-depth involvement, particularly in the eastern basin.

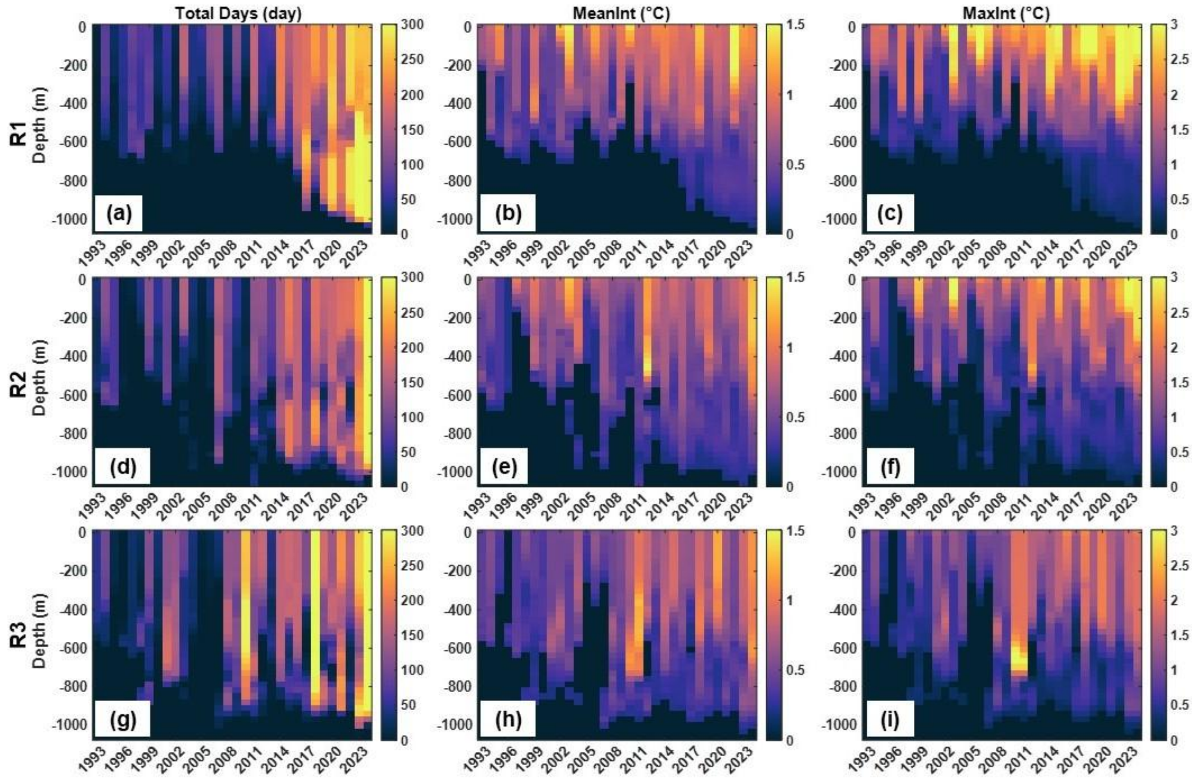

Figure 37. *Time–depth evolution of (left column) total MHW days (days), (middle column) mean intensity (°C), and (right column) maximum intensity (°C) for (a–c) WMB, (d–f) CMB, and (g–i) EMB. Depth (m) is shown on the vertical axis and year on the horizontal axis. The panels illustrate the temporal evolution of vertical penetration and intensity of subsurface MHWs across the Mediterranean sub-basins. The dark region indicates depths where temperature anomalies did not exceed the MHW threshold.*

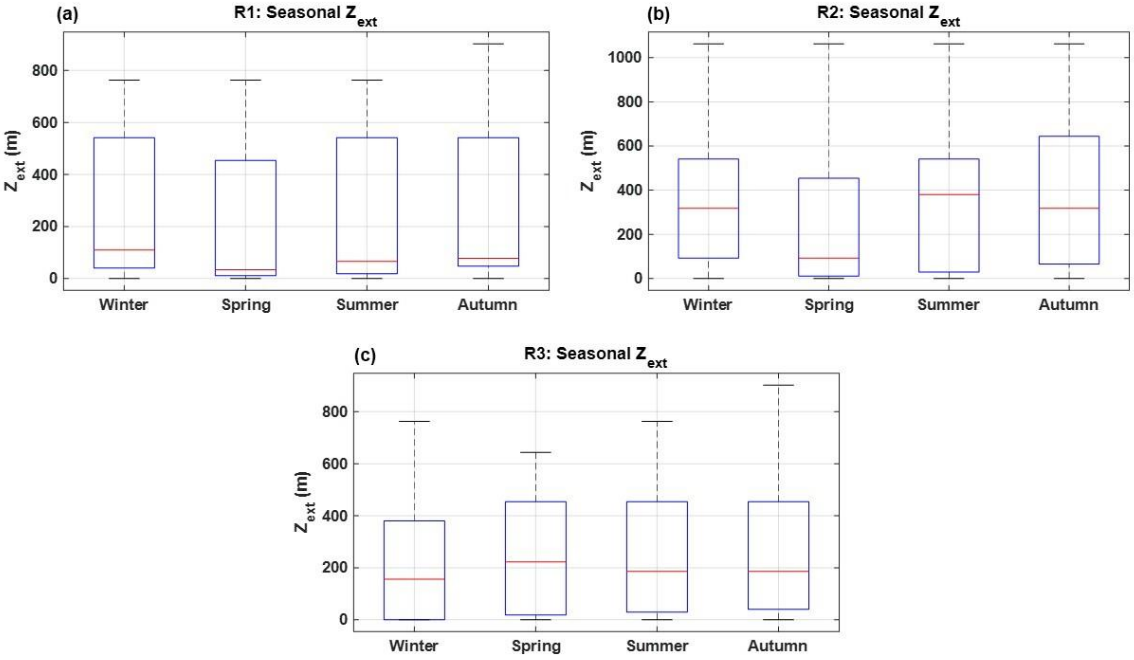

Figure 38. *Boxplots of seasonal Zext (m) for (a) WMB, (b) CMB, and (c) EMB during 1993–2024. Seasons are defined as winter (JFM), spring (AMJ), summer (JAS), and autumn (OND). Boxes indicate interquartile range, red lines show medians, whiskers represent the full data range excluding outliers.*

Seasonal distributions of average vertical maximum anomaly penetration depth (Zext) reveal subregional contrasts in subsurface MHW structure (Fig. 38). In the WMB (R1), median values remain relatively low throughout the year, generally below ~100 m, with slightly higher values in winter (~100 m) and autumn (~70–90 m), indicating predominantly shallow penetration depths with occasional deeper events reaching up to ~800–900 m (Fig. 38a). In the CMB (R2), median values are substantially higher, particularly during summer (~350–400 m) and autumn (~300–350 m), with a broad interquartile range and upper extremes exceeding ~1000 m, suggesting more frequent and deeper vertical extensions in this region (Fig. 38b). The EMB (R3) exhibits intermediate behaviour, with median values around ~150–220 m across seasons and relatively consistent variability, although slightly enhanced spread is observed during spring and summer (Fig. 38c). Across all regions, long upper whiskers indicate the occurrence of episodic deep-reaching events, especially during warmer seasons. Overall, these results highlight a marked eastward increase in both the magnitude and variability of Zext, with the CMB showing the deepest and most persistent vertical extensions compared to the WMB and EMB.

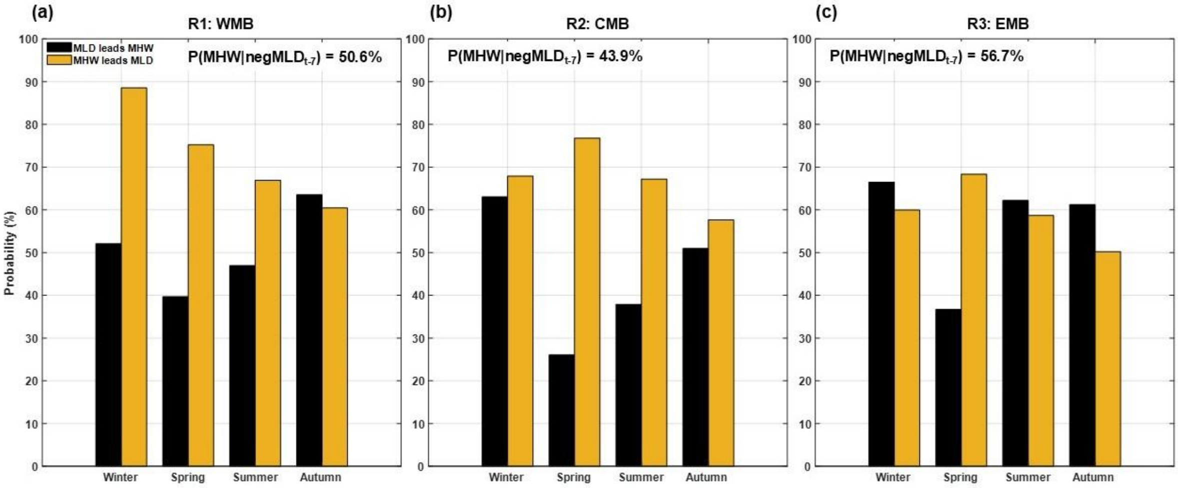

Figure 39. *Seasonal probability (%) that (black bars) MLD shoaling leads surface MHWs and (yellow bars) surface MHWs lead MLD shoaling by 7 days for (a) WMB, (b) CMB, and (c) EMB. The percentage shown above each panel indicates the conditional probability P(MHW | negative MLD anomaly at t-7). Results quantify the coupling between stratification changes and surface thermal extremes.*

To examine the role of stratification during Mediterranean MHWs, seasonal relationships between MLD anomalies and surface MHW onset were analysed (Fig. 39). In the WMB (Fig. 39a), the seasonal lead-lag analysis shows that, in most seasons, MHWs tend to occur before the mixed layer becomes anomalously shallow. In winter, spring, and summer, the probability that MHWs precede negative MLD anomalies is higher than the probability that shallow MLD anomalies precede MHWs. This suggests that surface warming during MHWs contributes to the shoaling of the mixed layer, rather than shallow mixed layers triggering MHWs. In autumn, the difference between the two probabilities is smaller, indicating a weaker and less systematic relationship between MHWs and MLD. Although these results show that in the WMB, MLD shoaling is more often a response to MHWs than an active factor enabling them, the probability of MLD shoaling within 7 days before MHWs is about 50% of all MHW events that occurred between 1993 and 2024.

In the CMB (Fig. 39b), the analysis shows that, in most seasons, MHWs tend to occur before the mixed layer becomes anomalously shallow. In winter, spring, and summer, the probability that MHWs precede negative MLD anomalies is higher than the probability that shallow MLD anomalies precede MHWs. This suggests that, similar to the WMB, MLD shoaling generally occurs as a response to MHWs rather than acting as a triggering factor. In autumn, the difference between the two probabilities is smaller, indicating a weaker and less consistent relationship between MHWs and MLD variability. The conditional probability of MLD shoaling within 7 days before MHWs onset is 43.9%. In the EMB (Fig. 39c), the analysis shows that, in most seasons, shallow MLD anomalies tend to occur before MHWs. In winter, summer, and autumn, the probability that negative MLD anomalies precede MHWs is higher, suggesting that stratification plays a more active role in enabling MHW development. In spring, however, the relationship is reversed, with MHWs more frequently preceding MLD shoaling, indicating that mixed layer changes may occur as a response to surface warming during this season. The conditional probability of MLD shoaling within 7 days before MHWs is 56.7% indicates that shallow mixed layer conditions are more often associated with the occurrence of MHWs in this basin. Overall, these results show a clear regional contrast, with MHWs generally preceding MLD shoaling in the WMB and CMB, while in the EMB, shallow mixed layer conditions more often precede MHWs, indicating a stronger role of stratification in MHW development in the eastern basin.

4.2.3 Subsurface MHWs in the Red Sea:

The vertical structure and temporal evolution of subsurface MHW characteristics in the RS reveal strong interannual variability and pronounced deep-reaching events, particularly after 2010 (Fig. 40). During the 1990s and early 2000s, MHW activity across all regions is higher in the upper 300-400 m, with limited penetration below 500 m. After approximately 2010, all regions show a clear increase in both the total number of days and the intensity of subsurface MHWs, with strong events reaching depths close to 800 m.

In the NRS (R1; Fig. 40a-c), subsurface MHWs are initially restricted to the upper 300-500 m, with weak and intermittent signals below this depth. However, after about 2010, several strong years show pronounced vertical penetration, with events extending to around 800 m and the highest number of MHW days occurring particularly around 2010, 2017-2018, and after 2021 (Fig. 40a). The mean intensity of NRS subsurface MHWs is about 1 °C, while during peak years it exceeds 1.5 °C (Fig. 40b). Maximum intensity exceeds 2 °C near the surface and frequently remains above 1-2 °C down to approximately 400-500 m during strong events (Fig. 40c), indicating episodic but significant deep-reaching anomalies. In the CRS (R2; Fig. 40d-f), subsurface MHW activity shows a similar vertical structure compared to the NRS but with less intense anomalies.

The SRS (R3; Fig. 40g-i) exhibits the deepest and most persistent subsurface MHW signal among the three regions. While early years show moderate activity mostly above 400-500 m, a strong intensification occurs after about 2010, with frequent events extending to around 800 m (Fig. 40g). Several years during the mid-to-late 2010s and early 2020s display sustained high MHW days across the water column. The SRS subsurface MHW mean intensity typically ranges between 0.8 and 1.2 °C. Notably, deeper layers (> 500 m) in 2000-2001 and after 2014 show relatively high mean intensities, often reaching about 1.5 °C, which is higher and more persistent than in the NRS and CRS (Fig. 40h). Moreover, the maximum intensity exceeds 2.5 °C in the deep layer during the same years (Fig. 40i), indicating strong deep subsurface involvement and sustained heat storage. When organized by depth, subsurface MHWs in the Red Sea show the strongest increase in total MHW days and intensity after 2010. The 400–600 m layer exhibits consistent and sustained involvement across all regions, particularly in the southern basin, which shows higher and more persistent intensities, indicating greater subsurface heat storage in the SRS.

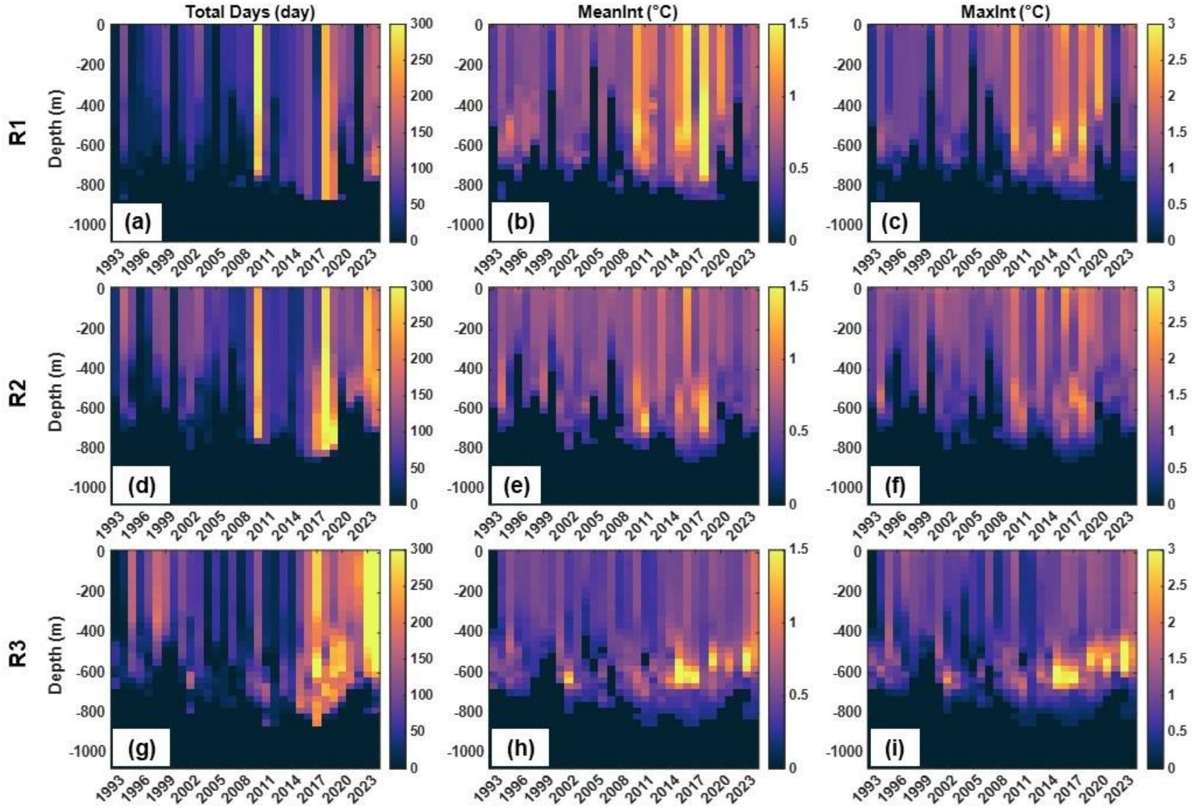

Figure 40. *Depth–time evolution of subsurface MHW metrics averaged over the three Red Sea subregions: Northern Red Sea (NRS; R1), Central Red Sea (CRS; R2), and Southern Red Sea (SRS; R3). Columns show (a,d,g) total MHW days (days), (b,e,h) mean intensity (°C), and (c,f,i) maximum intensity (°C). Rows correspond to R1-R3. Annual metrics are calculated at each depth relative to the 1993-2022 baseline. The dark region indicates depths where temperature anomalies did not exceed the MHW threshold.*

The seasonal distribution of Zext in the Red Sea shows clear regional variability and moderate seasonal dependence across the three sub-basins (Fig. 41). In the NRS (R1; Fig. 41a), median values remain relatively consistent across seasons, generally around 120-160 m, with slightly higher values in spring and autumn. The interquartile range is largest in spring, indicating increased variability during this season, while winter and summer show a more moderate spread. Upper extremes frequently exceed 300-500 m in all seasons, reflecting episodic deep-reaching events. In the CRS (R2; Fig. 41b), median values are generally lower than in the NRS, ranging between 60-110 m, with the highest values observed in winter and lower values during summer. The variability is relatively consistent across seasons, although spring and summer exhibit slightly broader distributions. Extreme values reach 500 m in all seasons, indicating that deep penetration occurs intermittently but without a strong seasonal preference.

The SRS (R3; Fig. 41c) displays median values between 70-110 m, with slightly higher values in summer. The interquartile range is relatively uniform across seasons, suggesting limited seasonal contrast in variability. However, frequent high outliers exceeding 400-500 m indicate recurrent deep-reaching events throughout the year, particularly during winter, summer, and autumn. Overall, the seasonal variability of Zext in the Red Sea is less pronounced than in the Mediterranean Sea, with relatively consistent median values across seasons in all regions. However, deep-reaching events remain a persistent feature across all sub-basins, particularly in the NRS and SRS, indicating that episodic vertical penetration occurs throughout the year rather than being strongly seasonally constrained.

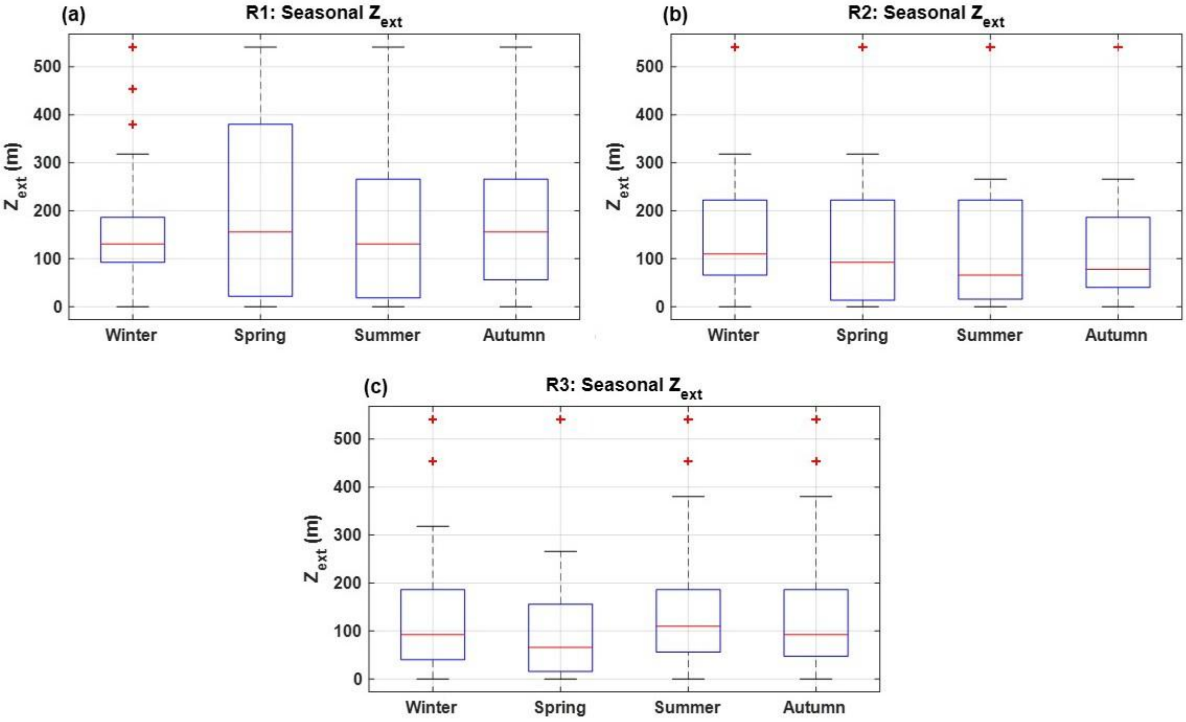

Figure 41. *Boxplots of seasonal Zext (m) for (a) NRS, (b) CRS, and (c) CRS during 1993-2024. Seasons are defined as winter (JFM), spring (AMJ), summer (JAS), and autumn (OND). Boxes indicate interquartile range, red lines show medians, whiskers represent the full data range excluding outliers.*

The role of seasonal variability in the MLD negative anomaly during Red Sea MHWs was analyzed and is shown in Figure 42. In the NRS (Fig. 42a), the seasonal lead-lag analysis shows that, in all seasons, MHWs tend to occur before the mixed layer becomes anomalously shallow, and the shoaling of the MLD is more likely to be caused by the occurrence of MHWs. The probability that the negative MLD anomaly precedes the onset of MHWs is about 37% of all MHW events that occurred between 1993 and 2024. This indicates that surface warming associated with MHWs contributes to mixed layer shoaling, rather than stratification acting as the primary triggering mechanism. In the CRS (Fig. 42b), the relationship between shallow MLD and MHW onset is more balanced in all seasons except in spring, when the difference between the two probabilities is higher. The conditional probability of MLD shoaling within 7 days before MHWs is about 50%. In the SRS (Fig. 42c), shallow MLD anomalies more often precede MHWs compared with the other two basins. In winter and autumn, the probability that negative MLD anomalies precede MHWs (approximately 55-60%) exceeds the probability that MHWs lead to MLD shoaling, indicating that stratification plays a more active role in enabling MHW development. Overall, the conditional probability of MLD shoaling within 7 days before MHWs is about 55.7%, which further supports the importance of preconditioning by shallow mixed layers in the southern basin.

In summary, these results reveal a clear north–south gradient in the role of stratification, with MLD shoaling primarily acting as a response to MHWs in the NRS, a more coupled interaction in the CRS, and a stronger preconditioning role of shallow MLD in the SRS.

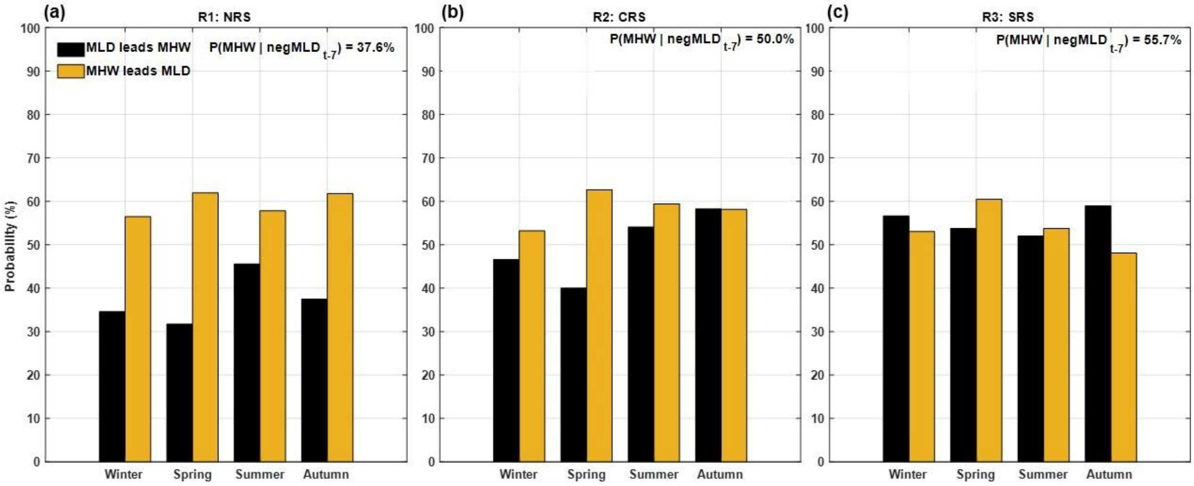

Figure 42. Seasonal probability (%) that (black bars) MLD shoaling leads surface MHWs and (yellow bars) surface MHWs lead MLD shoaling by 7 days for (a) NRS, (b) CRS, and (c) SRS. The percentage shown above each panel indicates the conditional probability P(MHW | negative MLD anomaly at t-7). Results quantify the coupling between stratification changes and surface thermal extremes.

4.2.4 Basin-Scale Comparison of Subsurface MHWs:

The interannual variability of basin-averaged maximum subsurface MHW penetration, calculated as the average of the sub-basins in each sea, reveals distinct temporal evolution in the Mediterranean Sea and the Red Sea (Fig. 43). During the 1990s and early 2000s, both basins show relatively shallow penetration depths, generally below approximately 400-600 m, with strong year-to-year variability. After about 2008-2010, both regions exhibit a marked increase in penetration depth. In the Mediterranean Sea, maximum penetration increases progressively, with several years exceeding approximately 900 m and reaching about 1000-1100 m after 2015. These deep-reaching values persist in most years from around 2016 onward, indicating sustained vertical expansion of MHWs. In the Red Sea, deep penetration also increases after about 2010, with several years, particularly around 2010-2012 and 2016-2018, exceeding approximately 1000 m. However, unlike the Mediterranean, these deep events are not sustained. After about 2019-2020, penetration depth decreases to approximately 300-700 m, indicating a reduction in deep-reaching events in recent years. Throughout the record, the Red Sea shows stronger interannual variability, with large fluctuations between shallow and deep penetration years.

Overall, both basins show a transition toward deeper subsurface MHW penetration after about 2010, but the Mediterranean Sea is characterized by sustained deep-reaching conditions in recent years, whereas the Red Sea exhibits intermittent deep events and higher interannual variability. This contrast indicates differences in the persistence of subsurface heat storage between the two basins.

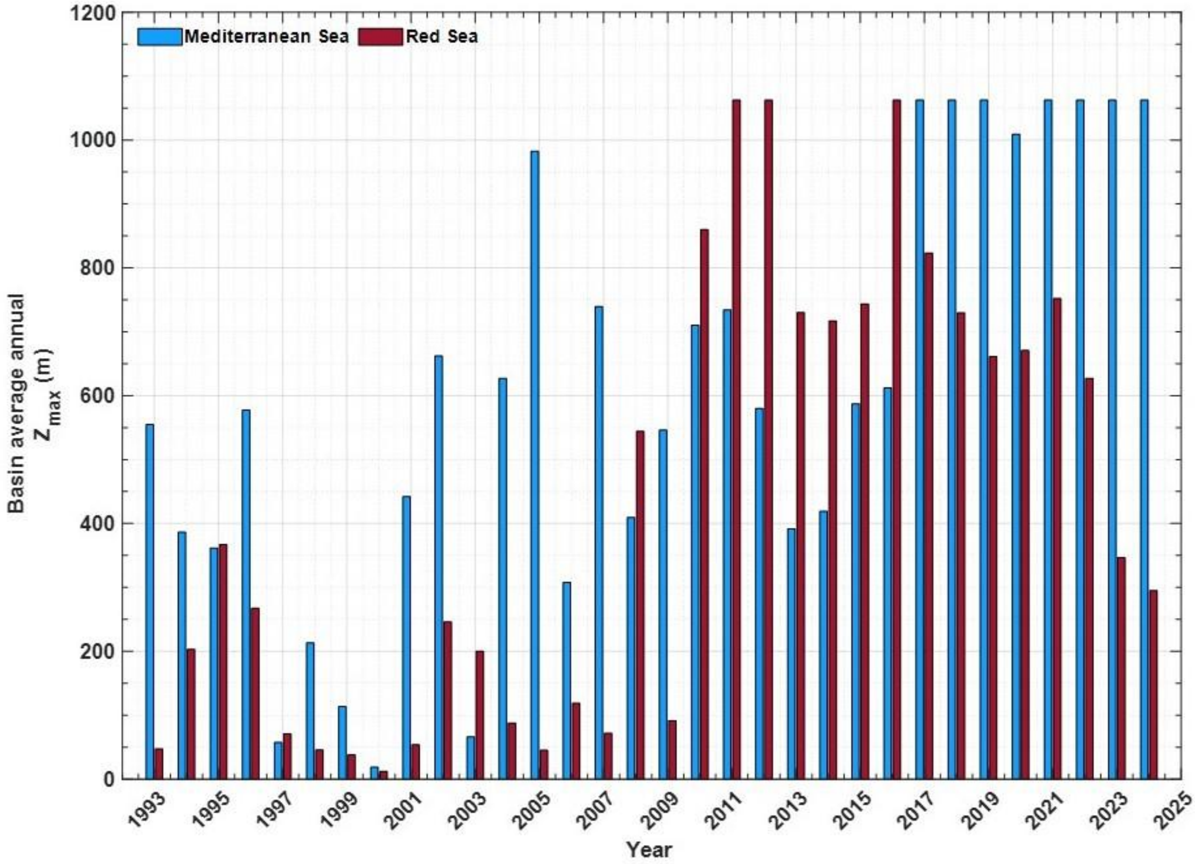

Figure 43. *Basin-mean annual maximum penetration depth (Zmax, m) of subsurface MHWs in the Mediterranean Sea (blue) and Red Sea (red) from 1993 to 2024.*

The long-term trends in subsurface MHW total days and mean intensity reveal distinct depth-dependent and regional patterns in both the Mediterranean Sea (Table 2) and the Red Sea (Table 3). In the Mediterranean, trends in MHW days are positive and statistically significant across most depths and subregions, with the strongest increases generally observed in the upper ocean. In the 0-50 m layer, trends range from approximately 44.8 to 57.8 days/decade across the WMB, CMB, and EMB, while in the 50-200 m layer, increases remain substantial (up to about 65.6 days/decade in the WMB). At intermediate depths (200-500 m), significant increases are observed in the CMB and EMB (about 58.0 and 51.5 days/decade), whereas the WMB shows no increase at this depth. In the deep layer (500-1100 m), trends remain positive and significant in the WMB and CMB, particularly in the CMB (about 64.7 days/decade), indicating enhanced deep-layer involvement. Trends in mean intensity are more heterogeneous, with modest positive values in most layers, particularly at depth in the WMB (about 0.092 °C/decade), while some negative trends appear in the upper layers (50-200 m) of the CMB and EMB, suggesting a redistribution of heat rather than uniform intensification.

In the Red Sea, trends in MHW days are also positive and significant but exhibit stronger regional contrasts. In the surface layer (0-50 m), increases range from about 21.1 days/decade in the NRS to about 44.2 days/decade in the SRS. The most pronounced increase occurs in the 50–200 m layer of the SRS (about 71.3 days/decade), indicating strong subsurface amplification in the southern basin. At intermediate depths (200-500 m), significant increases are observed mainly in the CRS (~50.6 days/decade), while the NRS and SRS show minimal changes. In the deep layer (500-1100 m), a significant increase is only evident in the CRS (~35.7 days/decade), whereas the NRS and SRS show no trend. Mean intensity trends in the Red Sea display a clear vertical and regional contrast, with strong positive trends in the SRS upper and intermediate layers (up to about 0.282 °C/decade), indicating substantial warming, while negative trends appear in deeper layers, particularly in the SRS (-0.319 °C/decade), suggesting reduced intensity in this layer.

Overall, both basins exhibit increasing MHW activity, but their vertical structures differ. The Mediterranean Sea shows a more vertically coherent intensification, with significant increases in MHW days extending from the surface to deep layers across multiple subregions, indicating sustained vertical expansion of MHWs. In contrast, the Red Sea displays a more heterogeneous structure, with strong increases concentrated in specific regions (notably the SRS and CRS) and limited or absent trends at depth in the NRS. Additionally, intensity trends in the Mediterranean are relatively moderate and spatially consistent, whereas the Red Sea shows stronger surface and intermediate warming but contrasting negative trends at depth, especially in the SRS. These differences indicate that subsurface MHW evolution in the Mediterranean is characterized by widespread and persistent vertical intensification, while in the Red Sea it is more regionally constrained and depth-dependent, reflecting differences in basin-scale circulation, stratification, and heat storage processes.

Table 2. *Linear trends in subsurface MHW total days (days/decade) and mean intensity (°C/decade) for the three Mediterranean subregions. Asterisks indicate statistically significant trends ($p < 0.05$).*

	Trend of the MHW Days (days/decade)			Trend of the MHW Intensity (°C/decade)		
Depth (m)	**WMB**	**CMB**	**EMB**	**WMB**	**CMB**	**EMB**
0–50	57.84*	44.81*	47.89*	0.087	0.042	0.016
50–200	65.62*	43.58*	32.47*	- 0.017	- 0.074	- 0.050
200–500	0.0*	58.01*	51.53*	0.098	0.027	0.067*
500–1100	5.92*	64.72*	28.97	0.092*	0.067	0.033

Table 3. *Linear trends in subsurface MHW total days (days/decade) and mean intensity (°C/decade) for the three Red Sea subregions. Asterisks indicate statistically significant trends ($p < 0.05$).*

	Trend of the MHW Days (days/decade)			Trend of the MHW Intensity (°C/decade)		
Depth (m)	**NRS**	**CRS**	**SRS**	**NRS**	**CRS**	**SRS**
0–50	21.14*	25.0*	44.19*	0.08	0.034	0.154*
50–200	6.75*	15.23*	71.27*	- 0.005	0.1	0.282*
200–500	0.0*	50.62*	5.0*	0.027	- 0.018	0.018
500–1100	0.0*	35.71*	0.0*	0.142	- 0.058	- 0.319*

4.3 Discussion:

The results show that both the Mediterranean Sea and the Red Sea have experienced a marked increase in surface MHW activity during the satellite era, with the strongest rise occurring after 2010, especially in the most recent decade. In both basins, the decomposition of MHW metrics indicates that this increase is primarily linked to long-term background warming, while internal variability modulates the year-to-year expression of events. This interpretation aligns with Denaxa et al., (2025), who found that the recent intensification of Mediterranean surface MHWs is largely explained by the long-term warming trend, with internal variability acting mainly as a regional modulator rather than the dominant cause of the observed increase.

Within the Mediterranean, the subregional contrasts identified here are consistent with previous studies. The stronger increase in maximum intensity in the western Mediterranean and the stronger increase in duration and cumulative exposure in the eastern Mediterranean match the subregional analysis of Juza et al., (2022) and Hamdeno and Alvera-Azcaráte, (2023), who reported that surface MHWs have accelerated across the basin, with marked regional differences in frequency, intensity, and duration. Their study also showed that the eastern Mediterranean tends to experience longer events, while more intense surface anomalies are often observed in western sectors.

The subsurface results demonstrate that recent MHW intensification is not limited to the surface but increasingly involves the upper and intermediate water column in both seas. In the Mediterranean, subsurface MHWs remain clearly surface intensified, yet the last decade is characterized by stronger downward propagation, with recurrent events reaching below 800 m and, in some years, approaching 1000 m. This is consistent with Juza et al., (2022), who showed that Mediterranean MHWs propagate below the surface with strong subregional and seasonal variability, and that vertical penetration can be much deeper in eastern sectors than in the western basin. It also aligns with the synthesis of Darmaraki et al., (2024), who emphasized that Mediterranean subsurface MHWs are often longer-lived than their surface expression, can exhibit strong spatial heterogeneity, and depend strongly on stratification, mixed-layer depth, wind-driven mixing, and vertical redistribution processes.

These results refine the Mediterranean picture by showing that the western basin is characterized by stronger near-surface intensity, whereas the eastern basin exhibits more persistent deep involvement and more frequent heat storage below 500 m. The penetration-depth analysis supports this contrast: Zext remains relatively shallow in the WMB, while the CMB and EMB show deeper and more variable vertical extension. This pattern supports the idea that deep Mediterranean subsurface MHW structure is influenced not only by surface warming magnitude but also by regional oceanographic setting, including stratification strength and circulation. This interpretation is consistent with Juza et al., (2022) and the broader Mediterranean review by Darmaraki et al., (2024).

The mixed-layer-depth lead-lag analysis further clarifies the role of stratification in the Mediterranean. In the WMB and CMB, MHWs more often occur before MLD shoaling, suggesting that mixed-layer shallowing is frequently a response to surface warming rather than a primary trigger. In contrast, in the EMB, negative MLD anomalies more often precede MHW onset, indicating a stronger preconditioning role of stratification in the eastern basin. This result corresponds with the deeper and more persistent subsurface signal observed in the EMB, and it agrees with Juza et al., (2022) and Darmaraki et al., (2024), who showed that MHWs enhance upper-ocean stratification and that the vertical response varies substantially among Mediterranean.

In the Red Sea, the vertical structure differs from the Mediterranean in an significant way. Although Red Sea subsurface MHWs are also surface intensified, the southern basin exhibits the deepest and most persistent subsurface signal, with relatively high mean and maximum intensities below 500 m and repeated deep-reaching events after 2010. This finding is consistent with Nadimpalli et al., (2025), who showed that subsurface marine heat anomalies in the southern Red Sea can be strongly influenced by remote forcing from the Gulf of Aden, and that subsurface heat-content anomalies down to 100 m help explain the severity of coral bleaching more effectively than SST alone. Their heat-budget analysis indicated that advection from the southern boundary is a primary heat source, implying that Red Sea subsurface MHW behaviour cannot be interpreted solely through local surface forcing.

The MLD analysis in the Red Sea also supports a north–south gradient in the role of stratification. In the NRS, MLD shoaling generally follows MHW onset, indicating that mixed-layer adjustment is mainly a response to warming. In the SRS, however, shallow MLD anomalies more often precede MHW onset, implying that upper-ocean stratification more clearly acts as a preconditioning factor. The CRS shows a more balanced interaction between the two processes. These results suggest that Red Sea subsurface MHW development becomes increasingly controlled by retained subsurface heat and stratification toward the southern basin. This interpretation is compatible with the regional mechanism proposed by Nadimpalli et al., (2025), in which subsurface heat anomalies and their advection into the southern Red Sea are critical for extreme warm events.

The basin-scale comparison highlights a clear distinction between the two seas. Both basins show a transition toward deeper subsurface MHW penetration after about 2010, but the Mediterranean exhibits more sustained deep penetration after 2015, whereas the Red Sea shows stronger interannual variability and more episodic deep-reaching years. This contrast is also reflected in the trend analysis. In the Mediterranean, positive trends in MHW days extend from the surface to the deep layer across most subregions, indicating a vertically coherent expansion of MHW activity. In the Red Sea, by contrast, the strongest increases are concentrated in the SRS and CRS, while deep-layer trends are weak or absent in NRS. Similarly, Mediterranean intensity trends are generally moderate but vertically consistent, whereas the Red Sea shows stronger positive trends in upper and intermediate layers combined with contrasting negative trends at depth, especially in the SRS. Overall, these differences suggest that the Mediterranean is undergoing a broader basin-scale vertical intensification, while the Red Sea response is more regionally focused and strongly influenced by southern-basin heat storage and remote forcing. This interpretation is consistent with Denaxa et al., (2025) for the role of warming in the Mediterranean, Juza et al., (2022) for the heterogeneous vertical response in the Mediterranean, and Nadimpalli et al., (2025) for the southern Red Sea subsurface mechanism.

Finally, the ecological relevance of these physical results should be emphasized. In the Mediterranean, the increasing vertical persistence of MHWs implies longer thermal exposure of subsurface ecosystems and stronger stratification effects on nutrient supply and biogeochemical exchanges. This is important because recent ecosystem modelling in the western Mediterranean by Artana et al., (2026) showed that MHWs can exacerbate long-term biomass declines and alter food-web structure beyond the effects of gradual warming alone. While that study focuses on ecosystem response rather than vertical heat structure, it reinforces the idea that the increasing persistence and downward propagation of thermal extremes found here are likely to have ecological consequences that extend well beyond the sea surface.

4.4 Conclusion:

This study provides a comprehensive assessment of MHWs in two climatically distinct but rapidly warming semi-enclosed basins, the Mediterranean Sea and the Red Sea, with a particular focus on their subsurface structure. The results demonstrate that MHWs have intensified significantly in both regions over recent decades, with a marked acceleration after 2010. This intensification is largely driven by long-term background warming, while internal variability modulates the timing and regional expression of extreme events.

Beyond surface warming, the analysis reveals that MHWs are three-dimensional phenomena, with enhanced vertical propagation into the subsurface ocean. In the Mediterranean Sea, MHWs exhibit a surface-intensified structure but show progressive and sustained deepening, particularly in the eastern basin, where there is persistent subsurface heat storage. In contrast, the Red Sea displays a more heterogeneous and regionally constrained response, with the southern basin showing the strongest subsurface intensification and deep heat storage, while the northern basin remains more in the near surface layer.

The role of stratification further highlights key regional differences. In the Mediterranean, stratification acts as a response to surface warming. In the Red Sea, a clear north-south gradient emerges, with stratification playing a dominant preconditioning role in the southern basin. These results emphasize the importance of mixed-layer dynamics and vertical heat redistribution in controlling the development and persistence of subsurface MHWs.

Overall, this study shows that while both basins are experiencing increasing MHW intensity and vertical expansion, the underlying mechanisms differ. The Mediterranean is characterized by basin-wide, persistent vertical intensification, whereas the Red Sea exhibits stronger regional variability and a greater influence of subsurface heat storage and remote forcing. These findings highlight the need to consider the full three-dimensional structure of MHWs when assessing their physical dynamics and potential ecological impacts, particularly in semi-enclosed seas that are highly sensitive to climate change.

Chapter Five: Drivers of MHWs in the Mediterranean and Red Sea

Foreword

This chapter investigates the physical drivers and mechanisms governing MHWs in the Mediterranean Sea and the Red Sea. While previous research has documented the increasing frequency and intensity of MHWs, the relative roles of atmospheric forcing and oceanic processes remain regionally dependent and not fully resolved, particularly in semi-enclosed basins with contrasting dynamics.

The primary objective of this chapter is to identify and quantify the drivers of MHW occurrence using a combination of composite analysis, upper-ocean diagnostics, and statistical modelling. By examining atmospheric conditions, air-sea heat fluxes, and subsurface ocean properties across different subregions, this study evaluates how MHWs are initiated, intensified, and sustained.

A key focus is the comparison between basins and subregions, including the Western and Eastern Mediterranean, as well as the Northern and Southern Red Sea. These regions exhibit distinct oceanographic and atmospheric characteristics, allowing for a systematic assessment of how local processes and large-scale conditions influence MHW dynamics.

This chapter contributes to the overall objectives of the thesis by linking surface and subsurface processes to the occurrence of MHWs and by providing a unified framework to interpret their drivers across different environments. The results offer new insights into the relative importance of atmospheric variability and oceanic heat storage in shaping MHW behaviour.

This research is currently being **prepared for submission to a peer-reviewed journal**.

5.1 Data and Methods:

5.1.1 SST data and MHW detection:

SST is obtained from the NOAA Optimum Interpolation SST version-2 (OISST v2) dataset, which combines satellite and in situ observations on a 0.25° grid with daily resolution (Reynolds et al., 2007).

MHWs are identified following the Hobday et al., (2016) framework, as explained in the previous chapters, relative to the 1993-2022 climatology. To assess the contribution of long-term warming, the linear SST trend is removed at each grid point using least-squares regression (Wilks, 2019). MHWs are then detected in both raw and detrended SST datasets, and the warming contribution is quantified as the difference between the two, following established approaches (Oliver et al., 2018b; Laufkötter et al., 2020). The MHWs calculations covers the period 1982-2024 and for the drivers analysis it covers 1993-2024 (the overlap period with the available oceanic variables).

5.1.2 Atmospheric Forcing:

Atmospheric variables are obtained from the ERA5 reanalysis produced by the European Centre for Medium-Range Weather Forecasts (ECMWF) (Hersbach et al., 2020). The dataset has a spatial resolution of 0.25° × 0.25°, and hourly fields are averaged to daily values. The atmospheric variables include 10 m wind components (U10, V10), 2m air temperature (Tair), 2m dew point temperature (d2m), mean sea level pressure (MSLP), shortwave radiation (Qs), longwave radiation (Qb), sensible heat flux (Qh), latent heat flux (Qe), and total cloud cover (TCC). These variables represent the main processes controlling air-sea heat exchange and upper-ocean forcing.

All atmospheric variables are expressed as daily anomalies relative to the 1993-2022 climatology, allowing consistent comparison across seasons and regions. Net surface heat flux (THF) and relative humidity (RH) are computed following the formulations described in Chapter 3 (Alduchov and Eskridge, 1996; Thomson and Emery, 2014; Nagy et al., 2017, 2021; Bawadekji et al., 2022). To investigate the role of atmospheric forcing in MHW development, composite analyses are performed by aligning all detected MHW events relative to their peak intensity. For each event, anomaly time series are extracted within a ±30 day window centred on the event peak, representing the temporal evolution of atmospheric conditions. Three phases are defined:

- **Pre-event phase**: -30 to -1 days before the event peak (preconditioning).
- **Peak phase**: day of maximum intensity.
- **Post-event phase**: +1 to +30 days after the event peak (decay).

Composite mean time series are computed across all events for each region and season. In addition, spatial composite maps are constructed to characterize the structure of anomalies during key stages of MHW evolution:

- **Pre-onset phase** (-5 to -1 days before event start).
- **Event phase** (event duration).
- **Decay phase** (+1 to +5 days after event end).

These composites allow identification of large-scale atmospheric patterns associated with MHW initiation, development, and decay.

5.1.3 Oceanic Processes and Upper Ocean Heat Content:

Subsurface temperatures and mixed layer depth (MLD) fields are obtained from the Copernicus Marine Service Global Ocean Reanalysis product GLORYS12V1 (Jean-Michel et al., 2021), which provides daily data at (~8 km) horizontal resolution. In this study, the upper 500 m of the water column are analysed. All data are interpolated to a common 0.25° grid. Oceanic variables are expressed as anomalies relative to the 1993-2022 climatology. The analysis focuses on upper-ocean processes controlling heat storage and vertical mixing.

Upper-ocean heat content is calculated as the vertical integral of temperature anomalies, providing a measure of subsurface heat storage (Levitus et al., 2012; Cheng et al., 2019). In addition, mean subsurface temperature anomalies and warm layer thickness are computed to characterize the intensity and vertical extent of warm anomalies. Oceanic composite analyses are performed using the same temporal and spatial framework as for atmospheric variables, allowing direct comparison between atmospheric forcing and oceanic preconditioning during MHW evolution.

5.1.4 Attribution of Atmospheric and Oceanic Contributions:

To quantify the relative roles of atmospheric and oceanic forcings to the occurrence of MHWs, standardized indices are constructed by combining key variables from each driver family. The atmospheric contribution index integrates anomalies in surface heat flux, wind speed, air temperature, and mean sea level pressure, capturing conditions that enhance surface heat input and suppress mixing. The oceanic contribution index combines mixed layer depth and upper-ocean heat content anomalies, representing stratification and subsurface heat storage.

Logistic regression is used to model the probability that a given day belongs to a MHW event as a function of these indices (Hosmer et al., 2013). All predictors are standardized prior to model fitting to allow direct comparison of their effects. Model performance is evaluated using the area under the receiver operating characteristic (ROC) curve (AUC), which provides a threshold-independent measure of the model's ability to discriminate between MHW and non-MHW days (Fawcett, 2006).

The relative importance of atmospheric and oceanic drivers is assessed using two complementary approaches. First, regression coefficients are expressed as odds ratios, quantifying how variations in each predictor influence the likelihood of MHW occurrence. Second, permutation importance analysis is applied by randomly perturbing each predictor and measuring the resulting decrease in model performance (AUC). This provides a robust estimate of the contribution of each driver family to MHW occurrence.

5.2 Results and discussion:

5.2.1 Contribution of Long-Term Warming to MHW Occurrence:

The contribution of long-term warming to MHW occurrence shows clear spatial and temporal intensification in both the Mediterranean Sea and the Red Sea (Figs. 44-45). In the

Mediterranean (Fig. 44a-b), the fraction of MHW days enabled by warming displays a pronounced eastward gradient, with values generally below ~30-40% in the Western Mediterranean and exceeding ~50-60% in the Eastern Mediterranean, particularly in the Levantine basin. A similar spatial pattern appears for the fraction of events dominated by warming, indicating that long-term temperature trends play a stronger role in controlling both the frequency and persistence of MHWs in the eastern basin compared to the west.

The temporal evolution further highlights the increasing importance of warming (Fig. 44c). Prior to ~2005, MHW variability is largely driven by internal variability, with warming contributing only a minor fraction of total MHW days. However, after ~2010, the warming-enabled component increases rapidly and becomes the dominant contribution in most years, especially after 2015. The most recent years (2020-2024) are almost entirely dominated by warming-driven MHW days, indicating a transition toward a regime in which background warming controls the occurrence of extreme events.

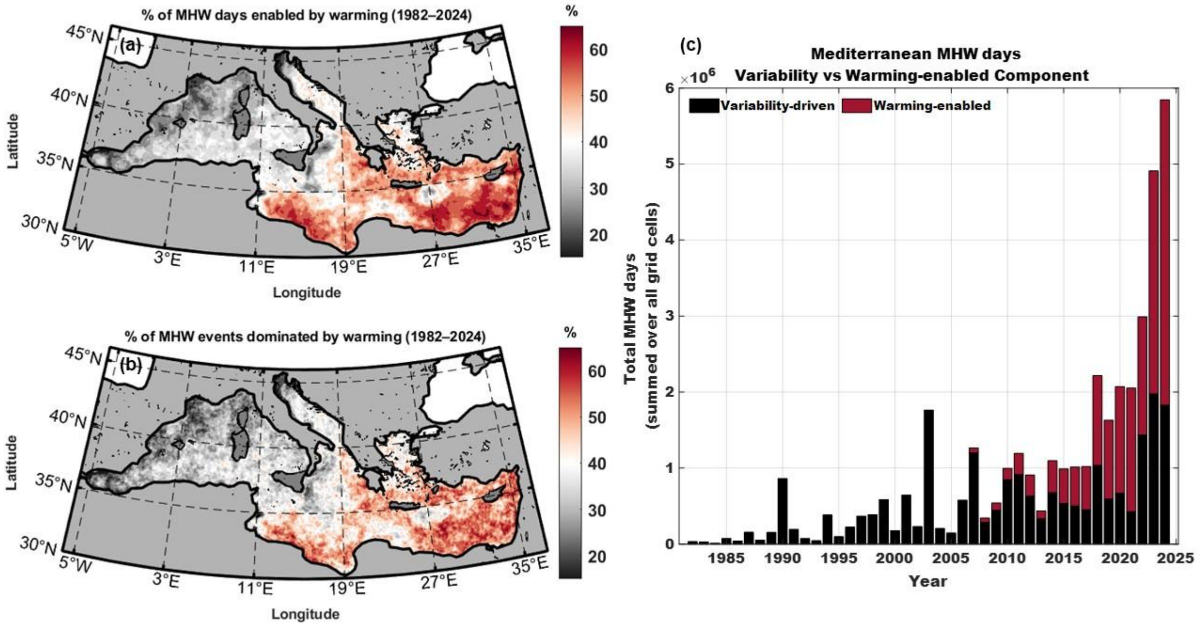

Figure 44. *The spatial distribution of the percentage of MHW days enabled by long-term warming (a) and the percentage of MHW events dominated by warming (b) over the period 1982–2024, together with the temporal evolution of total Mediterranean MHW days decomposed into variability-driven and warming-enabled components (c).*

These results are consistent with previous studies showing that long-term SST warming is the primary driver of increasing MHW activity in the Mediterranean. Simon et al., (2023) demonstrated that mean warming explains most of the increase in summer MHW activity, while interannual variability plays a secondary role, particularly in the western basin. Similarly, Denaxa et al., (2025) reported that warming dominates the increase in MHW days and cumulative intensity across most of the basin, with a stronger contribution in the eastern Mediterranean. The eastward increase in warming contribution identified here also aligns with studies linking enhanced stratification and reduced heat loss in the eastern basin to more persistent and longer MHWs (Juza et al., 2022; Hamdeno and Alvera-Azcaráte, 2023).

In the Red Sea (Fig. 45), the contribution of warming also shows a clear spatial gradient, but with a distinct north-south structure. The fraction of MHW days enabled by warming increases from ~30-40% in the northern basin to more than ~60-80% in the southern Red Sea. A similar pattern is observed for warming-dominated events, indicating that long-term warming exerts a stronger control on MHW occurrence in the southern basin.

The temporal evolution (Fig. 45c) reveals a marked shift after ~2010. Before this period, MHW occurrence is primarily driven by internal variability, with intermittent peaks associated with individual events. After ~2015, however, the warming-enabled component increases rapidly and becomes dominant in most years, with particularly strong amplification in the early 2020s.

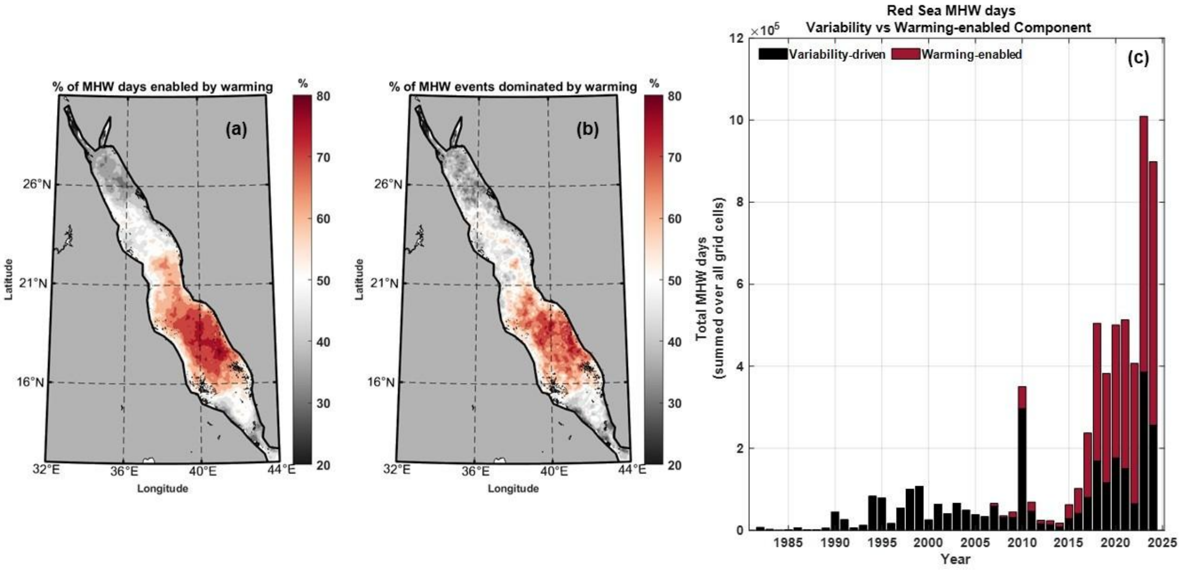

Figure 45. *The spatial distribution of the percentage of MHW days enabled by long-term warming (a) and the percentage of MHW events dominated by warming (b) over the period 1982-2024, together with the temporal evolution of total Red Sea MHW days decomposed into variability-driven and warming-enabled components (c).*

Although there are no studies yet have explicitly quantified the contribution of warming to Red Sea MHWs using a detrending framework, the present results are consistent with previous findings of rapid basin-wide warming and increasing MHW activity (Mohamed et al., 2021; Hamdeno et al., 2024). The stronger warming contribution in the southern Red Sea also consistent with studies highlighting enhanced subsurface heat storage and the role of advective processes in sustaining extreme events in this region (Nadimpalli et al., 2025).

In summery, both basins exhibit a clear transition toward warming-dominated MHW regimes over the past decade. However, the Mediterranean shows a more spatially coherent increase in warming contribution, particularly toward the eastern basin, whereas the Red Sea displays stronger regional contrasts and higher interannual variability. These differences reflect the distinct oceanographic and atmospheric conditions of the two basins, with the Mediterranean responding more uniformly to long-term warming, while the Red Sea remains more strongly influenced by regional circulation and subsurface processes.

5.2.2 Drivers of MHWs in the Western Mediterranean:

The drivers of MHWs in the Western Mediterranean consistently evolve from atmospheric preconditioning to oceanic amplification and delayed decay (Figs. 46-50). The pre-event composite maps (Fig. 46) show the early establishment of favourable atmospheric conditions, characterized by high THF, elevated air temperature, and positive MSLP over much of the basin. These anomalies coincide with reduced wind speeds and decreased cloud cover, indicating persistent anticyclonic conditions that enhance radiative heating and suppress turbulent heat loss. Simultaneously, oceanic conditions display a shallow MLD suggesting enhanced stratification that may lead to the heat accumulation in the upper ocean.

During the during event phase (Fig. 47), these patterns intensify and become spatially coherent across the basin. Strong positive SST and air temperature anomalies coincide with maximum downward heat flux, while weak winds and high-pressure systems persist, limiting evaporative cooling. The post-event composite maps (Fig. 48) show a rapid transition in atmospheric forcing, with negative heat flux anomalies, increasing wind speeds, and weakening MSLP, indicating the breakdown of the anticyclonic regime. However, SST anomalies remain positive, reflecting a delayed oceanic response.

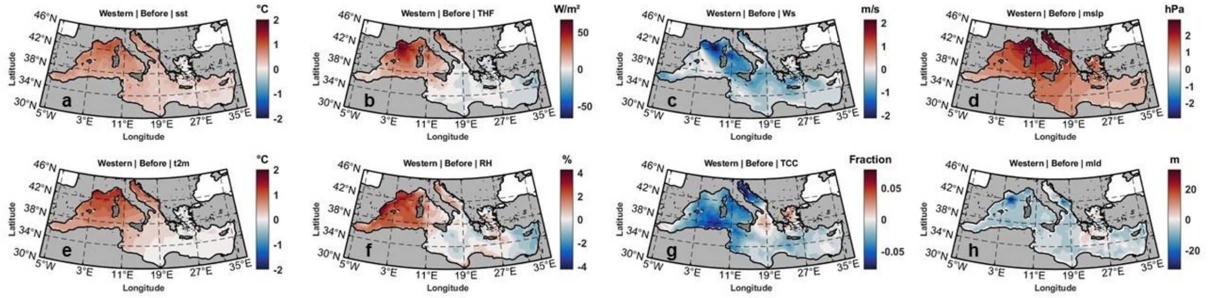

__Figure 46.__ Composite spatial anomalies the conditions __before__ MHW onset in the Western Mediterranean. Panels show SST (a), net surface heat flux (THF; b), wind speed (Ws; c), mean sea level pressure (MSLP; d), 2 m air temperature (T2m; e), relative humidity (RH; f), total cloud cover (TCC; g), and mixed layer depth (MLD; h).

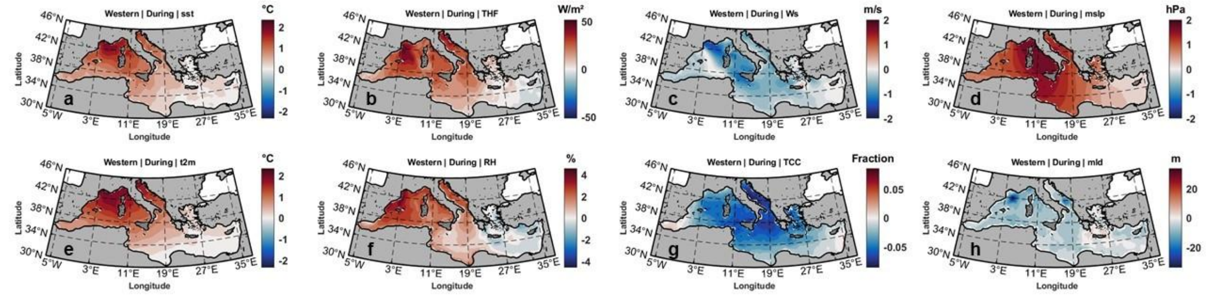

__Figure 47.__ Same as Fig. 46, but for the __during phase__ of the MHW in the Western Mediterranean.

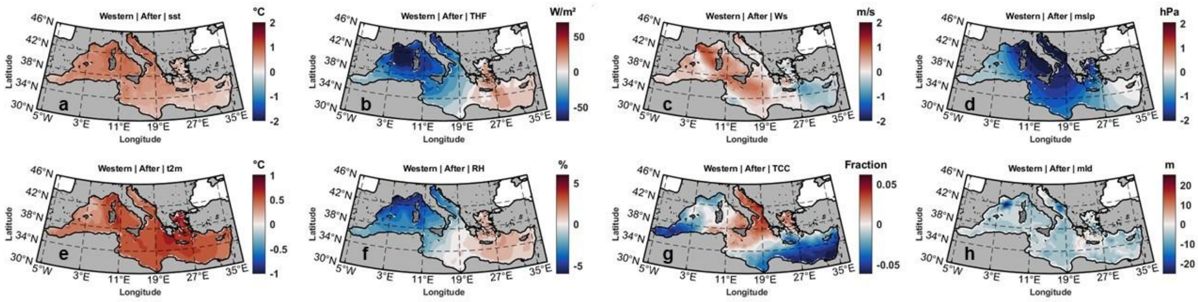

Figure 48. *Same as Fig. 46, but for the post-event phase of MHW in the Western Mediterranean.*

The temporal evolution of these drivers (Fig. 49) confirms this sequence. THF increases progressively prior to the event and peaks near the MHW maximum, while wind speed reaches a minimum around the peak, highlighting the role of reduced wind cooling in amplifying MHWs. Air temperature follows a similar evolution to SST, while MSLP shows a clear transition from positive anomalies before the peak to weaker or negative anomalies afterward.

Oceanic time series (Fig. 50) demonstrate that subsurface processes play a key role in sustaining MHWs. The MLD decreases before and during the peak, indicating enhanced stratification, while heat content, subsurface temperature (0-100 m), and warm layer thickness all increase and reach their maximum near the event peak. Notably, these subsurface anomalies decay more slowly than atmospheric forcing, confirming that stored heat in the upper ocean contributes to the persistence of MHW conditions even after atmospheric anomalies weaken.

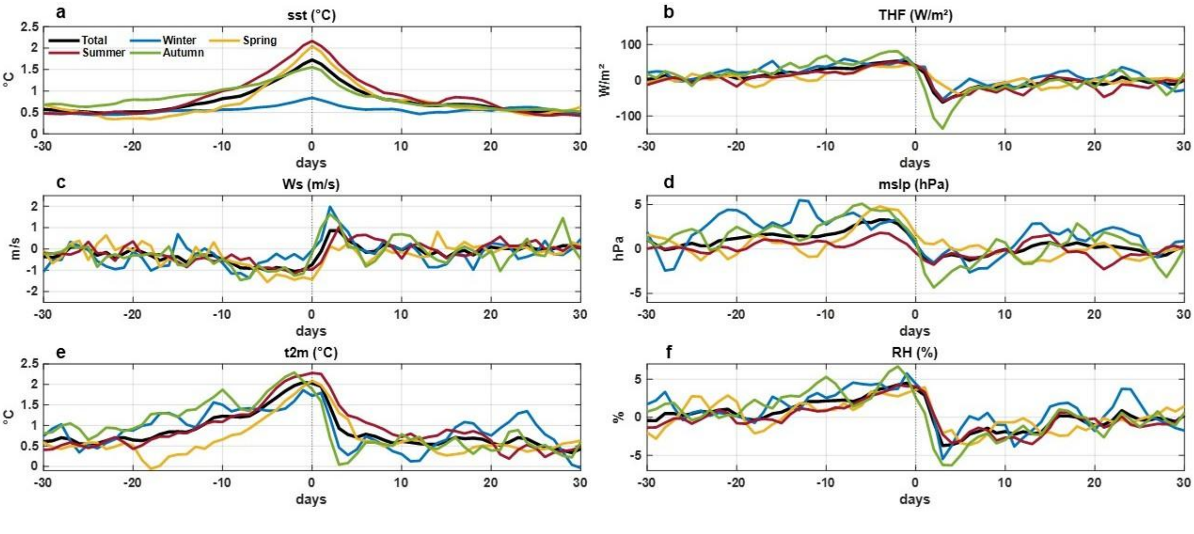

Figure 49. *Composite temporal evolution of atmospheric variables (SST (a), THF (b), Ws (c), MSLP (d), T2m (e), and RH (f)) from -30 to +30 days relative to MHW peak in the Western Mediterranean, including seasonal breakdown.*

In the Western Mediterranean, MHW activity shows strong summer dominance, as indicated by the atmospheric and oceanic time series (Figs. 49-50). The largest SST, air temperature, and net heat flux anomalies occur during summer, when reduced wind speeds and enhanced radiative forcing favor rapid surface warming. In contrast, winter atmospheric signals are weaker and more variable. In contrast, the oceanic signals are showing deeper heat penetration during winter. While the MLD is shallower during the MHWs of the winter than summer, but the upper layer heat content and warm layer thickness are peaking mainly during winter events indicating the role of the winter mixing in distributing the surface heat during occurrence of MHWs. This seasonal structure consistent with previous studies highlighting the role of summer atmospheric forcing, reduced latent heat loss, and high-pressure systems in driving Western Mediterranean MHWs (Darmaraki et al., 2024; Bonino et al., 2025; Denaxa et al., 2025), as well as the more limited subsurface involvement and deeper winter heat penetration (Juza et al., 2022; Darmaraki et al., 2024).

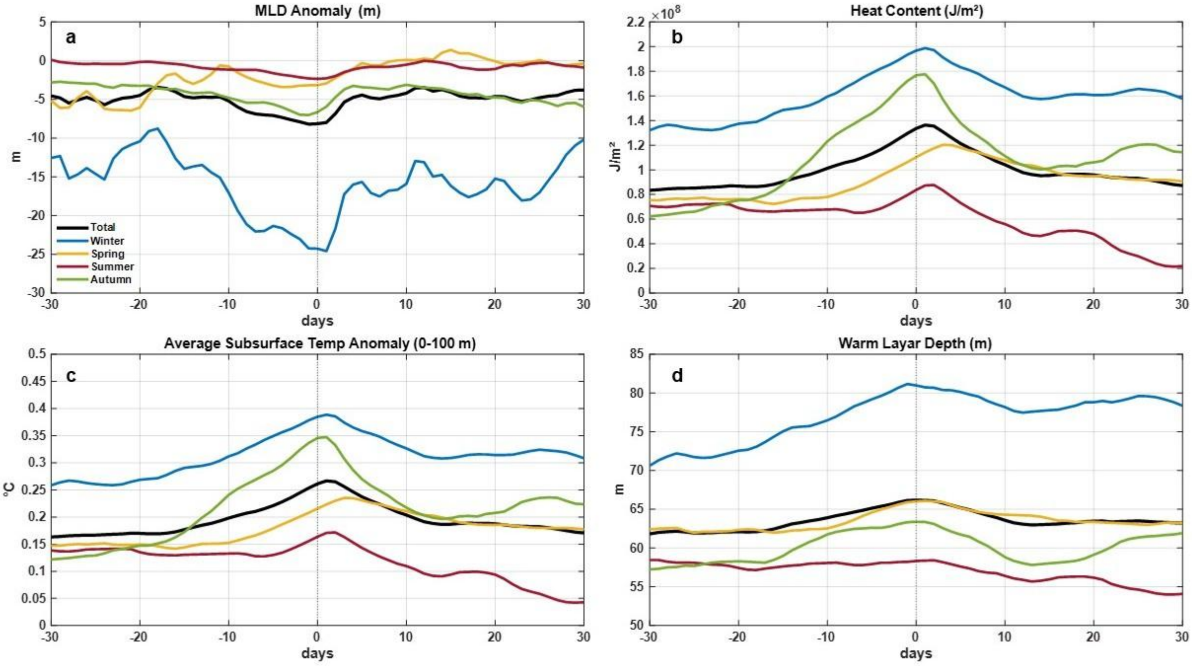

Figure 50. *Composite temporal evolution of oceanic variables MLD anomaly (a), heat content (b), subsurface temperature anomaly (0–100 m; c), and warm layer depth (d)) from -30 to +30 days relative to MHW peak in the Western Mediterranean, including seasonal breakdown.*

Overall, Western Mediterranean MHWs are driven by a combination of persistent anticyclonic atmospheric forcing and subsurface heat accumulation, with atmospheric processes controlling the onset and amplification phases and oceanic processes governing persistence. This mechanism consistent with previous studies highlighting the role of reduced winds, enhanced surface heat fluxes, and stratification in Mediterranean MHW development (Juza et al., 2022; Darmaraki et al., 2024; Bonino et al., 2025; Denaxa et al., 2025).

5.2.3 Drivers of MHWs in the Eastern Mediterranean:

The evolution of MHWs in the Eastern Mediterranean is characterized by combination of atmospheric forcing and pronounced subsurface heat storage (Figs. 51-55). The pre-event composite maps (Fig. 51) display widespread positive anomalies in SST, air temperature, and positive net surface heat flux, particularly over the Levantine basin. These conditions are associated with reduced wind speeds and increased relative humidity which indicating reduced evaporative cooling. Moreover, these atmospheric conditions coincide with shallow mixed layer depth which together may enhance the rising of SST.

During the MHWs (Fig. 52), these anomalies intensify and become spatially coherent. Strong positive SST and air temperature anomalies coincide with sustained positive THF, confirming continued atmospheric heat input. Weak winds persist, particularly over the Levantine basin, while relative humidity remains high, further suppressing latent heat loss. MSLP anomalies remain negative, contrasting with the anticyclonic pattern in the Western Mediterranean, but still maintaining conditions favourable for warming.

The post-event phase (Fig. 53) shows weakening atmospheric forcing, with decreasing THF and increasing wind speeds across the basin. However, SST anomalies remain positive, indicating delayed oceanic adjustment. The persistence of warm conditions despite reduced atmospheric forcing suggests a strong role for subsurface heat storage.

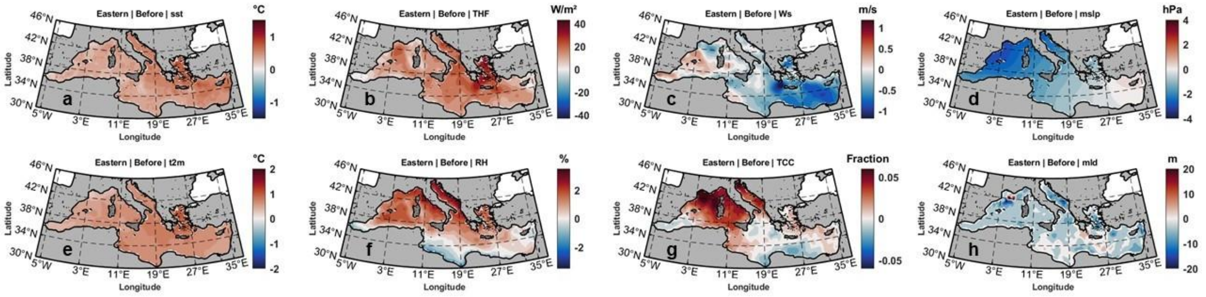

*__Figure 51.__ Composite spatial anomalies of atmospheric and oceanic variables **before** MHW onset in the Eastern Mediterranean (same variables as Fig. 46).*

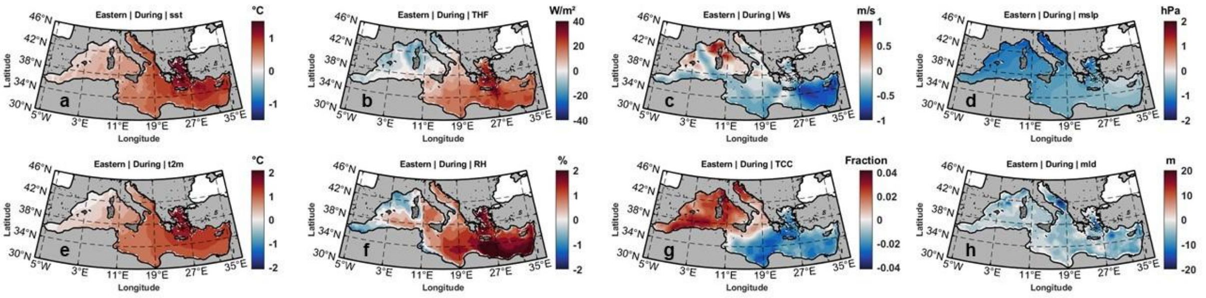

*__Figure 52.__ Same as Fig. 51, but for the **during phase** of MHWs in the Eastern Mediterranean.*

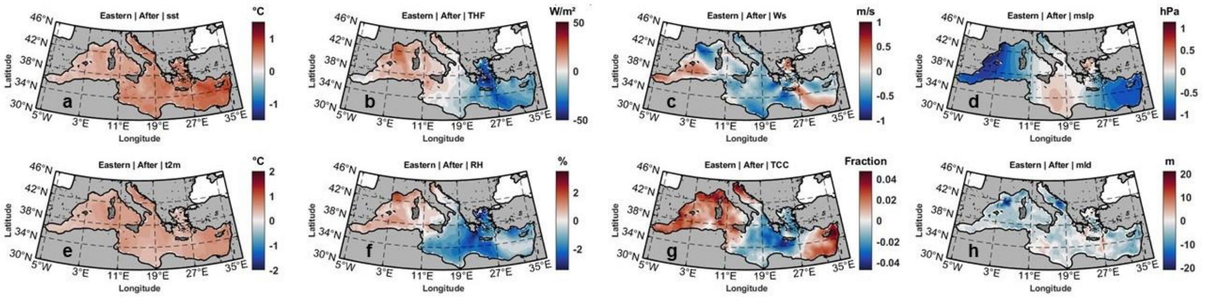

*__Figure 53.__ Same as Fig. 51, but for the **post-event phase** of MHWs in the Eastern Mediterranean.*

The temporal evolution (Fig. 54) confirms this sequence. THF increases before the event and peaks sharply at the MHW maximum, while wind speed reaches a minimum around the peak. Air temperature closely follows SST evolution, while MSLP remains predominantly negative throughout the event.

Oceanic time series (Fig. 55) demonstrate the dominant role of subsurface processes. The MLD decreases before and during the peak, indicating enhanced stratification, while heat content, subsurface temperature (0-100 m), and warm layer thickness increase strongly and peak near the event maximum. These anomalies are larger and more persistent than in the Western Mediterranean, and their decay is slower, indicating a stronger oceanic memory.

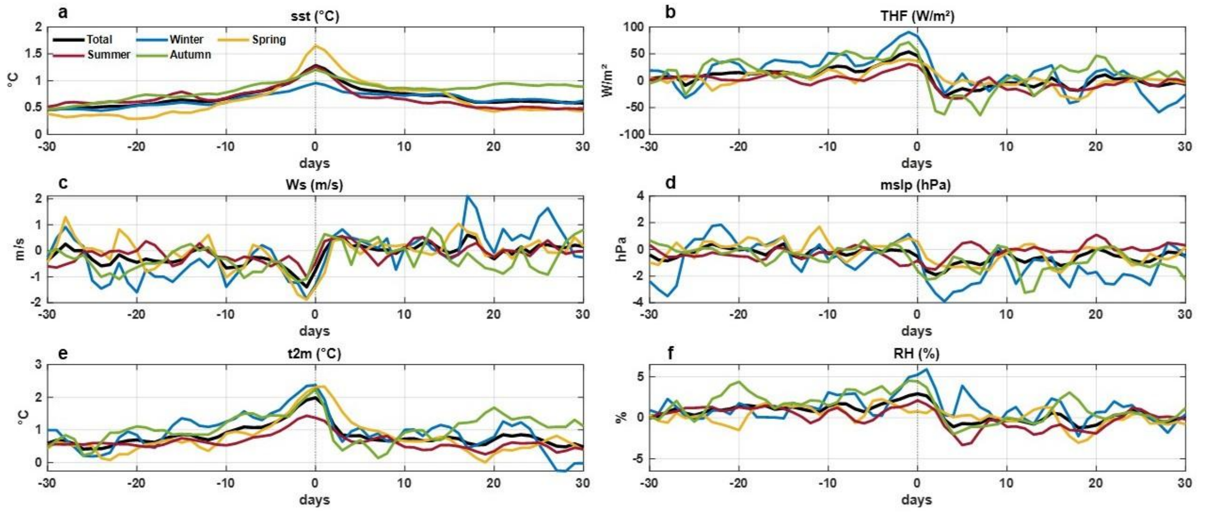

Figure 54. Composite temporal evolution of atmospheric variables relative to MHW peak in the Eastern Mediterranean, including seasonal breakdown.

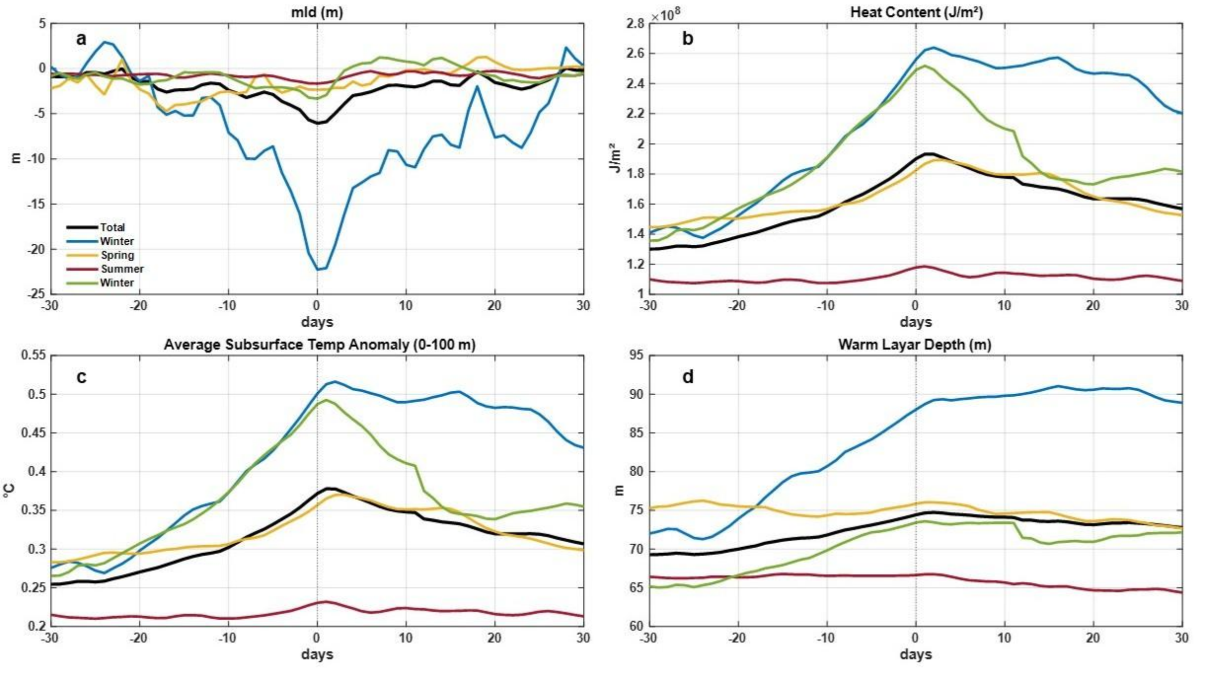

Figure 55. Composite temporal evolution of oceanic variables relative to MHW peak in the Eastern Mediterranean, including seasonal breakdown.

In the Eastern Mediterranean, MHW seasonality is less confined to summer and extends into spring and autumn, as shown by sustained anomalies in SST, heat flux, and oceanic variables (Figs. 54-55). While summer still exhibits strong surface warming, significant heat content, subsurface temperature, and warm layer thickness anomalies also occur during winter and transitional seasons. This reflects a stronger role of upper-ocean heat storage and stratification, which allows heat to accumulate and persist beyond peak summer conditions. The reduced seasonal contrast in MLD and the persistence of subsurface anomalies support longer-lasting events in this region. These findings are consistent with studies showing that the Eastern Mediterranean is characterized by enhanced stratification, deeper heat penetration, and prolonged MHW duration, with a stronger contribution from oceanic preconditioning compared to atmospheric forcing alone (Juza et al., 2022; Hamdeno and Alvera-Azcaráte, 2023; Darmaraki et al., 2024).

Overall, the Western Mediterranean responds more directly to short-term atmospheric variability, whereas the Eastern Mediterranean is more strongly influenced by subsurface heat accumulation and long-term warming, which enhance the persistence and vertical development of MHWs.

5.2.4 Drivers of MHWs in the Northern Red Sea:

The evolution of MHWs in the Northern Red Sea is characterized by strong atmospheric control combined with substantial subsurface heat storage (Figs. 56-60). The pre-event composite maps (Fig. 56) display pronounced positive anomalies in SST, air temperature, and net surface heat flux, particularly in the northern basin. These conditions are associated with reduced wind speeds and negative MSLP anomalies, indicating weakened ventilation and suppressed turbulent heat loss. Relative humidity increases, while cloud cover generally decreases over the northern region, further enhancing radiative heating. A shallow mixed layer depth coincide with the forementioned atmospheric conditions and rising subsurface temperature, suggesting early heat accumulation in the upper ocean.

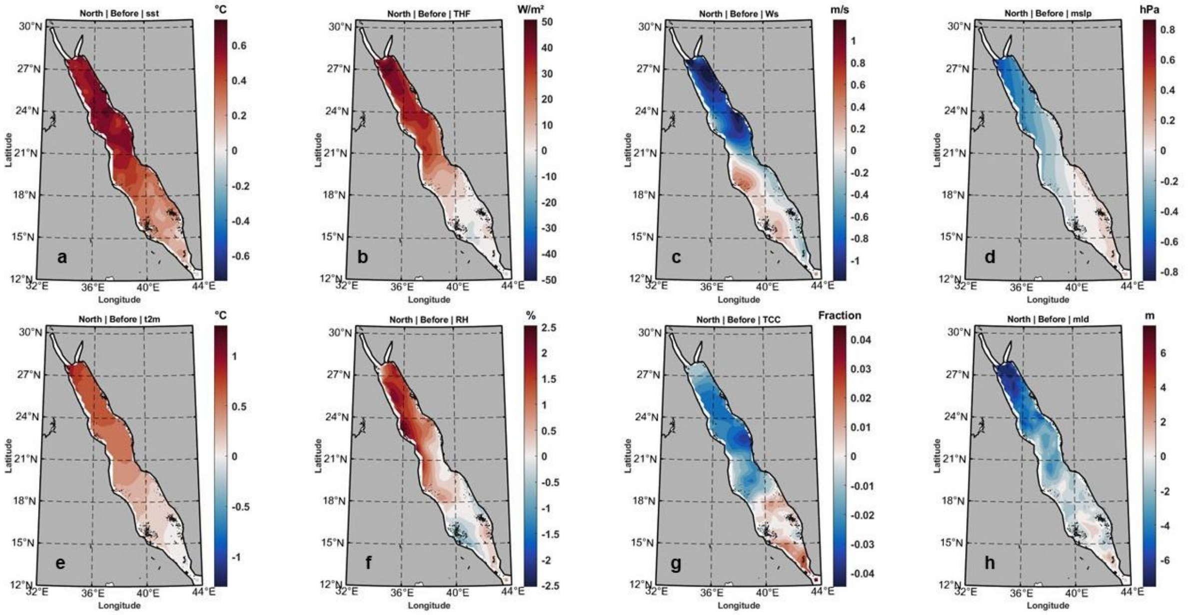

__Figure 56.__ Composite spatial anomalies of atmospheric and oceanic variables __before__ MHW onset in the Northern Red Sea (same variables as Fig. 46).

During the MHWs (Fig. 57), these anomalies intensify and become highly coherent. Strong positive SST and air temperature anomalies coincide with maximum THF, confirming sustained atmospheric heat input. Weak winds persist, particularly in the northern sector, limiting evaporative cooling, while relative humidity remains elevated.

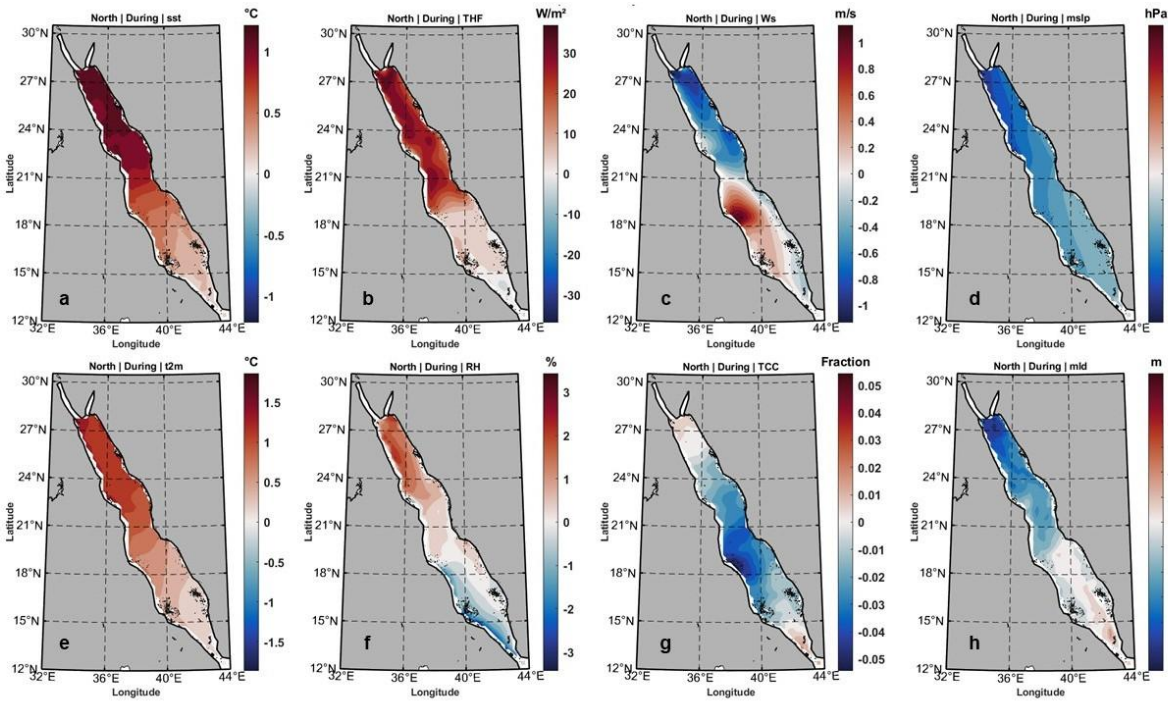

__Figure 57.__ Same as Fig. 56, but for the __during phase__ of MHWs in the Northern Red Sea.

The post-event phase (Fig. 58) shows a rapid reduction in atmospheric forcing, with negative THF anomalies and increasing wind speeds across the basin indicating the breakdown of favourable atmospheric conditions. However, SST anomalies remain positive, indicating a delayed oceanic response.

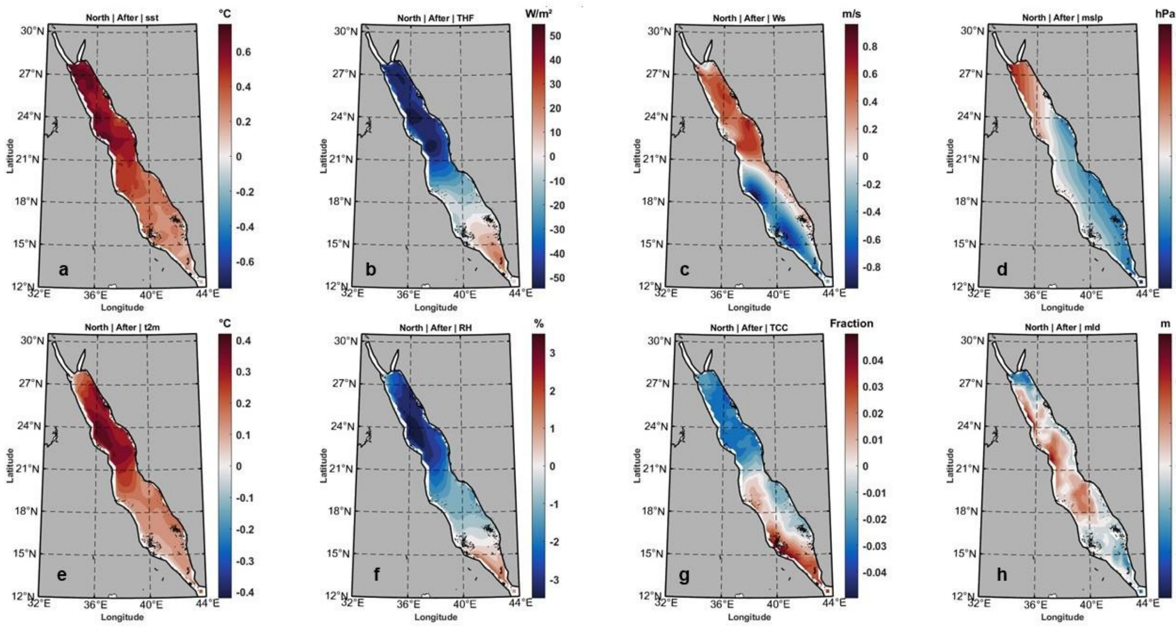

__Figure 58.__ Same as Fig. 56, but for the __post-event phase__ of MHWs in the Northern Red Sea.

The temporal evolution (Fig. 59) confirms this sequence. THF increases prior to the event and peaks near the MHW maximum, while wind speed reaches a minimum around the peak. Air temperature closely follows SST evolution, while MSLP remains predominantly negative during the event and recovers afterward. Oceanic time series (Fig. 60) reveal a strong subsurface contribution. The MLD decreases before and during the event, indicating enhanced stratification, while heat content, subsurface temperature (0-100 m), and warm layer thickness increase significantly and peak near the event maximum. These subsurface anomalies persist beyond the atmospheric forcing, indicating a strong oceanic memory that contributes to event persistence.

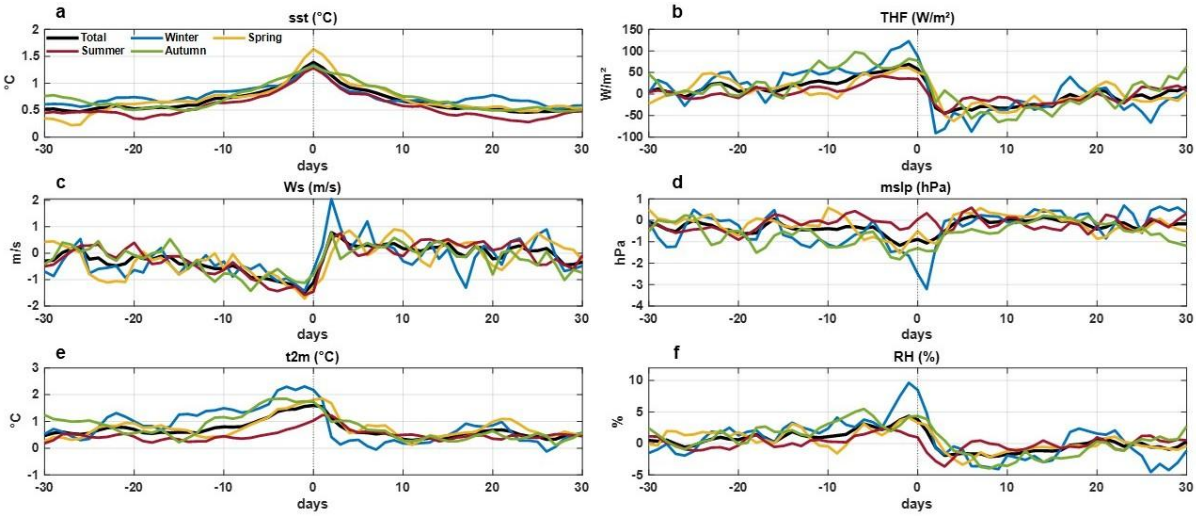

Figure 59. Composite temporal evolution of atmospheric variables relative to MHW peak in the Northern Red Sea, including seasonal breakdown.

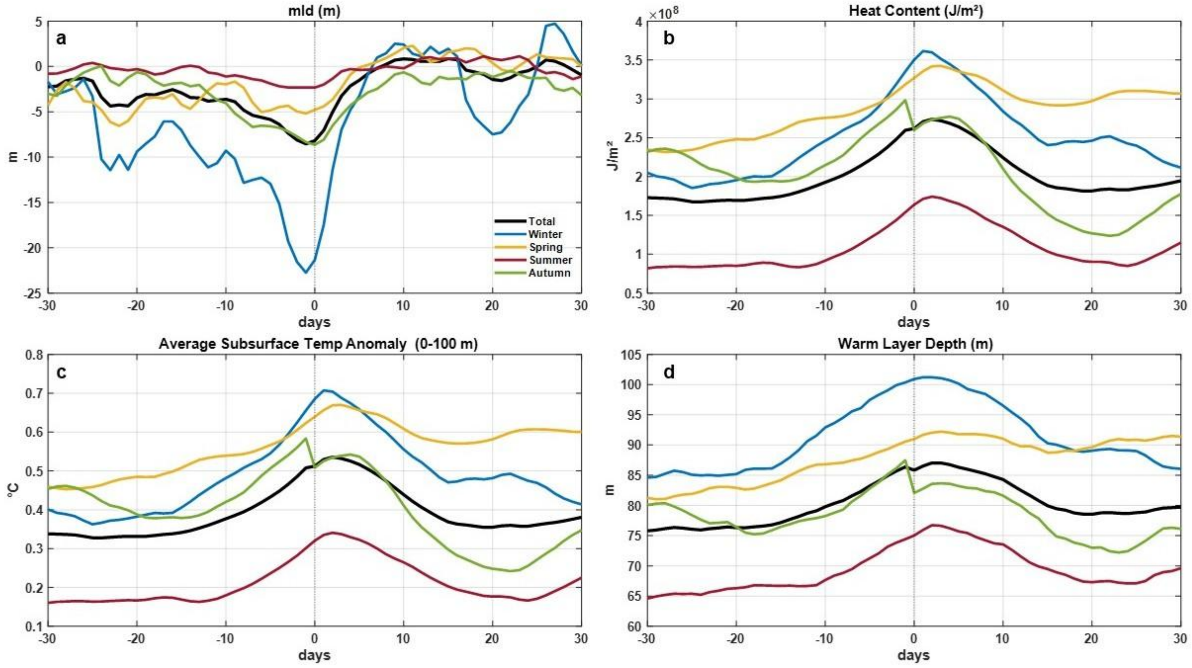

Figure 60. Composite temporal evolution of oceanic variables relative to MHW peak in the Northern Red Sea, including seasonal breakdown.

In the Northern Red Sea, MHW seasonality is characterized by a strong contribution from winter and spring, as indicated by pronounced anomalies in heat content, subsurface temperature, and warm layer thickness during these seasons (Fig. 60), together with corresponding atmospheric evolution (Fig. 59). Unlike the Mediterranean, peak subsurface heat storage does not coincide strictly with summer but is linked to seasonal stratification and preconditioning processes that begin earlier in the year. While summer events still show strong SST anomalies, the largest oceanic signals occur outside the peak summer season, indicating a dominant role of subsurface heat accumulation. This pattern is consistent with previous studies showing that Northern Red Sea MHWs are strongly influenced by seasonal stratification, reduced mixing, and accumulated upper-ocean heat, particularly during major events (Darmaraki et al., 2025)

Overall, MHWs in the Northern Red Sea are driven by a combination of enhanced atmospheric heat input, reduced wind-driven heat loss, and significant subsurface heat storage. This mechanism consistent with previous studies showing that Red Sea MHWs are associated with high air temperature, increased humidity, and weakened winds, particularly during major events such as 2010 (Hamdeno et al., 2024), and that subsurface heat content and stratification play a key role in sustaining extreme conditions (Darmaraki et al., 2025).

5.2.5 Drivers of MHWs in the Southern Red Sea

MHWs in the Southern Red Sea showing a clear contribution from subsurface heat storage (Figs. 61-65). During the pre-event phase (Fig. 61), positive anomalies in SST, air temperature, and surface heat flux are already established across the basin, accompanied by reduced wind speeds and elevated relative humidity. These conditions favor enhanced heat input and reduced evaporative cooling. At the same time, negative MLD anomalies indicate a shallower mixed layer, while oceanic time series (Fig. 65) show increasing heat content and subsurface temperature, pointing to early accumulation of heat in the upper ocean.

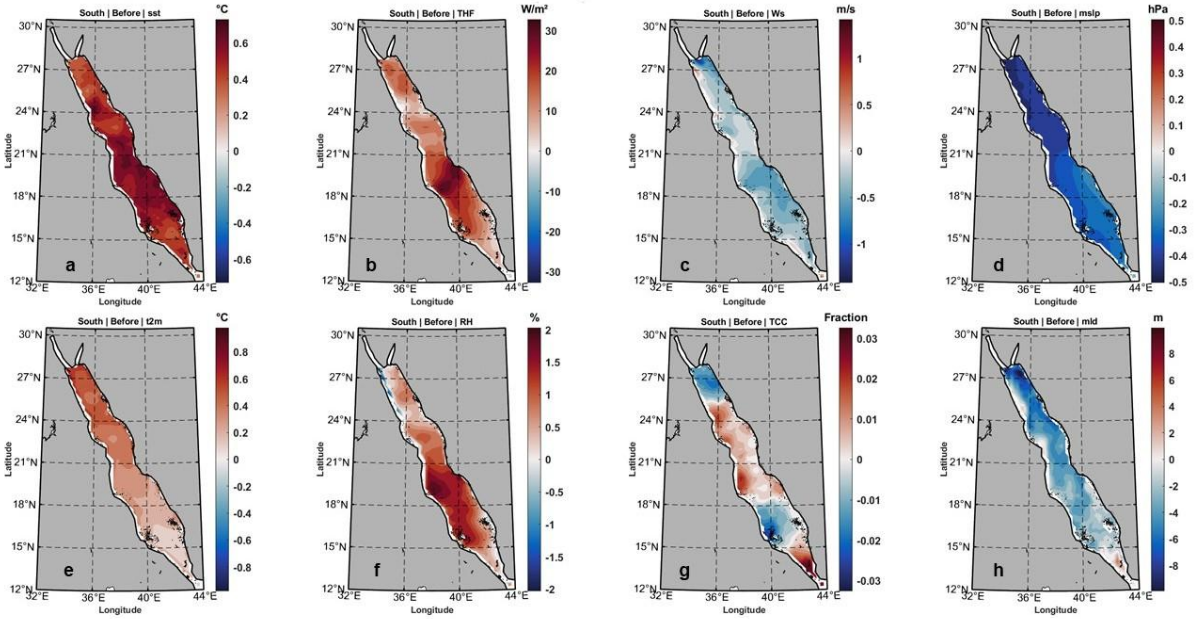

*Figure 61. Composite spatial anomalies of atmospheric and oceanic variables **before** MHW onset in the Southern Red Sea (same variables as Fig. 46).*

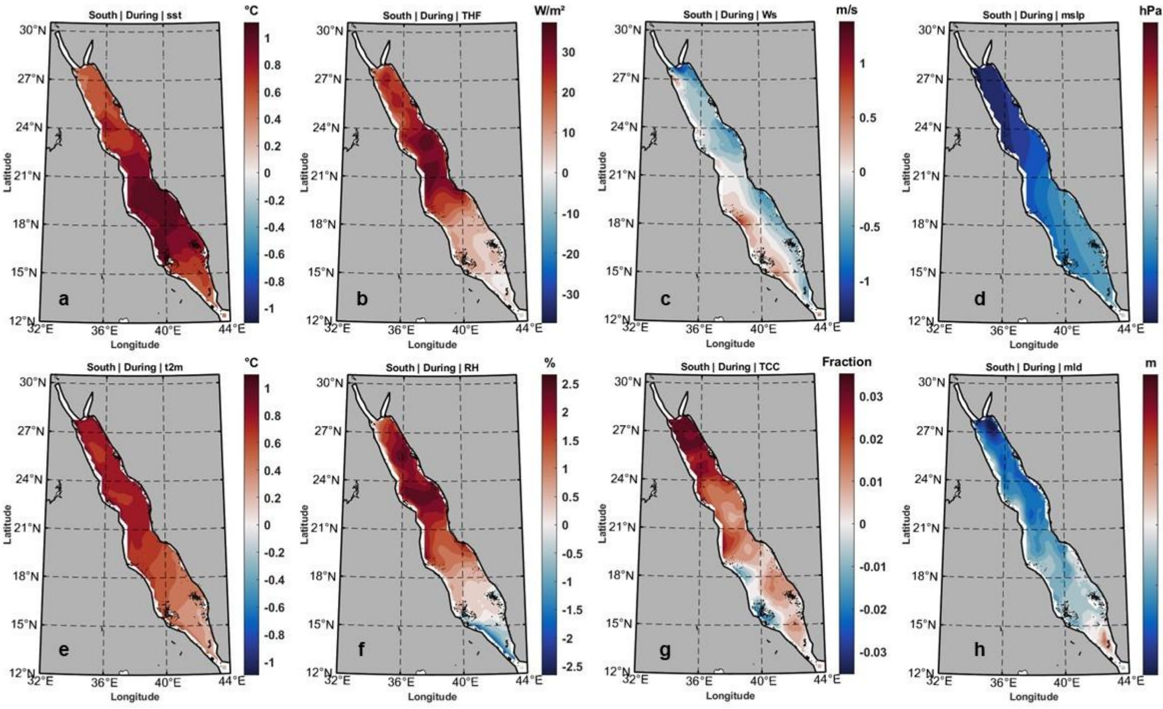

Figure 62. *Same as Fig. 61, but for the* ***during phase*** *of MHWs in the Southern Red Sea.*

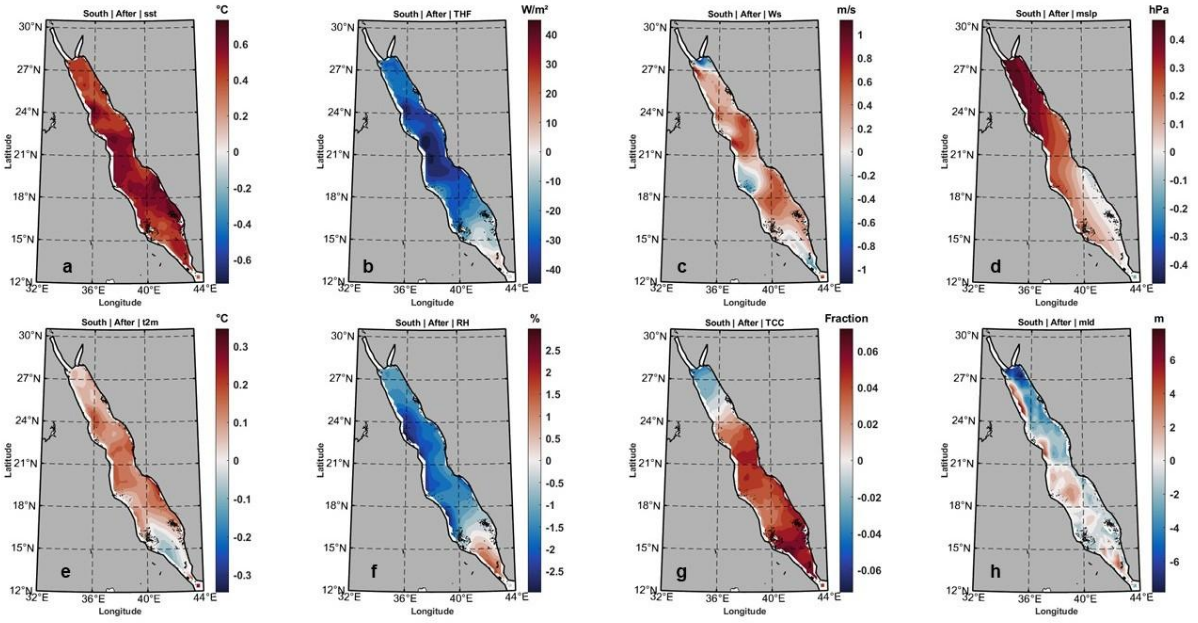

Figure 63. *Same as Fig. 61, but for the* ***post-event phase*** *of MHWs in the Southern Red Sea.*

During the peak phase (Fig. 62), atmospheric forcing remains favourable, with sustained positive THF, elevated air temperature, and weak winds. However, the persistence of the event is strongly supported by oceanic conditions, as heat content, subsurface temperature, and warm layer thickness reach their maximum around the event peak (Fig. 65), indicating a well-developed subsurface heat reservoir.

In the post-event phase (Fig. 63), atmospheric forcing weakens, with negative THF anomalies and increasing wind speeds promoting enhanced heat loss. Despite this, SST anomalies remain positive, and subsurface variables decrease more gradually, reflecting a delayed oceanic adjustment (Fig. 65).

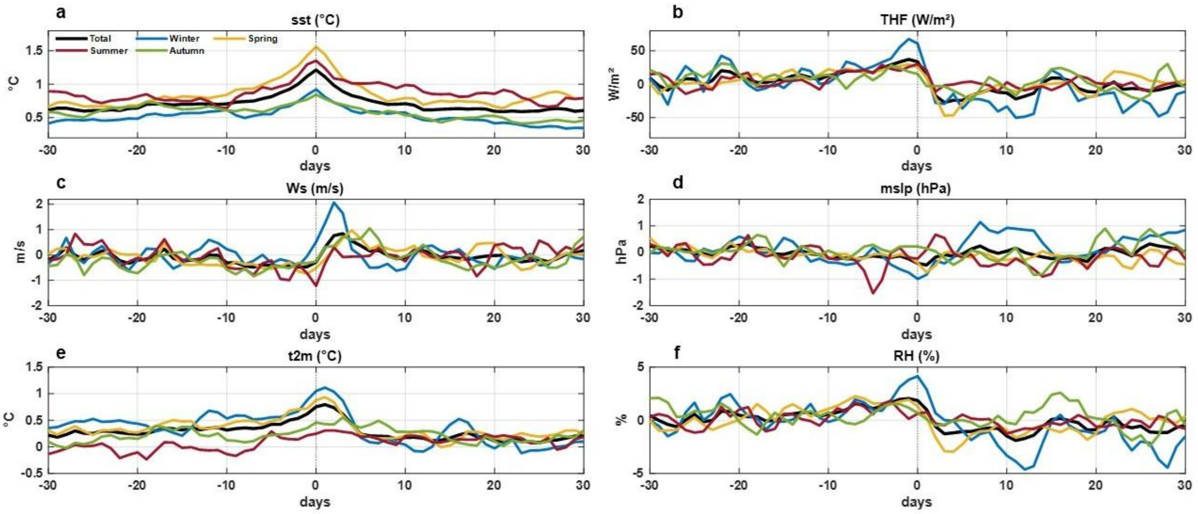

Figure 64. Composite temporal evolution of atmospheric variables relative to MHW peak in the Southern Red Sea, including seasonal breakdown.

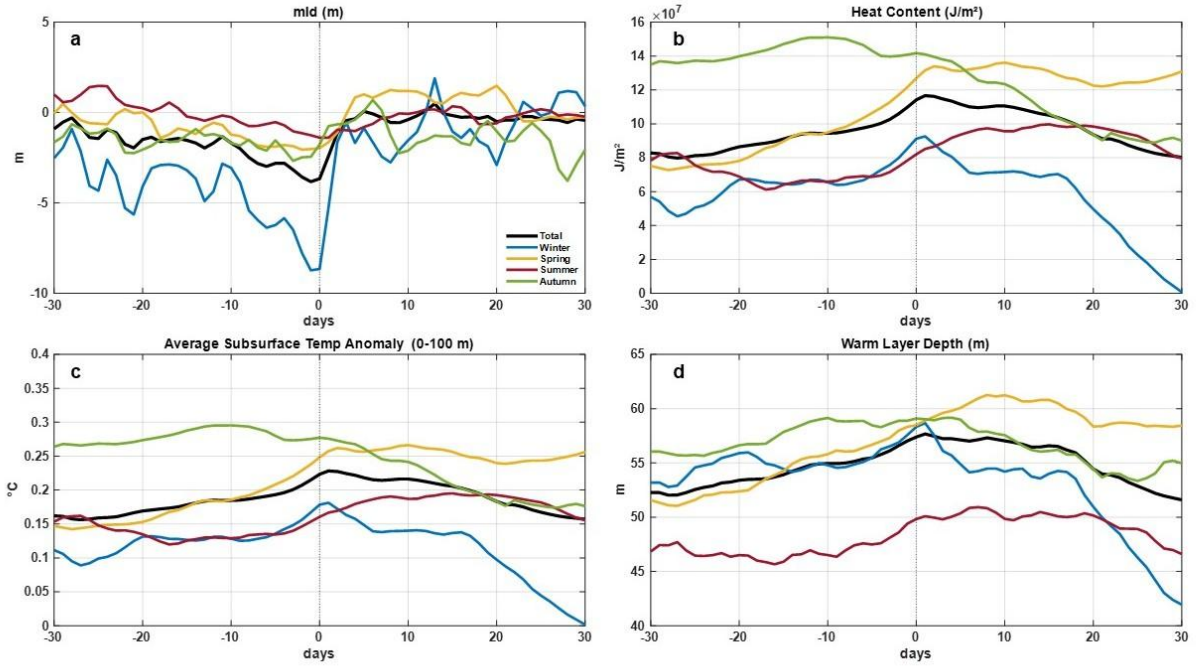

Figure 65. Composite temporal evolution of oceanic variables relative to MHW peak in the Southern Red Sea, including seasonal breakdown.

In the Southern Red Sea, MHWs display a broader seasonal distribution, with significant activity during spring and autumn, as reflected in the time series of heat content, subsurface temperature, and warm layer thickness (Fig. 65). Although summer shows enhanced SST and heat flux anomalies, subsurface signals are not limited to this season and remain elevated during transitional periods, indicating sustained upper-ocean heat storage. The relatively weak seasonal variability in atmospheric drivers (Fig. 64) compared to oceanic signals further highlights the importance of oceanic preconditioning. This pattern suggests that MHWs in the southern basin are less tightly coupled to peak summer forcing and more influenced by persistent subsurface heat reservoirs and regional ocean dynamics, consistent with studies emphasizing the role of remote forcing and heat advection from the Gulf of Aden, as well as upper-ocean heat content variability in the southern Red Sea (Chaidez et al., 2017; Darmaraki et al., 2025; Nadimpalli et al., 2025).

A contrast between the Northern and Southern Red Sea highlights differences in the relative role of atmospheric and oceanic processes. In the Northern Red Sea, MHWs are associated with stronger and more coherent atmospheric forcing, particularly through enhanced surface heat flux, and reduced winds, together with substantial subsurface heat storage. In the Southern Red Sea, atmospheric forcing also contributes to event development, but the evolution is more strongly influenced by upper-ocean preconditioning, with elevated heat content, subsurface temperature, and warm layer thickness present before and persisting after the event peak. This indicates a more pronounced role of oceanic memory in the southern basin.

5.2.6 The MHW Drivers Contribution in the Mediterranean and Red Seas:

The logistic regression results provide a quantitative assessment of the relative influence of atmospheric and oceanic drivers on MHW occurrence across the study regions (Figs. 66-67). In the Mediterranean Sea (Fig. 66), the model shows a clear contrast between sub-basins. In the Western Mediterranean, both atmospheric and oceanic predictors contribute to MHW occurrence, with comparable odds ratios, suggesting mixed control where surface forcing and upper-ocean conditions act together. In the Eastern Mediterranean, the oceanic contribution is relatively stronger, consistent with the composite analysis showing enhanced subsurface heat storage and stratification during MHW events.

In the Red Sea (Fig. 67), oceanic predictors generally have higher odds ratios than atmospheric predictors in both subregions, indicating a stronger association between MHW occurrence and upper-ocean conditions. This is particularly evident in the Southern Red Sea, where oceanic influence exceeds atmospheric forcing, consistent with the persistence of subsurface heat anomalies observed in the composite analysis. In the Northern Red Sea, both driver families contribute, although oceanic conditions remain an important component.

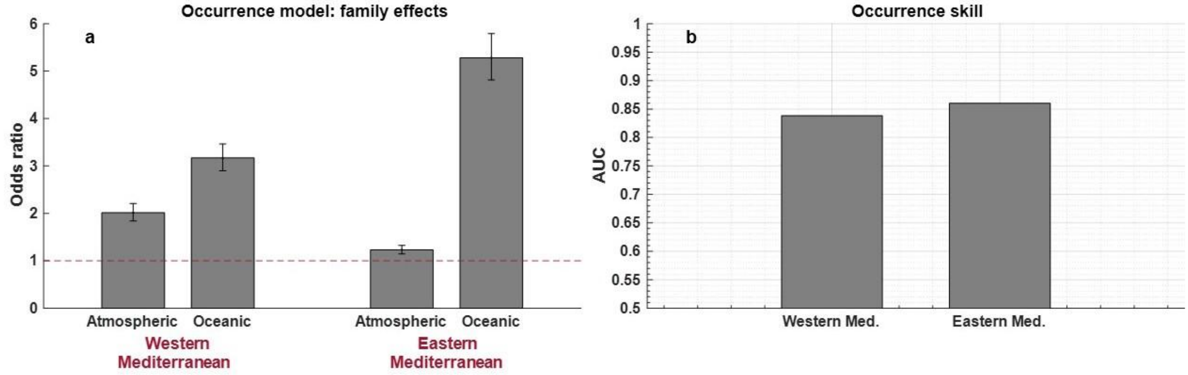

Figure 66. *(a) Odds ratios of atmospheric and oceanic driver families from the logistic regression model for MHW occurrence in the Western and Eastern Mediterranean. The dashed line indicates no effect (odds ratio = 1). Error bars represent confidence intervals. (b) Model performance (AUC) for the Mediterranean sub-basins.*

Model performance, as indicated by AUC values, is consistently above random classification in all regions, confirming that the selected predictors capture relevant aspects of MHW occurrence. Slightly higher AUC values in regions with stronger oceanic control suggest that subsurface heat content and stratification provide more consistent signals than atmospheric variability alone.

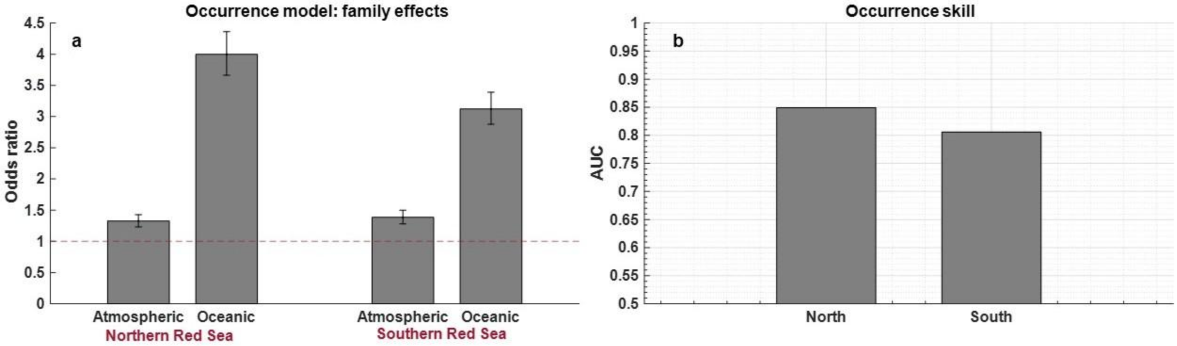

Figure 67. *(a) Same as Fig. 66a, but for the Northern and Southern Red Sea. (b) Model performance (AUC) for the Red Sea sub-basins.*

Overall, the model results support the interpretation from the composite analysis: MHW occurrence reflects a combination of atmospheric forcing and oceanic preconditioning, with the relative importance of each varying across regions. Rather than indicating strict dominance, the results highlight a shift from more balanced contributions in the Western Mediterranean to a stronger role for oceanic processes in the Eastern Mediterranean and Red Sea.

5.3 Conclusions:

This chapter provides a comprehensive assessment of the drivers of MHWs in the Mediterranean Sea and the Red Sea, combining composite analysis, upper-ocean diagnostics, and statistical modelling. The contribution of long-term background warming is also quantified, allowing a clear separation between externally forced trends and internal variability.

The results show that background warming plays a fundamental role in increasing MHW occurrence in both basins, particularly over the past decade. In the Mediterranean, the contribution of long-term warming becomes progressively dominant after the early 2000s, with a substantial increase in MHW frequency and cumulative intensity. In the Red Sea, this contribution is also significant but becomes more pronounced after approximately 2010, consistent with the strong recent amplification of surface temperatures. These findings confirm that long-term ocean warming acts as a baseline shift, increasing the likelihood of threshold exceedance and preconditioning the system for more frequent and persistent events (Oliver et al., 2018a; Laufkötter et al., 2020).

Superimposed on this long-term signal, the physical drivers of MHWs show clear spatial contrasts. In the Mediterranean Sea, a marked west-east gradient is observed. The Western Mediterranean is primarily controlled by atmospheric forcing, where enhanced surface heat fluxes, reduced wind-driven mixing, and high-pressure systems trigger rapid surface warming. In contrast, the Eastern Mediterranean is more strongly influenced by oceanic processes, with subsurface heat storage, increased stratification, and deeper heat penetration sustaining longer-lasting events. This transition reflects the combined effect of background warming and regional ocean dynamics, which enhance the persistence of thermal anomalies in the eastern basin.

In the Red Sea, MHWs are largely governed by oceanic preconditioning, with upper-ocean heat content and stratification playing a dominant role in both the Northern and Southern regions. The Northern Red Sea exhibits strong coupling between atmospheric forcing and subsurface heat storage, leading to coherent and persistent events. The Southern Red Sea, while still influenced by atmospheric fluxes, shows a stronger dependence on subsurface heat reservoirs and vertical structure, indicating enhanced oceanic control and longer memory of thermal anomalies. These differences highlight the importance of basin-specific circulation and stratification regimes in modulating MHW dynamics.

Seasonality further modulates these processes. In the Mediterranean, MHWs are strongly summer-dominated, particularly in the western basin where atmospheric forcing peaks. In contrast, the Eastern Mediterranean and the Red Sea display a broader seasonal distribution, with significant contributions from spring and autumn, reflecting the role of accumulated subsurface heat and stratification. This indicates that, in ocean-dominated regimes, MHWs are not solely tied to peak surface heating but also to preconditioning processes that develop over longer timescales.

In conclusion, this study demonstrates that MHW occurrence results from the combined effect of long-term warming and regional-scale drivers. Background warming increases the baseline likelihood of extreme events, while atmospheric forcing and oceanic processes control their initiation, amplification, and persistence. These findings highlight the increasing importance of subsurface processes under continued climate warming and underscore the need to consider both atmospheric variability and oceanic preconditioning when assessing future MHW risk in semi-enclosed basins.

Chapter Six: Impacts of MHWs in the Mediterranean and Red Sea

Foreword

This chapter investigates the ecological impacts of MHWs in the Mediterranean Sea and the Red Sea. While the physical drivers of MHWs are more studied, their consequences on marine ecosystems remain less constrained, particularly in regions characterized by strong stratification and nutrient limitation. Understanding how extreme warming events affect ocean structure and biological processes is essential for assessing ecosystem vulnerability under ongoing climate change.

The primary objective of this chapter is to quantify the environmental and biological responses associated with MHWs using a combination of basin-scale observations and controlled laboratory experiments. The analysis focuses on key indicators of ecosystem functioning, including mixed layer depth, chlorophyll-a, and nitrate concentrations, to evaluate how MHWs influence stratification, nutrient availability, and primary productivity. In addition, a compound event framework is applied to assess the co-occurrence of multiple stressors and their potential to amplify ecosystem impacts.

To complement the large-scale analysis, laboratory experiments are conducted to examine the response of zooplankton to elevated temperatures representative of MHW conditions. This combined approach provides a direct link between physical ocean changes and biological responses, offering new insight into the mechanisms through which MHWs affect marine ecosystems.

This chapter contributes to the broader objectives of the thesis by advancing the understanding of MHW impacts beyond physical characterization and by highlighting the role of compound stress and biological thresholds in shaping ecosystem responses to extreme warming events.

This research is currently being **prepared for submission to a peer-reviewed journal**.

6.1 Data and Methods:

6.1.1 SST and MHW detection:

Daily SST fields were obtained from the NOAA Optimum Interpolation SST dataset (OISST v2; Reynolds et al., (2007)). The analysis covers the period 1993-2024. MHWs were identified using the hierarchical framework of Hobday et al., (2016), as described in previous chapters.

6.1.2 Oceanic Variables:

MLD were obtained from the Copernicus Marine Service Global Ocean Reanalysis GLORYS12V1 (Jean-Michel et al., 2021). Biogeochemical variables, including chlorophyll-a (Chl-a) and nitrate (NO_3), were obtained from the Copernicus Marine biogeochemical hindcast for global ocean is produced at Mercator-Ocean. It provides 3D biogeochemical fields since year 1993 at 0.25°x0.25° spatial resolution, which provides global estimates of ocean productivity and nutrient fields based on data-assimilative models (European Union-Copernicus Marine Service, 2018).

To reduce skewness in chlorophyll-a distributions and stabilize variance, chlorophyll-a concentrations were log-transformed prior to analysis, a common approach in marine biogeochemical studies (Campbell, 1995; Behrenfeld and Boss, 2006). All variables were expressed as daily anomalies relative to the 1993-2022 climatology, following standard practices in climate variability and extreme event studies (Holbrook et al., 2019; Wilks, 2019).

6.1.3 Environmental Anomaly and Response Analysis:

Environmental responses to MHWs were quantified by systematically comparing physical and biogeochemical conditions during MHW events with baseline (non-MHW) conditions, following established approaches in MHW impact studies (Smale et al., 2019). This framework allows isolation of the specific contribution of extreme thermal events from background variability. Daily anomalies were first computed relative to the climatological seasonal cycle (1993-2022) to remove the dominant seasonal signal and ensure comparability across regions and time periods (Wilks, 2019).

Negative anomalies in mixed layer depth were interpreted as indicators of enhanced stratification and reduced vertical mixing, which limit the upward transport of nutrients from deeper layers. Similarly, negative anomalies in chlorophyll-a and nitrate were interpreted as indicators of reduced primary productivity and nutrient limitation, reflecting the suppression of biological activity under stratified conditions.

To further quantify the relationship between environmental variability and MHW intensity, statistical associations were evaluated using Pearson correlation analysis between environmental anomalies and SST anomalies during MHW days (Kirch, 2008). This analysis provides a measure of whether stronger heatwaves are associated with stronger ecological responses and has been used in previous studies to link thermal extremes with biogeochemical variability (Le Grix et al., 2021).

Temporal variability in environmental responses was examined at seasonal scales by grouping data into climatological seasons (winter: JFM, spring: AMJ, summer: JAS, autumn: OND). This approach allows assessment of how the magnitude and direction of ecosystem responses depend on background oceanographic conditions, such as seasonal stratification and nutrient availability (Smale et al., 2019; Le Grix et al., 2021, 2022). This seasonal framework is particularly important in semi-enclosed basins, where strong seasonal cycles modulate both physical and biological processes.

6.1.4 Compound Environmental Stress Analysis:

To assess the combined impact of multiple stressors, a compound event framework was applied to identify the co-occurrence of MHWs with unfavourable environmental conditions. This approach follows the conceptual framework introduced by Leonard et al., (2014) and Zscheischler et al., (2018, 2020), which emphasizes that extreme impacts often arise from the interaction of multiple drivers rather than individual variables.

Compound environmental stress events were defined as periods when MHW conditions coincide with negative anomalies in one or more ecosystem-relevant variables, including chlorophyll-a, nitrate, and mixed layer depth. These variables represent key components of the marine system, linking physical processes (stratification and mixing) with biogeochemical responses (productivity and nutrient availability).

The frequency of compound events was quantified at each grid point by calculating the fraction of days satisfying a given condition relative to the total number of valid observations. This probabilistic approach allows comparison across regions and variables and is commonly used in compound extreme analysis (Leonard et al., 2014; Zscheischler et al., 2018, 2020). Both pairwise combinations (e.g., MHW + low chlorophyll) and multivariable combinations (e.g., MHW + low chlorophyll + low nitrate + shallow MLD) were analysed to identify progressively stronger stress scenarios.

Temporal variability in compound stress events was examined at both seasonal and interannual scales. Seasonal analysis was conducted using climatological seasons (JFM, AMJ, JAS, OND), while interannual variability was assessed using annual averages of compound event frequency. This temporal framework allows evaluation of how compound stress evolves under changing environmental conditions and provides insight into the role of long-term warming in shaping ecosystem exposure to multiple stressors.

6.1.5 Copepods Lap Experimental Analysis:

To complement the basin-scale environmental analysis, a controlled laboratory experiment was conducted to investigate the biological response of zooplankton to temperature conditions representative of MHWs. The experiment focused on the copepod *Acartia tonsa*, a widely distributed species commonly used as a model organism in marine ecological studies due to its sensitivity to environmental variability and its key role in marine food webs (Kiørboe, 2011; Zervoudaki et al., 2024).

The experimental design consisted of two temperature treatments representing baseline (control) and heatwave conditions. The control treatment was maintained at 20 °C, representing typical non-extreme conditions, while the heatwave treatment simulated elevated temperatures consistent with observed MHW conditions in the study regions (Westen Mediterranean and Bay of Biscay MHW events). All experimental units were maintained under controlled laboratory conditions in a temperature-regulated water bath to ensure stable thermal environments throughout the experiment.

Each experimental unit consisted of 10 individuals placed in 50 mL of filtered seawater and supplied with a constant food concentration of approximately 3,000 cells/mL of the phytoplankton species *Isochrysis galbana* (Ulf Riebesell et al., 2011). To maintain water quality and food availability, partial water replacement (50%) was performed every two days, while preserving the temperature conditions of each treatment. The duration of the experiment ranged between 13 and 18 days, depending on the specific heatwave scenario.

Three key biological responses were monitored throughout the experiment. Mortality rates were assessed by recording daily survival, allowing quantification of the direct impact of elevated temperature on organism viability (Kiørboe, 2011). Swimming behaviour was qualitatively observed as an indicator of physiological and behavioural stress (Kiørboe, 2011). Grazing activity was evaluated by monitoring changes in phytoplankton concentration, providing insight into feeding efficiency under thermal stress (Zervoudaki et al., 2024).

This experimental approach offers a mechanistic perspective on the direct effects of elevated temperature on a key zooplankton species. By linking organism-level responses to the large-scale environmental changes identified in the basin-scale analysis, the experiment contributes to a more comprehensive understanding of how MHWs may impact marine ecosystems.

6.2 Results and Discussion:

6.2.1 Impacts of MHWs in the Mediterranean Sea:

The spatial distribution of MHW occurrence between 1993 to 2024 (Fig. 68) shows a clear basin-scale gradient, with higher event frequency in the WMB and parts of the central Mediterranean, and relatively lower counts in the EMB. This west-east contrast aligns with previous studies that report stronger variability and more intense air–sea interactions in the western basin, leading to increased MHW activity (Hamdeno and Alvera-Azcaráte, 2023).

Figure 69 shows both the co-variability between environmental anomalies and MHW intensity (upper panels) and the mean environmental response during MHW days relative to non-MHW days (lower panels). The upper panels indicate that SST anomalies are generally negatively correlated with mixed layer depth anomalies across most of the Mediterranean (Fig. 69a), meaning that stronger warm anomalies tend to occur with a shallower mixed layer and enhanced stratification. In contrast, SST anomalies show mostly positive correlations with chlorophyll-a (particularly in the central and eastern basin) and negative correlations in the WMB (Fig. 69b). The nitrate anomalies, correlates positively with MHW SST anomalies (Fig. 69c), indicating that where SST anomalies intensify, nitrate anomalies tend to vary in the same direction.. The lower panels clarify the average MHW response: MHW days are associated with predominantly negative MLD anomalies (Fig. 69d), confirming widespread mixed-layer shoaling during warm events, and broadly negative chlorophyll-a anomalies (Fig. 69e), especially in the western and northern Mediterranean, indicating reduced surface phytoplankton biomass during MHWs. Nitrate anomalies during MHW days are weaker and more spatially heterogeneous (Fig. 69f), but negative signals are evident in several subregions, suggesting reduced nutrient supply under enhanced stratification. This overall pattern is consistent with previous studies showing that Mediterranean MHWs are commonly associated with shallower mixed layers and suppressed biological productivity, particularly in stratified and nutrient-limited regions (Sen Gupta et al., 2020; Oliver et al., 2021; Smith et al., 2021; Hamdeno and Alvera-Azcaráte, 2023).

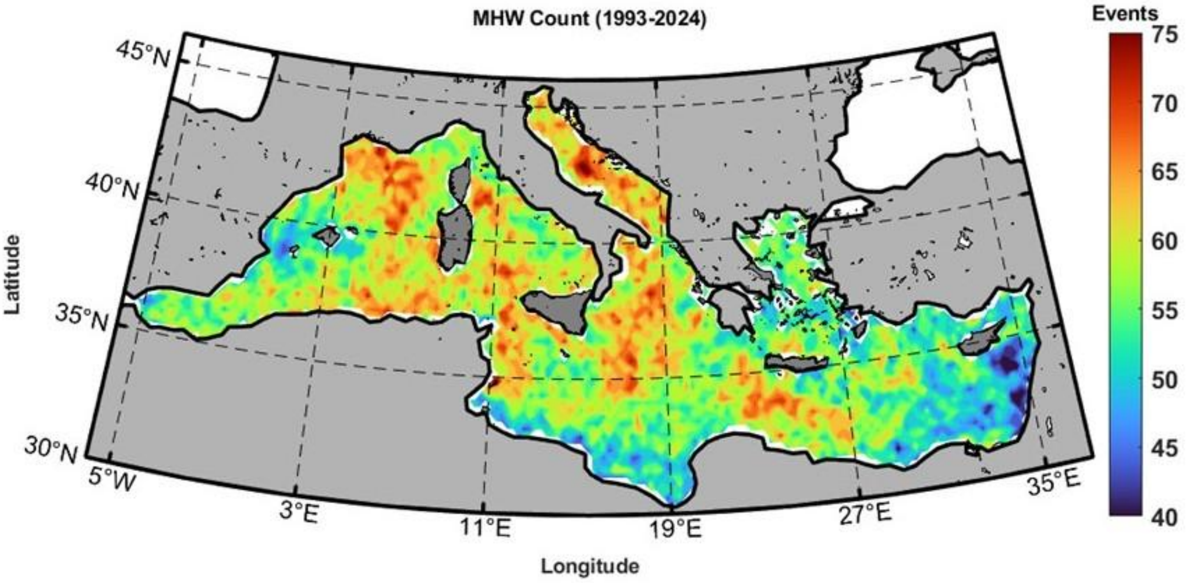

Figure 68. Spatial distribution of the total number of MHW events over the period 1993–2024 in the Mediterranean Sea.

The contrast between the upper and lower panels is important: the correlation maps describe how anomalies co-vary with MHW intensity, whereas the difference maps quantify the average shift in environmental conditions between MHW and non-MHW states. Together, they indicate that MHWs in the Mediterranean are characterized by stronger stratification and reduced surface biological productivity, even though the local anomaly response to increasing SST intensity may vary across the basin.

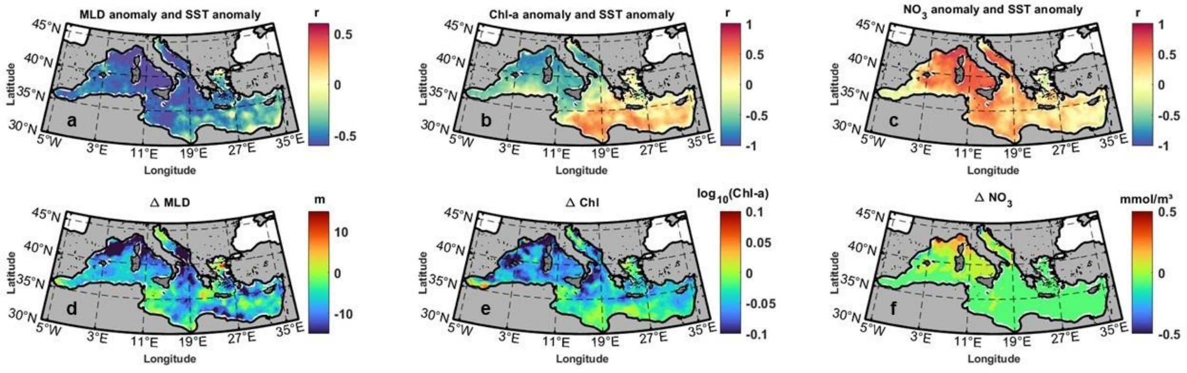

Figure 69. *Environmental covariability with MHW intensity and mean environmental response during MHW conditions in the Mediterranean Sea. Upper panels show the Pearson correlation between SST anomalies and anomalies in (a) mixed layer depth, (b) chlorophyll-a, and (c) nitrate. Lower panels show the mean difference between MHW days and non-MHW days for (d) mixed layer depth, (e) chlorophyll-a, and (f) nitrate. Negative mixed layer depth anomalies indicate mixed-layer shoaling and enhanced stratification, while negative chlorophyll-a and nitrate anomalies indicate reduced surface productivity and nutrient availability during MHW conditions.*

The co-occurrence analysis (Fig. 70) further demonstrates that MHWs are frequently associated with biogeochemical stress conditions, particularly in the WMB. High fractions of MHW + Chl-a reduction and MHW + NO_3 anomalies indicate that thermal extremes are often accompanied by unfavourable productivity conditions. In contrast, co-occurrence between Chl-a and NO_3 or Shallow MLD alone is generally weaker, suggesting that MHWs are a key organizing driver linking physical and biological responses. The spatial pattern shows a clear intensification of compound stress in the western and central Mediterranean, while the eastern basin exhibits lower co-occurrence fractions, consistent with its more oligotrophic and stable background state.

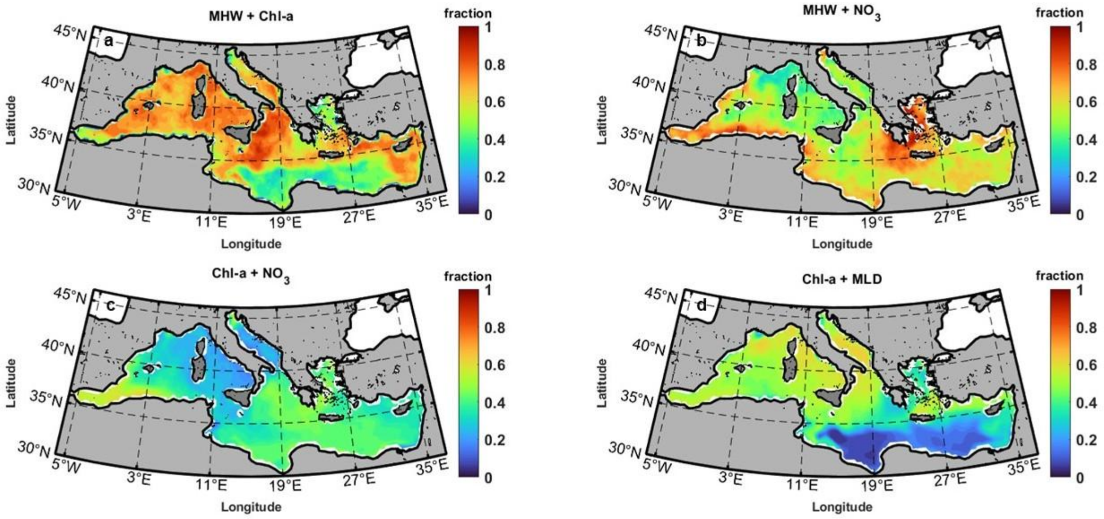

Figure 70. *Spatial distribution of pairwise co-occurrence fractions between environmental anomalies in the Mediterranean Sea. Panels show the fraction of days where MHWs coincide with -ve anomalies in (a) chlorophyll-a, (b) nitrate. The fraction of days where -ve anomalies of Chl-a coincide with MLD (c), and nitrate (d).*

Higher-order compound events (Fig. 71) reveal that multi-stressor conditions are not only present but widespread. The combination of MHWs with simultaneous reductions in Chl-a and MLD is particularly frequent in the WMB (Fig. 71a), while the combination of MHWs with simultaneous reductions in Chl-a and NO_3 is more evident in the Alboran Sea and Western and Eastern Mediterranean basins (Fig. 71b). The full compound condition (MHW + Chl-a + MLD + NO_3) reaches moderate but significant occurrence levels across the basin and shows highest cooccur in the Alboran Sea (Fig. 71c). These results are consistent with the global findings of Le Grix et al., (2021, 2022), who showed that compound MHW-low productivity events occur more frequently than expected and are strongly linked to stratification-driven nutrient limitation. The Mediterranean patterns suggest that such compound stress is regionally amplified in areas with strong seasonal mixing and biological productivity.

The seasonal evolution of co-occurrence events (Fig. 72) highlights a pronounced seasonal modulation of MHW impacts. Compound events involving MHWs and reduced Chl-a or NO_3 peak during autumn (OND) and spring (AMJ), while summer (JAS) shows elevated co-occurrence between Chl-a and MLD but weaker multi-variable combinations.

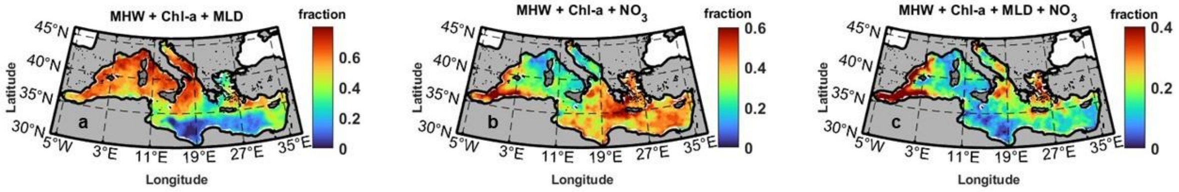

Figure 71. *Spatial distribution of compound environmental stress events in the Mediterranean Sea. Panels show the fraction of days where MHWs co-occur with multiple negative anomalies, including combinations of chlorophyll-a, nitrate, and mixed layer depth.*

Winter is characterized by strong co-occurrence of MHW+NO_3, MHW+Chl-a and a combination of three of them, reflecting the sensitivity of nutrient dynamics during the mixing season. Spring and summer Chl-a concentration are more affected by MHW and MLD anomaly. The Autumn season is showing transition condition between the other three seasons, with conditions more similar to the winter season. This seasonal structure indicates that MHW impacts are not confined to summer extremes but extend into transitional seasons when stratification and nutrient supply are rapidly evolving. Similar seasonal dependence of MHW-driven ecosystem responses has been reported in both regional and global studies (Smale et al., 2019; Oliver et al., 2021; Darmaraki et al., 2024).

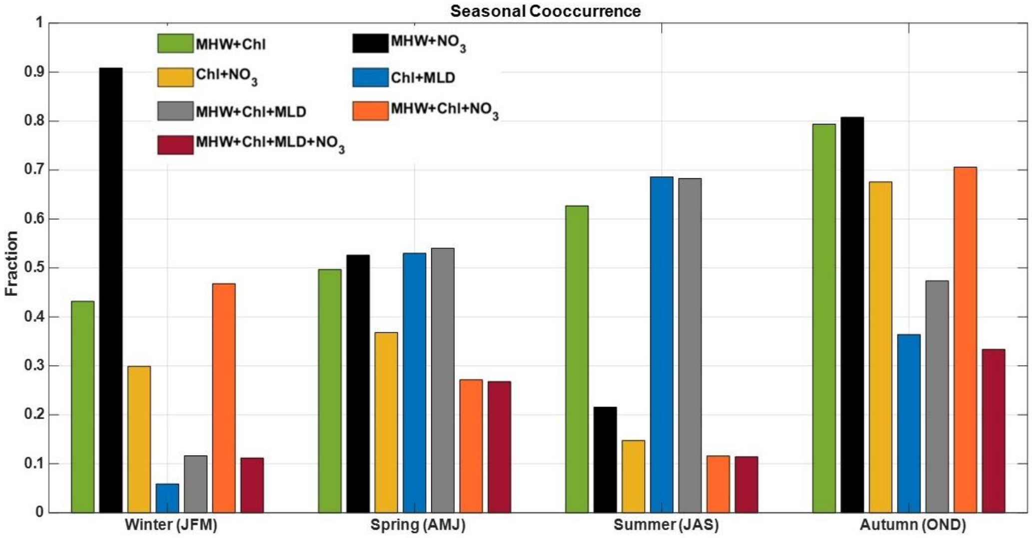

Figure 72. *Seasonal variability of co-occurrence fractions between MHWs and environmental anomalies in the Mediterranean Sea for winter (JFM), spring (AMJ), summer (JAS), and autumn (OND). Bars represent the fraction of days for each pairwise and compound condition.*

Interannual variability (Fig. 73) shows a clear increase in both pairwise and compound co-occurrence events over time, particularly after the mid-2000s. The frequency of MHW+Chl-a and MHW+NO_3 events has increased substantially in recent years (Fig. 73a), while compound events involving multiple stressors are showing strong interannual variability (Fig. 73b). This trend reflects the combined effect of increasing MHW frequency and intensity under climate warming, as well as the growing likelihood of concurrent physical and biogeochemical extremes. The amplification of compound events over time is consistent with global projections of increasing compound climate risks in the ocean (Le Grix et al., 2021, 2022, 2025; Hamdeno et al., 2022; Chen et al., 2023).

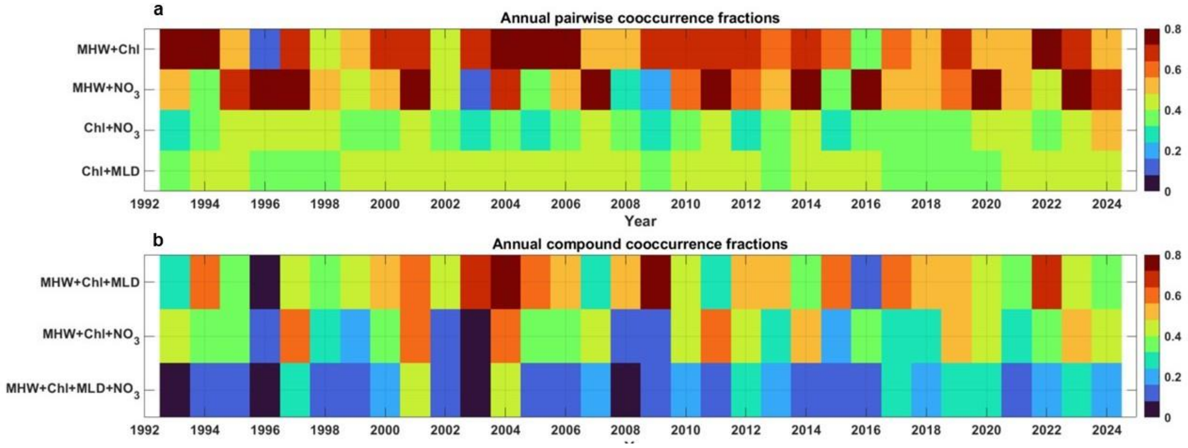

Figure 73. *Interannual variability of co-occurrence fractions between MHWs and environmental anomalies in the Mediterranean Sea over the period 1993–2024. Time series show annual fractions of pairwise and compound stress events.*

Overall, the results show that MHW impacts in the Mediterranean Sea are driven by a strong coupling between thermal extremes, stratification, and biogeochemical responses. MHWs consistently enhance stratification (reduced MLD), which limits vertical nutrient supply and leads to lower phytoplankton biomass, particularly in the more productive western basin. The spatial heterogeneity between the WMB and EMB reflects fundamental differences in basin structure: the WMB is characterized by active winter mixing and higher nutrient availability, making it more sensitive to stratification-induced productivity declines, while the EMB is persistently oligotrophic and thus shows weaker relative responses.

The high frequency of compound events and their strong seasonality highlight that MHW impacts are not isolated phenomena but part of a broader multi-stressor framework, where physical and biogeochemical processes interact to amplify ecosystem stress. The observed intensification of compound events over time further indicates that climate-driven increases in MHW occurrence are likely to increase the frequency and severity of ecological impacts in the Mediterranean.

These findings are fully consistent with the known characteristics of the Mediterranean Sea as a semi-enclosed, strongly stratified basin with pronounced west-east gradients in productivity and circulation, where relatively small changes in vertical mixing can lead to substantial ecological consequences.

6.2.2 Impacts of MHWs in the Red Sea:

The spatial distribution of MHW occurrence (Fig. 74) shows a clear north-south gradient, with the highest number of events concentrated in the central and southern Red Sea, while lower frequencies are observed in the northern basin. This pattern reflects the strong meridional thermal gradient and the enhanced background warming and stratification in the southern region, which has been identified as a hotspot for extreme warming events (Hamdeno et al., 2024).

Figure 75 shows the relationship between SST anomalies and environmental variables in the Red Sea, combining both correlation patterns (upper panels) and mean differences between MHW and non-MHW conditions (lower panels). The upper panels indicate that SST anomalies are predominantly negatively correlated with mixed layer depth anomalies throughout most of the basin (Fig. 75a), indicating that stronger warming is systematically associated with mixed-layer shoaling and intensified stratification. In contrast, SST anomalies show mostly positive correlations with chlorophyll-a and nitrate anomalies in the central Red Sea (Fig. 75b,c), suggesting that short-term variability in biological and nutrient fields may co-evolve with thermal anomalies, particularly in regions influenced by mesoscale processes and circulation variability.

The lower panels show the mean environmental response during MHW conditions. MHW days are characterized by strong negative MLD anomalies across the basin (Fig. 75d), confirming enhanced stratification as a dominant feature of Red Sea MHWs. Chlorophyll-a anomalies are generally negative, especially in the northern and southern regions (Fig. 75e), indicating reduced surface phytoplankton biomass under persistent warming conditions. Similarly, nitrate anomalies are predominantly negative throughout the basin (Fig. 75f), reflecting reduced nutrient availability in the euphotic layer due to suppressed vertical mixing. These patterns are consistent with the highly oligotrophic nature of the Red Sea, where nutrient supply is strongly controlled by vertical exchange processes and stratification (Raitsos et al., 2013; Krokos et al., 2019).

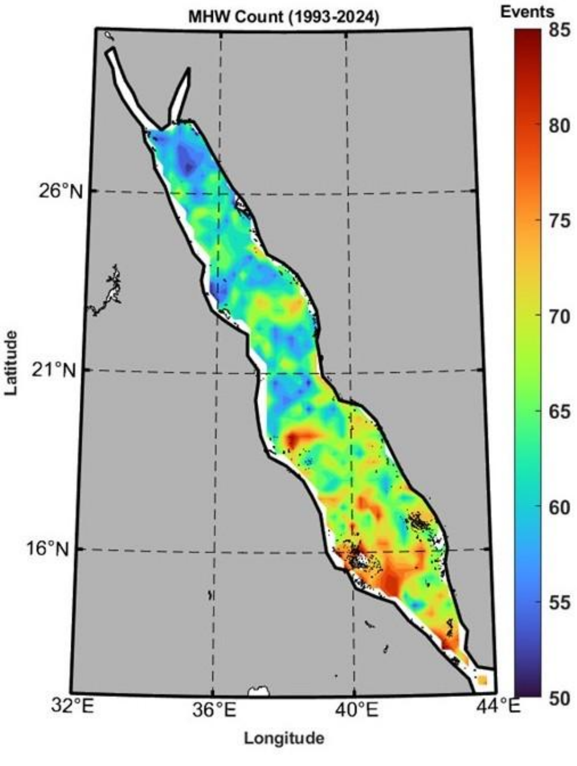

Figure 74. *Spatial distribution of the total number of MHW events over the period 1993–2024 in the Red Sea, highlighting the north–south gradient in MHW occurrence.*

The contrast between correlation and composite difference maps highlights that, although chlorophyll-a and nitrate anomalies may co-vary with SST anomalies on short timescales, the net effect of MHW conditions is a reduction in nutrient supply and biological productivity. This behaviour is consistent with previous studies showing that Red Sea MHWs are driven by atmospheric forcing and stratification processes, leading to enhanced upper-ocean stability and reduced nutrient entrainment (Raitsos et al., 2011, 2013; Chaidez et al., 2017). Overall, the results indicate that Red Sea MHWs amplify existing oligotrophic conditions, reinforcing nutrient limitation and suppressing biological productivity.

The co-occurrence patterns (Fig. 76) indicate that MHWs frequently coincide with Chl-a and NO_3 anomalies, with particularly high fractions in the northern and southern Red Sea. However, the co-occurrence between Chl-a and MLD/ NO_3 alone remains weaker, suggesting a less direct coupling between stratification and biological response. The strong MHW-biogeochemical co-occurrence likely reflects the dominant role of temperature as a stressor in an already nutrient-limited system, rather than a purely mixing-driven mechanism.

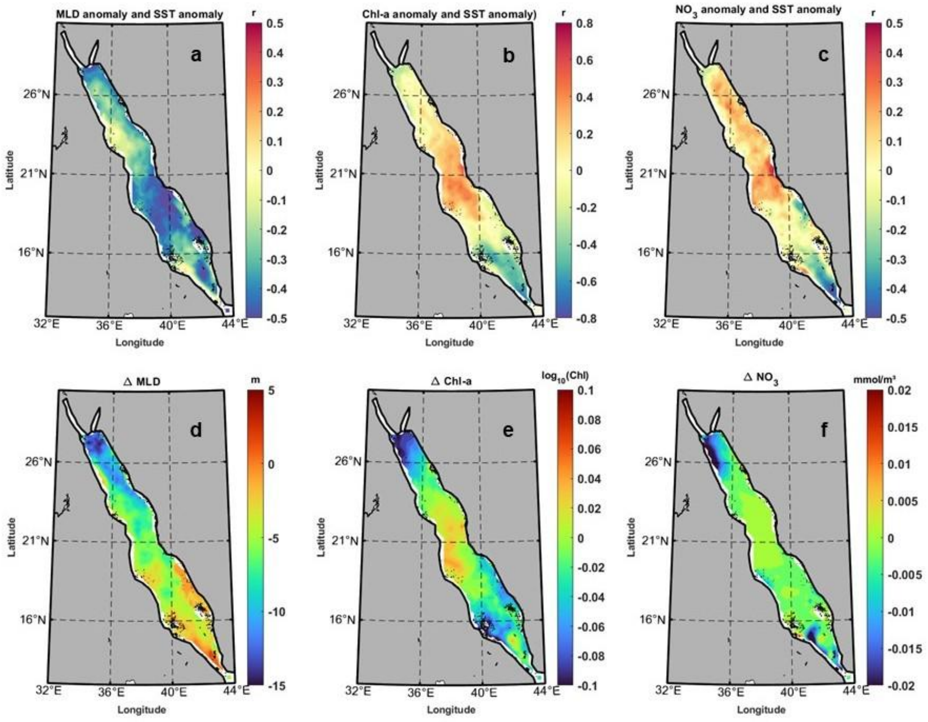

__Figure 75.__ Environmental covariability with MHW intensity and mean environmental response during MHW conditions in the Red Sea (same panels as Fig. 69).

Higher-order compound events (Fig. 77) confirm that multi-stressor conditions are widespread but spatially variable. The combination of MHWs with Chl-a and NO_3 anomalies is particularly pronounced in the northern southern basin, while the full compound condition (MHW + Chl-a + MLD + NO_3) occurs at moderate levels.

The seasonal variability of co-occurrence events (Fig. 78) shows a distinct pattern compared to the Mediterranean. Compound events peak during summer (JAS) and autumn (OND), when thermal stratification is strongest, and remain relatively elevated throughout the year. Winter (JFM) exhibits lower but still significant co-occurrence, particularly for MHW and NO_3 interactions. This reduced seasonality reflects the limited seasonal mixing in the Red Sea, where stratification persists year-round and biological responses are less strongly modulated by seasonal overturning compared to temperate basins (Raitsos et al., 2013). Interannual variability (Fig. 79) highlights a progressive intensification and high interannual variability of both pairwise and multi-compound events. The frequency of MHW + NO_3 and MHW + Chl-a events shows the highest occurrences across the study period (Fig. 79a), while among the multi-compound events the combination of MHW + Chl-a + NO_3 are the more likely to occur (Fig. 79b).

The results show that MHW impacts in the Red Sea are primarily governed by persistent thermal stress superimposed on a strongly stratified and oligotrophic system. Unlike the Mediterranean, where MHW impacts are closely linked to reductions in vertical mixing and nutrient supply, the Red Sea response is less directly controlled by MLD variability and more influenced by background nutrient limitation and the dominance of temperature as a stressor. The north-south gradient plays a key role in modulating these impacts: the northern Red Sea exhibits stronger stratification anomalies and more pronounced physical responses, while the southern basin shows higher MHW frequency and stronger compound biogeochemical stress. This reflects fundamental differences in circulation and nutrient dynamics, with the southern Red Sea influenced by Indian Ocean inflow and higher baseline productivity, making it more sensitive to compound stress conditions.

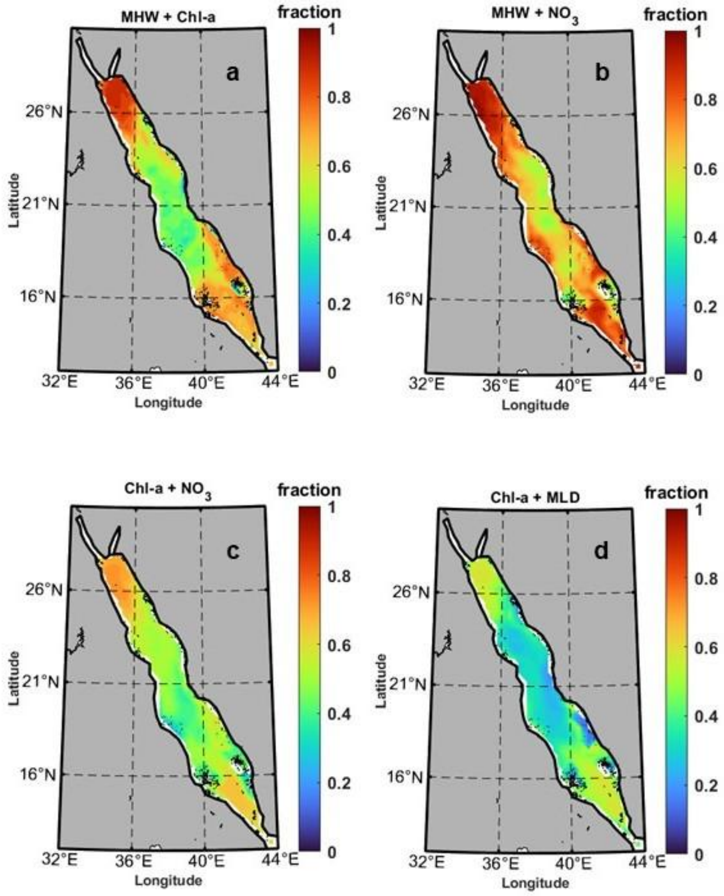

Figure 76. Spatial distribution of pairwise co-occurrence fractions between MHWs and environmental anomalies in the Red Sea.

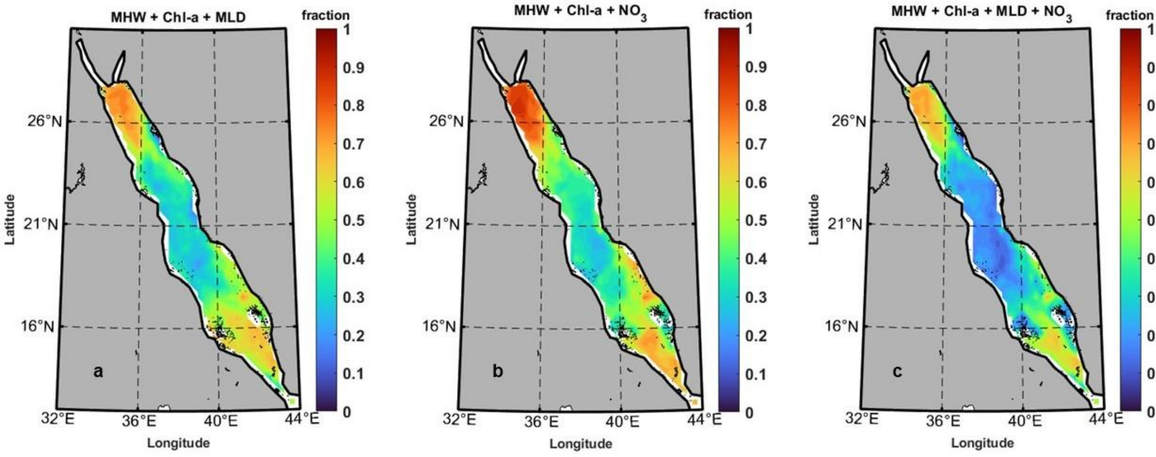

__Figure 77.__ Spatial distribution of compound environmental stress events in the Red Sea, showing the fraction of days where MHWs co-occur with multiple negative anomalies in chlorophyll-a, nitrate, and mixed layer depth.

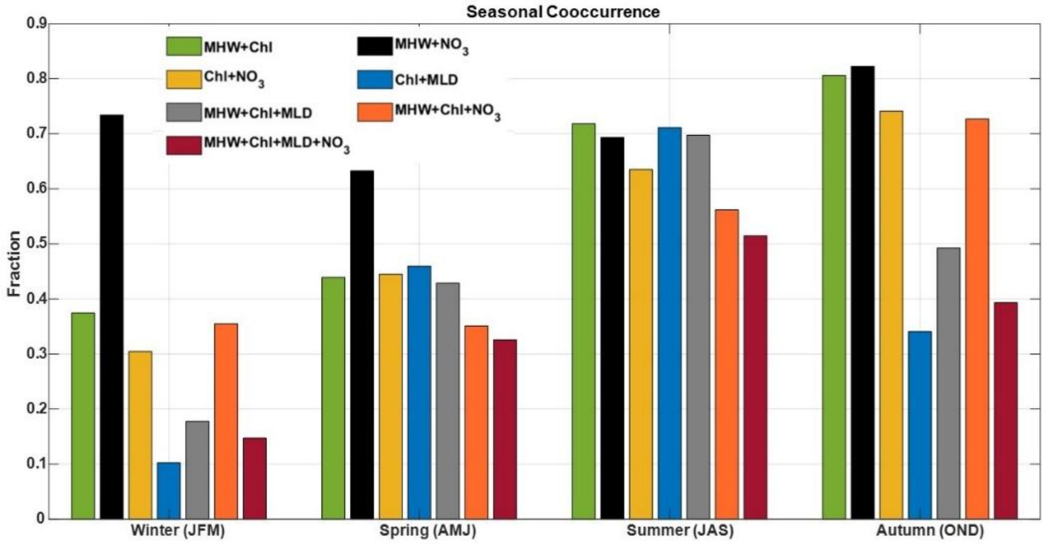

__Figure 78.__ Seasonal variability of co-occurrence fractions between MHWs and environmental anomalies in the Red Sea for winter (JFM), spring (AMJ), summer (JAS), and autumn (OND).

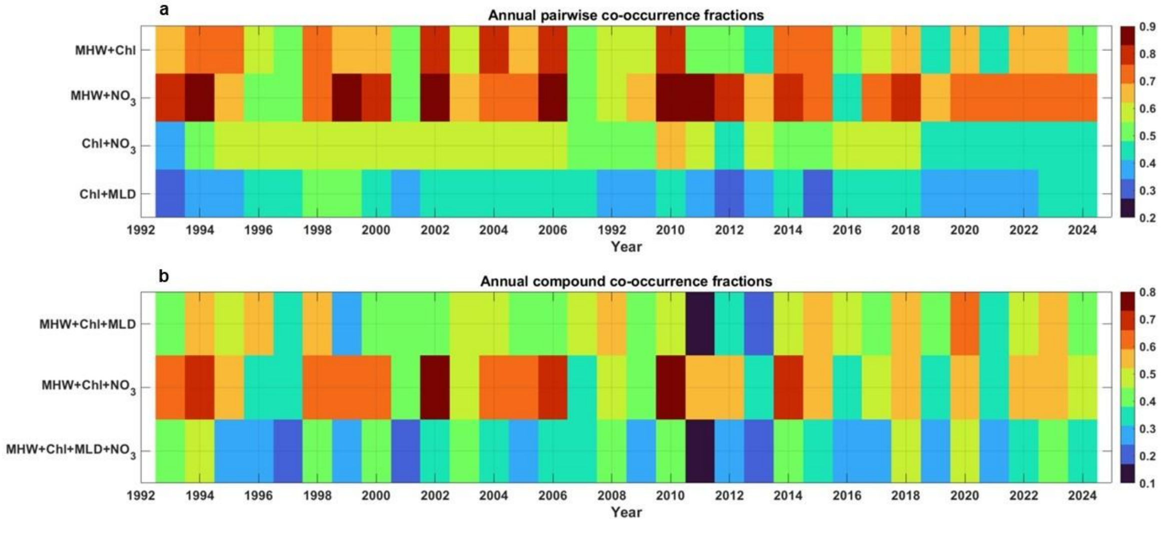

__Figure 79.__ Interannual variability of co-occurrence fractions between MHWs and environmental anomalies in the Red Sea over the period 1993–2024.

Overall, the Red Sea functions as a thermally dominated system, where MHWs amplify existing environmental constraints rather than fundamentally altering nutrient dynamics. The increasing frequency of compound events and their relatively weak seasonality indicate that ecosystem stress is becoming more persistent and less dependent on seasonal variability, highlighting the vulnerability of this basin under continued warming.

6.2.3 Role of Wind Systems, Nutrient Supply, and Bloom Seasonality in the Mediterranean and Red Sea:

The contrasting impacts of MHWs in the Mediterranean Sea and the Red Sea are primarily controlled by differences in wind-driven mixing, nutrient availability, and seasonal productivity regimes, which explain the patterns observed in Figs. 68–79.

In the Mediterranean Sea, regional wind systems such as the Mistral, Bora, and Etesian winds strongly regulate upper-ocean mixing and nutrient supply (D'Ortenzio and Ribera d'Alcalà, 2009; Josey et al., 2011). Winter mixing replenishes nutrients and supports the spring bloom, particularly in the western basin. This tight coupling between wind forcing and productivity explains why MHWs are associated with mixed-layer shoaling and reduced chlorophyll-a and nitrate concentrations (Fig. 69), reflecting suppressed vertical nutrient transport. The high occurrence of compound events (Figs. 70-71) further indicates that ecosystem responses are strongly controlled by stratification changes. These results are consistent with previous studies showing that Mediterranean productivity is highly sensitive to wind-driven mixing and stratification variability (D'Ortenzio et al., 2014; Hamdeno and Alvera-Azcaráte, 2023; Darmaraki et al., 2024).

In contrast, the Red Sea is dominated by along-basin winds and monsoon variability, with persistent stratification and limited deep mixing (Zhai and Bower, 2013; Yao et al., 2014). As a result, mixed-layer variability is weaker and primarily controlled by surface heat fluxes rather than wind-driven turbulence (Raitsos et al., 2013; Krokos et al., 2022). This explains why MHWs occur frequently (Fig. 74) but are associated with relatively uniform MLD anomalies (Fig. 75), indicating sustained stratification. Biological responses are weaker and more heterogeneous, with reduced and spatially variable chlorophyll-a and nitrate anomalies (Fig. 75), reflecting strong background oligotrophy. Compound events (Figs. 76-77) are widespread but less tightly linked to mixing, consistent with studies showing that Red Sea productivity is primarily limited by nutrient availability and influenced by lateral inputs (Raitsos et al., 2013; López-Sandoval et al., 2019).

Overall, the key difference between the two basins lies in the efficiency of wind-nutrient coupling. In the Mediterranean, wind-driven mixing tightly links physical and biological processes, leading to strong ecosystem responses to MHW-induced stratification. In the Red Sea, persistent stratification weakens this coupling, resulting in a more thermally dominated and spatially heterogeneous response. This explains the stronger and more coherent biogeochemical impacts of MHWs in the Mediterranean compared to the more diffuse response in the Red Sea.

6.2.4 Effects of a Simulated Marine Heatwave on Copepods:

The lab experiment reveals a strong and direct response of zooplankton survivorship to MHW intensity and thermal structure. The selection of the events was based on their severity and duration (maximum duration of 20 days to suit the lab experiment conditions). The most intense events in the Western Mediterranean were Category II events that occurred in summers 2018 and 2019, while the Bay of Biscay (BB) intense event occurred in July 2013 with Category IV (Hobday et al., 2018). In order to simulate the same category observed in the BB MHW event, the Mediterranean MHW events were intensified to represent the worst-case scenario (WCS) of the same events (their temperature was increased to match the same period and peak day, but with SST exceeding four times the threshold baseline).

The temperature evolution of the Mediterranean MHW events (Figs. 80 and 81) shows that even moderate Category II events are characterized by sustained temperature anomalies above the climatological threshold, while the synthetic worst-case scenarios (WCS; Category IV) reach substantially higher peak temperatures and sharper gradients. The temporal evolution of copepod survivorship highlights a rapid decline under elevated temperature conditions (Figs. 82 and 83). During the July-August 2018 event (Fig. 82), survivorship decreases progressively under observed MHW conditions, reaching near-zero values within approximately 9 days. Under the WCS scenario, mortality occurs much faster, with survivorship collapsing within about 6 days. A similar pattern is observed for the June-July 2019 event (Fig. 83), where survivorship declines more gradually under real conditions but exhibits a rapid and near-complete collapse under intensified warming.

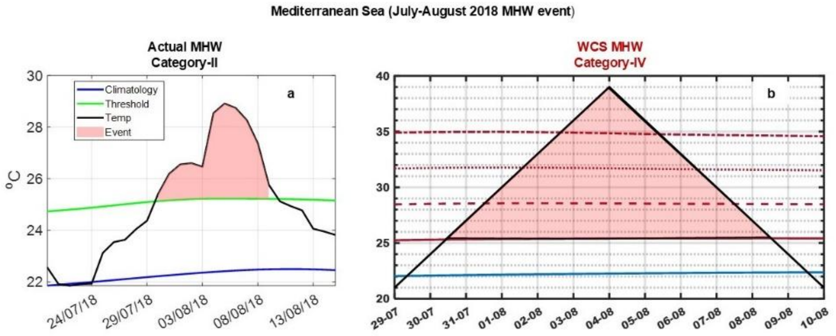

__Figure 80.__ Time series of SST (°C) during the July–August 2018 Mediterranean MHW event, showing actual observed temperatures (a), and synthetic worst-case scenario (WCS; b).

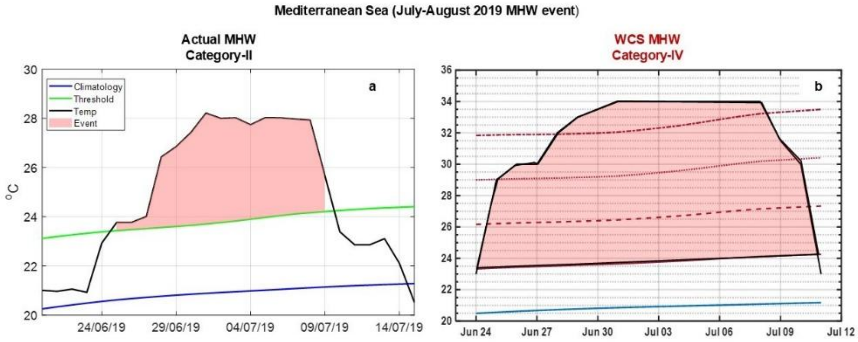

__Figure 81.__ Time series of SST (°C) during the June–July 2019 Mediterranean MHW event, including climatology, threshold, observed temperatures, and worst-case scenario (WCS).

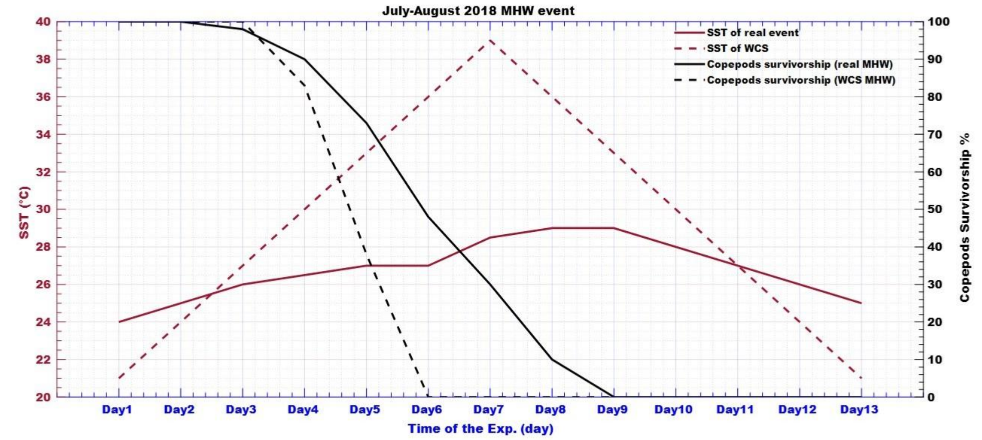

Figure 82. *Temporal evolution of copepod survivorship (%) during the July–August 2018 experiment for observed MHW, and worst-case scenario (WCS).*

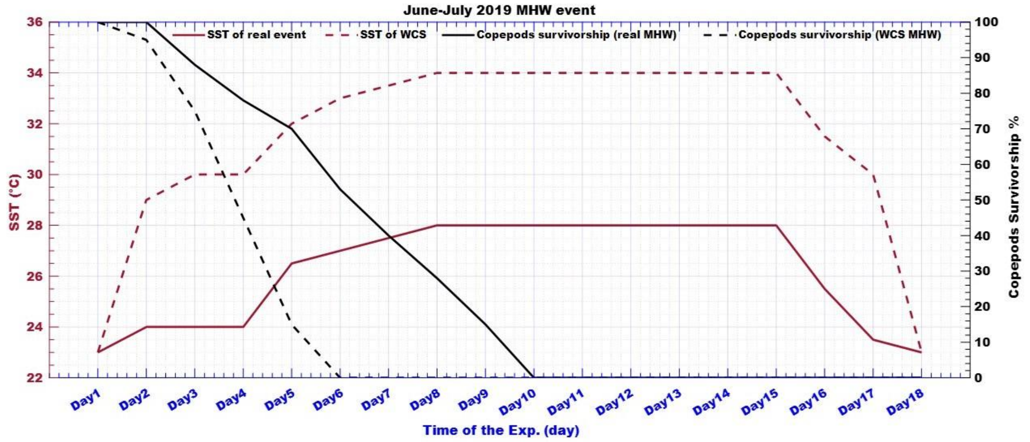

Figure 83. *Temporal evolution of copepod survivorship (%) during the June–July 2019 experiment for observed MHW, and WCS conditions.*

The MHW event that occurred in July-2013 in the BB is shown in Figure 84. The event is wide spread in the basin with temperature anomaly about 4° C on the peak day. During the July 2013 event (Fig. 85), survivorship decreases progressively under observed MHW conditions, reaching 10% within 13 days (period of the MHW event). The comparison between observed Mediterranean and BB copepods survivorship provides important context for interpreting the severity of Mediterranean heatwaves. Despite being classified as a lower category event, the Mediterranean MHW produces a stronger and faster decline in survivorship compared to the BB case. This indicates that absolute temperature levels and baseline thermal conditions play a critical role in biological response, beyond categorical classification alone. The BB event shows a more gradual mortality curve, suggesting that organisms exposed to cooler baseline conditions may exhibit higher thermal tolerance or slower stress accumulation.

The aggregated comparison of survivorship across experiments (Fig. 86 and 87) further emphasizes these differences. Mediterranean events, particularly under WCS conditions, consistently show the most rapid decline in survivorship, followed by the BB event, while control conditions maintain high survival rates throughout the experiment. This confirms that temperature intensity and exposure duration jointly control mortality rates, with nonlinear responses under extreme warming.

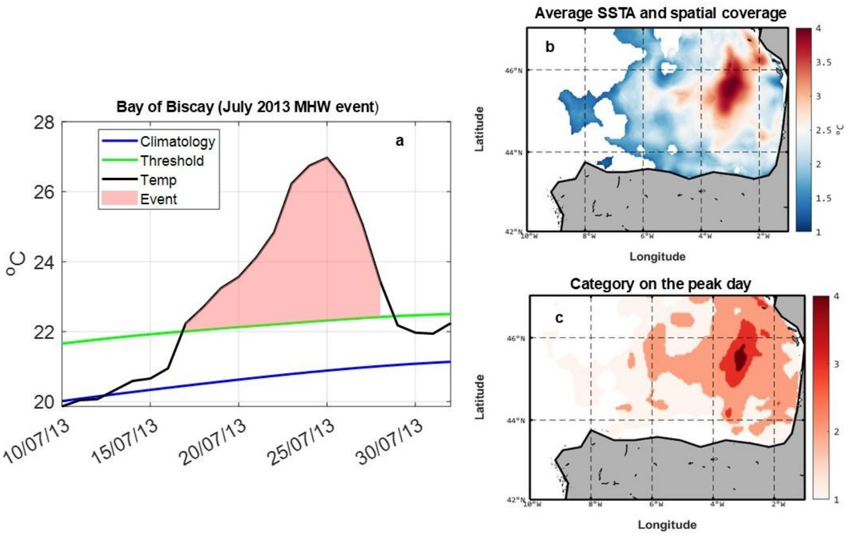

Figure 84. *The temperature evolution (a), average SSTA (b), and category (c) of the Bay of Biscay July-2013 MHW event.*

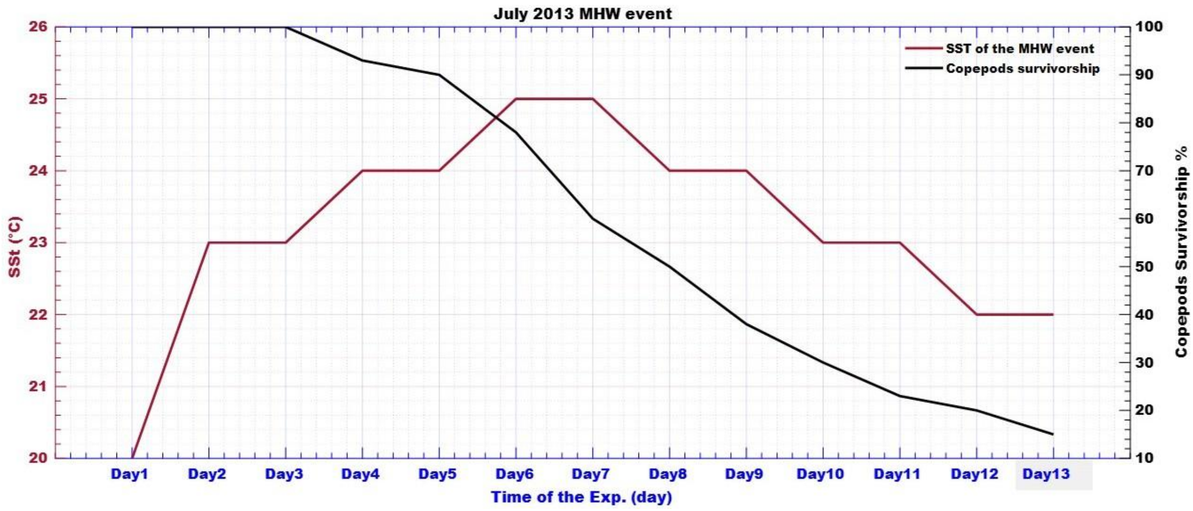

Figure 85. *Temporal evolution of copepod survivorship (%) during the July-2013 experiment for observed Bay of Biscay MHW event.*

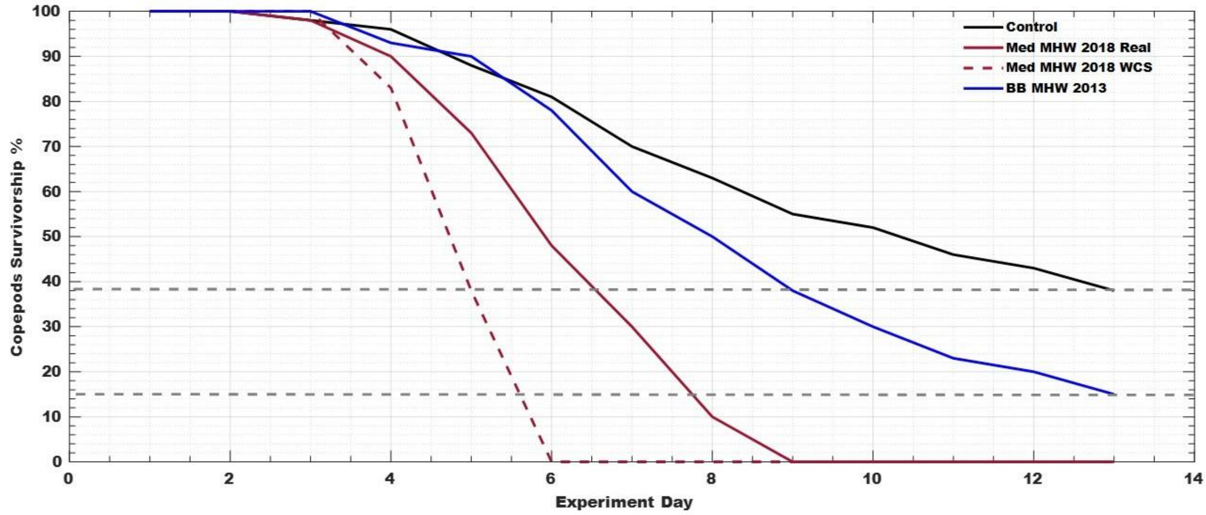

Figure 86. *Comparison of copepod survivorship (%) across experiments, including Mediterranean 2018 event, Bay of Biscay event, and control conditions (13-days experiments).*

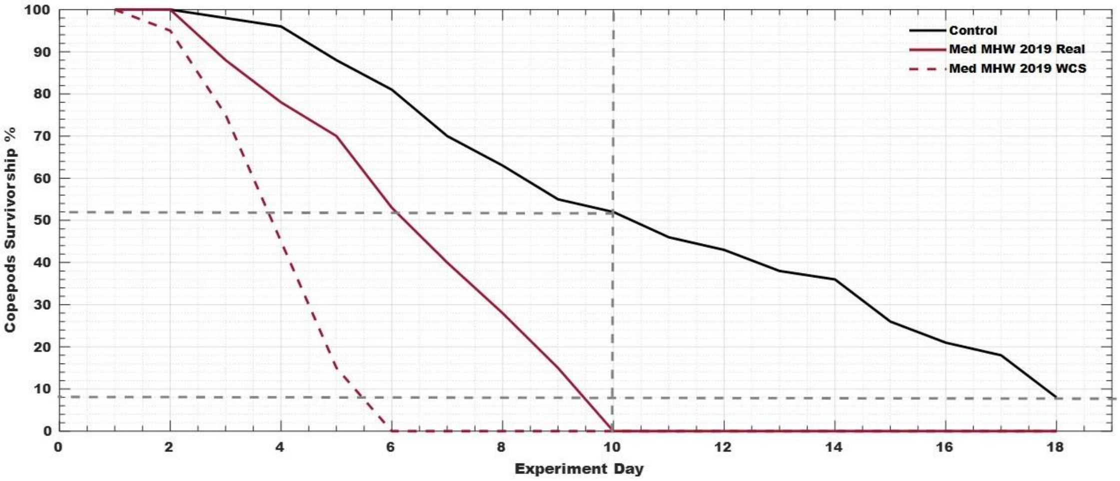

Figure 87. *Comparison of copepod survivorship (%) across experiments, including Mediterranean 2019 event and control conditions (18-days experiments).*

The extended survivorship analysis (Figs. 86-87) reinforces the robustness of these findings across different experimental durations. In both Mediterranean cases, survivorship declines steadily under real MHW conditions but reaches zero significantly earlier under WCS forcing. The persistence of individuals under control conditions highlights that mortality is primarily driven by thermal stress rather than experimental artifacts.

These results demonstrate that MHWs exert a strong physiological impact on zooplankton, primarily through increased mortality rather than behavioural changes. The absence of significant changes in swimming or grazing behaviour observed during the experiment suggests that lethal thermal thresholds are reached before substantial sublethal behavioural responses occur, indicating a rapid transition from tolerance to mortality under extreme conditions.

Importantly, the comparison across regions shows that Mediterranean MHWs are more biologically severe than Bay of Biscay events, even when classified at lower intensity categories. This reflects the influence of warmer baseline conditions in the Mediterranean, where organisms are already closer to their upper thermal limits, making them more vulnerable to additional warming.

6.3 Conclusion:

MHWs have significant and consistent impacts on marine ecosystems in both the Mediterranean Sea and the Red Sea. At the basin scale, MHWs are associated with enhanced stratification, reduced mixed layer depth, and lower nutrient availability, resulting in declines in chlorophyll-a and indicating suppressed primary productivity. These effects are particularly pronounced in oligotrophic regions, where limited nutrient supply amplifies ecosystem sensitivity to warming. Co-occurrence analysis shows that MHWs often coincide with multiple unfavourable environmental conditions, creating compound stress events that intensify ecosystem impacts. These compound conditions are widespread in both basins and display strong seasonal variability, peaking during stratified periods. Differences between basins reflect their contrasting oceanographic regimes: the Mediterranean shows greater spatial variability due to dynamic mixing, while the Red Sea shows more persistent and coherent responses driven by strong stratification.

Experimental results demonstrate that elevated temperatures associated with MHWs directly increase zooplankton mortality, with rapid declines in survivorship under both observed and intensified warming scenarios. Mediterranean heatwaves, in particular, cause stronger biological impacts than events in cooler regions, underscoring the influence of baseline temperature on organismal vulnerability. Behavioural responses are limited, indicating that lethal thresholds are reached before significant physiological adaptation occurs.

These findings show that MHW impacts result from the combined effects of physical stratification, nutrient limitation, and direct thermal stress, with potential cascading consequences across trophic levels. As background ocean warming continues, MHWs are expected to become more frequent, intense, and persistent, further increasing compound environmental stress and ecosystem vulnerability, especially in semi-enclosed and oligotrophic basins.

Chapter Seven: Compound Marine and Atmospheric Extremes in the Mediterranean Sea: Co-occurrence of MHWs, Atmospheric Heatwaves, and Medicanes

Foreword

Extreme events in the Mediterranean Sea are increasingly recognized as interconnected phenomena rather than isolated processes. MHWs, atmospheric heatwaves (AHWs), and Mediterranean tropical-like cyclones (Medicanes) each represent distinct expressions of climate variability, yet they are fundamentally linked through air-sea interactions and shared physical drivers. Understanding these connections is essential for capturing the full complexity of regional climate extremes.

Previous studies have largely examined these phenomena independently, focusing either on oceanic heatwaves, atmospheric extremes, or individual storm events. However, recent evidence suggests that their co-occurrence and interaction can amplify impacts and modify underlying dynamics. In particular, the Mediterranean basin, characterized by strong stratification and tight air-sea coupling, provides a natural laboratory for investigating compound extremes.

This chapter builds on the analysis of MHWs presented in earlier chapters by extending the framework to include atmospheric heatwaves and Medicanes. It aims to quantify their co-occurrence, identify their dynamical links, and assess how ocean-atmosphere coupling influences both surface and subsurface responses. By combining statistical analysis, composite diagnostics, and case studies, this chapter provides a comprehensive perspective on compound extreme events in the Mediterranean Sea.

Ultimately, the goal is to move beyond a single-variable view of extremes and toward an integrated understanding of the coupled processes that govern their evolution, intensity, and impacts.

This research is currently being **prepared for submission to a peer-reviewed journal**.

7.1 Data and Methods:

7.1.1 Datasets:

This chapter examines compound extremes involving MHWs , atmospheric heatwaves (AHWs), and Mediterranean tropical-like cyclones (medicanes) over the Mediterranean Sea. SST is obtained from the NOAA Optimum Interpolation SST version-2 (OISST v2) dataset, which combines satellite and in situ observations on a 0.25° grid with daily resolution (Reynolds et al., 2007). Subsurface temperatures and mixed layer depth (MLD) fields are obtained from the Copernicus Marine Service Global Ocean Reanalysis product GLORYS12V1 (Jean-Michel et al., 2021)

Atmospheric variables are obtained from the ERA5 reanalysis produced by the European Centre for Medium-Range Weather Forecasts (ECMWF) (Hersbach et al., 2020). The dataset has a spatial resolution of 0.25° × 0.25°, and hourly fields are averaged to daily values. The atmospheric variables include 10 m wind components (U10, V10), 2m air temperature (Tair), 2m dew point temperature (d2m), mean sea level pressure (MSLP), shortwave radiation (Qs), longwave radiation (Qb), sensible heat flux (Qh), latent heat flux (Qe), and total cloud cover (TCC). These variables represent the main processes controlling air-sea heat exchange and upper-ocean forcing.

All atmospheric variables are expressed as daily anomalies relative to the 1993-2022 climatology, allowing consistent comparison across seasons and regions. Net surface heat flux (THF) and relative humidity (RH) are computed following the formulations described in Chapter 3 (Alduchov and Eskridge, 1996; Thomson and Emery, 2014; Nagy et al., 2017, 2021; Bawadekji et al., 2022).

A medicane event catalogue covering 1995-2023 was compiled from published case studies, documented storm lists (https://zivipotty.hu/tcr.html), and operational best-track information. For each event, storm timing, track, and intensity were identified from the literature and ERA5 sea level pressure fields. This study presents 23 medicanes distributed across the western, central, and eastern Mediterranean. For each storm, the genesis, peak intensity, and dissipation stages were defined to characterize the storm life cycle.

To evaluate the consistency between observationally reported medicane characteristics (https://zivipotty.hu/tcr.html) and ERA5-derived estimates, a comparative analysis was performed for events with available information in both datasets. A subset of 16 medicanes with documented minimum MSLP and maximum wind speed from observational reports was matched with corresponding ERA5-derived values at the time of peak intensity. Such intercomparison approaches are commonly used to assess the reliability of reanalysis products for representing Mediterranean cyclones and small-scale extreme systems (Hersbach et al., 2020; Gandoin and Garza, 2024). For each paired event, differences between reported and ERA5 values were quantified to assess systematic biases. Linear regression models were applied to evaluate the relationship between the two datasets:

$$\mathbf{X_{obs} = a + b \cdot X_{ERA5}}$$

X represents either minimum MSLP or maximum wind speed. Bias was defined as the mean difference between ERA5 and reported values. This type of regression-based calibration has been widely applied in cyclone intensity validation and reanalysis evaluation studies (Miglietta et al., 2013, 2025; Miglietta and Rotunno, 2019). Temporal trends in medicane intensity were estimated independently for reported data and ERA5 using least-squares regression (Wilks, 2019) applied to peak intensity values as a function of time.

7.1.2 Detection of Marine and Atmospheric Heatwaves:

MHWs were identified following the framework of Hobday et al. (2016), as described in previous chapters. AHWs were detected using an analogous threshold-based approach applied to daily T2m, following methods commonly used for heatwave detection in climate studies (Perkins and Alexander, 2013; Wilks, 2019). For each grid point, a daily climatology and corresponding 90th percentile threshold were computed from the full record. MHWs were defined as periods of at least five consecutive days with SST above the local threshold, while AHWs were defined as periods of at least three consecutive days with T2m above the local threshold (Perkins and Alexander, 2013; Hobday et al., 2016). The categories of both heat extremes were calculated using Hobday et al., (2018) categorizing method.

For both MHWs and AHWs, event properties including start and end date, duration, mean exceedance, maximum exceedance, and cumulative exceedance were computed and stored in event tables. Daily binary masks were then constructed to identify the occurrence of marine and atmospheric heatwaves at each grid cell. Compound marine-atmospheric heatwave days were defined as days when MHWs and AHWs occurred simultaneously at the same location. In addition to exact overlap, each MHW event was matched to the nearest AHW event within a ±30 day temporal window to assess lead-lag relationships between marine and atmospheric extremes. This framework enables quantification of both concurrent events and temporally related atmospheric–oceanic extremes.

Several metrics were used to characterize compound MHW-AHW occurrence. These include the fraction of MHW days that coincide with AHWs and the mean number of compound days per year. Seasonal analyses were conducted for winter (JFM), spring (AMJ), summer (JAS), and autumn (OND) to examine the temporal structure of compound heat extremes. To investigate whether compound marine-atmospheric heatwaves modify upper-ocean structure relative to ocean-only heatwaves, anomalies in mixed layer depth and subsurface layer temperature were analysed. Daily anomalies were calculated by removing the day-of-year climatology at each grid point and, for subsurface temperature, at each depth level using 1993-2022 climatology.

Composite analyses were then performed for two categories of days as compound MHW/AHW days, and MHW-only days. Differences between these composites were used to assess whether concurrent atmospheric heatwaves intensify upper-ocean stratification or enhance the downward penetration of warming. For subsurface temperature, composite vertical profiles were constructed for both categories, and the depth of heat penetration was quantified as the deepest level where the mean anomaly exceeded a fixed threshold. Basin-scale vertical profiles were also calculated to compare the mean subsurface structure of compound and ocean-only events.

7.1.3 Medicane Tracking and Warm-Ocean Interaction:

Storm trajectories were reconstructed from ERA5 mean sea level pressure fields by identifying the local pressure minimum around the previous storm position, following common cyclone-tracking approaches used in Mediterranean studies (Hodges, 1995; Campins et al., 2011). Starting from the reported genesis location, the storm center was updated every 6 hours, producing continuous storm tracks consistent with the synoptic evolution of each event.

To assess the interaction between medicanes and warm ocean conditions, a circular storm footprint with a radius of 200 km was defined around each storm center. At each time step, the fraction of the footprint overlapping with positive SST anomalies or active MHW conditions was calculated following the method of (Choi et al., 2024). Based on this overlap, storms were classified according to whether warm anomalies were absent, present during genesis, present near peak intensification, or persistent throughout most of the storm life cycle. This classification distinguished between storms that developed independently of anomalous ocean warmth and those whose evolution occurred in the presence of pre-existing marine heat extremes.

Composite analyses were then performed by separating storms into two groups:

- Storms interacting with positive SST anomalies or MHWs, and
- Storms without significant warm-ocean interaction.

For each group, atmospheric and oceanic variables were composited relative to the time of storm peak intensity, using a window extending from five days before to five days after the peak following the method of (Choi et al., 2024). Within the storms interacting with positive SST anomalies or MHWs, a comparison between the strong and weak storms characteristics were performed. The strong or weak classification was based on their minimum MSLP and maximum wind speed during their peak days. Strong medicanes are those that have wind speed > 20 m/s and MSLP < 1000 hPa, and the weak events have wind speed < 20 m/s and MSLP > 1000 hPa (Based on ERA5 data).

In addition to the statistical analysis, three selected case studies were examined in detail using spatial maps of SST anomalies, atmospheric circulation, surface fluxes, and upper-ocean temperature structure over the full storm life cycle. These event-scale analyses provide a mechanistic perspective on how pre-existing marine heat anomalies may influence storm development and how storm passage modifies the ocean surface and subsurface layers.

7.2 Results and Discussion:

7.2.1 Atmospheric and Oceanic Heatwaves Characteristics in the Mediterranean Sea:

The spatial structure of AHWs over the Mediterranean Sea shows a spatial variability in both mean characteristics and long-term trends (Figs. 88-89). On average, AHW frequency is highest over the northern Adriatic and parts of the central and eastern basins, where values exceed about four events per year, while the western basin generally shows lower frequencies (Fig. 88a). In contrast, AHW duration is longest in the western Mediterranean and along the northwestern African margin, where mean events typically last 7-8 days, while shorter events occur in parts of the eastern basin (Fig. 88b). Mean and maximum intensity also display strong regional contrasts: the eastern Mediterranean and adjacent land-influenced sectors show the highest mean intensity, and the southern-central Mediterranean and eastern basin exhibit enhanced maximum intensity (Fig. 88c-d). Cumulative intensity which the integrated anomaly over the AHW period shows highest values in the western and central Mediterranean (Fig. 88e). Total AHW days are also elevated in the western basin and parts of the Adriatic-Ionian sector (Fig. 88f), indicating that different AHW metrics peak in different subregions rather than forming a single Mediterranean-wide hotspot. This spatial heterogeneity aligns with previous work showing that Mediterranean atmospheric heat extremes are strongly shaped by local land-sea contrasts, regional circulation, and persistent subsidence associated with summer anticyclonic conditions (Aboelkhair et al., 2023; Paredes-Fortuny et al., 2025).

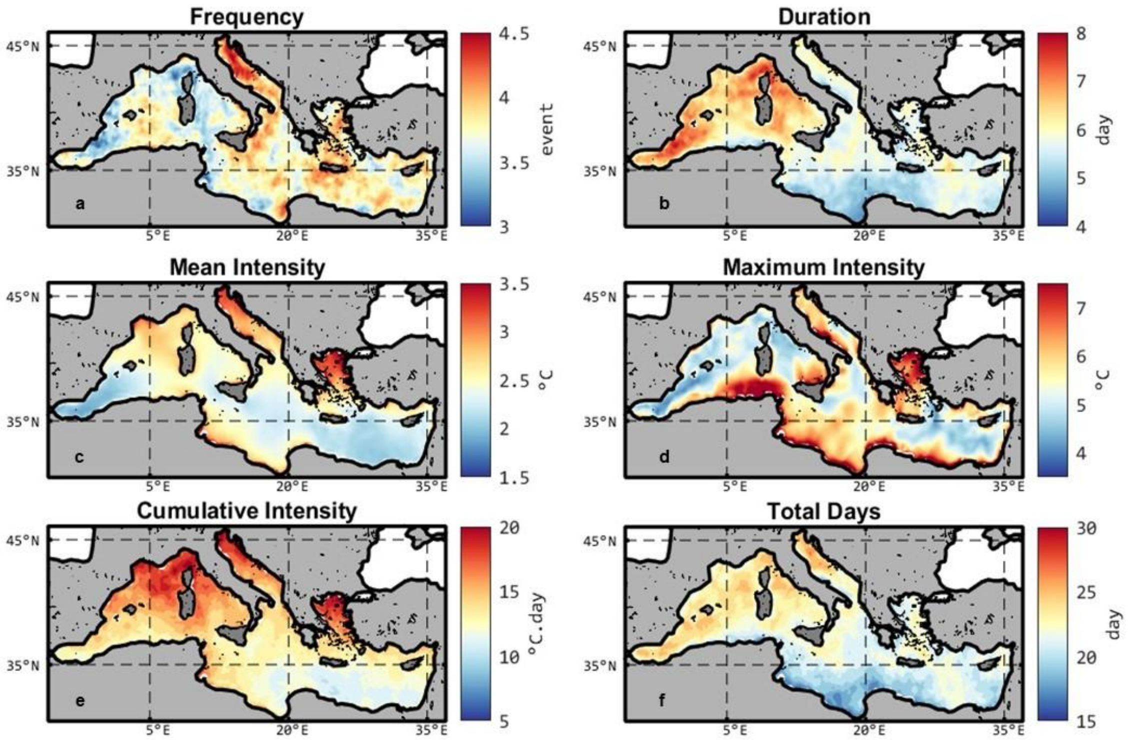

Figure 88. *Atmospheric heatwave (AHW) mean characteristics in the Mediterranean Sea. Spatial distribution of (a) frequency, (b) duration, (c) mean intensity, (d) maximum intensity, (e) cumulative intensity, and (f) total AHW days over the study period.*

Trend maps indicate that AHWs have intensified across most of the basin during the study period, although the magnitude of change varies regionally (Fig. 89). AHW frequency increases almost everywhere, with the strongest positive trends in the eastern Mediterranean and Adriatic sector, while duration also increases over large parts of the basin, particularly in the central and eastern Mediterranean (Fig. 89a-b). Mean intensity trends are generally across the entire basin (Fig. 89c), whereas the strongest increase in maximum intensity appears over the Aegean-Levantine region and south of the Ionian sea, where trends locally exceed 0.5 °C/decade (Fig. 89d). Cumulative intensity and total AHW days also show basin-wide positive trends, with the largest increases in the eastern and central Mediterranean (Fig. 89e-f). These patterns indicate that atmospheric heat extremes in the Mediterranean are not only becoming more frequent, but also longer and more energetically persistent, consistent with recent Mediterranean-scale studies documenting rapid intensification of compound and concurrent heat extremes under ongoing regional warming (Paredes-Fortuny et al., 2025).

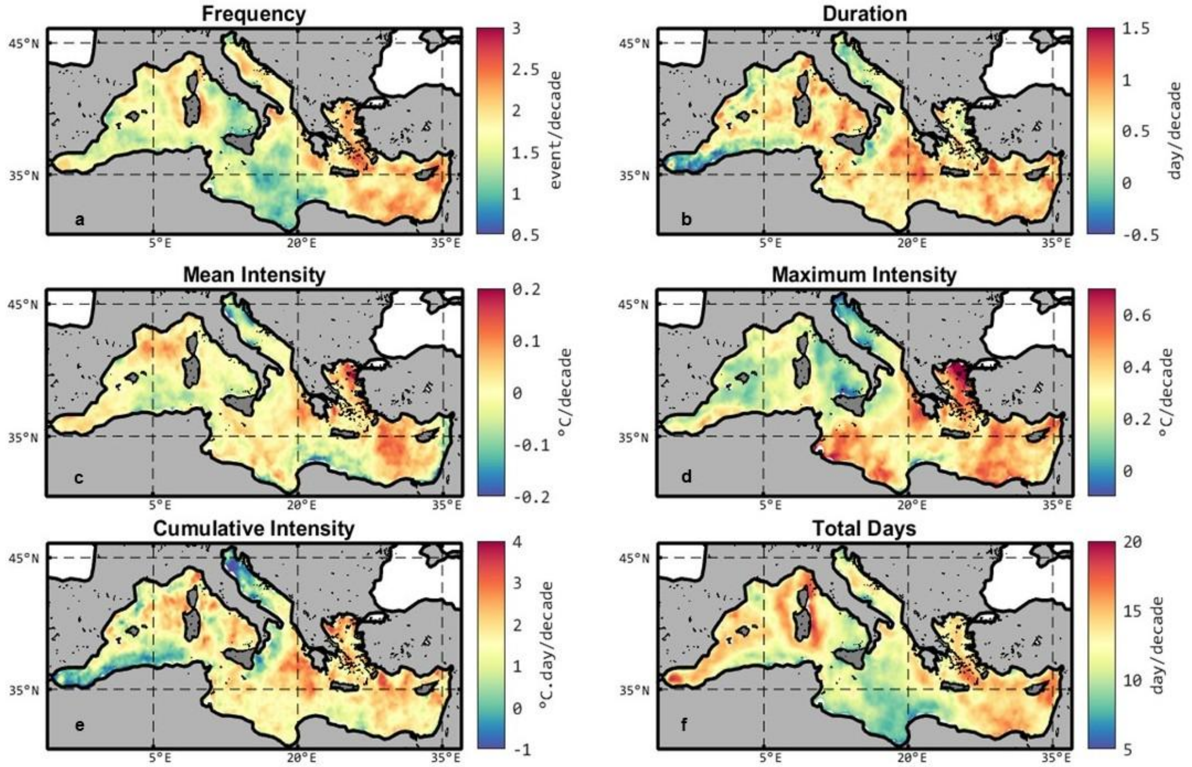

Figure 89. *Trends in atmospheric heatwave (AHW) characteristics. Spatial trends (per decade) of (a) frequency, (b) duration, (c) mean intensity, (d) maximum intensity, (e) cumulative intensity, and (f) total AHW days across the Mediterranean basin.*

The classification analysis further confirms that AHWs across the Mediterranean are dominated by moderate events, while strong events are concentrated mainly along the southern Mediterranean margin and the Levantine basin (Fig. 90). Moderate AHWs occur widely at rates of roughly three to six events per year and account for most annual heatwave days (Fig. 90b,c), indicating that recurrent moderate atmospheric extremes are the background state of Mediterranean summer warming. Strong AHWs are less frequent but cluster in the North African coastal zone and eastern Mediterranean, where their frequency and annual duration are clearly enhanced (Fig. 90d,e). This spatial distribution is physically consistent with stronger continental influence and greater lower-tropospheric heating over the southern and eastern Mediterranean, where land-sea thermal contrasts favor more persistent air temperature extremes.

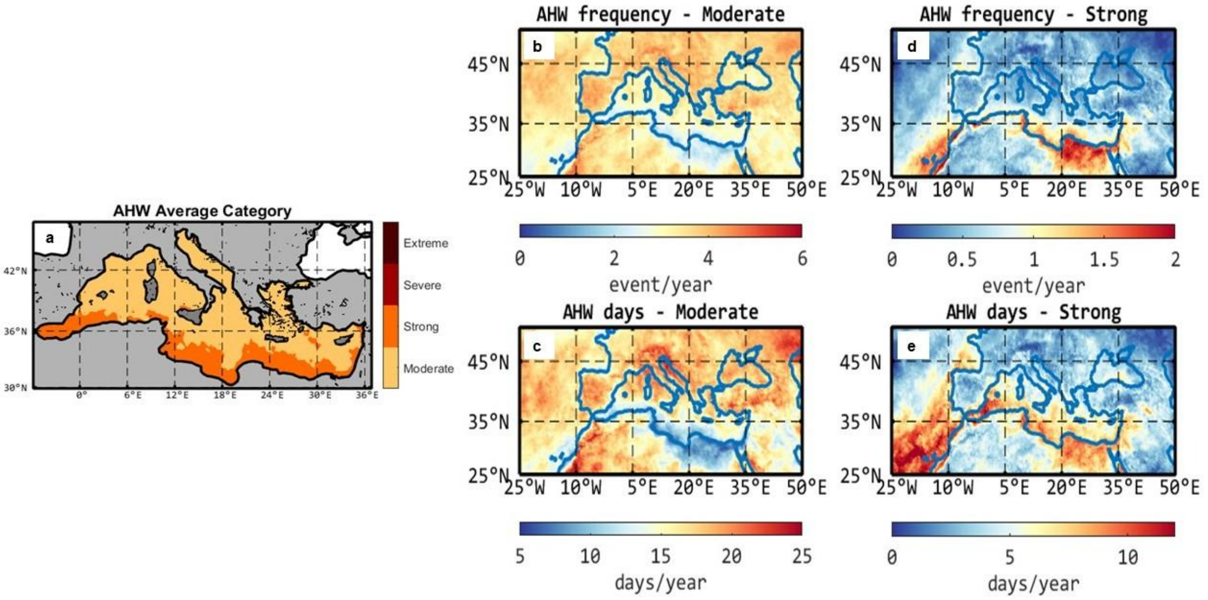

Figure 90. *Atmospheric heatwave (AHW) categories and occurrence. (a) Spatial distribution of mean AHW category. (b-e) Frequency and number of days associated with moderate and strong AHW events.*

MHW characteristics show some similar but not identical spatial patterns (Fig. 91). As discussed in detail in Chapter 2, Mediterranean MHWs have intensified markedly in recent decades, with a broad west-east contrast: the western basin tends to experience stronger and more frequent surface anomalies, while the eastern basin tends to show longer and more persistent events (Hamdeno and Alvera-Azcárate, 2023). The mean MHW category map also indicates that most of the basin remains in the moderate class, with localized transitions toward stronger categories in the eastern basin and some western subregions (Fig. 91a). In the present classification maps, moderate MHWs are widespread across nearly the entire basin and dominate the annual event count and annual MHW days (Fig. 91b-c). In contrast, strong MHWs are comparatively rare and spatially patchy, with higher occurrence in parts of the Alboran sea and the eastern Mediterranean (Fig. 91d-e). These patterns align with the established Mediterranean tendency for frequent moderate thermal anomalies, punctuated by regionally intense events, and support the basin's known sensitivity to both atmospheric forcing and accumulated ocean heat content (Pastor et al., 2020; Ibrahim et al., 2021; Hamdeno and Alvera-Azcaráte, 2023; Simon et al., 2023; Darmaraki et al., 2024).

A direct comparison of the AHW and MHW distributions reveals both strong coupling and significant regional asymmetries. Both types of extremes are widespread and predominantly moderate, with stronger signatures in the eastern and southern Mediterranean sectors. However, AHWs are more clearly organized by proximity to the southern land margins and eastern continental influence, while MHWs retain a stronger ocean-basin structure, with enhanced moderate-event activity across most of the open Mediterranean and more localized strong-event hotspots. In particular, strong AHW categories are more concentrated along the North African margin, while strong MHW occurrences are more spatially dispersed. This reflects the fact that atmospheric heat extremes respond rapidly to land-air forcing, whereas marine heat extremes integrate both atmospheric forcing and oceanic memory.

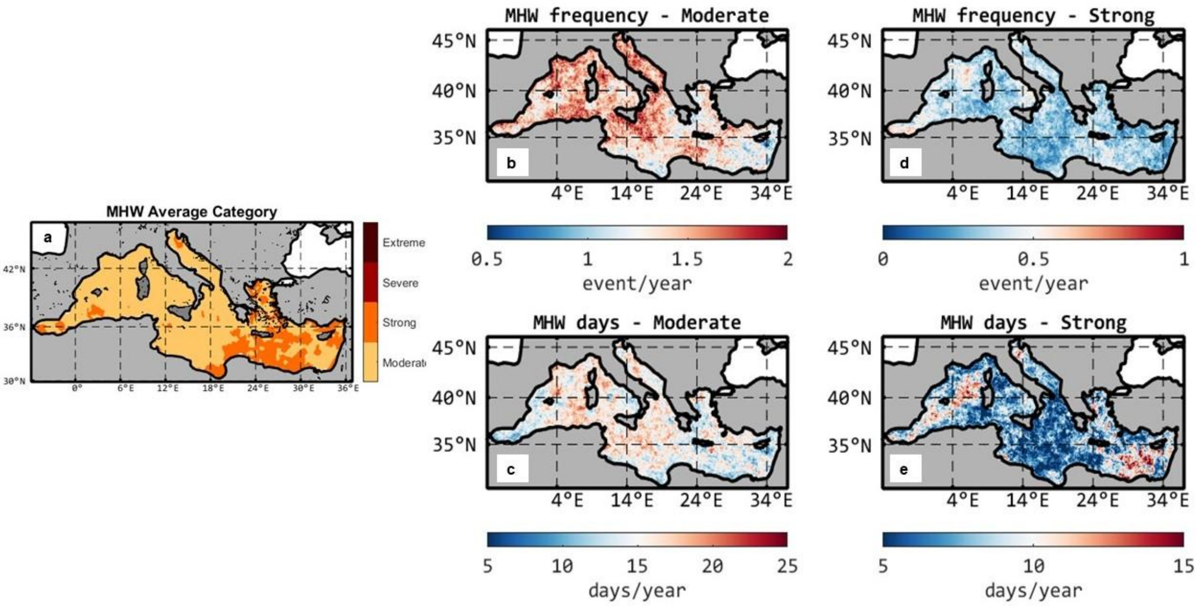

Figure 91. MHW categories and occurrence. (a) Spatial distribution of mean MHW category. (b-e) Frequency and number of days associated with moderate and strong MHW events.

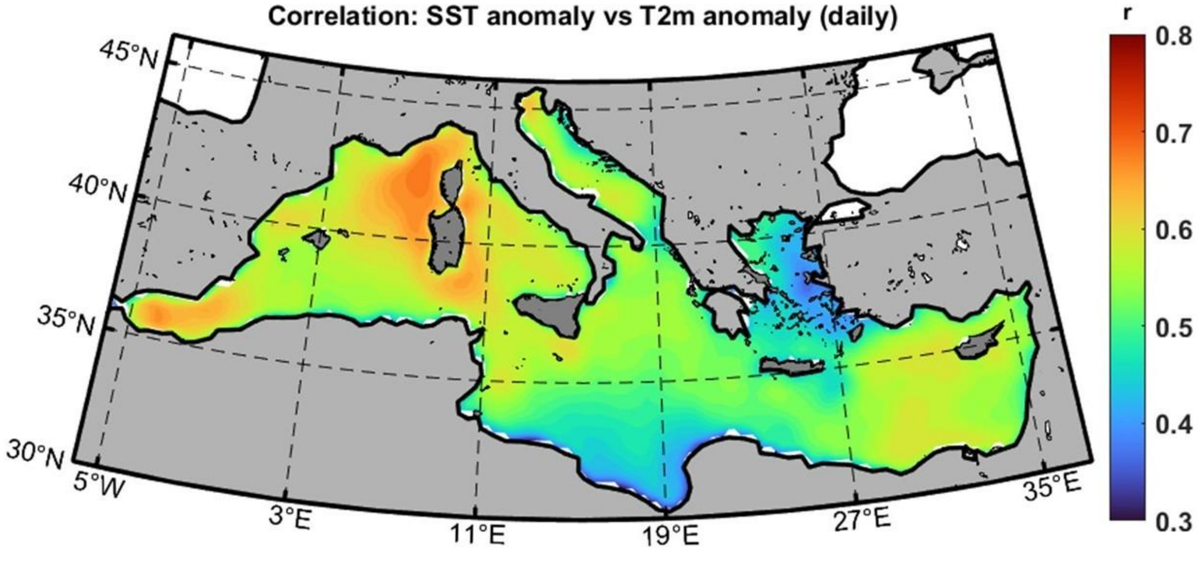

Figure 92. Spatial distribution of the Pearson correlation coefficient between daily SST anomalies and near-surface air temperature anomalies.

The daily correlation between SST anomalies and T2m anomalies confirms that the two systems are strongly linked across most of the Mediterranean (Fig. 92). Correlation coefficients are generally positive throughout the basin, reaching values above 0.6 in the western and central Mediterranean, with the strongest coupling in the northwestern basin and around the Balearic-Tyrrhenian sector. Lower correlations occur in the Aegean and parts of the central southern Mediterranean, where local circulation, shallow seas, and complex coastal geometry may weaken direct air-sea coherence. The strongest correlations in the western basin indicate that atmospheric temperature anomalies are efficiently translated into SST anomalies there, consistent with previous studies showing that Mediterranean MHWs are often triggered or amplified by warm atmospheric conditions, weaker winds, and altered surface heat fluxes (Hamdeno and Alvera-Azcaráte, 2023; Darmaraki et al., 2024). The basin-wide positive correlation pattern also supports the interpretation that Mediterranean MHWs and AHWs are not independent phenomena, but rather expressions of a coupled ocean-atmosphere extreme state, as shown by Paredes-Fortuny et al., (2025), who linked that intensification to changes in air-sea heat exchange.

7.2.2 Co-occurrence of Marine and Atmospheric Heatwaves in the Mediterranean Sea:

The temporal evolution of compound marine-atmospheric heatwave events shows a clear intensification over the study period (Fig. 93a). Mean compound days remain relatively low prior to the early 2000s but increase markedly afterward, with a sharp acceleration after approximately 2015 and peak values exceeding 80 days per year in recent years. This pattern indicates that compound extremes are not only becoming more frequent but are also persisting longer. Such a rapid increase is consistent with previous findings that concurrent ocean-atmosphere heat extremes are amplified under background warming and enhanced air-sea coupling in the Mediterranean (Pastor et al., 2024; Paredes-Fortuny et al., 2025).

The lag analysis further clarifies the temporal relationship between atmospheric and marine extremes (Fig. 93b). The distribution is strongly centred around zero lag, with the highest probability between approximately -3 and +3 days, indicating that MHWs and AHWs tend to occur nearly simultaneously. A slight asymmetry toward positive lags suggests that atmospheric heatwaves may, in some cases, precede or coincide with the development of MHWs. This supports the interpretation that atmospheric forcing plays a key role in triggering or intensifying ocean surface warming through enhanced heat fluxes and reduced mixing, as documented in previous Mediterranean studies (Pastor and Khodayar, 2023; Simon et al., 2023).

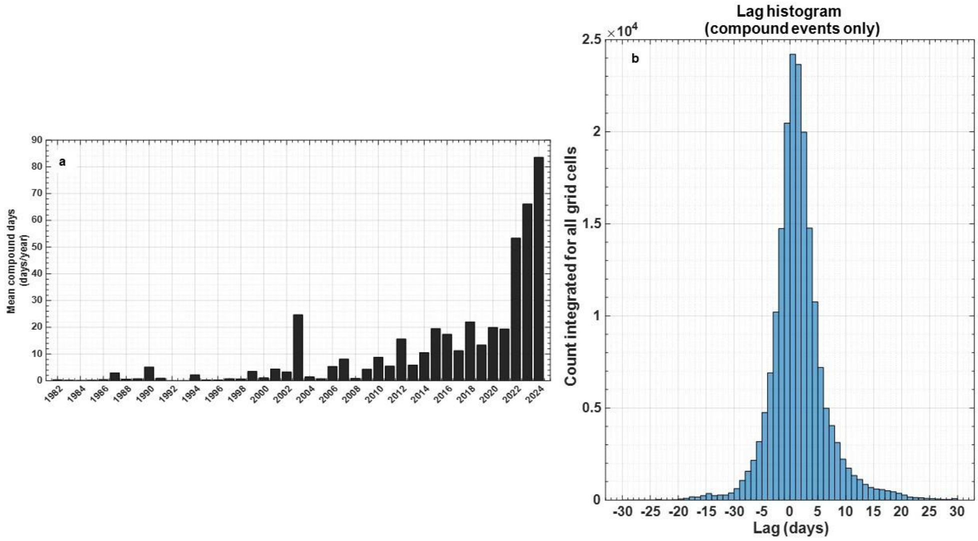

Figure 93. *temporal evolution of compound MHW–AHW events. (a) Annual mean number of compound days across the Mediterranean Sea. (b) Distribution of temporal lag between AHW and MHW occurrences, computed for compound events.*

Seasonal variability reveals a strong modulation of co-occurrence throughout the year (Fig. 94). The highest co-occurrence fractions are observed during summer (JAS), commonly ranging between 50% and 80%, followed by spring (AMJ) with intermediate values (about 40-70%). In contrast, winter (JFM) shows the lowest co-occurrence, typically below 40%, while autumn (OND) exhibits moderate values (about 30-50%). This seasonal structure reflects the dominant role of summer atmospheric conditions in driving coupled extremes. During summer, persistent anticyclonic systems, clear-sky conditions, and weak winds promote strong air-sea heat exchange and reduced vertical mixing, favouring simultaneous atmospheric and oceanic warming. In winter, enhanced mixing and more dynamic atmospheric circulation weaken this coupling, reducing the likelihood of concurrent extremes. These findings are consistent with previous work highlighting the strong seasonality of Mediterranean compound heat events and their association with summer stratification regimes (Holbrook et al., 2019; Smale et al., 2019; Oliver et al., 2021).

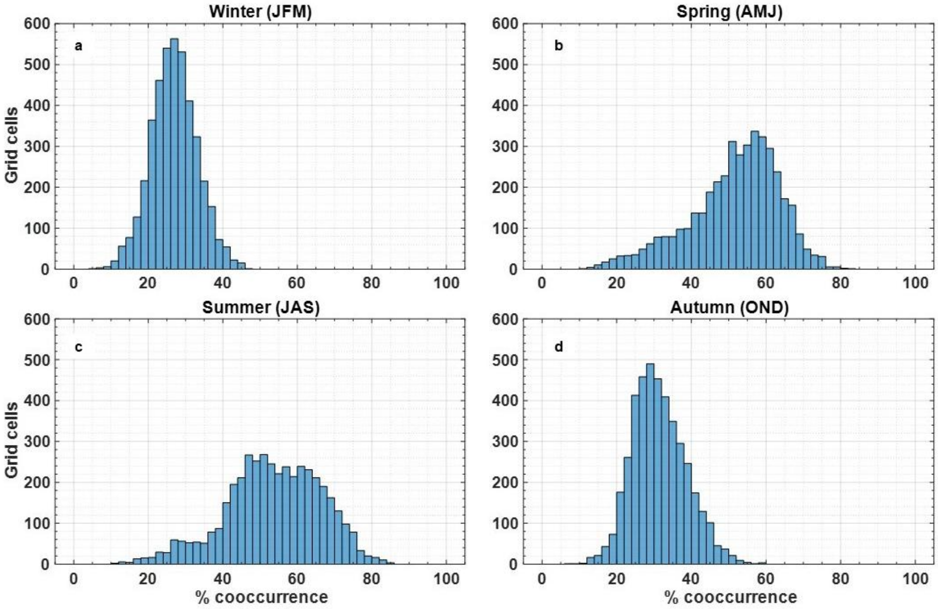

Figure 94. *Seasonal distribution of compound MHW–AHW co-occurrence. Histograms of co-occurrence fraction (%) for winter (JFM), spring (AMJ), summer (JAS), and autumn (OND), illustrating seasonal variability in compound event likelihood.*

The spatial distribution of co-occurrence further emphasizes basin-scale contrasts (Fig. 95). On average, the highest co-occurrence fractions (up to about 60-65%) are observed in the western Mediterranean, particularly in the Alboran, Balearic, and Tyrrhenian regions (Fig. 95a). In contrast, lower values (about 20-40%) dominate the southern and southeastern Mediterranean, indicating weaker coupling in these regions. Seasonal maps show that this pattern is strongly modulated by the annual cycle. In winter (JFM), co-occurrence is low across the entire basin (Fig. 95b). In spring (AMJ), co-occurrence increases in the western and central Mediterranean (Fig. 95c), while in summer (JAS) it reaches its maximum extent and intensity, covering most of the basin with particularly high values in the western and central regions (Fig. 95d). In autumn (OND), co-occurrence decreases again but remains elevated in parts of the western basin (Fig. 95e).

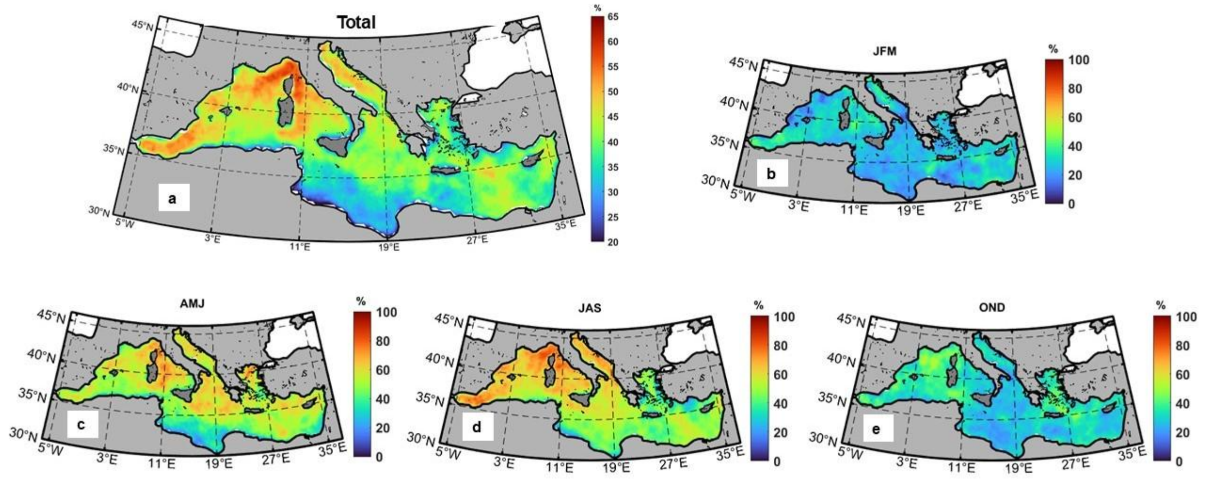

Figure 95. *Spatial distribution of compound MHW-AHW co-occurrence. (a) total co-occurrence fraction (1982-2024). (b–e) Seasonal co-occurrence fractions for JFM, AMJ, JAS, and OND, respectively.*

The stronger co-occurrence in the western Mediterranean aligns with the higher SST and air temperature correlation observed earlier (Fig. 92) and reflects more efficient air-sea coupling in this region. This can be attributed to the combination of stronger atmospheric control, relatively shallower mixed layers during summer, and enhanced sensitivity of SST to atmospheric forcing. In contrast, the eastern Mediterranean, although experiencing strong atmospheric heat extremes, shows lower co-occurrence fractions, likely due to higher stratification, different circulation regimes, and a reduced immediate ocean response to atmospheric variability.

Overall, these results demonstrate that compound MHW-AHW events in the Mediterranean are increasing rapidly in both frequency and persistence, are strongly synchronized in time, and are highly seasonal, with a clear peak during summer. Their spatial distribution highlights stronger coupling in the western basin compared to the eastern Mediterranean, reflecting underlying differences in air-sea interaction and oceanographic structure. These findings reinforce the idea that Mediterranean heat extremes are increasingly governed by coupled ocean-atmosphere dynamics rather than isolated processes.

7.2.3 Impacts of Compound Heatwaves on Stratification and Vertical Heat Distribution:

Compound MHW-AHW events exert a clear influence on upper-ocean stratification across the Mediterranean, as indicated by MLD anomalies (Fig. 96). Both compound and MHW-only conditions are associated with predominantly negative MLD anomalies, reflecting general shoaling of the mixed layer and increased stratification (Fig. 96a,b). However, the difference map (compound − MHW-only) shows a spatially heterogeneous response (Fig. 96c). In parts of the western and central Mediterranean, compound events exhibit slightly weaker shoaling compared to MHW-only conditions, while in the eastern basin, shoaling remains equally strong or is slightly enhanced.

The vertical heat distribution further highlights these differences (Fig. 97). The penetration depth difference (compound − MHW-only) shows that compound events are generally associated with deeper heat penetration, particularly in the Alboran sea , central, and eastern Mediterranean, where positive differences dominate (Fig. 97a). Surface-layer temperature anomalies remain positive under both conditions (Fig. 97b,c), but their difference shows a basin-scale contrast, with reduced surface intensification in parts of the western basin and enhanced anomalies in the eastern Mediterranean (Fig. 97d). This indicates that compound events modify not only the magnitude but also the vertical redistribution of heat, with a tendency toward increased subsurface storage.

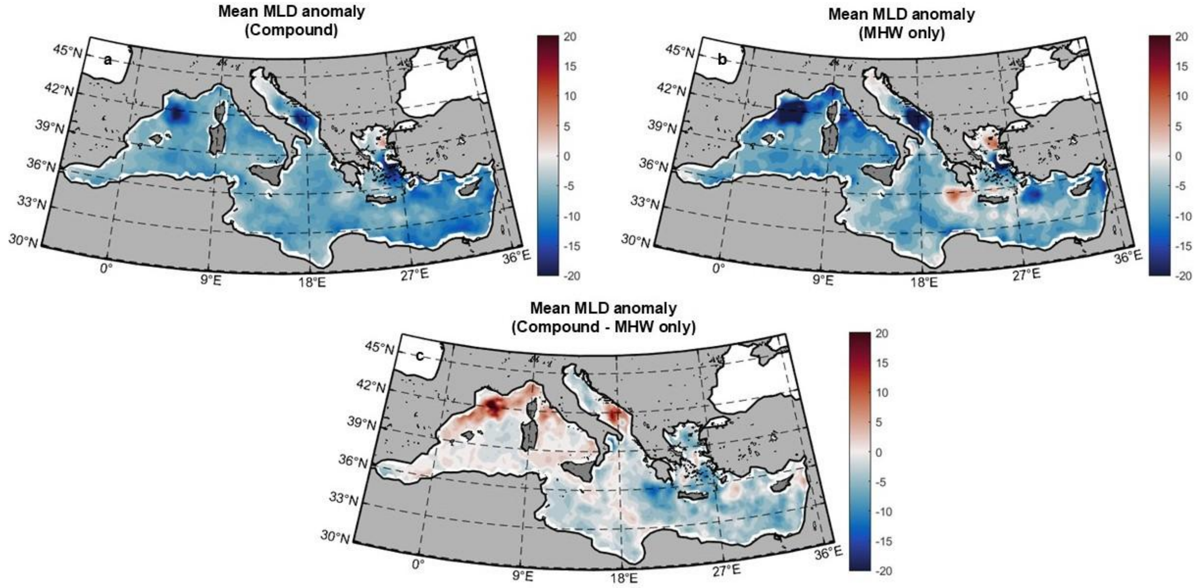

__Figure 96.__ Mean MLD anomalies during (a) compound MHW and AHW events and (b) MHW-only events. (c) Difference between compound and MHW-only conditions, highlighting the impact of atmospheric forcing on upper-ocean stratification.

The basin-mean vertical profiles provide a clearer view of this redistribution (Fig. 98). Both compound and MHW-only events show strong surface-intensified warming (Fig. 98a), but the difference profile (compound − MHW-only) reveals a distinct three-layer structure (Fig. 98b). The anomaly is positive at the surface, indicating stronger near-surface warming during compound events. Between approximately 25 and 100 m, the anomaly becomes negative, showing reduced warming within the upper thermocline. Below this layer, from about 100 m down to 300–500 m, the anomaly becomes positive again, indicating enhanced subsurface warming. Several of these depth ranges are statistically significant, confirming a robust vertical reorganization of heat. This pattern demonstrates that compound events do not simply intensify warming but instead redistribute heat vertically, enhancing both surface and deep anomalies while weakening the intermediate layer.

The statistical distributions further support this interpretation (Fig. 99). The MLD anomaly distribution shows that both compound and MHW-only events are dominated by negative values, consistent with enhanced stratification, although compound events display a slightly broader range, including more extreme shoaling cases (Fig. 99a). More importantly, the penetration depth distribution shifts toward greater depths during compound events, with a higher probability of anomalies extending beyond ~300–500 m compared to MHW-only conditions (Fig. 99b). This confirms that compound heatwaves are associated with a deeper vertical footprint of warming.

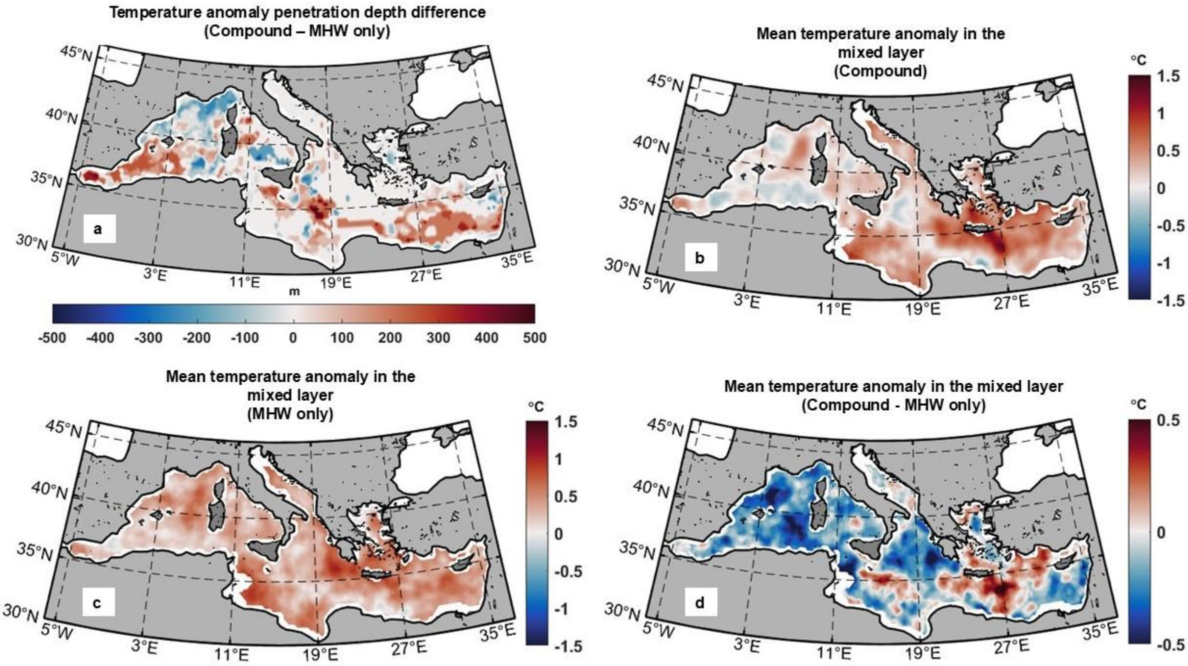

__Figure 97.__ Vertical heat distribution and penetration depth. (a) Difference in temperature anomaly penetration depth (compound – MHW-only). (b-c) Mean temperature anomalies in the mixed layer for compound and MHW-only conditions. (d) Difference between the two conditions.

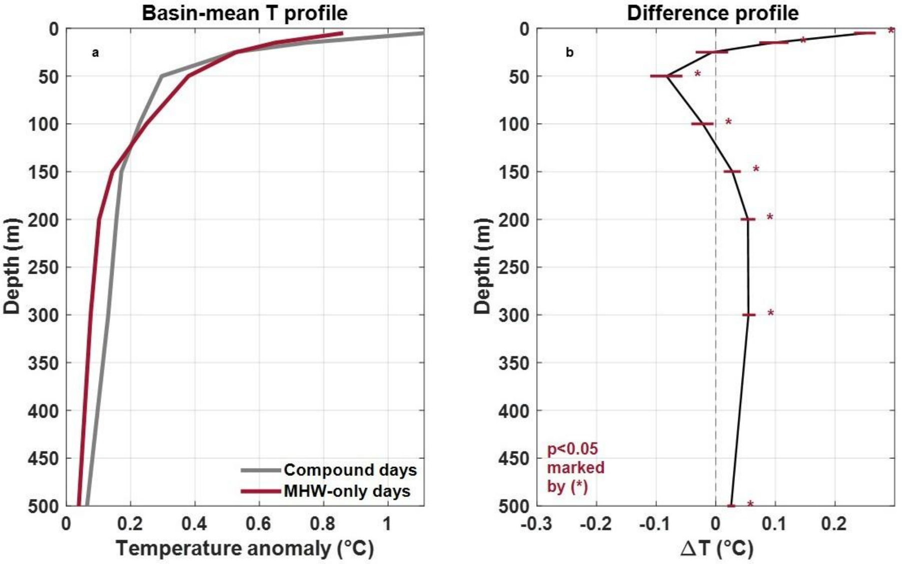

__Figure 98.__ Basin-mean vertical temperature structure. (a) Basin-averaged vertical temperature profiles for compound and MHW-only events. (b) Difference profile (compound – MHW-only), with statistically significant differences ($p < 0.05$) indicated.

Overall, these results show that compound MHW-AHW events modify both stratification and heat distribution in a non-uniform way. While stratification is enhanced under both conditions, compound events are characterized by a more complex vertical structure, with stronger surface warming, reduced anomalies in the upper thermocline, and enhanced warming at depth. This indicates a more efficient redistribution of heat into the subsurface, increasing the persistence of thermal anomalies below the mixed layer. Such behaviour is consistent with previous studies showing that coupled ocean-atmosphere extremes can alter air-sea heat fluxes and mixing processes, leading to enhanced subsurface heat storage and prolonged oceanic impacts (Holbrook et al., 2019; Sen Gupta et al., 2020; Oliver et al., 2021).

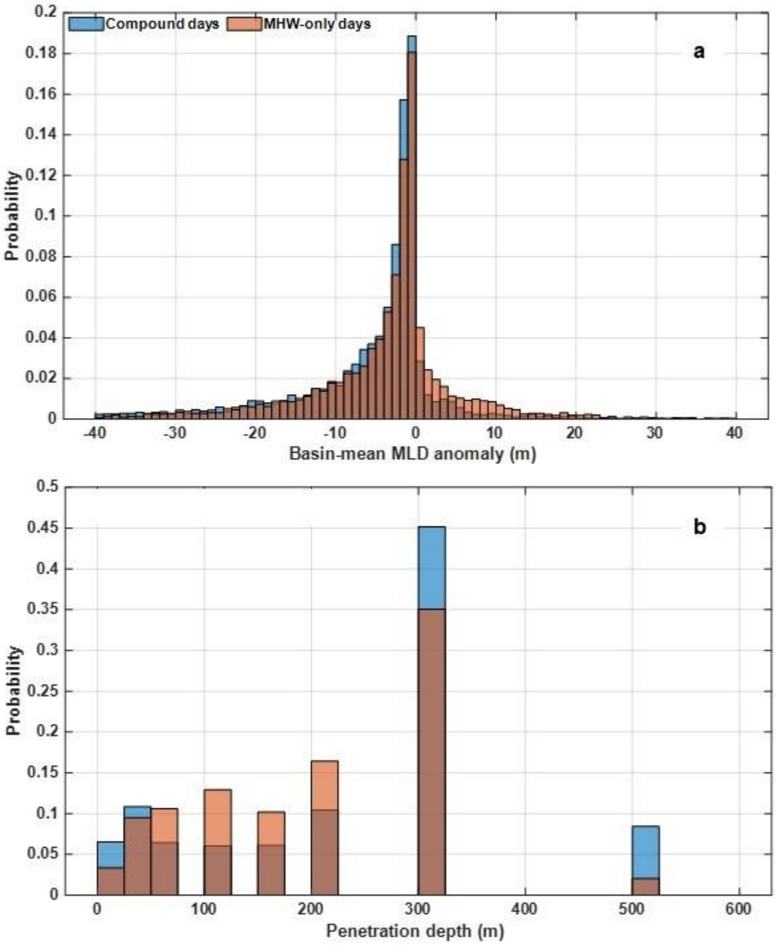

Figure 99. *Statistical distribution of stratification and penetration depth. (a) Probability distribution of basin-mean MLD anomalies for compound and MHW-only events. (b) Distribution of heat penetration depth under both conditions.*

7.2.4 Medicanes Spatial Distribution and Dataset Consistency:

The spatial and temporal distribution of Medicane events reveals a heterogeneous yet well-defined pattern across the Mediterranean basin (Fig. 100). Peak intensity locations are concentrated mainly in the central Mediterranean, particularly in the Ionian Sea and surrounding areas, with secondary clusters in the western Mediterranean (Balearic and Sardinia region) then the eastern basin (Levantine area). This spatial distribution aligns with previous studies identifying the central Mediterranean as a key hotspot for Medicane development due to favourable thermodynamic and dynamical conditions, including strong air-sea fluxes and upper-level forcing (Tous et al., 2013; Borzì et al., 2024; Miglietta et al., 2025).

The minimum MSLP distribution shows that the most intense systems tend to occur in the central and eastern Mediterranean, consistent with earlier analyses indicating that these regions support stronger cyclone intensification due to warmer SSTs and increased instability

(Miglietta et al., 2013, 2025; Miglietta and Rotunno, 2019). The co-location of lower MSLP and higher wind speeds further reflects the coherent structure of these systems, consistent with the tropical-like characteristics described in previous Medicane case studies (Romero and Emanuel, 2013; Jangir et al., 2024).

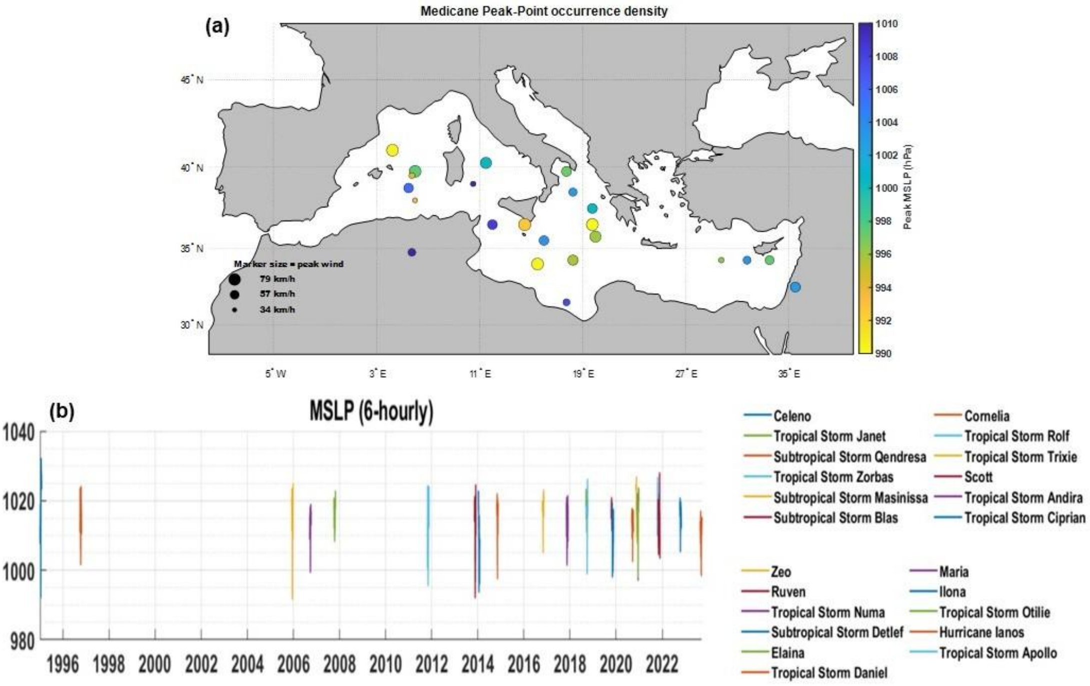

Figure 100. *Spatial and temporal distribution of Medicanes (1995–2023). (a) Peak intensity locations of 23 Medicane events, with marker size representing maximum wind speed and color indicating minimum sea-level pressure. (b) Temporal distribution of events and associated pressure evolution.*

The temporal distribution (Fig. 100b) highlights the intermittent occurrence of Medicanes, with relatively few events before the mid-2000s and a higher concentration in recent years. Although part of this increase may be due to improved detection and reporting, several studies suggest that Medicane activity may be sensitive to changes in SST and atmospheric conditions, particularly in a warming Mediterranean (Romero and Emanuel, 2013; Tous et al., 2013). However, given the limited number of events, robust trend attribution remains challenging.

The comparison between reported Medicane characteristics and ERA5-derived estimates (Fig. 101) provides insight into dataset consistency and known reanalysis limitations. For minimum MSLP (Fig. 101a), both reported data and ERA5 indicate a weak decreasing trend, suggesting a tendency toward stronger systems over time. However, ERA5 generally produces slightly higher (weaker by 5.73 hPa) minimum pressures compared to observations, as confirmed by the positive bias in the calibration analysis (Fig. 101c). This behaviour is consistent with previous evaluations of ERA5, which show that while it captures cyclone structure and evolution well, it tends to smooth intensity extremes, particularly for small-scale systems (Hersbach et al., 2020; Gandoin and Garza, 2024).

For maximum wind speed (Fig. 101b), discrepancies between datasets are more pronounced. Reported data suggest a slight intensification, whereas ERA5 indicates weak or neutral trends. The calibration results (Fig. 101d) confirm a systematic underestimation of wind speeds in ERA5 by 9.34 m/s, consistent with known limitations of reanalysis products in resolving the compact core and peak winds of Medicanes (Miglietta et al., 2013; Borzì et al., 2024; Gandoin and Garza, 2024). Despite this bias, ERA5 reproduces the relative variability and inter-event differences reasonably well.

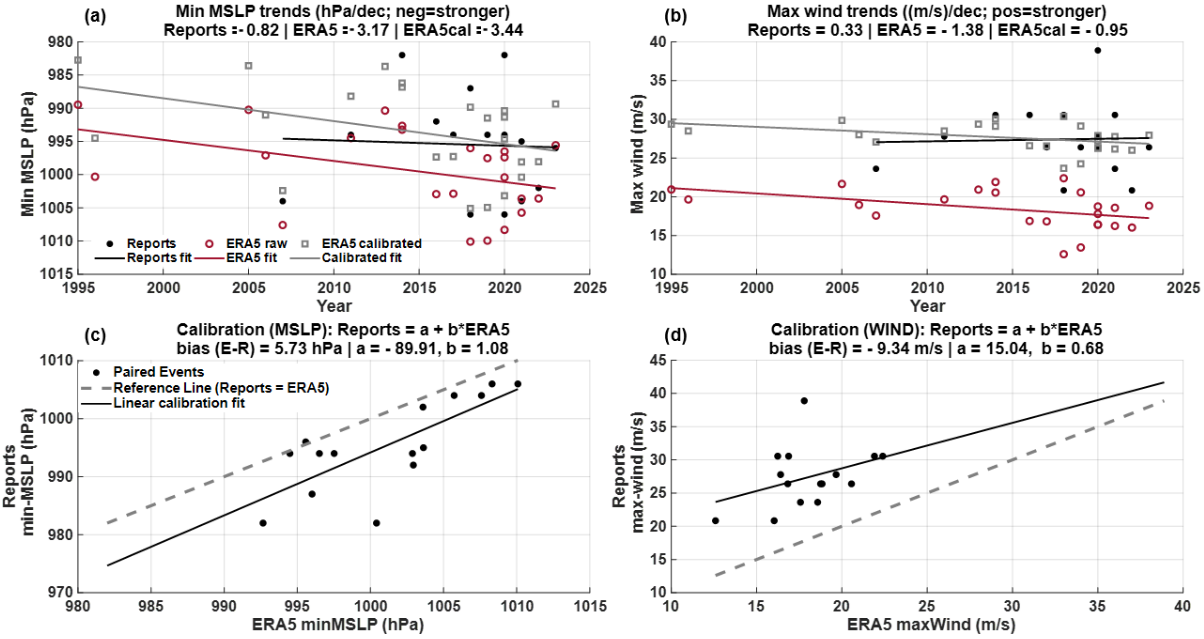

Figure 101. *Comparison between reported and ERA5-derived Medicane characteristics. (a–b) Trends in minimum sea-level pressure and maximum wind speed. (c–d) Calibration relationships between reported observations and ERA5 estimates.*

Overall, the comparison demonstrates that ERA5 provides a robust representation of Medicane dynamics and variability, particularly for pressure-based metrics, but requires caution when interpreting intensity, especially wind speed. These findings are consistent with previous studies highlighting the usefulness of ERA5 for climatological and composite analyses of Mediterranean cyclones, while emphasizing the need for bias awareness in intensity-related diagnostics (Hersbach et al., 2020; Gandoin and Garza, 2024)

7.2.5 Interaction Between MHWs and Medicanes:

The interaction between Medicanes and MHWs is examined through composite analyses of atmospheric and oceanic conditions, distinguishing events that occur with and without positive SST anomalies (SSTA) (Figs. 102–104).

- **Atmospheric response to warm ocean conditions**

The atmospheric composites reveal clear differences between Medicanes developing over positive SST anomalies and those occurring under neutral or negative conditions (Fig. 102). Storms associated with warm ocean anomalies exhibit slightly deeper minimum sea-level pressure (MSLP) at peak intensity (lag 0), indicating enhanced cyclone development (Fig. 102a). This is accompanied by stronger near-surface winds, particularly during the intensification phase, suggesting a more energetic system (Fig. 102b).

Precipitation shows distinct modulation, with reduced peak precipitation but a broader temporal distribution under warm conditions (Fig. 102c), indicating more sustained but less concentrated convective activity. Cloud cover is generally higher and more persistent around peak intensity (Fig. 102d), consistent with enhanced atmospheric moisture availability.

Surface turbulent heat fluxes provide key insight into air-sea coupling. Both latent and sensible heat fluxes show stronger negative anomalies (enhanced upward fluxes from ocean to atmosphere) during Medicanes over warm SSTs (Fig. 102e,f). This indicates increased energy transfer from the ocean to the atmosphere, supporting cyclone maintenance and intensification. In contrast, near-surface air temperature is slightly lower during these events (Fig. 102g), reflecting stronger air-sea temperature gradients that enhance turbulent heat exchange.

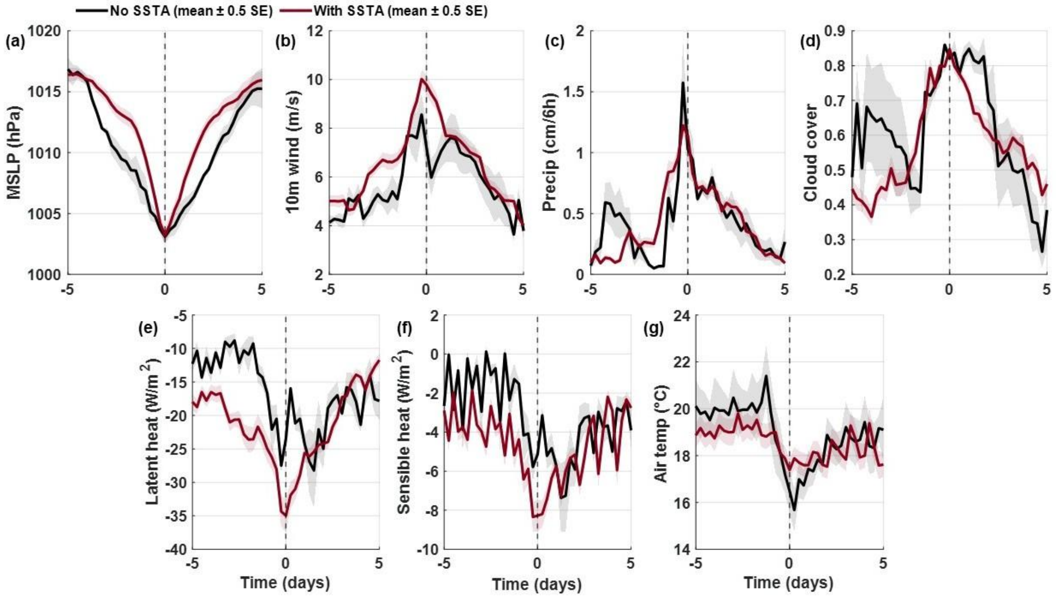

Figure 102. Atmospheric composites of Medicanes with and without SST anomalies. Evolution of (a) sea-level pressure, (b) wind speed, (c) precipitation, (d) cloud cover, (e) latent heat flux, (f) sensible heat flux, and (g) air temperature relative to storm peak.

Overall, these results indicate that Medicanes interacting with warm ocean anomalies are associated with enhanced air-sea fluxes and more favourable thermodynamic conditions, which support cyclone intensification, consistent with previous studies on tropical-like cyclone energetics (Tous et al., 2013; Miglietta and Rotunno, 2019; Jangir et al., 2024).

- **Oceanic response and feedbacks**

The oceanic composites further highlight the role of pre-existing warm anomalies (Fig. 103). Medicanes developing over positive SSTA occur over a warmer ocean background, with SST anomalies remaining positive throughout the storm life cycle (Fig. 103a). In contrast, storms without SSTA are associated with near-neutral or slightly negative anomalies.

The fraction of the storm footprint overlapping with MHW conditions is substantially higher for storms over warm anomalies (Fig. 103b), confirming that these events are strongly coupled with MHW conditions. MLD shows a deeper mixed layer during and after storm passage in both cases, but the increase is more gradual and sustained under warm conditions

(Fig. 103c), and it also shows in general a shallower MLD in the case of medicanes associated with positive SSTA. As discussed in Ch. 5, the Mediterranean MHW is highly associated with enhanced stratification which explain the results seen in (Fig. 103c).

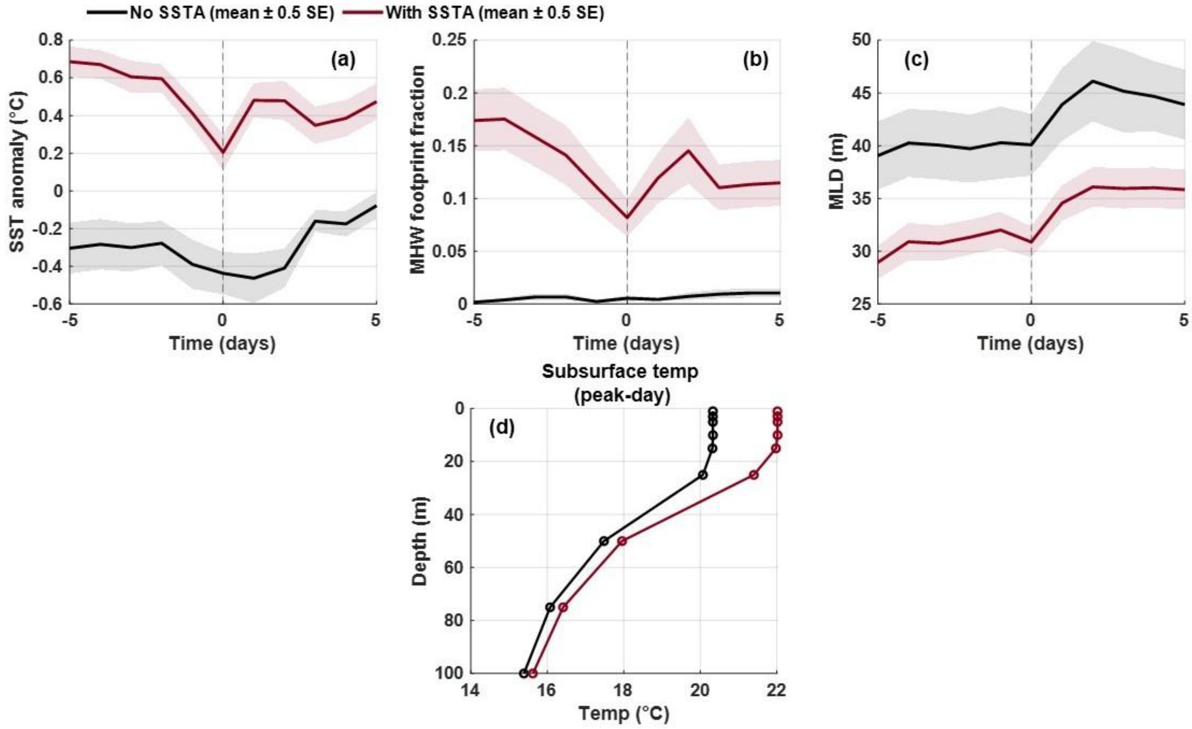

Figure 103. *Oceanic response to Medicanes under different SST conditions. (a) SST anomalies, (b) fraction of storm footprint overlapping with MHW conditions, (c) mixed layer depth, and (d) subsurface temperature profiles at peak intensity.*

The subsurface temperature structure at peak intensity reveals that storms over positive SSTA are associated with warmer upper-ocean profiles extending deeper into the water column (Fig. 103d). This indicates that pre-existing heat content plays a key role in modulating the ocean response and provides a reservoir of energy available for air-sea exchange. Together, these results demonstrate that Medicanes interacting with MHWs are embedded in a preconditioned ocean state characterized by elevated heat content and enhanced vertical coherence of warming, which supports sustained air-sea coupling during storm evolution.

- **Differences between weak and strong Medicanes under warm conditions:**

Further insight is provided by separating Medicanes occurring over positive SSTA into weak and strong systems (Fig. 104). Strong Medicanes are characterized by lower minimum MSLP and higher wind speeds, confirming a more intense cyclone structure (Fig. 104a,b). Precipitation is also enhanced in strong systems, particularly near peak intensity (Fig. 104c), indicating stronger convective activity.

Surface heat fluxes show a clear intensification signal, with larger latent heat fluxes in strong Medicanes, reflecting stronger ocean-to-atmosphere energy transfer (Fig. 104d). Sensible heat flux differences are present but less pronounced (Fig. 104e), suggesting that latent heat plays the dominant role in storm intensification.

Atmospheric conditions also differ markedly, with strong Medicanes associated with lower air temperatures and higher cloud cover (Fig. 104f,g), consistent with more vigorous convection and deeper atmospheric coupling. At the same time, SST anomalies remain elevated but are slightly reduced at peak intensity (Fig. 104h), likely reflecting enhanced ocean cooling due to stronger mixing.

The fraction of MHW conditions within the storm footprint is lower for strong Medicanes at peak intensity (Fig. 104i), suggesting that intense storms may partially erode surface warm anomalies through mixing and heat fluxes. This is supported by the MLD evolution, which shows deeper mixed layers in strong events (Fig. 104j), indicating stronger vertical mixing.

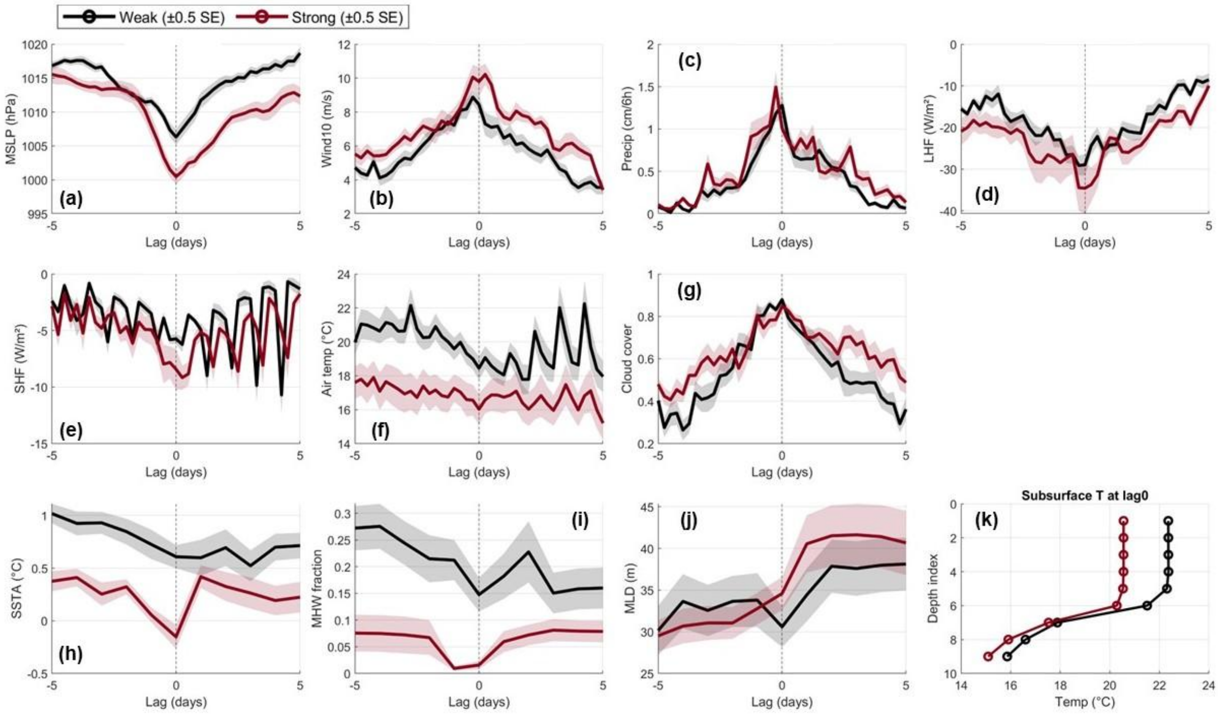

__Figure 104.__ Comparison between weak and strong Medicanes under warm SST conditions. Atmospheric and oceanic evolution of (a) pressure, (b) wind speed, (c) precipitation, (d–e) heat fluxes, (f) air temperature, (g) cloud cover, (h) SST anomalies, (i) MHW fraction, (j) mixed layer depth, and (k) subsurface temperature profiles.

Subsurface temperature profiles confirm that strong Medicanes are associated with deeper penetration of thermal anomalies, although surface anomalies may be reduced due to mixing (Fig. 104k). This highlights a key feedback: while warm ocean conditions support storm intensification, the storms themselves redistribute and partially dissipate this heat vertically.

Overall, the interaction between Medicanes and MHWs is characterized by two-way coupling. Pre-existing warm ocean conditions enhance cyclone intensity through increased air-sea fluxes and available heat content, while the passage of strong Medicanes modifies the ocean state by deepening the mixed layer and redistributing heat into the subsurface. This feedback mechanism highlights the importance of considering both atmospheric and oceanic processes when assessing the role of extreme events in the Mediterranean system.

7.2.6 Case Studies of Medicanes:

To further investigate the mechanisms linking Medicanes and MHWs, three representative events, Zorbas (2018), Ianos (2020), and Daniel (2023), were analysed in detail (Figs. 105-108). These case studies provide insight into the temporal evolution of oceanic preconditioning, air-sea fluxes, and atmospheric responses during storm development.

- **Medicane Zorbas (September–October 2018):**

The Zorbas event developed over a region characterized by persistent positive SSTA exceeding about 2 °C before storm formation (Fig. 105d), indicating strong oceanic preconditioning. The MHW time series confirms that the event occurred during an active MHW period, with SST exceeding the climatological threshold for several weeks (Fig. 105b). The vertical structure shows that this warming extended below the mixed layer, with anomalies penetrating to approximately 30 to 40 m depth (Fig. 105c), indicating elevated upper-ocean heat content.

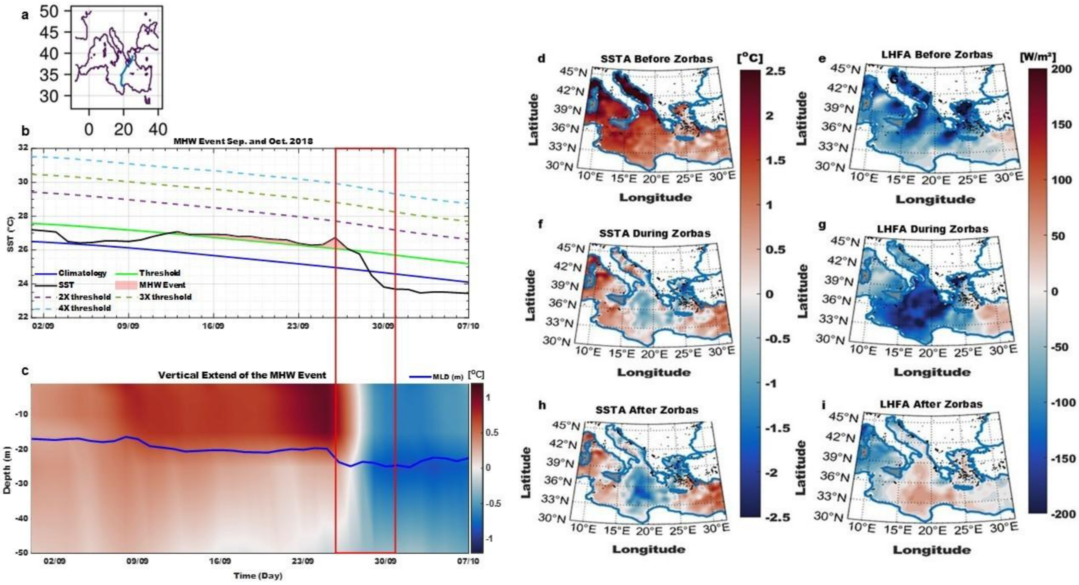

Figure 105. Medicane Zorbas (2018) preconditioning and evolution. (a) Event track. (b) MHW event. (c) Vertical temperature structure and mixed layer depth. (d–i) Spatial evolution of SST anomalies and latent heat flux before, during, and after the event.

During storm passage, SST anomalies rapidly decreased (Fig. 105f-h), accompanied by a marked increase in upward latent heat fluxes, reaching values below -150 W/m² (Fig. 105g,i). This reflects intense air-sea energy transfer, consistent with the strong cooling observed after the event. Time series analysis (Fig. 106) shows that peak storm intensity coincides with maximum wind speed and precipitation, while the air-sea temperature difference (ΔT) reaches its maximum before peak intensity, supporting enhanced turbulent heat exchange.

These results are consistent with previous analyses of Zorbas, which identified the role of warm SSTs and strong air-sea fluxes in sustaining cyclone intensity (Avolio et al., 2024). The rapid post-storm cooling and mixed-layer deepening reflect strong ocean feedbacks, a common feature of tropical-like cyclones interacting with pre-existing warm anomalies (Romero and Emanuel, 2013; Miglietta and Rotunno, 2019).

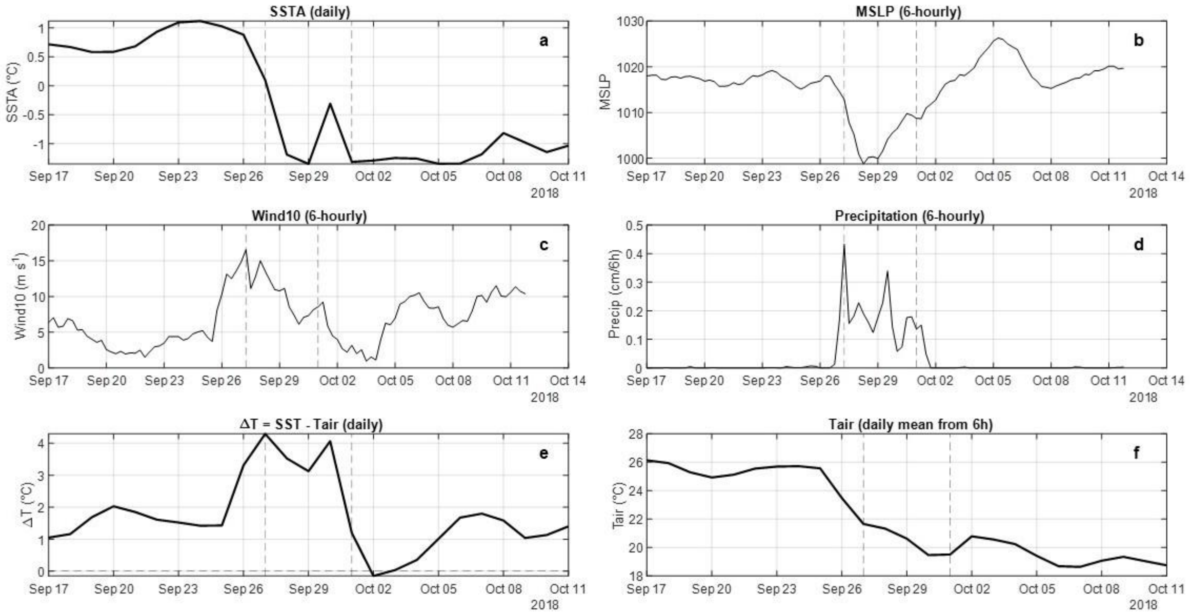

Figure 106. *Medicane Zorbas (2018). Temporal evolution of (a) SST anomaly, (b) sea-level pressure, (c) wind speed, (d) precipitation, (e) air–sea temperature difference, and (f) air temperature.*

- **Medicane Ianos (September 2020):**

The Ianos event represents a particularly intense Medicane developing over an exceptionally warm Mediterranean background, with basin-wide SSTA exceeding 2 °C (Fig. 107a). The associated MHW persisted throughout the preconditioning phase, with SST consistently above the climatological threshold (Fig. 107b). The vertical structure indicates deep penetration of warm anomalies before storm arrival, suggesting a substantial reservoir of upper-ocean heat (Fig. 107c). During the storm, a sharp SST drop is observed, indicating strong ocean cooling due to vertical mixing and heat loss. Atmospheric variables show a clear intensification phase characterized by decreasing MSLP, increasing wind speeds, and enhanced precipitation (Fig. 107d–f). Latent heat fluxes exhibit strong negative values during peak intensity (Fig. 107g), confirming intense ocean-to-atmosphere energy transfer. These features are consistent with previous studies of Ianos, which highlighted the importance of high ocean heat content and strong air-sea coupling in driving its rapid intensification (Tous et al., 2013; Avolio et al., 2024; Jangir et al., 2024).

- **Medicane Daniel (September 2023):**

The Daniel event further illustrates the role of coupled ocean-atmosphere processes, although with a somewhat different structure (Fig. 108). SST anomalies before storm development are positive but more spatially heterogeneous (Fig. 108a), and the fraction of the storm track overlapping with MHW conditions is more localized (Fig. 108b). Surface heat flux patterns show strong regional contrasts, with intense latent heat fluxes along the storm trajectory (Fig. 108c,d). The air-sea temperature difference (ΔT) is particularly high along the storm path (Fig. 108e), indicating favourable conditions for heat transfer. Precipitation is strongly concentrated near the storm center (Fig. 108f), consistent with the extreme rainfall associated with this event (Hewson et al., 2024). Atmospheric fields show a well-defined low-pressure system and strong winds aligned with the storm track (Fig. 108g-h).

Time series analysis indicates rapid intensification followed by a decay phase, with peak precipitation and wind coinciding with minimum MSLP (Fig. 108i-k). Latent heat fluxes remain strongly negative during intensification (Fig. 108l), while air temperature decreases significantly during peak activity (Fig. 108m), enhancing air-sea gradients. These characteristics are consistent with recent analyses of Daniel, which emphasize the combined role of warm SST anomalies and atmospheric instability in producing extreme precipitation and storm intensity (Argüeso et al., 2024; Hewson et al., 2024).

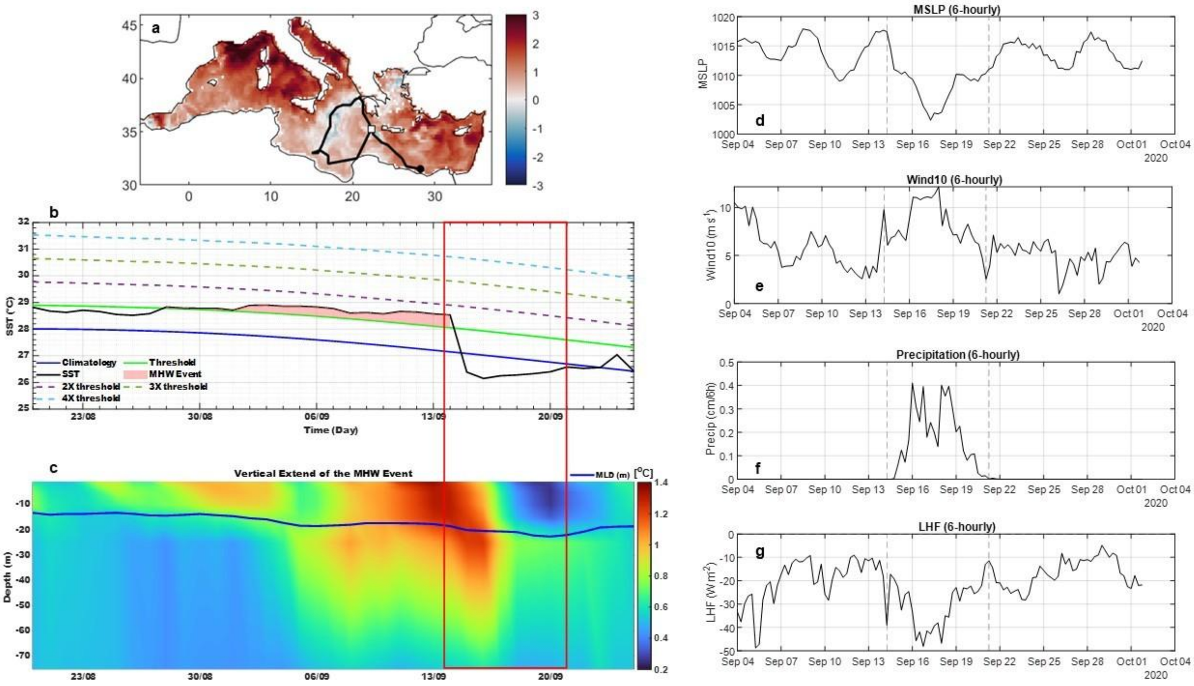

Figure 107. *Medicane Ianos (2020). (a) Spatial SST anomaly distribution. (b) SST evolution and thresholds. (c) Vertical temperature structure. (d–g) Atmospheric evolution including pressure, wind, precipitation, and latent heat flux.*

Across all three events, a consistent pattern emerges. Medicanes develop over pre-existing warm ocean conditions, often associated with MHWs, which provide enhanced heat content and favourable air-sea temperature gradients. During storm intensification, latent heat fluxes increase substantially, transferring energy from the ocean to the atmosphere and supporting cyclone development. At the same time, storms induce strong ocean feedbacks, including surface cooling, mixed-layer deepening, and vertical heat redistribution.

These results confirm that Medicanes and MHWs are tightly coupled phenomena, with two-way interactions that influence both storm intensity and ocean state, in agreement with previous studies on Mediterranean cyclones and tropical-like systems (Tous et al., 2013; Miglietta and Rotunno, 2019; Avolio et al., 2024; Borzì et al., 2024; Jangir et al., 2024).

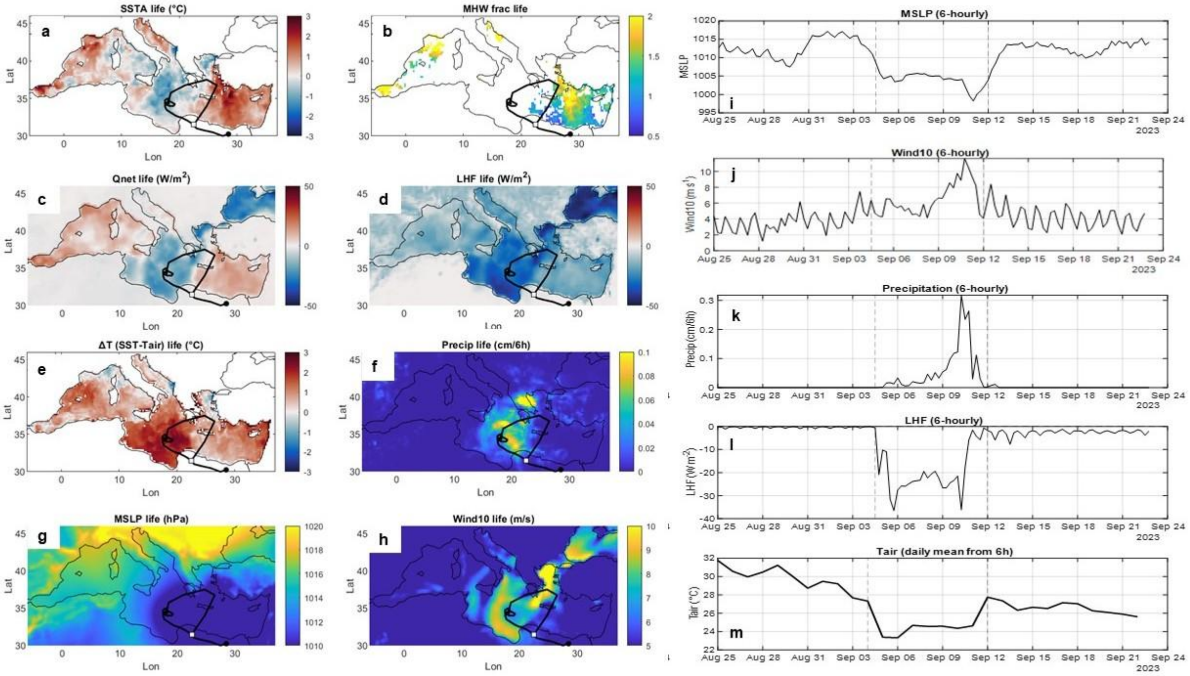

Figure 108. *Medicane Daniel (2023). (a-b) SST anomaly and MHW footprint. (c-f) Surface heat fluxes, precipitation, and air–sea temperature contrast. (g-h) pressure and wind evolution. (i-m) time series of atmospheric variables during storm evolution.*

7.3 Conclusions:

This chapter provides a comprehensive assessment of compound extremes in the Mediterranean Sea by examining the co-occurrence and interactions among MHWs, AHWs, and Medicanes. The results reveal a tightly coupled ocean-atmosphere system in which extreme events do not occur in isolation but rather reinforce each other across temporal and spatial scales.

Analysis of MHW and AHW characteristics demonstrates clear spatial coherence between oceanic and atmospheric warming patterns, with both extremes intensifying in the eastern Mediterranean and along southern regions. The strong correlation between SST anomalies and near-surface air temperature confirms that air-sea coupling plays a fundamental role in shaping heatwave dynamics. The co-occurrence analysis further shows that compound MHW-AHW events are not random but statistically favoured, with occurrences exceeding expectations based on independent probabilities. The increasing frequency of compound days since the early 2000s reflects an emerging regime of persistent coupled extremes. Lead-lag analysis indicates that atmospheric heatwaves generally precede or coincide with MHWs, pointing to a dominant role of atmospheric forcing in initiating ocean warming, followed by oceanic persistence due to thermal inertia. Seasonal patterns reinforce this interpretation, with the highest co-occurrence observed during summer, when stratification and radiative forcing maximize air-sea feedbacks. The vertical ocean response highlights the critical role of compound events in modifying upper-ocean structure. The redistribution of heat indicates that atmospheric forcing not only amplifies surface anomalies but also alters the vertical structure of MHWs.

The interaction between MHWs and Medicanes reveals an additional layer of complexity. Statistical analysis shows that storms developing over warm SST anomalies exhibit stronger air-sea fluxes, deeper pressure minima, and enhanced wind speeds, indicating that oceanic preconditioning contributes to storm intensification. At the same time, Medicanes exert strong feedback on the ocean through rapid surface cooling, mixed-layer deepening, and vertical mixing. Comparison between weak and strong storms further confirms that higher SST anomalies are associated with more intense atmospheric responses.

Case studies of Zorbas (2018), Ianos (2020), and Daniel (2023) provide process-level evidence supporting these statistical relationships. All three events developed over pre-existing warm anomalies, often linked to MHWs, and exhibited strong air-sea heat fluxes during intensification. Differences between events reflect variations in the spatial extent of oceanic preconditioning and atmospheric forcing, but the underlying mechanism remains consistent: warm ocean conditions enhance energy transfer to the atmosphere, while storms subsequently redistribute and reduce upper-ocean heat content.

Taken together, these results demonstrate that the Mediterranean is transitioning toward a regime characterized by increasingly frequent and intense compound extremes, driven by the coupling between oceanic and atmospheric processes. MHWs, atmospheric heatwaves, and Medicanes are interconnected components of a broader system of climate extremes, where each process influences and amplifies the others.

The intensification of compound extremes has important implications for both climate dynamics and impacts. Enhanced co-occurrence of MHWs and AHWs suggests a higher likelihood of persistent heat stress across marine and terrestrial systems, while interaction with Medicanes points to increased risks of extreme storms fuelled by anomalously warm oceans. These coupled processes may lead to cascading impacts, including ecosystem disruption, altered biogeochemical cycles, and intensified hydrometeorological hazards.

Chapter Eight: MarineHeatwaves.jl A High-Performance Framework for MHW Detection

8.1 Introduction:

MHWs are prolonged periods of anomalously warm ocean temperatures that have become increasingly frequent and intense under anthropogenic climate change, with significant ecological, biogeochemical, and socio-economic impacts (Holbrook et al., 2019; Smale et al., 2019; Oliver et al., 2021). The standardized definition introduced by Hobday et al., (2016) provides a consistent framework for detecting and characterizing these events, and has been widely adopted in oceanographic and climate studies.

With the rapid growth of high-resolution and long-term SST datasets, the need for efficient, scalable, and reproducible computational tools for MHW detection has become increasingly important. Several implementations of the Hobday et al., (2016) framework have been developed in Python, R, and MATLAB, each with specific advantages and limitations. However, computational efficiency and scalability remain key challenges when analysing large datasets or performing repeated analyses.

In this context, this chapter introduces **MarineHeatwaves.jl**, a Julia-based implementation of MHW detection designed to combine methodological rigor with high computational performance. The chapter also provides a comparative overview of existing implementations across programming languages, highlighting their respective strengths and limitations.

8.2 Methodological Framework:

8.2.1 Definition of MHWs:

All major implementations of MHW detection are based on the hierarchical framework proposed by Hobday et al., (2016). According to this definition, a MHW is identified when:

- SST exceeds a seasonally varying climatological threshold (typically the 90th percentile),
- The exceedance persists for at least five consecutive days,
- Events separated by gaps of two days or less are merged into a single event.

This definition ensures methodological consistency across studies and allows robust comparison of MHW characteristics across regions and time periods (Hobday et al., 2016; Oliver et al., 2018a). The climatology is computed relative to a baseline period using a moving window cantered on each calendar day, which accounts for the seasonal cycle and ensures that anomalies are defined relative to local climatological conditions (Perkins and Alexander, 2013; Hobday et al., 2016).

8.2.2 Detection Algorithm:

The computational workflow for MHW detection is consistent across implementations and includes four main steps:

1. **Climatology estimation**: Calculation of daily climatological mean and percentile thresholds using a sliding window approach.
2. **Threshold exceedance detection:** Identification of time steps where SST exceeds the climatological threshold.
3. **Event identification:** Grouping of consecutive exceedances into events, applying minimum duration and gap-merging criteria.
4. **Event characterization:** Computation of event properties, including:

    - Frequency
    - Duration
    - Maximum intensity
    - Mean intensity
    - Cumulative intensity
    - Rates of onset and decline

This standardized workflow ensures that differences between implementations are primarily related to computational design rather than methodological definition (Hobday et al., 2016; Oliver et al., 2018a).

8.3 Existing Implementations:

8.3.1 Python Implementation:

The reference implementation of the Hobday framework is the **marineHeatWaves** Python module developed by Oliver et al., (2018a). This implementation is widely used and serves as the basis for many MHW studies (Holbrook et al., 2019).

Key features include:

- Transparent and reproducible implementation of the detection algorithm.
- Integration with standard scientific libraries.
- Flexibility for time series analysis.

However, performance limitations may arise when applying the algorithm to large spatial datasets or long time series, particularly when computational optimization is limited (Oliver et al., 2018a).

8.3.2 R Implementations:

In R, the Hobday et al., (2016) framework is implemented through the **heatwaveR** package (W Schlegel and J Smit, 2018; Schlegel et al., 2021).

These packages provide:

- Extended functionality, including cold-spell detection.
- Event categorization and additional diagnostics.
- Strong integration with statistical workflows.

The heatwaveR package improves performance through optimized data handling and compiled code components. Nevertheless, computational challenges may still arise for very large datasets or high-resolution applications (W Schlegel and J Smit, 2018).

8.3.3 MATLAB Implementation:

MHW detection has also been implemented in MATLAB through the **m_mhw toolbox** developed by Zhao and Marin (2019). This toolbox follows the Hobday et al. (2016) framework and is specifically designed for spatial MHW analysis.

The MATLAB implementation provides:

- Efficient matrix-based computation.
- Direct application to gridded datasets.
- Additional tools for trend analysis, composites, and spatial diagnostics.

The toolbox includes core functions for event detection and analysis, as well as routines for evaluating seasonal variability and large-scale patterns. It also supports the detection of marine cold spells following (Schlegel et al., 2021). While MATLAB offers strong performance for matrix operations, limitations include reduced accessibility due to licensing requirements and less flexibility for integration with modern open-source data science ecosystems (Zhao and Marin, 2019).

8.4 MarineHeatwaves.jl: Julia-Based Implementation

8.4.1 Design and Implementation:

MarineHeatwaves.jl is a Julia-based package designed to implement MHW detection following Hobday et al., (2016), while addressing computational limitations of existing tools. The package is structured as a modular and extensible framework, enabling efficient processing of both time series and gridded datasets. The implementation leverages Julia's array-based operations and type system, allowing efficient handling of large datasets and flexible integration with scientific workflows.

A key advantage of MarineHeatwaves.jl lies in its computational performance. Julia's just-in-time compilation enables near-compiled execution speeds for numerical routines, providing:

- Efficient processing of long time series.
- Scalability to high-resolution spatial datasets.
- Reduced computational cost for repeated analyses.

These characteristics make the package well suited for large-scale oceanographic and climate applications.

8.4.2 Reproducibility and Open Science:

MarineHeatwaves.jl is distributed as an open-source package, ensuring transparency, reproducibility, and accessibility (https://github.com/keduba/MarineHeatwaves.jl). Open-source implementations are essential for enabling consistent application of detection methods across studies and facilitating intercomparison of results. The use of a standardized framework further ensures compatibility with existing literature and supports reproducible scientific workflows. The package is still being updated, and examples for MHW, MCS, AHWs and other ocean or atmospheric extremes, defined using percentile method, will be added. The output provide mean metrics, trends, event tables, anomalies, and categories according to Hobday et al., (2016, 2018).

8.5 Discussion and Conclusion:

The development of multiple implementations of the Hobday et al., (2016, 2018) framework reflects the increasing importance of MHW research and the growing demand for scalable computational tools. While methodological consistency has largely been achieved, the primary challenge has shifted toward efficient data processing and analysis. High-performance languages such as Julia offer a promising solution to these challenges, particularly for large-scale and high-resolution applications. At the same time, Python, R, and MATLAB implementations remain essential due to their widespread adoption and integration within existing research ecosystems. The coexistence of these tools enables flexibility and adaptability, allowing researchers to select the most appropriate implementation for their specific needs.

By combining methodological rigor with computational efficiency, the package contributes to the development of scalable tools for analysing marine heat extremes. The comparison with existing Python, R, and MATLAB implementations highlights that while the methodological foundation is well established, computational approaches continue to evolve. The availability of diverse and complementary tools is essential for advancing MHW research in the context of increasing data availability and complexity.

Chapter Nine: General Discussion

9.1 Surface and Subsurface Marine Heatwaves in the Mediterranean and Red Sea:

The global climate system is undergoing rapid transformation as a consequence of increasing greenhouse gas concentrations from human activities (IPCC, 2018, 2019, 2022). The ocean has absorbed the vast majority of this excess heat, approximately 89% over recent decades, while much smaller fractions have been stored in land, the atmosphere, and the cryosphere (Cheng et al., 2017; von Schuckmann et al., 2020; IPCC, 2022). This dominant role of the ocean in heat uptake has fundamentally altered its thermal structure and circulation, leading to an intensification of extreme events. Among these, MHWs have emerged as one of the most significant manifestations of climate variability and long-term ocean warming (Frölicher et al., 2018; Oliver et al., 2018a; Holbrook et al., 2019; Smale et al., 2019; Sen Gupta et al., 2020; Benedetti-Cecchi, 2021). However, their dynamics remain insufficiently resolved in semi-enclosed basins such as the Mediterranean Sea and the Red Sea, where regional processes strongly modulate their evolution.

Semi-enclosed basins are inherently sensitive to warming due to their restricted exchange with the open ocean, strong stratification, and intense air–sea coupling. These characteristics enhance heat retention and amplify variability, making them hotspots for marine extremes (Darmaraki et al., 2019a, 2024, 2025; Genevier et al., 2019; Pisano et al., 2020; Bawadekji et al., 2021; Mohamed et al., 2021; Juza et al., 2022). Building on the results of this thesis, a consistent picture emerges in which MHWs in both basins are intensifying, but their spatial and vertical expressions differ markedly due to contrasting oceanographic settings.

At the surface, both the Mediterranean Sea and the Red Sea exhibit robust warming trends of approximately 0.3-0.4 °C per decade, in agreement with previous studies (Raitsos et al., 2011; Skliris et al., 2012; Chaidez et al., 2017; Pastor et al., 2020; Ibrahim et al., 2021; Liu and Yao, 2022). This warming has translated into a clear intensification of MHW characteristics, with increases in frequency, duration, and cumulative intensity across both basins. These trends reflect the combined influence of a rising thermal baseline and enhanced variability, indicating that climate change is amplifying not only mean conditions but also extremes.

Despite this common intensification signal, the spatial structure of MHWs differs substantially between the two basins. In the Mediterranean Sea, a pronounced west-east contrast is observed. The western basin is characterized by more frequent and intense events, while the eastern basin exhibits longer-lasting MHWs. This distinction reflects differences in circulation, stratification, and ventilation, with the eastern Mediterranean favouring heat accumulation and persistence. In contrast, the Red Sea displays a clear north-south gradient, where the northern basin experiences longer and more intense events, while the southern basin is dominated by more frequent occurrences. These contrasting patterns highlight that the regional expression of MHWs is strongly controlled by basin geometry and oceanographic structure (Hamdeno and Alvera-Azcaráte, 2023; Hamdeno et al., 2024).

Beyond surface intensification, a key finding of this thesis is that MHWs are increasingly extending into the subsurface ocean. In the Mediterranean Sea, subsurface MHWs remain surface-intensified but show a clear tendency toward deeper penetration in recent years, with anomalies extending to several hundred meters and occasionally approaching 1000 m. This behaviour is consistent with previous studies emphasizing strong vertical variability and regional dependence of MHW penetration (Juza et al., 2022; Dayan et al., 2023; Darmaraki et al., 2024). Importantly, a basin-scale contrast emerges: the western Mediterranean is dominated by strong near-surface signals, whereas the central and eastern basins exhibit more persistent subsurface heat storage and deeper vertical extension. This indicates that stratification and regional circulation play a key role in modulating vertical heat redistribution.

The analysis of mixed layer dynamics further clarifies these mechanisms. In the western and central Mediterranean, MHWs typically precede mixed layer shoaling, suggesting that stratification changes are largely a response to surface warming. In contrast, in the eastern basin, shallow mixed layers often precede MHW onset, indicating that stratification acts as a preconditioning factor. This difference explains the stronger subsurface persistence observed in the eastern Mediterranean and aligns with previous findings on the role of stratification in MHW development (Juza et al., 2022; Dayan et al., 2023; Darmaraki et al., 2024).

In the Red Sea, subsurface MHW structure exhibits a distinct behaviour. While events remain surface-intensified, the southern basin shows a persistent subsurface warming, with repeated deep-reaching anomalies in recent decades. This pattern is consistent with studies highlighting the role of remote forcing and heat advection from the Gulf of Aden in shaping subsurface variability (Nadimpalli et al., 2025). In this context, subsurface heat storage becomes a dominant mechanism sustaining extreme events, indicating that Red Sea MHW dynamics cannot be interpreted solely through local surface forcing.

The role of stratification in the Red Sea also varies regionally. In the northern basin, mixed layer changes tend to follow MHW development, suggesting that stratification is primarily a response to warming. In contrast, in the southern basin, shallow mixed layers frequently precede MHW onset, indicating a stronger preconditioning role. This north-south contrast implies that subsurface heat retention and stratification become increasingly important toward the southern Red Sea, where basin connectivity and remote forcing exert greater influence.

A comparison between the two basins reveals both convergence and divergence in their response to climate change. In both the Mediterranean Sea and the Red Sea, there is a clear shift toward increased subsurface involvement of MHWs, reflecting a growing role of ocean heat storage and memory. However, the Mediterranean exhibits a more coherent basin-wide vertical intensification, with consistent increases in MHW occurrence and duration across depth. In contrast, the Red Sea shows a more heterogeneous response, with strong subsurface intensification concentrated in the southern basin and more limited changes in the north.

Overall, these results demonstrate that MHWs in semi-enclosed basins are evolving from predominantly surface-confined anomalies into vertically structured extremes governed by the interaction of stratification, circulation, and heat storage. While both basins experience intensification under ongoing warming, the mechanisms controlling their spatial and vertical structure differ significantly. This highlights a central conclusion of this thesis: understanding MHW evolution requires not only consideration of surface warming, but also explicit integration of subsurface processes and basin-specific dynamics, which together determine the persistence, depth, and impact of extreme marine events.

9.2 Drivers of MHW: background warming, atmospheric triggering, and oceanic persistence:

Understanding the development of MHWs requires a shift from single-driver explanations toward a multi-scale framework in which processes interact across temporal and spatial scales. The results of this thesis demonstrate that MHWs in the Mediterranean Sea and the Red Sea arise from the combined influence of three key components: (i) long-term background warming, which elevates the thermal baseline; (ii) short-term atmospheric forcing, which initiates events; and (iii) oceanic processes, which regulate their persistence, vertical structure, and spatial coherence. This integrated perspective provides a consistent explanation for both the timing and evolution of MHWs across contrasting basins.

At the most fundamental level, long-term ocean warming acts as a preconditioning mechanism. The progressive increase in sea surface temperature raises the climatological baseline, increasing the likelihood that even moderate variability exceeds extreme thresholds. In both basins, detrended analyses confirm that a substantial fraction of MHW occurrence is linked to this background warming. However, the persistence of variability after detrending indicates that warming alone is not sufficient to explain event dynamics. Instead, it establishes a thermodynamic environment that favours extremes, while other processes determine their onset and evolution.

The contribution of background warming shows clear spatial and temporal intensification in both basins, although with distinct regional patterns. In the Mediterranean Sea, the influence of warming increases eastward, with a stronger contribution to both MHW frequency and persistence in the eastern basin compared to the west. This spatial gradient reflects enhanced stratification, reduced heat loss, and greater heat retention in the Levantine region, which favour longer-lasting events. Temporally, a marked transition occurs after approximately 2010, when warming becomes the dominant contributor to MHW occurrence, particularly in recent years. These findings are consistent with previous studies demonstrating that long-term warming explains a large fraction of the increase in MHW activity, especially in the eastern Mediterranean (Juza et al., 2022; Hamdeno and Alvera-Azcaráte, 2023; Simon et al., 2023; Denaxa et al., 2025).

In the Red Sea, the contribution of warming also increases over time but follows a different spatial structure. A clear north-south gradient is observed, with a stronger influence of warming in the southern basin compared to the north. This pattern reflects differences in stratification, circulation, and heat storage, with the southern Red Sea exhibiting enhanced subsurface heat accumulation and reduced ventilation. As in the Mediterranean, a transition toward a warming-dominated regime occurs after approximately 2010, although with greater interannual variability. These results align with previous studies documenting rapid warming and increasing MHW activity in the Red Sea, as well as the role of subsurface heat storage and advective processes in sustaining extremes (Genevier et al., 2019; Mohamed et al., 2021; Hamdeno et al., 2024; Darmaraki et al., 2025; Nadimpalli et al., 2025).

While background warming sets the stage, atmospheric forcing acts as the primary trigger of individual MHW events. In both basins, MHW onset is associated with periods of enhanced surface heat flux, reduced wind-driven mixing, and persistent high-pressure systems. These conditions favour rapid surface warming by increasing net heat input and suppressing vertical heat loss. The importance of atmospheric forcing is particularly evident in regions where MHWs respond rapidly to short-term variability.

In the Mediterranean Sea, a clear west-east contrast emerges in the relative role of atmospheric and oceanic processes. In the western basin, MHWs are strongly driven by atmospheric forcing, with events closely linked to anomalous heat fluxes, reduced winds, and anticyclonic conditions. This leads to rapid surface warming and relatively high-intensity events. In contrast, the eastern Mediterranean exhibits stronger oceanic control, where enhanced stratification and substantial subsurface heat storage sustain MHWs over longer periods. This distinction explains why events in the eastern basin tend to be more persistent and vertically developed, while those in the west are more closely tied to short-term atmospheric variability (Darmaraki et al., 2024; Bonino et al., 2025; Denaxa et al., 2025).

A similar contrast is observed in the Red Sea, but with a north-south structure. In the northern Red Sea, MHWs are associated with relatively strong atmospheric forcing, including enhanced heat fluxes and reduced wind mixing, combined with subsurface heat storage. In the southern basin, however, oceanic preconditioning plays a more dominant role. Elevated heat content, subsurface temperature anomalies, and warm layer thickness are often present prior to MHW onset and persist after peak conditions, indicating a stronger influence of ocean memory. This suggests that, in the southern Red Sea, MHW evolution is less dependent on immediate atmospheric forcing and more strongly controlled by subsurface heat retention and remote forcing processes (Chaidez et al., 2017; Nadimpalli et al., 2025).

The role of oceanic processes in sustaining MHWs is further supported by the statistical analysis. The logistic regression results show that both atmospheric and oceanic predictors contribute to MHW occurrence, but their relative importance varies regionally. In the Mediterranean Sea, the western basin exhibits a more balanced contribution from atmospheric and oceanic drivers, while the eastern basin shows a stronger influence of oceanic conditions, consistent with enhanced stratification and subsurface heat storage. In the Red Sea, oceanic predictors generally exhibit a stronger association with MHW occurrence, particularly in the southern basin, where subsurface heat anomalies provide a persistent signal. The higher predictive skill associated with oceanic variables suggests that subsurface conditions offer more stable indicators of MHW development than atmospheric variability alone.

Taken together, these results demonstrate that MHW development is governed by the interaction of slow and fast components of the climate system. Background warming increases the likelihood of extremes, atmospheric forcing determines their initiation, and oceanic processes control their persistence and vertical extent. However, the balance between these components is strongly region-dependent. The Mediterranean Sea shows a transition from atmospheric dominance in the west to oceanic control in the east, while the Red Sea exhibits a shift from mixed control in the north to stronger oceanic influence in the south.

This basin-scale comparison highlights a central conclusion of this thesis: MHWs cannot be attributed to a single driver, but instead emerge from the coupling between atmospheric variability and oceanic memory under a warming climate. Understanding this interplay is essential for interpreting regional differences, improving prediction, and assessing how MHW dynamics will evolve in semi-enclosed basins in the future.

9.3 From physical Extremes to Ecological Stress: linking stratification, nutrients, and biological response:

While MHWs are fundamentally physical phenomena, their most significant consequences arise through their impact on marine ecosystems. The results of this thesis demonstrate that the translation from physical extremes to ecological stress is not controlled by temperature alone, but by a cascade of interconnected processes linking stratification, nutrient availability, and biological response. This coupling is particularly important in semi-enclosed basins such as the Mediterranean Sea and the Red Sea, where small changes in upper-ocean structure can lead to disproportionate ecological impacts.

In the Mediterranean Sea, MHW impacts are strongly governed by the interaction between thermal anomalies and stratification-driven nutrient limitation. MHW events consistently enhance upper-ocean stratification through reduced mixed layer depth, which suppresses vertical mixing and limits the upward supply of nutrients, particularly nitrate. This leads to a reduction in phytoplankton biomass, as reflected by declines in chlorophyll-a. However, the magnitude of this response varies across the basin, revealing a strong west-east contrast. The western Mediterranean, characterized by active winter mixing and relatively higher nutrient availability, shows a more pronounced biological response to MHW-induced stratification, as productivity is highly sensitive to disruptions in nutrient supply. In contrast, the eastern Mediterranean is persistently oligotrophic, and therefore exhibits weaker relative changes, as nutrient limitation is already a dominant constraint on biological activity. This spatial heterogeneity reflects fundamental differences in basin structure, circulation, and baseline productivity.

The ecological response in the Mediterranean is further shaped by strong coupling between atmospheric forcing, mixing, and seasonal productivity cycles. Regional wind systems, including the Mistral, Bora, and Etesian winds, regulate vertical mixing and drive a well-defined seasonal nutrient cycle, with winter mixing replenishing nutrients and supporting spring phytoplankton blooms (D’Ortenzio and Ribera d’Alcalà, 2009; Josey et al., 2011). MHW-induced stratification disrupts this cycle, particularly during transitional seasons when ecosystems are most sensitive to changes in mixing. As a result, compound events involving MHWs, reduced mixing, and biological decline occur more frequently and exhibit clear seasonal modulation. This confirms that Mediterranean ecosystems are tightly controlled by wind-driven nutrient entrainment and are therefore highly vulnerable to stratification anomalies (D’Ortenzio et al., 2014; Hamdeno and Alvera-Azcaráte, 2023; Darmaraki et al., 2024).

In contrast, the Red Sea exhibits a fundamentally different ecological response to MHWs, reflecting its persistently stratified and oligotrophic nature. Here, MHW impacts are primarily governed by sustained thermal stress superimposed on an already nutrient-limited system. Unlike the Mediterranean, where changes in mixing directly control nutrient supply, the Red Sea shows a weaker coupling between mixed layer variability and biological response. Stratification remains strong throughout most of the year, and variability in nutrient availability is more strongly influenced by lateral inputs and basin-scale circulation than by vertical mixing (Raitsos et al., 2013; López-Sandoval et al., 2019; Krokos et al., 2022).

A pronounced north-south gradient further modulates ecological responses in the Red Sea. The northern basin exhibits stronger physical anomalies associated with MHWs, including changes in stratification and heat flux, while the southern basin is characterized by higher MHW frequency and more persistent compound stress. The southern Red Sea is influenced by monsoon-driven inflow from the Gulf of Aden, which introduces additional variability in nutrient supply and productivity (Raitsos et al., 2013; Yao et al., 2014; Krokos et al., 2019; López-Sandoval et al., 2019; Alawad et al., 2020; Bawadekji et al., 2021; Hoteit et al., 2021). As a result, ecosystem responses in this region are shaped by the interaction between persistent thermal stress and variable nutrient inputs, leading to a more spatially heterogeneous but sustained ecological impact.

This contrast between the two basins highlights a key difference in ecosystem sensitivity: in the Mediterranean, ecological responses are primarily controlled by disruptions to wind-driven mixing and nutrient supply, whereas in the Red Sea, they are dominated by persistent thermal stress acting on an already constrained system. Consequently, MHWs in the Mediterranean tend to produce strong but seasonally modulated biological responses, while in the Red Sea they generate more continuous and less seasonally dependent stress.

The role of compound events further amplifies these impacts. In both basins, the co-occurrence of MHWs with stratification anomalies and reduced nutrient availability intensifies ecosystem stress. However, this coupling is stronger and more coherent in the Mediterranean, where physical and biogeochemical processes are tightly linked. In the Red Sea, compound stress is more diffuse and persistent, reflecting weaker coupling between physical drivers and biological variability. The increasing frequency of such compound events suggests that ecological impacts will intensify under continued warming.

In addition to indirect effects mediated through nutrient limitation, this thesis demonstrates that MHWs exert direct thermal stress on marine organisms. A controlled laboratory experiment was conducted to investigate the response of zooplankton to temperature conditions representative of marine heatwaves, using the copepod *Acartia tonsa* as a model organism. The experimental design was based on representative MHW events selected according to their intensity and duration, with a maximum duration of 20 days to match laboratory constraints. Moderate to strong events from the Western Mediterranean (Category II, summers 2018 and 2019) were compared with an extreme event from the Bay of Biscay (Category IV, July 2013). To ensure comparability and explore upper-bound responses, Mediterranean events were further intensified to simulate a worst-case scenario, with temperatures exceeding four times the climatological threshold.

The results reveal a strong and direct physiological response of zooplankton to MHW intensity and thermal structure, with mortality emerging as the dominant response. In contrast, no significant changes were observed in swimming or grazing behaviour. This indicates that lethal thermal thresholds are reached rapidly, before substantial sublethal behavioural adjustments can occur. These findings suggest that under extreme MHW conditions, zooplankton responses are characterized by a sharp transition from tolerance to mortality, rather than gradual behavioural adaptation. This highlights the vulnerability of lower trophic levels to intense and prolonged thermal stress, and provides experimental evidence linking basin-scale thermal extremes to organism-level impacts (Zervoudaki et al., 2024).

The vertical structure of MHWs adds further complexity to these interactions. Subsurface warming extends thermal stress beyond the surface layer, exposing organisms throughout the water column to elevated temperatures. At the same time, nutrient limitation remains largely confined to the upper ocean, creating a vertical decoupling between thermal and biogeochemical stressors. This mismatch can alter ecosystem structure and functioning in ways that are not captured by surface observations alone (Doney et al., 2012; Sen Gupta et al., 2020; Smith et al., 2021; Darmaraki et al., 2025; Nadimpalli et al., 2025).

Overall, the comparison between the Mediterranean Sea and the Red Sea demonstrates that MHWs act as compound physical-biogeochemical disturbances, with impacts determined by the interaction between stratification, nutrient dynamics, and biological sensitivity. While both basins are vulnerable to increasing thermal extremes, the mechanisms driving ecological responses differ fundamentally. The Mediterranean exhibits strong coupling between physical forcing and ecosystem response, leading to pronounced but seasonally dependent impacts, whereas the Red Sea is characterized by persistent, thermally dominated stress with weaker dependence on mixing variability. This distinction underscores the importance of considering both physical structure and ecosystem context when assessing the impacts of marine heatwaves in a changing climate.

9.4 Compound Extremes in the Mediterranean Sea:

A major advancement of this thesis is the treatment of MHWs as components of a broader system of compound climate extremes, rather than isolated events. In semi-enclosed basins such as the Mediterranean Sea, where strong air-sea coupling and pronounced atmospheric variability coexist, MHWs frequently co-occur with AHWs and interact with intense cyclonic systems such as Medicanes.

In the Mediterranean Sea, compound MHW-AHW events show a clear increase in both frequency and persistence over recent decades, indicating a transition toward more tightly coupled ocean-atmosphere extremes. These events are strongly synchronized in time and exhibit a pronounced seasonal cycle, with a peak during summer when radiative forcing and stratification are maximized. Spatially, compound events are more prevalent in the western Mediterranean than in the eastern basin, reflecting regional differences in air-sea interaction. The stronger co-occurrence in the western basin is consistent with more efficient air-sea coupling, driven by stronger atmospheric control, shallower summer mixed layers, and a more rapid oceanic response to atmospheric forcing. In contrast, the eastern Mediterranean, although experiencing intense atmospheric heat extremes, shows weaker co-occurrence, likely due to stronger stratification and a greater role of oceanic inertia in modulating surface responses.

The vertical structure of compound events further highlights their distinct dynamics compared to MHWs occurring in isolation. While both compound and single MHW events are associated with enhanced stratification, compound events exhibit a deeper vertical footprint, with thermal anomalies extending further into the water column. This indicates that coupled ocean-atmosphere extremes not only intensify surface warming but also promote more efficient redistribution of heat into subsurface layers. As a result, compound events enhance ocean heat storage and prolong the persistence of anomalies, reinforcing the role of ocean memory in sustaining MHW conditions. These findings are consistent with previous studies showing that combined atmospheric and oceanic extremes can modify air-sea heat fluxes and vertical mixing, leading to deeper and longer-lasting warming (Holbrook et al., 2019; Sen Gupta et al., 2020, p. 20; Oliver et al., 2021; Aboelkhair et al., 2023; Pastor and Khodayar, 2023; Pastor et al., 2024; Paredes-Fortuny et al., 2025).

Lead-lag relationships further clarify the dynamics of compound MHW-AHW events. Atmospheric heatwaves typically precede or coincide with MHW onset, indicating that atmospheric forcing plays a dominant role in initiating ocean warming. However, once established, oceanic processes, particularly subsurface heat storage and reduced mixing, control the persistence and vertical development of the event. This sequence confirms a two-stage mechanism, in which atmospheric variability triggers MHWs, while oceanic memory sustains them.

In addition to co-occurring heatwaves, the interaction between MHWs and Medicanes introduces a further level of complexity through bidirectional coupling between oceanic and atmospheric extremes. Pre-existing warm ocean conditions, often associated with MHWs, enhance cyclone development by increasing ocean heat content and strengthening air-sea heat fluxes. Warmer SSTs and deeper heat reservoirs provide additional energy to the atmosphere, supporting storm intensification. At the same time, Medicanes exert a strong feedback on the ocean, inducing rapid surface cooling, deepening the mixed layer, and redistributing heat vertically. This redistribution does not eliminate stored heat but instead transfers it to deeper layers, potentially contributing to subsequent re-emergence of thermal anomalies (Romero and Emanuel, 2013; Tous et al., 2013; Borzì et al., 2024; Miglietta et al., 2025).

Case studies of recent Medicanes, including Zorbas (2018), Ianos (2020), and Daniel (2023), provide consistent process-level evidence for this interaction. In each case, storms developed over pre-existing warm anomalies, often linked to MHW conditions, and were associated with strong latent heat fluxes during intensification. Differences between events reflect variations in atmospheric forcing and oceanic preconditioning, but the underlying mechanism remains consistent: warm ocean conditions enhance energy transfer to the atmosphere, while storms subsequently modify the ocean thermal structure through mixing and cooling. These findings are in agreement with previous studies on Mediterranean cyclones and tropical-like systems (Tous et al., 2013; Avolio et al., 2024; Borzì et al., 2024; Hewson et al., 2024; Jangir et al., 2024).

Taken together, the results demonstrate that the Mediterranean Sea is transitioning toward a regime characterized by increasingly frequent and intense compound extremes. MHWs, atmospheric heatwaves, and Medicanes are not independent phenomena, but interconnected components of a coupled climate system in which each process influences and amplifies the others. This shift has important implications for both physical dynamics and impacts. Enhanced co-occurrence of MHWs and AHWs increases the likelihood of prolonged heat stress across marine and terrestrial systems, while interactions with Medicanes suggest an elevated risk of intense storms fuelled by anomalously warm oceans.

More broadly, these findings highlight that compound extremes amplify both the intensity and persistence of climate anomalies, alter vertical heat distribution, and introduce feedback mechanisms that are not captured when events are considered in isolation. As such, understanding MHW dynamics in semi-enclosed basins requires a systems-based perspective that explicitly accounts for interactions between oceanic and atmospheric processes. This integrated view is essential for improving the prediction of extreme events and assessing their ecological and societal impacts in a warming climate.

9.5 Advances Beyond Previous Studies: what this thesis adds to the field:

MHWs have been widely documented over the past decade, with significant progress in describing their surface characteristics, temporal trends, and large-scale drivers. However, much of the existing literature has remained either global in scope or focused on individual basins, often emphasizing SST metrics and short-term atmospheric forcing. As a result, key aspects of MHW dynamics, particularly their vertical structure, regional variability, ecological impacts, and interaction with other extremes, remain insufficiently resolved. In this context, this thesis provides a substantial advance by developing an integrated, process-based framework for understanding MHWs in semi-enclosed basins.

A first major contribution of this work is the establishment of a **comparative basin-scale perspective**. By analysing the Mediterranean Sea and the Red Sea within a unified framework, this thesis demonstrates that MHW intensification is a shared response to global warming, but that its expression is strongly modulated by regional oceanographic and atmospheric conditions. This comparative approach reveals systematic contrasts (i.e., west-east in the Mediterranean and north-south in the Red Sea) and shows that basin geometry, circulation, and stratification fundamentally control how heat extremes develop and persist. This represents a clear step beyond previous studies that have largely treated these basins independently, and highlights the importance of regional context in shaping extreme-event dynamics.

A second key advance lies in the explicit integration of the **vertical dimension of MHWs**, which emerges as a central theme of this thesis. While most previous studies have focused on SST-based definitions, this work demonstrates that subsurface processes, including heat storage, vertical penetration, and ocean memory, are essential for understanding the full structure and persistence of MHWs. The results show that MHWs are increasingly extending below the surface and that subsurface heat reservoirs play a critical role in sustaining and re-intensifying events. This shifts the interpretation of MHWs from surface anomalies to **three-dimensional, vertically coherent extremes**, representing a significant conceptual advance in the field.

Third, this thesis advances the **process-based understanding of MHW drivers** by clearly disentangling and then reconnecting the roles of background warming, atmospheric forcing, and oceanic persistence. Rather than attributing MHWs to a single dominant mechanism, the results demonstrate that these events emerge from a hierarchical interaction across timescales: long-term warming sets the baseline, atmospheric variability triggers events, and oceanic processes control their persistence and vertical development. The use of detrended analyses further shows that, even under strong climate warming, internal variability and atmospheric forcing remain critical. This integrated framework provides a more complete and physically consistent interpretation of MHW dynamics than approaches that consider these drivers in isolation.

A fourth major contribution is the explicit coupling of **physical processes with ecological responses**. This thesis demonstrates that the ecological impacts of MHWs are mediated through changes in stratification and nutrient supply, rather than temperature alone. By linking mixed layer dynamics, nutrient limitation, and phytoplankton variability, the results provide a mechanistic explanation for observed biological responses. Importantly, this work also incorporates experimental evidence, showing that MHW conditions can induce direct physiological stress on zooplankton, leading to increased mortality. This dual perspective, combining basin-scale diagnostics with organism-level experiments, represents a significant step toward bridging physical oceanography and marine ecology in the study of climate extremes.

Fifth, this thesis introduces a **compound-event framework** that places MHWs within a broader system of interacting extremes. The results demonstrate that co-occurring MHW-AHW events are becoming more frequent and persistent, leading to amplified thermal stress through strong air-sea feedbacks. In addition, the interaction between MHWs and Medicanes reveals a two-way coupling in which warm ocean conditions enhance storm intensity, while storms redistribute heat vertically and modify ocean structure. This systems-based perspective shows that MHWs cannot be fully understood in isolation, but must be considered as part of a network of coupled ocean–atmosphere processes. This represents an important conceptual shift in how marine climate extremes are interpreted.

In addition to these scientific contributions, this thesis also provides a **methodological advancement** through the development of a consistent and reproducible analysis framework. The workflow enables the integration of multiple datasets, variables, and regions within a unified approach, allowing surface, subsurface, and ecological processes to be analysed together. This not only strengthens the robustness of the results but also facilitates future applications and extensions of the methodology.

Taken together, these advances demonstrate that MHWs in semi-enclosed basins are not simply increasing in frequency and intensity, but are undergoing a fundamental transformation in their structure and dynamics. The results of this thesis show that MHWs are evolving into **persistent, vertically structured, and dynamically coupled extremes**, governed by interactions between climate warming, atmospheric forcing, oceanic memory, and ecosystem response.

The overarching contribution of this work is therefore to move the field beyond a descriptive, surface-focused paradigm toward an **integrated, multi-dimensional understanding of marine heatwaves**. By combining comparative basin analysis, vertical structure, driver attribution, ecological coupling, and compound-event dynamics, this thesis provides a coherent framework for interpreting present-day MHWs and anticipating their future evolution. This perspective not only advances scientific understanding, but also establishes a foundation for improving prediction, assessing ecosystem vulnerability, and supporting adaptation strategies in a rapidly changing ocean.

Chapter Ten: Conclusions

This thesis investigates the characteristics, drivers, and impacts of MHWs in two semi-enclosed basins – the Mediterranean Sea and the Red Sea – using an integrated, multi-dimensional approach. By combining surface and subsurface analyses, atmospheric and oceanic drivers, ecological indicators, and compound-event frameworks, this work offers a comprehensive understanding of how MHWs develop, evolve, and affect marine systems in a warming climate.

The results show that MHWs in both basins have clearly intensified in recent decades, with increases in frequency, duration, and cumulative intensity. This intensification reflects the combined influence of long-term ocean warming and short-term variability, confirming that climate change is not only shifting mean conditions but also amplifying extreme thermal events. A central finding of this thesis is that MHW development is governed by a hierarchical interaction of processes. Long-term background warming raises the thermal baseline, increasing the likelihood of extreme conditions. Superimposed on this baseline, atmospheric forcing serves as the primary trigger for MHW onset. Oceanic processes, particularly stratification, mixed layer variability, and subsurface heat storage, then control the persistence, intensity, and spatial structure of events. This process-based framework provides a coherent explanation for the lifecycle of MHWs across contrasting regions.

The comparative analysis between the Mediterranean Sea and the Red Sea shows that, although both basins experience similar intensification trends, their regional expressions differ significantly. In the Mediterranean, strong air-sea coupling and regional atmospheric variability play a dominant role, while in the Red Sea, oceanic structure and stratification exert stronger control on event evolution. These differences emphasize that MHW dynamics are not universal but are shaped by basin-specific characteristics, including circulation, geometry, and vertical structure.

Another major contribution of this thesis is the demonstration that MHWs are three-dimensional phenomena. Subsurface heat storage, vertical penetration of thermal anomalies, and ocean memory are fundamental components of MHW dynamics. The presence of subsurface heat reservoirs allows anomalies to persist beyond atmospheric forcing and, in some cases, to re-emerge at the surface. This vertical perspective challenges the traditional surface-focused view of MHWs and highlights the importance of considering the full water column when assessing their intensity and impacts.

The thesis further establishes that the impacts of MHWs are mediated through coupled physical-biogeochemical processes. Enhanced stratification during MHWs reduces vertical nutrient supply, leading to declines in primary productivity, while direct thermal stress affects organismal performance and ecosystem structure. The integration of basin-scale analyses with zooplankton experiments shows that ecological responses arise from both indirect effects (via nutrient limitation) and direct temperature stress, providing a more mechanistic understanding of ecosystem vulnerability.

In addition, this work advances the understanding of MHWs by situating them within a compound-event framework. The co-occurrence of marine and atmospheric heatwaves amplifies thermal extremes through reinforcing air-sea feedbacks, while interactions between MHWs and Medicanes reveal a bidirectional coupling between oceanic and atmospheric processes. These findings highlight that MHWs are embedded within a network of interacting extremes, rather than occurring in isolation.

This thesis contributes to the field of marine climate extremes through several key advances:

- It provides a comparative, basin-scale analysis of MHWs in the Mediterranean Sea and the Red Sea, revealing both common trends and region-specific dynamics.
- It advances a process-based framework for MHW development, integrating background warming, atmospheric forcing, and oceanic persistence.
- It demonstrates the critical importance of the vertical dimension, including subsurface heat storage, penetration, and ocean memory.
- It establishes explicit links between physical processes and ecological responses, highlighting the role of stratification and nutrient limitation.
- It introduces a compound-extreme perspective, emphasizing interactions between MHWs, atmospheric heatwaves, and Medicanes.
- It implements a reproducible methodological framework for multi-variable MHW analysis across different basins.
- It introduces MarineHeatwaves.jl, a Julia-based implementation of MHW detection designed to combine methodological rigor with high computational performance.

Together, these contributions move the field beyond a surface-based and event-focused paradigm toward a more integrated understanding of MHWs as multi-scale, coupled phenomena. The results of this thesis indicate that MHWs in semi-enclosed basins are likely to become more frequent, more persistent, and more vertically extensive under continued climate warming. The increasing importance of subsurface heat storage and ocean memory suggests that future events may last longer and have greater cumulative impacts, while the rising likelihood of compound extremes will further amplify risks.

From an ecological perspective, the intensification of MHWs presents significant challenges for marine ecosystems, particularly in oligotrophic regions such as the Mediterranean and the Red Sea. Increased stratification, reduced nutrient supply, and prolonged thermal stress are likely to affect productivity, species distribution, and ecosystem functioning. The presence of vertically extended MHWs further implies that impacts will propagate throughout the water column, affecting a broader range of habitats.

These findings highlight the need for integrated management and adaptation strategies that address the increasing frequency and complexity of extreme events. This includes developing monitoring systems that combine satellite and in situ observations, as well as adaptive frameworks for fisheries, conservation, and coastal resource management.

Building on the results of this thesis, several avenues for future research emerge:

- Improving the representation of subsurface processes through higher-resolution observations and data assimilation.
- Developing coupled ocean-atmosphere models to better resolve causal mechanisms and feedbacks.
- Expanding the analysis of compound extremes to include additional drivers and longer time series.
- Incorporating more comprehensive ecosystem indicators, including species-level responses and trophic interactions.
- Advancing predictive models that integrate atmospheric, oceanic, and ecological variables.

In conclusion, this thesis demonstrates that marine heatwaves in semi-enclosed basins are complex, dynamically coupled extremes arising from the interaction of climate change, atmospheric variability, oceanic structure, and ecosystem sensitivity. By integrating these components into a unified framework, this work advances the understanding of MHWs from surface anomalies to fully coupled, three-dimensional phenomena. This perspective is essential for improving prediction, assessing impacts, and developing effective responses to marine climate extremes in a rapidly changing ocean.

Chapter Eleven: Supplementary Materials

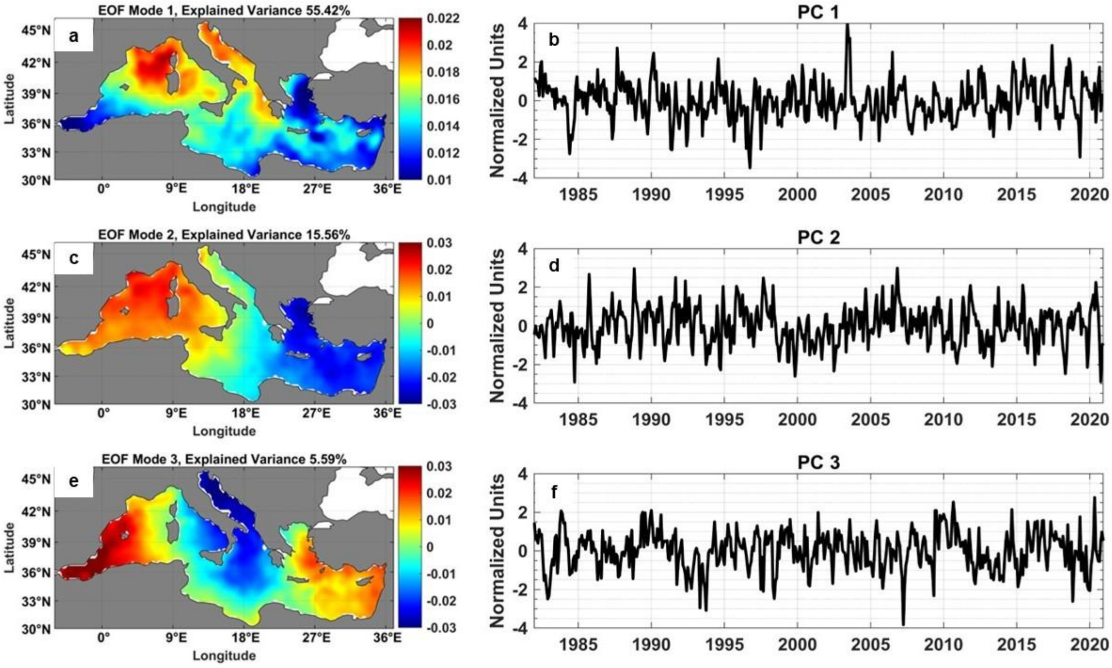

Supplementary Figure 1. *The first three EOF (left)/PC (right) (spatial variation/temporal variation) modes of SSTA in the Mediterranean Sea from 1982 to 2020.*

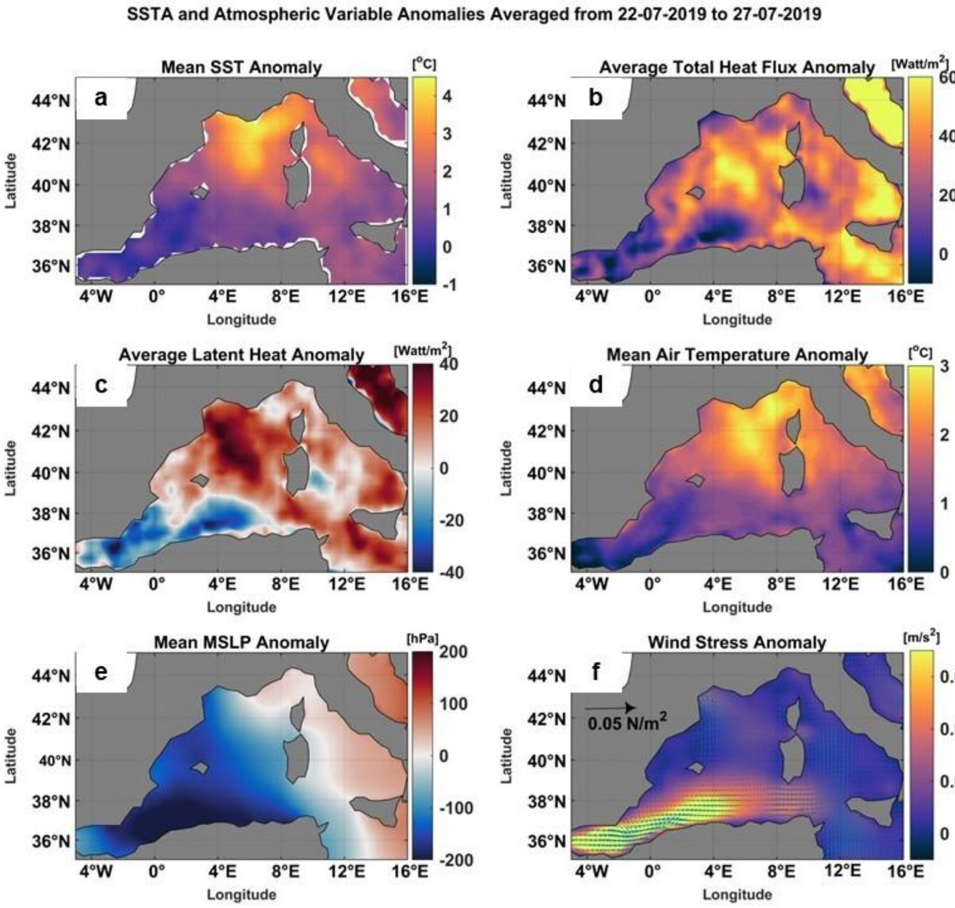

SSTA and Atmospheric Variable Anomalies Averaged from 22-07-2019 to 27-07-2019

Mean SST Anomaly

Average Total Heat Flux Anomaly

Average Latent Heat Anomaly

Mean Air Temperature Anomaly

Mean MSLP Anomaly

Wind Stress Anomaly

Supplementary Figure 2. *The mean (a) SST anomaly [°C], (b) total heat flux anomaly [W/m²], (c) latent heat flux anomaly [W/m²], (d) air temperature anomaly [°C], (e) mean sea level pressure anomaly [hPa], and (f) wind stress anomaly [N/m²] during the MHW event (22 July-27 July 2019) in the WMB. Note that the anomalies were calculated based on 1982-2020 climatology from ERA5 hourly data.*

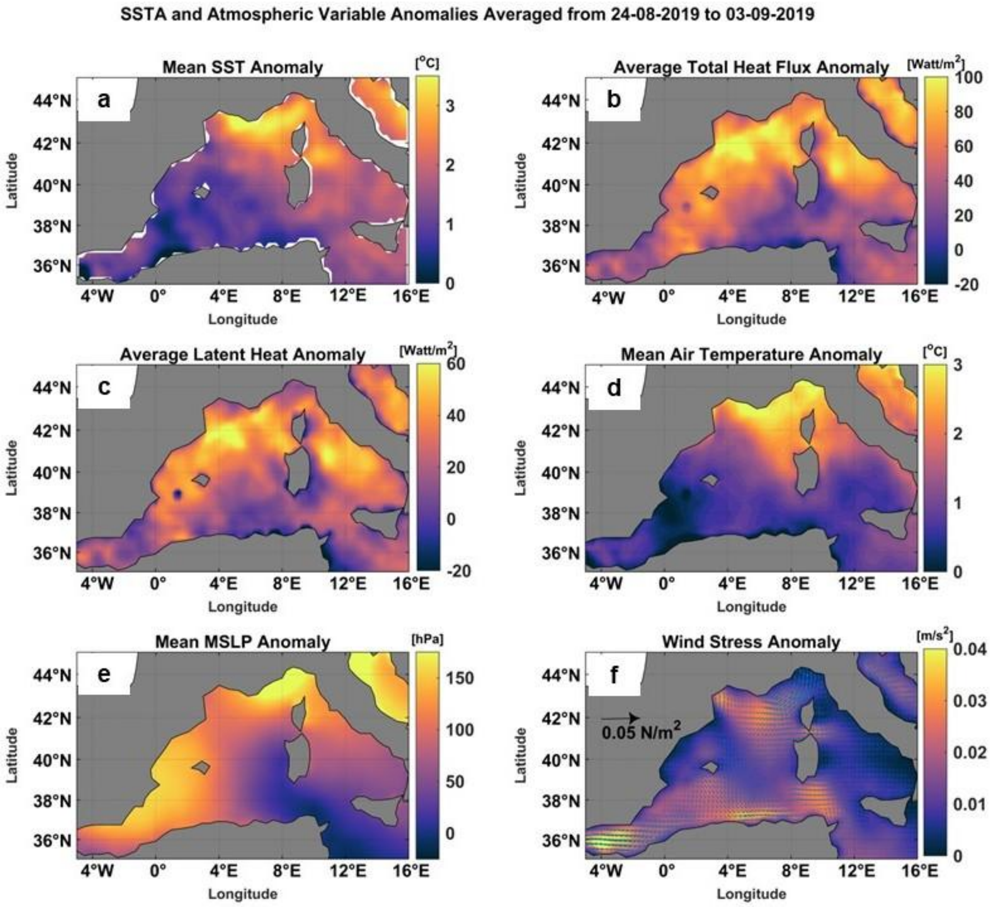

Supplementary Figure 3. *The mean (a) SST anomaly [°C], (b) total heat flux anomaly [W/m²], (c) latent heat flux anomaly [W/m²], (d) air temperature anomaly [°C], (e) mean sea level pressure anomaly [hPa], and (f) wind stress anomaly [N/m²] during the MHW event (24 August-3 September 2019) in the WMB. Note that the anomalies were calculated based on 1982-2020 climatology from ERA5 hourly data.*

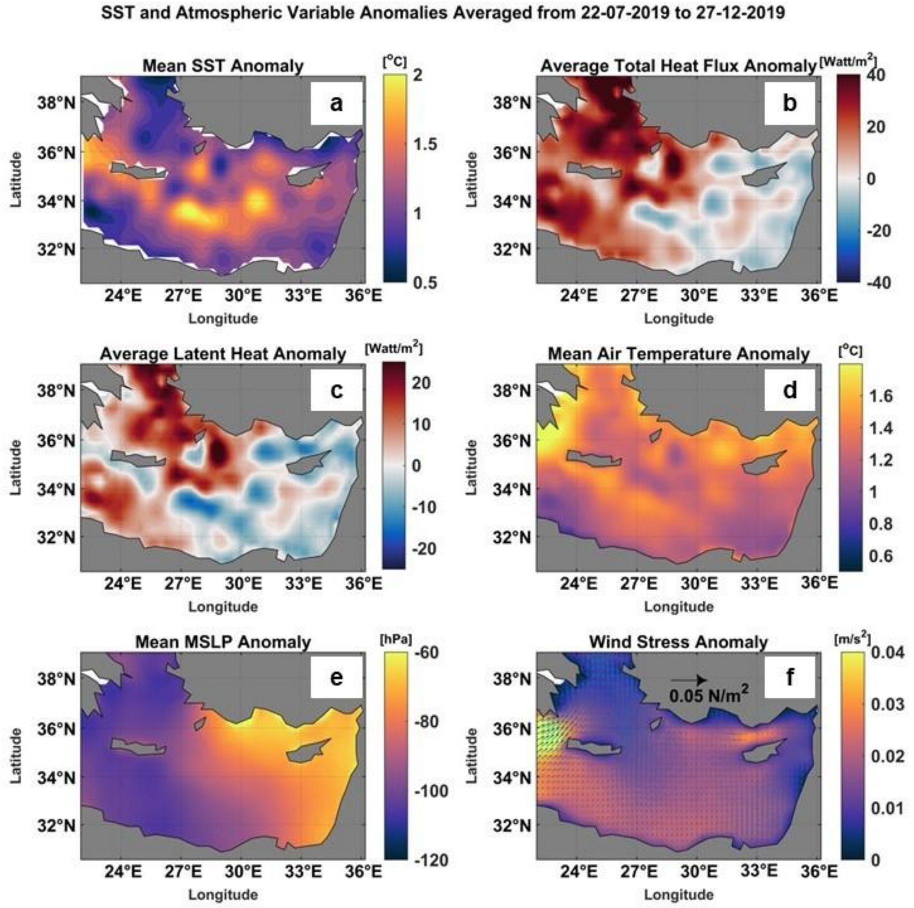

Supplementary Figure 4. *The mean (a) SST anomaly [°C], (b) total heat flux anomaly [W/m²], (c) latent heat flux anomaly [W/m²], (d) air temperature anomaly [°C], (e) mean sea level pressure anomaly [hPa], and (f) wind stress anomaly [N/m²] during the MHW event (22 July-27 December 2019) in the EMB. Note that the anomalies were calculated based on 1982-2020 climatology from ERA5 hourly data.*

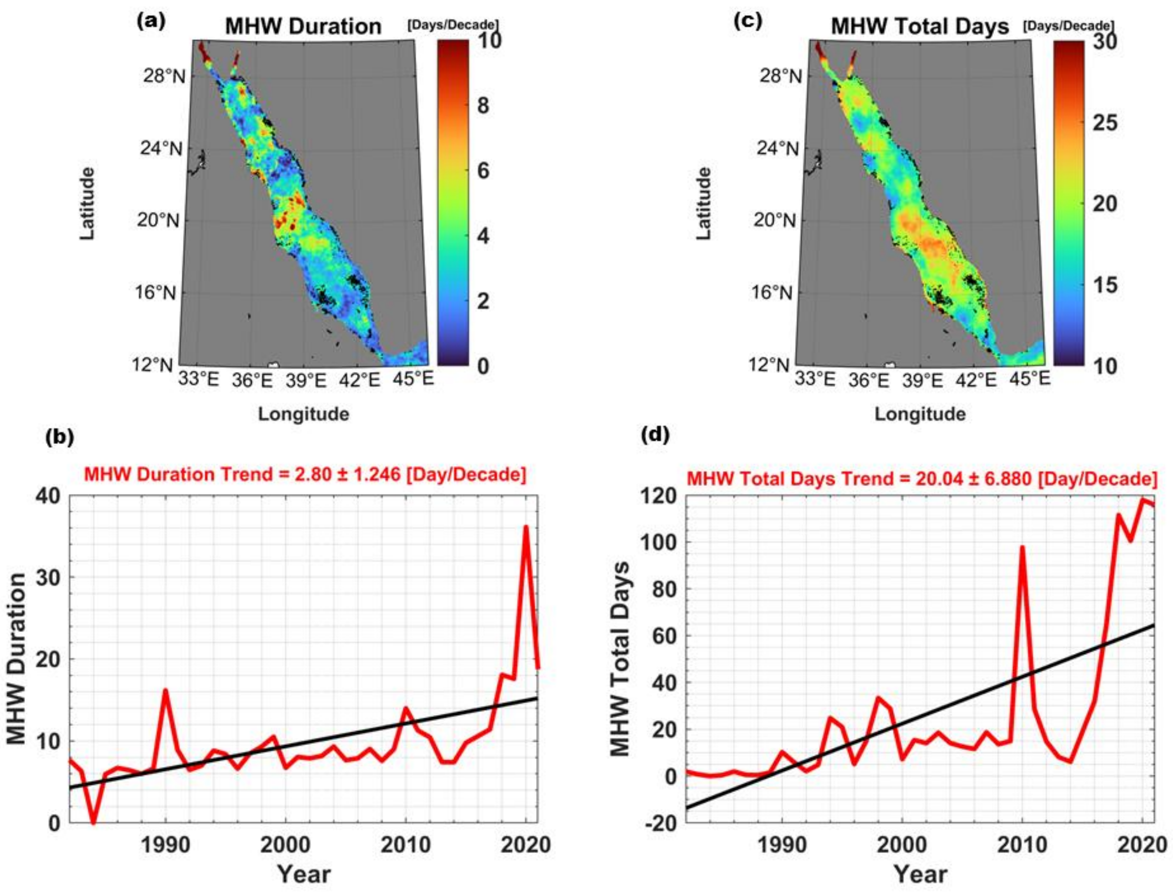

Supplementary Figure 5. *Spatial and temporal trends of marine heatwave duration (a, b) and total days (c,d) in the Red Sea from 1982-2021.*

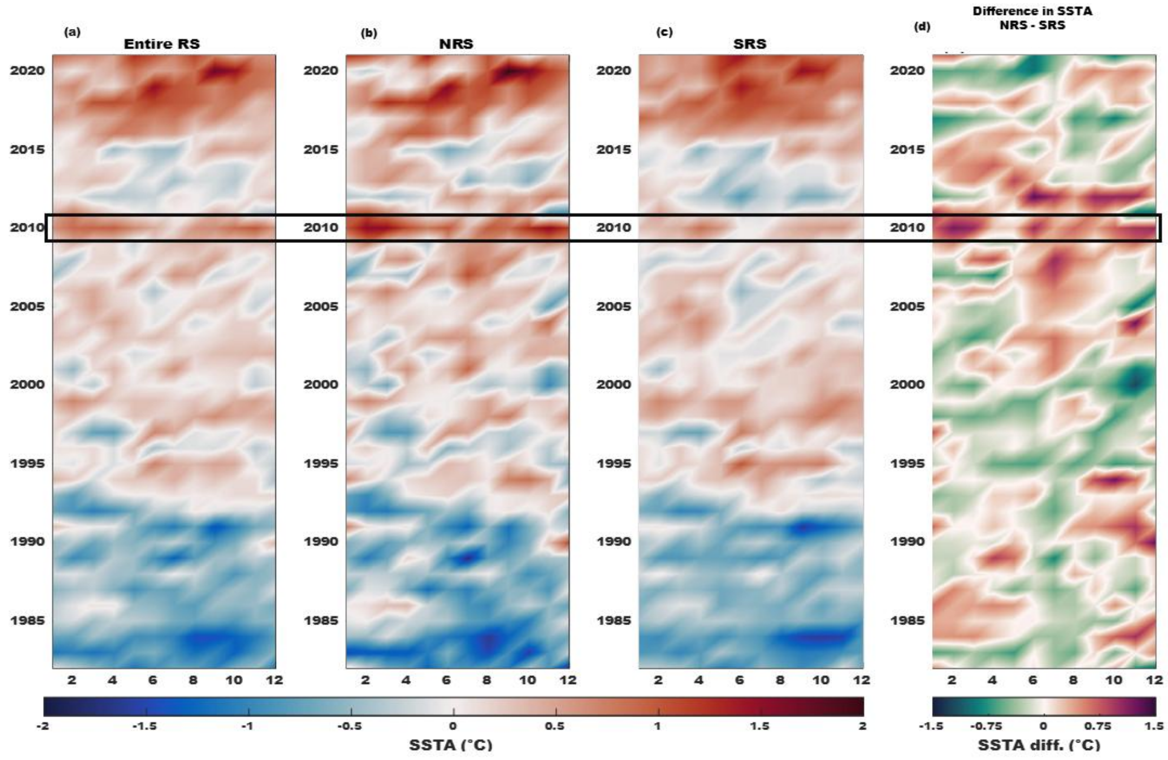

Supplementary Figure 6*. Monthly sea surface temperature anomaly patterns from 1982 to 2021. (A-C) Monthly SSTA time series for the entire Red Sea (RS), northern Red Sea (NRS), and southern Red Sea (SRS), respectively. (D) Monthly SSTA difference between NRS and SRS, where red indicates periods when SSTA was higher in NRS than in SRS, and green indicates periods when SSTA was higher in SRS than in NRS.*

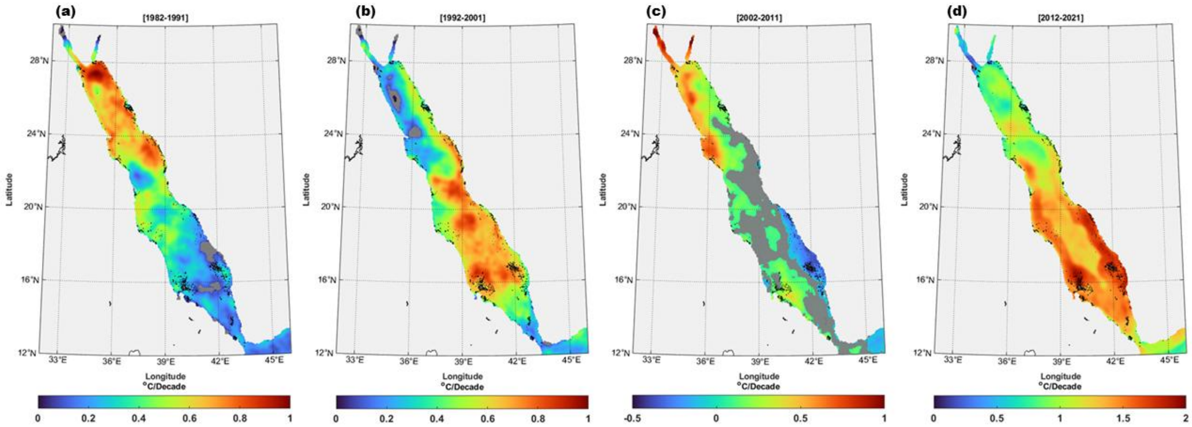

Supplementary Figure 7*. Decadal spatial trends in sea surface temperature (°C/decade) in the Red Sea. (a) 1982 - 1991, (b) 1992 - 2001, (c) 2002 - 2011, and (d) 2012 - 2021.*

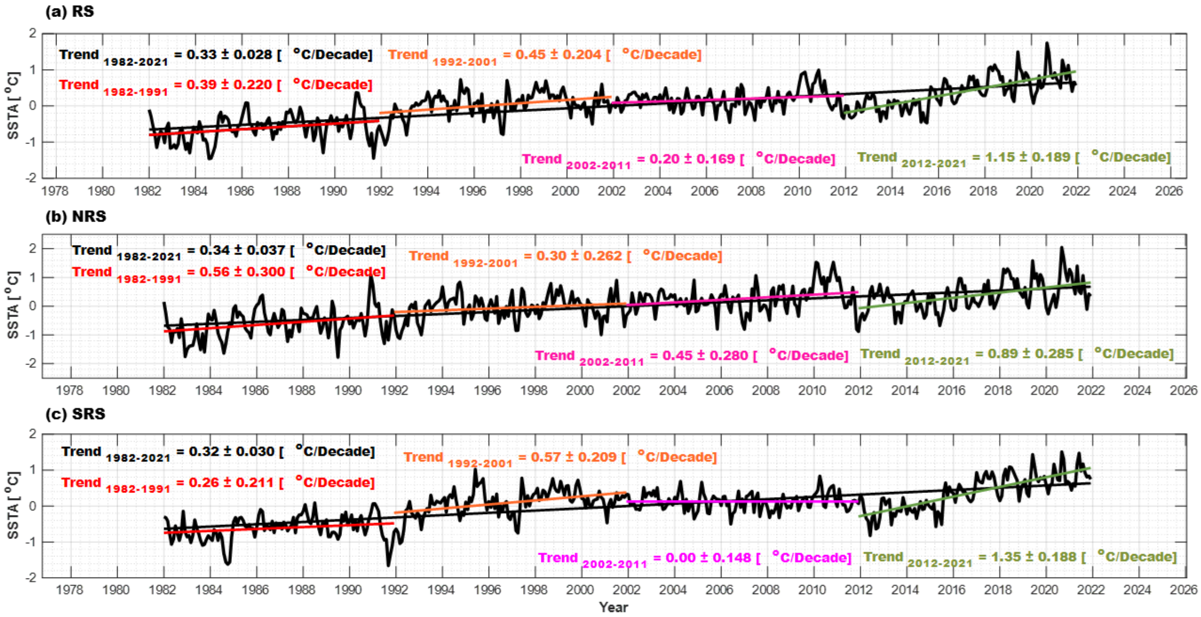

Supplementary Figure 8. *Temporal evolution and decadal trends of sea surface temperature anomalies (°C) in the entire Red Sea (a), northern Red Sea (b), and southern Red Sea (c) from 1982 to 2021.*

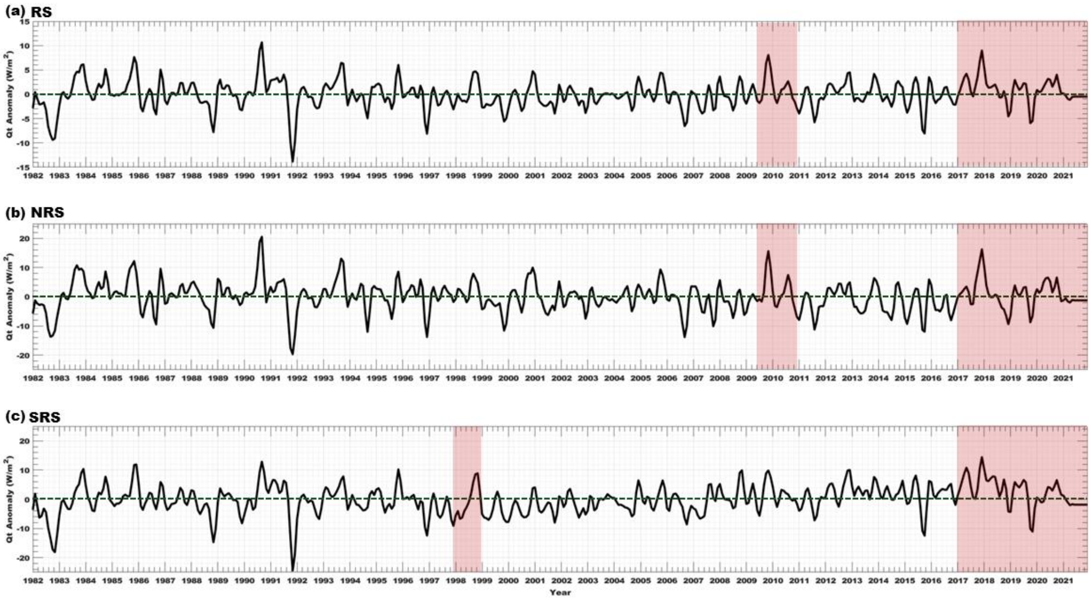

Supplementary Figure 9. *Temporal evolution of total heat flux anomalies (in W/m²) in the entire Red Sea (A), northern Red Sea (B), and southern Red Sea (C) between 1982 and 2021. The red shaded areas indicate the years with the highest marine heatwave (MHW) frequency in each basin.*

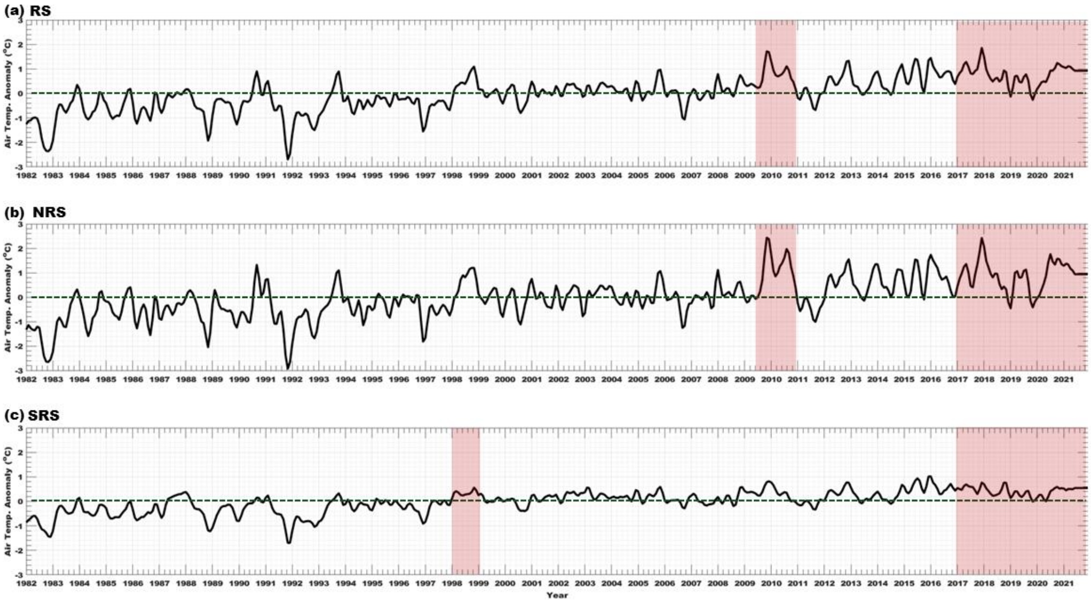

Supplementary Figure 10. *Temporal evolution of the atmospheric temperature anomalies (in °C) in the entire Red Sea (A), northern Red Sea (B), and southern Red Sea (C) between 1982 and 2021. The red shaded areas indicate the years with the highest marine heatwave (MHW) frequency in each basin.*

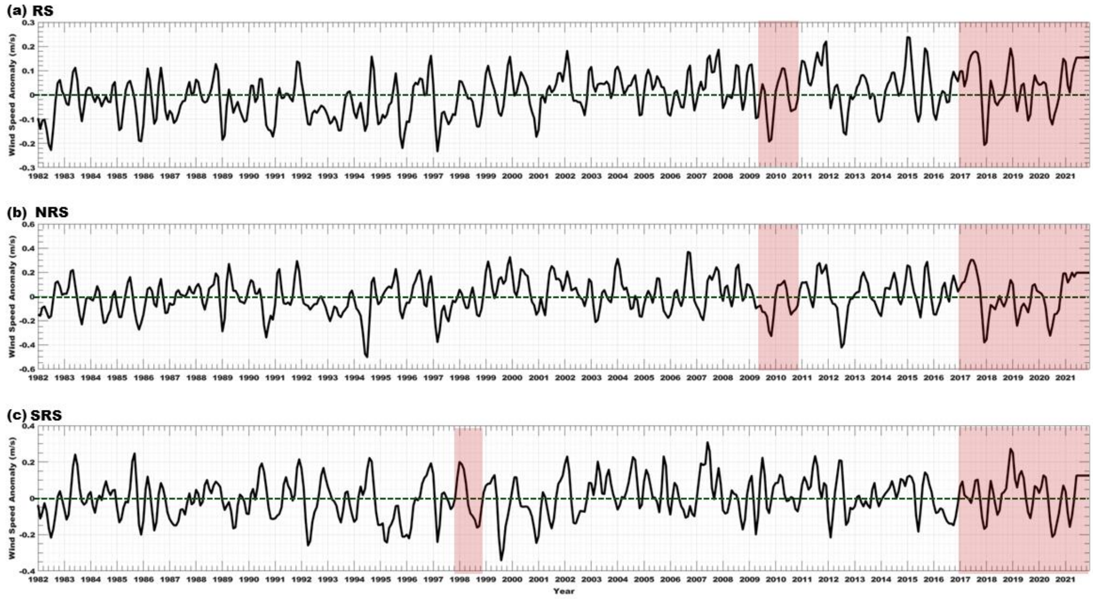

Supplementary Figure 11. *Temporal evolution of the wind speed anomalies (in m/s) in the entire Red Sea (A), northern Red Sea (B), and southern Red Sea (C) between 1982 and 2021. The red shaded areas indicate the years with the highest marine heatwave (MHW) frequency in each basin.*

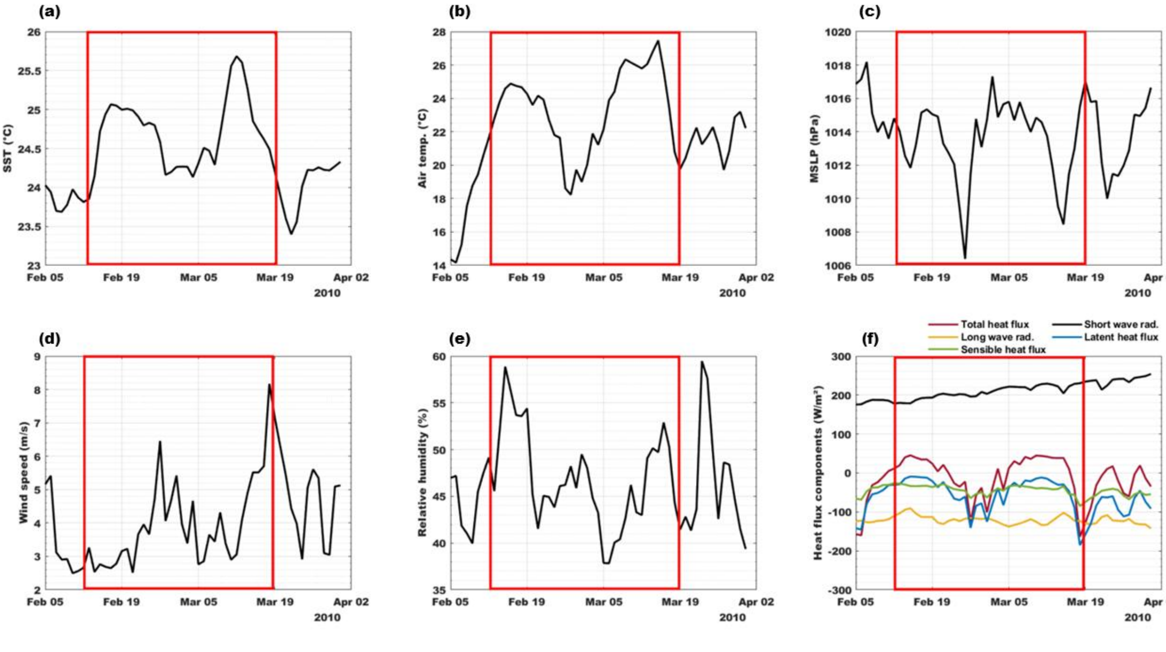

Supplementary Figure 12. *The time series of different atmospheric covering the period of the 2010 MHW event in the NRS. The panels display (a) sea surface temperature (°C), (b) air temperature (°C), (c) mean sea level pressure (hPa), (d) wind speed (m/s), (e) relative humidity (%), and (f) heat flux components (W/m²). The MHW event period is highlighted with a red box.*

Chapter Twelve: References

- Aboelkhair, H., Mohamed, B., Morsy, M., and Nagy, H. (2023). Co-Occurrence of Atmospheric and Oceanic Heatwaves in the Eastern Mediterranean over the Last Four Decades. *Remote Sensing* 15, 1841. doi: 10.3390/rs15071841
- AghaKouchak, A., Chiang, F., Huning, L. S., Love, C. A., Mallakpour, I., Mazdiyasni, O., et al. (2020). Climate Extremes and Compound Hazards in a Warming World. *Annual Review of Earth and Planetary Sciences* 48, 519–548. doi: 10.1146/annurev-earth-071719-055228
- Alawad, K. A., Al-Subhi, A. M., Alsaafani, M. A., and Alraddadi, T. M. (2020). Atmospheric Forcing of the High and Low Extremes in the Sea Surface Temperature over the Red Sea and Associated Chlorophyll-a Concentration. *Remote Sensing* 12, 2227. doi: 10.3390/rs12142227
- Alduchov, O. A., and Eskridge, R. E. (1996). Improved Magnus Form Approximation of Saturation Vapor Pressure. Available at: https://journals.ametsoc.org/view/journals/apme/35/4/1520-0450_1996_035_0601_imfaos_2_0_co_2.xml (Accessed June 20, 2024).
- Al-Horani, F. A., Al-Rousan, S. A., Al-Zibdeh, M., and Khalaf, M. A. (2006). The status of coral reefs on the Jordanian coast of the Gulf of Aqaba, Red Sea. *Zoology in the Middle East* 38, 99–110. doi: 10.1080/09397140.2006.10638171
- Allam, A., Moussa, R., Najem, W., and Bocquillon, C. (2020). "Chapter 1 - Hydrological cycle, Mediterranean basins hydrology," in *Water Resources in the Mediterranean Region*, eds. M. Zribi, L. Brocca, Y. Tramblay, and F. Molle (Elsevier), 1–21. doi: 10.1016/B978-0-12-818086-0.00001-7
- Amaya, D. J., Alexander, M. A., Capotondi, A., Deser, C., Karnauskas, K. B., Miller, A. J., et al. (2021). Are Long-Term Changes in Mixed Layer Depth Influencing North Pacific Marine Heatwaves? *Bulletin of the American Meteorological Society* 102, S59–S66. doi: 10.1175/BAMS-D-20-0144.1
- Amaya, D. J., Miller, A. J., Xie, S.-P., and Kosaka, Y. (2020). Physical drivers of the summer 2019 North Pacific marine heatwave. *Nat Commun* 11, 1903. doi: 10.1038/s41467-020-15820-w
- Arafeh-Dalmau, N., Montaño-Moctezuma, G., Martínez, J. A., Beas-Luna, R., Schoeman, D. S., and Torres-Moye, G. (2019). Extreme Marine Heatwaves Alter Kelp Forest Community Near Its Equatorward Distribution Limit. *Front. Mar. Sci.* 6, 499. doi: 10.3389/fmars.2019.00499
- Argüeso, D., Marcos, M., and Amores, A. (2024). Storm Daniel fueled by anomalously high sea surface temperatures in the Mediterranean. *npj Clim Atmos Sci* 7, 307. doi: 10.1038/s41612-024-00872-2
- Artana, C., Kaplan, A., Ramírez, F., Ortega, M., Steenbeek, J. G., and Coll, M. (2026). Marine heatwaves are transforming Western mediterranean marine ecosystems. *Sci Rep* 16, 5843. doi: 10.1038/s41598-026-35813-x

- Arteaga, L. A., and Rousseaux, C. S. (2023). Impact of Pacific Ocean heatwaves on phytoplankton community composition. *Commun Biol* 6, 263. doi: 10.1038/s42003-023-04645-0
- Avolio, E., Fanelli, C., Pisano, A., and Miglietta, M. M. (2024). Unveiling the Relationship Between Mediterranean Tropical-Like Cyclones and Rising Sea Surface Temperature. *Geophysical Research Letters* 51, e2024GL109921. doi: 10.1029/2024GL109921
- Barcikowska, M. J., Kapnick, S. B., and Feser, F. (2018). Impact of large-scale circulation changes in the North Atlantic sector on the current and future Mediterranean winter hydroclimate. *Climate Dynamics* 50, 2039–2059. doi: 10.1007/s00382-017-3735-5
- Barnston, A. G., and Livezey, R. E. (1987). Classification, Seasonality and Persistence of Low-Frequency Atmospheric Circulation Patterns. *Monthly Weather Review* 115, 1083–1126. doi: 10.1175/1520-0493(1987)115%3C1083:CSAPOL%3E2.0.CO;2
- Barros, V. R., Field, C. B., Dokken, D. J., Mastrandrea, M. D., and Mach, K. J. eds. (2014). *Climate Change 2014: Impacts, Adaptation and Vulnerability: Working Group II Contribution to the IPCC Fifth Assessment Report of the Integovernmental Panel on Climate Change*. Cambridge: Cambridge University Press. doi: 10.1017/CBO9781107415386
- Bawadekji, A., Tonbol, K., Ghazouani, N., Becheikh, N., and Shaltout, M. (2021). General and Local Characteristics of Current Marine Heatwave in the Red Sea. *JMSE* 9, 1048. doi: 10.3390/jmse9101048
- Bawadekji, A., Tonbol, K., Ghazouani, N., Becheikh, N., and Shaltout, M. (2022). Recent atmospheric changes and future projections along the Saudi Arabian Red Sea Coast. *Sci Rep* 12, 160. doi: 10.1038/s41598-021-04200-z
- Behera, S. K., Doi, T., and Ratnam, J. V. (2021). "5 - Air–sea interactions in tropical Indian Ocean: The Indian Ocean Dipole," in *Tropical and Extratropical Air-Sea Interactions*, ed. S. K. Behera (Elsevier), 115–139. doi: 10.1016/B978-0-12-818156-0.00001-0
- Behrenfeld, M., and Boss, E. (2006). Beam attenuation and chlorophyll concentration as alternative optical indices of phytoplankton biomass. *Journal of Marine Research* 64. Available at: https://elischolar.library.yale.edu/journal_of_marine_research/134
- Benedetti-Cecchi, L. (2021). Complex networks of marine heatwaves reveal abrupt transitions in the global ocean. *Sci Rep* 11, 1739. doi: 10.1038/s41598-021-81369-3
- Bian, C., Jing, Z., Wang, H., and Wu, L. (2024). Scale-Dependent Drivers of Marine Heatwaves Globally. *Geophysical Research Letters* 51, e2023GL107306. doi: 10.1029/2023GL107306
- Bjerknes, J. (1969). ATMOSPHERIC TELECONNECTIONS FROM THE EQUATORIAL PACIFIC. *Monthly Weather Review* 97, 163–172. doi: 10.1175/1520-0493(1969)097%3C0163:ATFTEP%3E2.3.CO;2
- Bond, N. A., Cronin, M. F., Freeland, H., and Mantua, N. (2015). Causes and impacts of the 2014 warm anomaly in the NE Pacific. *Geophysical Research Letters* 42, 3414–3420. doi: 10.1002/2015GL063306

- Bonino, G., McAdam, R., Athanasiadis, P., Cavicchia, L., Rodrigues, R. R., Scoccimarro, E., et al. (2025). Mediterranean summer marine heatwaves triggered by weaker winds under subtropical ridges. *Nat. Geosci.* 18, 848–853. doi: 10.1038/s41561-025-01762-9
- Borzì, A. M., Minio, V., De Plaen, R., Lecocq, T., Cannavò, F., Ciraolo, G., et al. (2024). Long-term analysis of microseism during extreme weather events: Medicanes and common storms in the Mediterranean Sea. *Science of The Total Environment* 915, 169989. doi: 10.1016/j.scitotenv.2024.169989
- Breitburg, D., Levin, L. A., Oschlies, A., Grégoire, M., Chavez, F. P., Conley, D. J., et al. (2018). Declining oxygen in the global ocean and coastal waters. *Science* 359, eaam7240. doi: 10.1126/science.aam7240
- Brenner, S. (1993). Long-term evolution and dynamics of a persistent warm core eddy in the Eastern Mediterranean Sea. *Deep Sea Research Part II: Topical Studies in Oceanography* 40, 1193–1206. doi: 10.1016/0967-0645(93)90067-W
- Burger, F., Terhaar, J., and Frölicher, T. (2022). Compound marine heatwaves and ocean acidity extremes. *Nature Communications* 13. doi: 10.1038/s41467-022-32120-7
- Cai, W., Wang, G., Li, Z., Zheng, X., Yang, K., and Ng, B. (2021). “Chapter 21 - Response of the positive Indian Ocean dipole to climate change and impact on Indian summer monsoon rainfall,” in *Indian Summer Monsoon Variability*, eds. J. Chowdary, A. Parekh, and C. Gnanaseelan (Elsevier), 413–432. doi: 10.1016/B978-0-12-822402-1.00010-7
- Campbell, J. W. (1995). The lognormal distribution as a model for bio-optical variability in the sea. *J. Geophys. Res.* 100, 13237–13254. doi: 10.1029/95JC00458
- Campins, J., Genovés, A., Picornell, M. A., and Jansà, A. (2011). Climatology of Mediterranean cyclones using the ERA-40 dataset. *International Journal of Climatology* 31, 1596–1614. doi: 10.1002/joc.2183
- Carvalho, S., Kürten, B., Krokos, G., Hoteit, I., and Ellis, J. (2019). “The Red Sea,” in *World Seas: an Environmental Evaluation*, (Elsevier), 49–74. doi: 10.1016/B978-0-08-100853-9.00004-X
- Cerutti, J. M. B., Holzman, R., Kiflawi, M., and Fine, M. (2025). Regionalisation of Red Sea coral reefs based on remotely sensed environmental data identifies two distinct regions that align with large-scale climatic forcings. *Coral Reefs* 44, 1127–1142. doi: 10.1007/s00338-025-02668-z
- Chaidez, V., Dreano, D., Agusti, S., Duarte, C. M., and Hoteit, I. (2017). Decadal trends in Red Sea maximum surface temperature. *Sci Rep* 7, 8144. doi: 10.1038/s41598-017-08146-z
- Chefaoui, R. M., Duarte, C. M., and Serrão, E. A. (2018). Dramatic loss of seagrass habitat under projected climate change in the Mediterranean Sea. *Glob Change Biol* 24, 4919–4928. doi: 10.1111/gcb.14401
- Chen, Q., Li, D., Feng, J., Zhao, L., Qi, J., and Yin, B. (2023). Understanding the compound marine heatwave and low-chlorophyll extremes in the western Pacific Ocean. *Front. Mar. Sci.* 10. doi: 10.3389/fmars.2023.1303663

- Cheng, L., Abraham, J., Hausfather, Z., and Trenberth, K. E. (2019). How fast are the oceans warming? *Science* 363, 128–129. doi: 10.1126/science.aav7619
- Cheng, L., Trenberth, K. E., Fasullo, J., Boyer, T., Abraham, J., and Zhu, J. (2017). Improved estimates of ocean heat content from 1960 to 2015. *Sci Adv* 3, e1601545. doi: 10.1126/sciadv.1601545
- Cheng, Y., Zhang, M., Song, Z., Wang, G., Zhao, C., Shu, Q., et al. (2023). A quantitative analysis of marine heatwaves in response to rising sea surface temperature. *Science of The Total Environment* 881, 163396. doi: 10.1016/j.scitotenv.2023.163396
- Choi, H.-Y., Park, M.-S., Kim, H.-S., and Lee, S. (2024). Marine heatwave events strengthen the intensity of tropical cyclones. *Commun Earth Environ* 5, 1–8. doi: 10.1038/s43247-024-01239-4
- Cochran, J. E. M., Kattan, A., Langner, U., Knochel, A. M., Carvalho, S., Coker, D. J., et al. (2024). Fine-scale spatial and temporal trends in Red Sea coral reef research. *Regional Studies in Marine Science* 71, 103404. doi: 10.1016/j.rsma.2024.103404
- Collins, M., Sutherland, M., Bouwer, L., Cheong, S.-M., Frölicher, T., Jacot Des Combes, H., et al. (2019). Extremes, Abrupt Changes and Managing Risk. In: IPCC Special Report on the Ocean and Cryosphere in a Changing Climate. Available at: https://www.ipcc.ch/site/assets/uploads/sites/3/2019/11/10_SROCC_Ch06_FINAL.pdf
- Darmaraki, S., Denaxa, D., Theodorou, I., Livanou, E., Rigatou, D., Raitsos E., D., et al. (2024). Marine Heatwaves in the Mediterranean Sea: A Literature Review. *Mediterr. Mar. Sci.* 25, 586–620. doi: 10.12681/mms.38392
- Darmaraki, S., Krokos, G., Genevier, L., Hoteit, I., and Raitsos, D. E. (2025). Drivers of marine heatwaves in coral bleaching regions of the Red Sea. *Commun Earth Environ* 6, 120. doi: 10.1038/s43247-025-02096-5
- Darmaraki, S., Somot, S., Sevault, F., and Nabat, P. (2019a). Past Variability of Mediterranean Sea Marine Heatwaves. *Geophys. Res. Lett.* 46, 9813–9823. doi: 10.1029/2019GL082933
- Darmaraki, S., Somot, S., Sevault, F., Nabat, P., Cabos Narvaez, W. D., Cavicchia, L., et al. (2019b). Future evolution of Marine Heatwaves in the Mediterranean Sea. *Clim Dyn* 53, 1371–1392. doi: 10.1007/s00382-019-04661-z
- Davis, S. R., Pratt, L. J., and Jiang, H. (2015). The Tokar Gap Jet: Regional Circulation, Diurnal Variability, and Moisture Transport Based on Numerical Simulations. *Journal of Climate* 28, 5885–5907. doi: 10.1175/JCLI-D-14-00635.1
- Dayan, H., McAdam, R., Juza, M., Masina, S., and Speich, S. (2023). Marine heat waves in the Mediterranean Sea: An assessment from the surface to the subsurface to meet national needs. *Front. Mar. Sci.* 10. doi: 10.3389/fmars.2023.1045138
- Denaxa, D., Korres, G., Darmaraki, S., and Hatzaki, M. (2025). Insights into sea surface temperature variability and the impact of long-term warming on marine heatwaves in the Mediterranean Sea. *State of the Planet* 6-osr9, 1–11. doi: 10.5194/sp-6-osr9-10-2025

- Di Lorenzo, E., and Mantua, N. (2016). Multi-year persistence of the 2014/15 North Pacific marine heatwave. *Nature Clim Change* 6, 1042–1047. doi: 10.1038/nclimate3082
- Diaz-Almela, E., Marbà, N., and Duarte, C. M. (2007). Consequences of Mediterranean warming events in seagrass (Posidonia oceanica) flowering records. *Global Change Biol* 13, 224–235. doi: 10.1111/j.1365-2486.2006.01260.x
- Doney, S. C., Ruckelshaus, M., Emmett Duffy, J., Barry, J. P., Chan, F., English, C. A., et al. (2012). Climate Change Impacts on Marine Ecosystems. *Annu. Rev. Mar. Sci.* 4, 11–37. doi: 10.1146/annurev-marine-041911-111611
- D'Ortenzio, F., Lavigne, H., Besson, F., Claustre, H., Coppola, L., Garcia, N., et al. (2014). Observing mixed layer depth, nitrate and chlorophyll concentrations in the northwestern Mediterranean: A combined satellite and NO3 profiling floats experiment. *Geophysical Research Letters* 41, 6443–6451. doi: 10.1002/2014GL061020
- D'Ortenzio, F., and Ribera d'Alcalà, M. (2009). On the trophic regimes of the Mediterranean Sea: a satellite analysis. *Biogeosciences* 6, 139–148. doi: 10.5194/bg-6-139-2009
- Escudier, R., Clementi, E., Omar, M., Cipollone, A., Pistoia, J., Aydogdu, A., et al. (2020). Mediterranean Sea Physical Reanalysis (CMEMS MED-Currents, E3R1 system): MEDSEA_MULTIYEAR_PHY_006_004. doi: 10.25423/CMCC/MEDSEA_MULTIYEAR_PHY_006_004_E3R1
- European Union-Copernicus Marine Service (2018). Global ocean biogeochemistry hindcast. doi: 10.48670/MOI-00019
- Fawcett, T. (2006). An introduction to ROC analysis. *Pattern Recognition Letters* 27, 861–874. doi: 10.1016/j.patrec.2005.10.010
- Fenoglio-Marc, L., Schöne, T., Illigner, J., Becker, M., Manurung, P., and Khafid (2012). Sea Level Change and Vertical Motion from Satellite Altimetry, Tide Gauges and GPS in the Indonesian Region. *Marine Geodesy* 35, 137–150. doi: 10.1080/01490419.2012.718682
- Fernández-Álvarez, B., Barceló-Llull, B., and Pascual, A. (2025). Tracking marine heatwaves in the Balearic Sea: temperature trends and the role of detection methods. *Ocean Science* 21, 1987–1999. doi: 10.5194/os-21-1987-2025
- Fine, M., Gildor, H., and Genin, A. (2013). A coral reef refuge in the Red Sea. *Glob Chang Biol* 19, 3640–3647. doi: 10.1111/gcb.12356
- Fredston, A. L., Cheung, W. W. L., Frölicher, T. L., Kitchel, Z. J., Maureaud, A. A., Thorson, J. T., et al. (2023). Marine heatwaves are not a dominant driver of change in demersal fishes. *Nature* 621, 324–329. doi: 10.1038/s41586-023-06449-y
- Frölicher, T. L., Fischer, E. M., and Gruber, N. (2018). Marine heatwaves under global warming. *Nature* 560, 360–364. doi: 10.1038/s41586-018-0383-9
- Gandoin, R., and Garza, J. (2024). Underestimation of strong wind speeds offshore in ERA5: evidence, discussion and correction. *Wind Energy Science* 9, 1727–1745. doi: 10.5194/wes-9-1727-2024

- Garnesson, P., Mangin, A., and Bretagnon, M. (2022). OCEAN COLOUR PRODUCTION CENTRE Satellite Observation Copernicus-GlobColour Products. doi: https://doi.org/10.48670/moi-00281
- Garrabou, J., Coma, R., Bensoussan, N., Bally, M., Chevaldonné, P., Cigliano, M., et al. (2009). Mass mortality in Northwestern Mediterranean rocky benthic communities: effects of the 2003 heat wave. *Global Change Biology* 15, 1090–1103. doi: 10.1111/j.1365-2486.2008.01823.x
- Genevier, L. G. C., Jamil, T., Raitsos, D. E., Krokos, G., and Hoteit, I. (2019). Marine heatwaves reveal coral reef zones susceptible to bleaching in the Red Sea. *Glob Change Biol* 25, 2338–2351. doi: 10.1111/gcb.14652
- Gonzalez, K., Daraghmeh, N., Lozano-Cortés, D., Benzoni, F., Berumen, M. L., and Carvalho, S. (2024). Differential spatio-temporal responses of Red Sea coral reef benthic communities to a mass bleaching event. *Sci Rep* 14, 24229. doi: 10.1038/s41598-024-74956-7
- Good, S., Fiedler, E., Mao, C., Martin, M. J., Maycock, A., Reid, R., et al. (2020). The Current Configuration of the OSTIA System for Operational Production of Foundation Sea Surface Temperature and Ice Concentration Analyses. *Remote Sensing* 12, 720. doi: 10.3390/rs12040720
- Greenhough, H., Smith, K. F., Vignier, J., Miller, M. R., Passfield, E., Kenny, N. J., et al. (2025). Impacts of marine heatwave stress and harmful algal (Alexandrium spp.) exposure on subadult green-lipped mussels (Perna canaliculus). *Ecotoxicol Environ Saf* 304, 119112. doi: 10.1016/j.ecoenv.2025.119112
- Gröger, M., Dutheil, C., Börgel, F., and Meier, M. H. E. (2024). Drivers of marine heatwaves in a stratified marginal sea. *Clim Dyn* 62, 3231–3243. doi: 10.1007/s00382-023-07062-5
- Guerrero-Meseguer, L., Marín, A., and Sanz-Lázaro, C. (2017). Future heat waves due to climate change threaten the survival of Posidonia oceanica seedlings. *Environmental Pollution* 230, 40–45. doi: 10.1016/j.envpol.2017.06.039
- Guerrero-Meseguer, L., Marín, A., and Sanz-Lázaro, C. (2020). Heat wave intensity can vary the cumulative effects of multiple environmental stressors on Posidonia oceanica seedlings. *Marine Environmental Research* 159, 105001. doi: 10.1016/j.marenvres.2020.105001
- Hamdeno, M., and Alvera-Azcaráte, A. (2023). Marine heatwaves characteristics in the Mediterranean Sea: Case study the 2019 heatwave events. *Front. Mar. Sci.* 10, 1093760. doi: 10.3389/fmars.2023.1093760
- Hamdeno, M., Alvera-Azcárate, A., Krokos, G., and Hoteit, I. (2024). Investigating the long-term variability of the Red Sea marine heatwaves and their relationship to different climate modes: focus on 2010 events in the northern basin. *Ocean Science* 20, 1087–1107. doi: 10.5194/os-20-1087-2024
- Hamdeno, M., Nagy, H., Ibrahim, O., and Mohamed, B. (2022). Responses of Satellite Chlorophyll-a to the Extreme Sea Surface Temperatures over the Arabian and Omani Gulf. *Remote Sensing* 14, 4653. doi: 10.3390/rs14184653

- Hamed, K. H., and Ramachandra Rao, A. (1998). A modified Mann-Kendall trend test for autocorrelated data. *Journal of Hydrology* 204, 182–196. doi: 10.1016/S0022-1694(97)00125-X
- Hayashida, H., Matear, R. J., and Strutton, P. G. (2020). Background nutrient concentration determines phytoplankton bloom response to marine heatwaves. *Global Change Biology* 26, 4800–4811. doi: 10.1111/gcb.15255
- Hellerman, S., and Rosenstein, M. (1983). Normal Monthly Wind Stress Over the World Ocean with Error Estimates. *J. Phys. Oceanogr.* 13, 1093–1104. doi: 10.1175/1520-0485(1983)013%3C1093:NMWSOT%3E2.0.CO;2
- Hersbach, H., Bell, B., Berrisford, P., Hirahara, S., Horányi, A., Muñoz-Sabater, J., et al. (2020). The ERA5 global reanalysis. *Q.J.R. Meteorol. Soc.* 146, 1999–2049. doi: 10.1002/qj.3803
- Hewson, T., Ashoor, A., Boussetta, S., Emanuel, K., Lagouvardos, K., Lavers, D., et al. (2024). Medicane Daniel: an extraordinary cyclone with devastating impacts. doi: 10.21957/TH3WXK861D
- Hobday, A. J., Alexander, L. V., Perkins, S. E., Smale, D. A., Straub, S. C., Oliver, E. C. J., et al. (2016). A hierarchical approach to defining marine heatwaves. *Progress in Oceanography* 141, 227–238. doi: 10.1016/j.pocean.2015.12.014
- Hobday, A., Oliver, E., Sen Gupta, A., Benthuysen, J., Burrows, M., Donat, M., et al. (2018). Categorizing and Naming Marine Heatwaves. *Oceanog* 31. doi: 10.5670/oceanog.2018.205
- Hodges, K. I. (1995). Feature Tracking on the Unit Sphere. *Monthly Weather Review* 123, 3458–3465. doi: 10.1175/1520-0493(1995)123%3C3458:FTOTUS%3E2.0.CO;2
- Holbrook, N. J., Scannell, H. A., Sen Gupta, A., Benthuysen, J. A., Feng, M., Oliver, E. C. J., et al. (2019). A global assessment of marine heatwaves and their drivers. *Nat Commun* 10, 2624. doi: 10.1038/s41467-019-10206-z
- Holbrook, N. J., Sen Gupta, A., Oliver, E. C. J., Hobday, A. J., Benthuysen, J. A., Scannell, H. A., et al. (2020). Keeping pace with marine heatwaves. *Nat Rev Earth Environ* 1, 482–493. doi: 10.1038/s43017-020-0068-4
- Hosmer, D. W., Lemeshow, S., and Sturdivant, R. X. (2013). *Applied Logistic Regression.*, 1st Edn. Wiley. doi: 10.1002/9781118548387
- Hoteit, I., Abualnaja, Y., Afzal, S., Ait-El-Fquih, B., Akylas, T., Antony, C., et al. (2021). Towards an End-to-End Analysis and Prediction System for Weather, Climate, and Marine Applications in the Red Sea. *Bulletin of the American Meteorological Society* 102, E99–E122. doi: 10.1175/BAMS-D-19-0005.1
- Hughes, T. P., Anderson, K. D., Connolly, S. R., Heron, S. F., Kerry, J. T., Lough, J. M., et al. (2018). Spatial and temporal patterns of mass bleaching of corals in the Anthropocene. *Science* 359, 80–83. doi: 10.1126/science.aan8048
- Hurrell, J. W., Kushnir, Y., Ottersen, G., and Visbeck, M. (2003). An Overview of the North Atlantic Oscillation. 134. doi: doi:10.1029/134GM01
- Ibrahim, O., Mohamed, B., and Nagy, H. (2021). Spatial Variability and Trends of Marine Heat Waves in the Eastern Mediterranean Sea over 39 Years. *JMSE* 9, 643. doi: 10.3390/jmse9060643

- IPCC (2014). AR5 Synthesis Report: Climate Change 2014 — IPCC. Available at: https://www.ipcc.ch/report/ar5/syr/ (Accessed July 21, 2021).
- IPCC (2018). Global Warming of 1.5°C. An IPCC Special Report on the impacts of global warming of 1.5°C above pre-industrial levels and related global greenhouse gas emission pathways, in the context of strengthening the global response to the threat of climate change, sustainable development, and efforts to eradicate poverty. Available at: https://www.ipcc.ch/sr15/download/
- IPCC (2019). IPCC Special Report on the Ocean and Cryosphere in a Changing Climate. Available at: https://www.ipcc.ch/srocc/download/
- Ipcc (2022). *The Ocean and Cryosphere in a Changing Climate: Special Report of the Intergovernmental Panel on Climate Change.*, 1st Edn. Cambridge University Press. doi: 10.1017/9781009157964
- Jangir, B., Mishra, A. K., and Strobach, E. (2024). The interplay between medicanes and the Mediterranean Sea in the presence of sea surface temperature anomalies. *Atmospheric Research* 310, 107625. doi: 10.1016/j.atmosres.2024.107625
- Jean-Michel, L., Eric, G., Romain, B.-B., Gilles, G., Angélique, M., Marie, D., et al. (2021). The Copernicus Global 1/12° Oceanic and Sea Ice GLORYS12 Reanalysis. *Front. Earth Sci.* 9, 698876. doi: 10.3389/feart.2021.698876
- Jiang, H., Farrar, J. T., Beardsley, R. C., Chen, R., and Chen, C. (2009). Zonal surface wind jets across the Red Sea due to mountain gap forcing along both sides of the Red Sea. *Geophysical Research Letters* 36. doi: 10.1029/2009GL040008
- Josey, S. A., Somot, S., and Tsimplis, M. (2011). Impacts of atmospheric modes of variability on Mediterranean Sea surface heat exchange. *Journal of Geophysical Research: Oceans* 116. doi: 10.1029/2010JC006685
- Juza, M., Fernández-Mora, À., and Tintoré, J. (2022). Sub-Regional Marine Heat Waves in the Mediterranean Sea From Observations: Long-Term Surface Changes, Sub-Surface and Coastal Responses. *Frontiers in Marine Science* 9. Available at: https://www.frontiersin.org/article/10.3389/fmars.2022.785771 (Accessed March 25, 2022).
- Karnauskas, K. B., and Jones, B. H. (2018). The Interannual Variability of Sea Surface Temperature in the Red Sea From 35 Years of Satellite and In Situ Observations. *Journal of Geophysical Research: Oceans* 123, 5824–5841. doi: 10.1029/2017JC013320
- Katsanevakis, S., Coll, M., Piroddi, C., Steenbeek, J., Ben Rais Lasram, F., Zenetos, A., et al. (2014). Invading the Mediterranean Sea: biodiversity patterns shaped by human activities. *Front. Mar. Sci.* 1. doi: 10.3389/fmars.2014.00032
- Kheireddine, M., Ouhssain, M., Claustre, H., Uitz, J., Gentili, B., and Jones, B. H. (2017). Assessing Pigment-Based Phytoplankton Community Distributions in the Red Sea. *Front. Mar. Sci.* 4. doi: 10.3389/fmars.2017.00132
- Kiørboe, T. (2011). What makes pelagic copepods so successful? *Journal of Plankton Research* 33, 677–685. doi: 10.1093/plankt/fbq159

- Kirch, W. ed. (2008). "Pearson's Correlation Coefficient," in *Encyclopedia of Public Health*, (Dordrecht: Springer Netherlands), 1090–1091. doi: 10.1007/978-1-4020-5614-7_2569
- Krokos, G., Cerovečki, I., Papadopoulos, V. P., Hendershott, M. C., and Hoteit, I. (2022). Processes Governing the Seasonal Evolution of Mixed Layers in the Red Sea. *Journal of Geophysical Research: Oceans* 127, e2021JC017369. doi: 10.1029/2021JC017369
- Krokos, G., Cerovecki, I., Zhan, P., Hendershott, M., and Hoteit, I. (2021). *Seasonal Evolution of Mixed Layers in the Red Sea and the Relative Contribution of Atmospheric Buoyancy and Momentum Forcing*.
- Krokos, G., Papadopoulos, V. P., Sofianos, S. S., Ombao, H., Dybczak, P., and Hoteit, I. (2019). Natural Climate Oscillations may Counteract Red Sea Warming Over the Coming Decades. *Geophysical Research Letters* 46, 3454–3461. doi: 10.1029/2018GL081397
- Langodan, S., Cavaleri, L., Pomaro, A., V, Y., Bertotti, L., and Hoteit, I. (2017a). The climatology of the Red Sea - part 2: The waves. *International Journal of Climatology* 37, n/a-n/a. doi: 10.1002/joc.5101
- Langodan, S., Cavaleri, L., Vishwanadhapalli, Y., Pomaro, A., Bertotti, L., and Hoteit, I. (2017b). The climatology of the Red Sea – part 1: the wind. *International Journal of Climatology* 37, 4509–4517. doi: 10.1002/joc.5103
- Laufkötter, C., Zscheischler, J., and Frölicher, T. L. (2020). High-impact marine heatwaves attributable to human-induced global warming. *Science* 369, 1621–1625. doi: https://doi.org/10.1126/science.aba0690
- Le Grix, N., Burger, F. A., and Frölicher, T. L. (2025). Surface and Subsurface Compound Marine Heatwave and Biogeochemical Extremes Under Climate Change. *Global Biogeochemical Cycles* 39, e2025GB008514. doi: 10.1029/2025GB008514
- Le Grix, N., Zscheischler, J., Laufkötter, C., Rousseaux, C. S., and Frölicher, T. L. (2021). Compound high-temperature and low-chlorophyll extremes in the ocean over the satellite period. *Biogeosciences* 18, 2119–2137. doi: 10.5194/bg-18-2119-2021
- Le Grix, N., Zscheischler, J., Rodgers, K. B., Yamaguchi, R., and Frölicher, T. L. (2022). Hotspots and drivers of compound marine heatwaves and low net primary production extremes. *Biogeosciences* 19, 5807–5835. doi: 10.5194/bg-19-5807-2022
- Leonard, M., Westra, S., Phatak, A., Lambert, M., van den Hurk, B., McInnes, K., et al. (2014). A compound event framework for understanding extreme impacts. *WIREs Climate Change* 5, 113–128. doi: 10.1002/wcc.252
- Levitus, S., Antonov, J. I., Boyer, T. P., Baranova, O. K., Garcia, H. E., Locarnini, R. A., et al. (2012). World ocean heat content and thermosteric sea level change (0–2000 m), 1955–2010. *Geophysical Research Letters* 39. doi: 10.1029/2012GL051106
- Lionello, P., Malanotte-Rizzoli, P., Boscolo, R., Alpert, P., Artale, V., Li, L., et al. (2006). "The Mediterranean climate: An overview of the main characteristics and issues," in *Developments in Earth and Environmental Sciences*, eds. P. Lionello, P. Malanotte-Rizzoli, and R. Boscolo (Elsevier), 1–26. doi: 10.1016/S1571-9197(06)80003-0

- Liu, X., and Yao, F. (2022). Relationship of the Warming of Red Sea Surface Water over 140 Years with External Heat Elements. *Journal of Marine Science and Engineering* 10, 846. doi: 10.3390/jmse10070846
- López-Sandoval, D. C., Rowe, K., Carillo-de-Albonoz, P., Duarte, C. M., and Agustí, S. (2019). Rates and drivers of Red Sea plankton community metabolism. *Biogeosciences* 16, 2983–2995. doi: 10.5194/bg-16-2983-2019
- Mannino, A. M., Balistreri, P., and Deidun, A. (2017). *The Marine Biodiversity of the Mediterranean Sea in a Changing Climate: The Impact of Biological Invasions*. IntechOpen. doi: 10.5772/intechopen.69214
- Marshall, J., Adcroft, A., Hill, C., Perelman, L., and Heisey, C. (1997). A finite-volume, incompressible Navier Stokes model for studies of the ocean on parallel computers. *Journal of Geophysical Research: Oceans* 102, 5753–5766. doi: 10.1029/96JC02775
- McPhaden, M. J., Zebiak, S. E., and Glantz, M. H. (2006). ENSO as an Integrating Concept in Earth Science. *Science* 314, 1740–1745. doi: 10.1126/science.1132588
- Miglietta, M. M., Flaounas, E., González-Alemán, J. J., Panegrossi, G., Gaertner, M. A., Pantillon, F., et al. (2025). Defining Medicanes: Bridging the Knowledge Gap between Tropical and Extratropical Cyclones in the Mediterranean. *Bulletin of the American Meteorological Society* 106, E1955–E1971. doi: 10.1175/BAMS-D-24-0289.1
- Miglietta, M. M., Laviola, S., Malvaldi, A., Conte, D., Levizzani, V., and Price, C. (2013). Analysis of tropical-like cyclones over the Mediterranean Sea through a combined modeling and satellite approach. *Geophysical Research Letters* 40, 2400–2405. doi: 10.1002/grl.50432
- Miglietta, M. M., and Rotunno, R. (2019). Development mechanisms for Mediterranean tropical-like cyclones (medicanes). *Quarterly Journal of the Royal Meteorological Society* 145, 1444–1460. doi: 10.1002/qj.3503
- Mills, K. E., PERSHING, A. J., BROWN, C. J., CHEN, Y., CHIANG, F.-S., HOLLAND, D. S., et al. (2013). Fisheries Management in a Changing Climate: Lessons from the 2012 Ocean Heat Wave in the Northwest Atlantic. *Oceanography* 26, 191–195. Available at: https://www.jstor.org/stable/24862052 (Accessed July 9, 2021).
- Mohamed, B., Abdallah, A. M., Alam El-Din, K., Nagy, H., and Shaltout, M. (2019). Inter-Annual Variability and Trends of Sea Level and Sea Surface Temperature in the Mediterranean Sea over the Last 25 Years. *Pure Appl. Geophys.* 176, 3787–3810. doi: 10.1007/s00024-019-02156-w
- Mohamed, B., Ibrahim, O., and Nagy, H. (2022a). Sea Surface Temperature Variability and Marine Heatwaves in the Black Sea. *Remote Sensing* 14, 2383. doi: 10.3390/rs14102383
- Mohamed, B., Nagy, H., and Ibrahim, O. (2021). Spatiotemporal Variability and Trends of Marine Heat Waves in the Red Sea over 38 Years. *JMSE* 9, 842. doi: 10.3390/jmse9080842
- Mohamed, B., Nilsen, F., and Skogseth, R. (2022b). Marine Heatwaves Characteristics in the Barents Sea Based on High Resolution Satellite Data (1982–2020). *Frontiers in Marine Science* 9. Available at:

https://www.frontiersin.org/article/10.3389/fmars.2022.821646 (Accessed June 12, 2022).

- Nadimpalli, J. R., Sanikommu, S., Subramanian, A. C., Giglio, D., and Hoteit, I. (2025). Subsurface marine heat waves and coral bleaching in the southern red sea linked to remote forcing. *Weather and Climate Extremes* 48, 100771. doi: 10.1016/j.wace.2025.100771
- Nagy, H., Elgindy, A., Pinardi, N., Zavatarelli, M., and Oddo, P. (2017). A nested pre-operational model for the Egyptian shelf zone: Model configuration and validation/calibration. *Dynamics of Atmospheres and Oceans* 80, 75–96. doi: 10.1016/j.dynatmoce.2017.10.003
- Nagy, H., Lyons, K., Nolan, G., Cure, M., and Dabrowski, T. (2020). A Regional Operational Model for the North East Atlantic: Model Configuration and Validation. *Journal of Marine Science and Engineering* 8, 673. doi: 10.3390/jmse8090673
- Nagy, H., Mohamed, B., and Ibrahim, O. (2021). Variability of Heat and Water Fluxes in the Red Sea Using ERA5 Data (1981–2020). *Journal of Marine Science and Engineering* 9, 1276. doi: 10.3390/jmse9111276
- Oliver, E. C., Benthuysen, J. A., Bindoff, N. L., Hobday, A. J., Holbrook, N. J., Mundy, C. N., et al. (2017). The unprecedented 2015/16 Tasman Sea marine heatwave. *Nature communications* 8, 16101. doi: 10.1038/ncomms16101
- Oliver, E. C. J., Benthuysen, J. A., Darmaraki, S., Donat, M. G., Hobday, A. J., Holbrook, N. J., et al. (2021). Marine Heatwaves. *Annu. Rev. Mar. Sci.* 13, 313–342. doi: 10.1146/annurev-marine-032720-095144
- Oliver, E. C. J., Donat, M. G., Burrows, M. T., Moore, P. J., Smale, D. A., Alexander, L. V., et al. (2018a). Longer and more frequent marine heatwaves over the past century. *Nat Commun* 9, 1324. doi: 10.1038/s41467-018-03732-9
- Oliver, E. C., Lago, V., Hobday, A. J., Holbrook, N. J., Ling, S. D., and Mundy, C. N. (2018b). Marine heatwaves off eastern Tasmania: Trends, interannual variability, and predictability. *Progress in Oceanography* 161, 116–130. doi: 10.1016/j.pocean.2018.02.007
- Papadopoulos, V., Abualnaja, Y., Josey, S., Bower, A., Dionysios, Raitsos, E., et al. (2013). Atmospheric Forcing of the Winter Air–Sea Heat Fluxes over the Northern Red Sea. *Journal of Climate* 26, 1685–1701. doi: 10.1175/JCLI-D-12-00267.1
- Paredes-Fortuny, L., Pastor, F., and Khodayar, S. (2025). Concurrent atmospheric heatwaves intensify marine heatwaves through air-sea heat flux change in the Mediterranean Sea. *Commun Earth Environ* 6, 638. doi: 10.1038/s43247-025-02633-2
- Pastor, F., and Khodayar, S. (2023). Marine heat waves: Characterizing a major climate impact in the Mediterranean. *Science of The Total Environment* 861, 160621. doi: 10.1016/j.scitotenv.2022.160621
- Pastor, F., Paredes-Fortuny, L., and Khodayar, S. (2024). Mediterranean marine heatwaves intensify in the presence of concurrent atmospheric heatwaves. *Commun Earth Environ* 5, 797. doi: 10.1038/s43247-024-01982-8

- Pastor, F., Valiente, J. A., and Khodayar, S. (2020). A Warming Mediterranean: 38 Years of Increasing Sea Surface Temperature. *Remote Sensing* 12, 2687. doi: 10.3390/rs12172687
- Pastor, F., Valiente, J. A., and Palau, J. L. (2018). Sea Surface Temperature in the Mediterranean: Trends and Spatial Patterns (1982–2016). *Pure Appl. Geophys.* 175, 4017–4029. doi: 10.1007/s00024-017-1739-z
- Patten, M. L., and Newhart, M. (2017). *Understanding Research Methods: An Overview of the Essentials*., 10th Edn. Tenth edition. | New York, NY : Routledge, 2017.: Routledge. doi: 10.4324/9781315213033
- Perkins, S. E., and Alexander, L. V. (2013). On the Measurement of Heat Waves. *Journal of Climate* 26, 4500–4517. doi: 10.1175/JCLI-D-12-00383.1
- Pinardi, N., Allen, I., Demirov, E., De Mey, P., Korres, G., Lascaratos, A., et al. (2003). The Mediterranean ocean forecasting system: first phase of implementation (1998–2001). *Annales Geophysicae* 21, 3–20. doi: 10.5194/angeo-21-3-2003
- Pinardi, N., Cessi, P., Borile, F., and Wolfe, C. L. P. (2019). The Mediterranean Sea Overturning Circulation. *Journal of Physical Oceanography* 49, 1699–1721. doi: 10.1175/JPO-D-18-0254.1
- Pisano, A., Marullo, S., Artale, V., Falcini, F., Yang, C., Leonelli, F., et al. (2020). New Evidence of Mediterranean Climate Change and Variability from Sea Surface Temperature Observations. *Remote Sensing* 12. doi: 10.3390/rs12010132
- Racault, M.-F., Le Quéré, C., Buitenhuis, E., Sathyendranath, S., and Platt, T. (2012). Phytoplankton phenology in the global ocean. *Ecological Indicators* 14, 152–163. doi: 10.1016/j.ecolind.2011.07.010
- Raitsos, D. E., Pradhan, Y., Brewin, R. J. W., Stenchikov, G., and Hoteit, I. (2013). Remote Sensing the Phytoplankton Seasonal Succession of the Red Sea. *PLOS ONE* 8, e64909. doi: 10.1371/journal.pone.0064909
- Raitsos, D., Hoteit, I., Prihartato, P., Chronis, T., Triantafyllou, G., and Abualnaja, Y. (2011). Abrupt warming of the Red Sea. *Geophysical Research Letters - GEOPHYS RES LETT* 38. doi: 10.1029/2011GL047984
- Rasul, N. M. A., and Stewart, I. C. F. eds. (2015). *The Red Sea: The Formation, Morphology, Oceanography and Environment of a Young Ocean Basin*. Berlin, Heidelberg: Springer Berlin Heidelberg. doi: 10.1007/978-3-662-45201-1
- Reynolds, R. W., Smith, T. M., Liu, C., Chelton, D. B., Casey, K. S., and Schlax, M. G. (2007). Daily High-Resolution-Blended Analyses for Sea Surface Temperature. *Journal of Climate* 20, 5473–5496. doi: 10.1175/2007JCLI1824.1
- Rivetti, I., Fraschetti, S., Lionello, P., Zambianchi, E., and Boero, F. (2014). Global Warming and Mass Mortalities of Benthic Invertebrates in the Mediterranean Sea. *PLOS ONE* 9, e115655. doi: 10.1371/journal.pone.0115655
- Romero, R., and Emanuel, K. (2013). Medicane risk in a changing climate. *Journal of Geophysical Research: Atmospheres* 118, 5992–6001. doi: 10.1002/jgrd.50475
- Russo, A., Santos, R., and Gouveia, C. M. (2026). Compound atmospheric and marine hot extremes coupled with droughts in Madagascar. *Weather and Climate Extremes*, 100884. doi: 10.1016/j.wace.2026.100884

- Schenke, H.-W. (2013). “GEBCO,” in *Encyclopedia of Marine Geosciences*, eds. J. Harff, M. Meschede, S. Petersen, and J. Thiede (Dordrecht: Springer Netherlands), 1–2. doi: 10.1007/978-94-007-6644-0_63-3
- Schlegel, R. W., Darmaraki, S., Benthuysen, J. A., Filbee-Dexter, K., and Oliver, E. C. J. (2021). Marine cold-spells. *Progress in Oceanography* 198, 102684. doi: 10.1016/j.pocean.2021.102684
- Schneider, D. P., Deser, C., Fasullo, J., and Trenberth, K. E. (2013). Climate Data Guide Spurs Discovery and Understanding. *Eos Trans. AGU* 94, 121–122. doi: 10.1002/2013EO130001
- Sen Gupta, A., Thomsen, M., Benthuysen, J. A., Hobday, A. J., Oliver, E., Alexander, L. V., et al. (2020). Drivers and impacts of the most extreme marine heatwave events. *Sci Rep* 10, 19359. doi: 10.1038/s41598-020-75445-3
- Sen, P. K. (1968). Estimates of the Regression Coefficient Based on Kendall’s Tau. *Journal of the American Statistical Association* 63, 1379–1389. doi: 10.1080/01621459.1968.10480934
- Shaltout, M. (2019). Recent sea surface temperature trends and future scenarios for the Red Sea. *Oceanologia* 61, 484–504. doi: 10.1016/j.oceano.2019.05.002
- Simon, A., Pires, C., Frölicher, T. L., and Russo, A. (2023). Long-term warming and interannual variability contributions’ to marine heatwaves in the Mediterranean. *Weather and Climate Extremes* 42, 100619. doi: 10.1016/j.wace.2023.100619
- Skliris, N., Sofianos, S., Gkanasos, A., Mantziafou, A., Vervatis, V., Axaopoulos, P., et al. (2012). Decadal scale variability of sea surface temperature in the Mediterranean Sea in relation to atmospheric variability. *Ocean Dynamics* 62, 13–30. doi: 10.1007/s10236-011-0493-5
- Skliris, N., Sofianos, S. S., Gkanasos, A., Axaopoulos, P., Mantziafou, A., and Vervatis, V. (2011). Long-term sea surface temperature variability in the Aegean Sea. *Advances in Oceanography and Limnology* 2, 125–139. doi: 10.1080/19475721.2011.601325
- Smale, D. A., Wernberg, T., Oliver, E. C. J., Thomsen, M., Harvey, B. P., Straub, S. C., et al. (2019). Marine heatwaves threaten global biodiversity and the provision of ecosystem services. *Nat. Clim. Chang.* 9, 306–312. doi: 10.1038/s41558-019-0412-1
- Smith, K. E., Burrows, M. T., Hobday, A. J., Sen Gupta, A., Moore, P. J., Thomsen, M., et al. (2021). Socioeconomic impacts of marine heatwaves: Global issues and opportunities. *Science* 374, eabj3593. doi: 10.1126/science.abj3593
- Smith, K. E., Sen Gupta, A., Amaya, D., Benthuysen, J. A., Burrows, M. T., Capotondi, A., et al. (2025). Baseline matters: Challenges and implications of different marine heatwave baselines. *Progress in Oceanography* 231, 103404. doi: 10.1016/j.pocean.2024.103404
- Sofianos, S., and Johns, W. E. (2015). “Water Mass Formation, Overturning Circulation, and the Exchange of the Red Sea with the Adjacent Basins,” in *The Red Sea*, eds. N. M. A. Rasul and I. C. F. Stewart (Berlin, Heidelberg: Springer Berlin Heidelberg), 343–353. doi: 10.1007/978-3-662-45201-1_20

- Sofianos, S., and Johns, W. E. (2017). The Summer Circulation in the Gulf of Suez and Its Influence in the Red Sea Thermohaline Circulation. *Journal of Physical Oceanography* 47, 2047–2053. doi: 10.1175/JPO-D-16-0282.1
- Sofianos, S. S., and Johns, W. E. (2003). An Oceanic General Circulation Model (OGCM) investigation of the Red Sea circulation: 2. Three-dimensional circulation in the Red Sea. *Journal of Geophysical Research: Oceans* 108. doi: 10.1029/2001JC001185
- Sofianos, S. S., Johns, W. E., and Murray, S. P. (2002). Heat and freshwater budgets in the Red Sea from direct observations at Bab el Mandeb. *Deep Sea Research Part II: Topical Studies in Oceanography* 49, 1323–1340. doi: 10.1016/S0967-0645(01)00164-3
- Tanhua, T., Hainbucher, D., Schroeder, K., Cardin, V., Álvarez, M., and Civitarese, G. (2013). The Mediterranean Sea system: a review and an introduction to the special issue. *Ocean Science* 9, 789–803. doi: 10.5194/os-9-789-2013
- Theodorou, I., Krokos, G., Gittings, J. A., Darmaraki, S., Hoteit, I., and Raitsos, D. E. (2025). Response of Red Sea phytoplankton biomass to marine heatwaves and cold-spells. *Sci Rep* 15, 5109. doi: 10.1038/s41598-025-88727-5
- Thomson, R. E., and Emery, W. J. (2014). *Data Analysis Methods in Physical Oceanography*. Elsevier. doi: 10.1016/C2010-0-66362-0
- Tous, M., Romero, R., and Ramis, C. (2013). Surface heat fluxes influence on medicane trajectories and intensification. *Atmospheric Research* 123, 400–411. doi: 10.1016/j.atmosres.2012.05.022
- Trenberth, K. E. (2020). Understanding climate change through Earth’s energy flows. *Journal of the Royal Society of New Zealand* 50, 331–347. doi: 10.1080/03036758.2020.1741404
- Ulf Riebesell, J. Fabry, V., Hansson, L., and Gattuso, J.-P. (2011). *Guide to best practices for ocean acidification research and data reporting.* LU: Publications Office. doi: 10.2777/66906
- Vautard, R., Aalst, M. van, Boucher, O., Drouin, A., Haustein, K., Kreienkamp, F., et al. (2020). Human contribution to the record-breaking June and July 2019 heatwaves in Western Europe. *Environ. Res. Lett.* 15, 094077. doi: 10.1088/1748-9326/aba3d4
- Viswanadhapalli, Y., Dasari, H. P., Langodan, S., Challa, V. S., and Hoteit, I. (2017). Climatic features of the Red Sea from a regional assimilative model. *Intl Journal of Climatology* 37, 2563–2581. doi: 10.1002/joc.4865
- Vogt, L., Burger, F. A., Griffies, S. M., and Frölicher, T. L. (2022). Local Drivers of Marine Heatwaves: A Global Analysis With an Earth System Model. *Front. Clim.* 4. doi: 10.3389/fclim.2022.847995
- von Schuckmann, K., Le Traon, P.-Y., Smith, N., Pascual, A., Djavidnia, S., Gattuso, J.-P., et al. (2020). Copernicus Marine Service Ocean State Report, Issue 4. *Journal of Operational Oceanography* 13, S1–S172. doi: 10.1080/1755876X.2020.1785097
- W Schlegel, R., and J Smit, A. (2018). heatwaveR: A central algorithm for the detection of heatwaves and cold-spells. *The Journal of Open Source Software* 3, 821. doi: 10.21105/joss.00821

- Wang, F., Shao, W., Yu, H., Kan, G., He, X., Zhang, D., et al. (2020). Re-evaluation of the Power of the Mann-Kendall Test for Detecting Monotonic Trends in Hydrometeorological Time Series. *Frontiers in Earth Science* 8. Available at: https://www.frontiersin.org/article/10.3389/feart.2020.00014 (Accessed March 10, 2022).
- Weatherall, P., Marks, K. M., Jakobsson, M., Schmitt, T., Tani, S., Arndt, J. E., et al. (2015). A new digital bathymetric model of the world's oceans. *Earth and Space Science* 2, 331–345. doi: 10.1002/2015EA000107
- Wilks, D. S. (2019). *Statistical Methods in the Atmospheric Sciences*. Elsevier. doi: 10.1016/C2017-0-03921-6
- Yao, F., and Hoteit, I. (2018). Rapid Red Sea Deep Water renewals caused by volcanic eruptions and the North Atlantic Oscillation. *Sci Adv* 4, eaar5637. doi: 10.1126/sciadv.aar5637
- Yao, F., Hoteit, I., Pratt, L. J., Bower, A. S., Zhai, P., Köhl, A., et al. (2014). Seasonal overturning circulation in the Red Sea: 1. Model validation and summer circulation. *Journal of Geophysical Research: Oceans* 119, 2238–2262. doi: 10.1002/2013JC009004
- Zervoudaki, S., Protopapa, M., Koutsandrea, A., Jansson, A., von Weissenberg, E., Fyttis, G., et al. (2024). Zooplankton responses to simulated marine heatwave in the Mediterranean Sea using in situ mesocosms. *PLoS One* 19, e0308846. doi: 10.1371/journal.pone.0308846
- Zhan, P., Gopalakrishnan, G., Subramanian, A. C., Guo, D., and Hoteit, I. (2018). Sensitivity Studies of the Red Sea Eddies Using Adjoint Method. *Journal of Geophysical Research: Oceans* 123, 8329–8345. doi: 10.1029/2018JC014531
- Zhan, P., Krokos, G., Guo, D., and Hoteit, I. (2019). Three-Dimensional Signature of the Red Sea Eddies and Eddy-Induced Transport. *Geophysical Research Letters* 46, 2167–2177. doi: 10.1029/2018GL081387
- Zhan, P., Subramanian, A. C., Yao, F., Kartadikaria, A. R., Guo, D., and Hoteit, I. (2016). The eddy kinetic energy budget in the Red Sea. *Journal of Geophysical Research: Oceans* 121, 4732–4747. doi: 10.1002/2015JC011589
- Zhang, R. (2007). Anticorrelated multidecadal variations between surface and subsurface tropical North Atlantic. *Geophysical Research Letters* 34. doi: 10.1029/2007GL030225
- Zhao, Z., and Marin, M. (2019). A MATLAB toolbox to detect and analyze marine heatwaves. *JOSS* 4, 1124. doi: 10.21105/joss.01124
- Zhou, X., Xu, K., Ashok, K., Shi, J., Zhang, L., Yu, J.-Y., et al. (2025). Compound marine heatwaves and tropical cyclones delay the onset of the Bay of Bengal summer monsoon. *npj Clim Atmos Sci* 8, 162. doi: 10.1038/s41612-025-01061-5
- Zscheischler, J., Martius, O., Westra, S., Bevacqua, E., Raymond, C., Horton, R. M., et al. (2020). A typology of compound weather and climate events. *Nat Rev Earth Environ* 1, 333–347. doi: 10.1038/s43017-020-0060-z

- Zscheischler, J., Westra, S., van den Hurk, B. J. J. M., Seneviratne, S. I., Ward, P. J., Pitman, A., et al. (2018). Future climate risk from compound events. *Nature Climate Change* 8, 469–477. doi: 10.1038/s41558-018-0156-3

Chapter Thirteen: List of Publications

Papers:

- **Hamdeno, M.**, Uba, K., Barth, A., and Alvera-Azcárate, A. (**2024**). Investigating the interaction between Mediterranean extremes: A deep dive into Medicane Zorbas 2018. Rapports et Communications de la Commission Internationale pour l'Exploration Scientifique de la Mer Méditerranée (CIESM) **43**, 16. (**Conference proceedings paper**).
- **Hamdeno, M.**, Alvera-Azcárate, A., Krokos, G., and Hoteit, I. (**2024**). Investigating the long-term variability of the Red Sea marine heatwaves and their relationship to different climate modes: focus on 2010 events in the northern basin. Ocean Sci. 20, 1087–1107. doi: 10.5194/os-20-1087-2024. (**Published**).
- **Hamdeno, M.**, and Alvera-Azcaráte, A. (**2023**). Marine heatwaves characteristics in the Mediterranean Sea: Case study the 2019 heatwave events. Front. Mar. Sci. 10,1093760. doi: 10.3389/fmars.2023.1093760. (**Published**).

Oral Presentations and Posters:

- **Hamdeno, M.**, and Alvera-Azcárate, A. (May 2022). Spatial and temporal variability of marine heatwaves in the Mediterranean Sea over 39 years and their possible physical drivers. **Oral presentation** at the European Geosciences Union General Assembly 2022 (EGU 2022).
- **Hamdeno, M.**, and Alvera-Azcárate, A. (May 2022). The 2019 marine heatwaves in the Western Mediterranean Sea: atmospheric drivers and effects on chlorophyll-a concentration. **Poster presentation** at the Living Planet Symposium 2022 (LPS 2022), Bonn, Germany.
- **Hamdeno, M.**, and Alvera-Azcárate, A. (September 2022). A long-term study of marine heatwaves in the Western Mediterranean Sea and the Red Sea. **Oral presentation** at the MER+ Summit 2022, Spain.
- **Hamdeno, M.**, Alvera-Azcárate, A., Krokos, G., and Hoteit, I. (May 2023). Characteristics of marine heatwaves in the Red Sea and their relation to climate modes. **Poster presentation** at the 54th Liège Colloquium, Liège, Belgium.
- **Hamdeno, M.**, Alvera-Azcárate, A., Krokos, G., and Hoteit, I. (November 2023). Marine heatwaves in the Red Sea and their relationship to different climate modes: case study of the 2010 events in the northern Red Sea. **Poster presentation** at the 3rd International Conference on Marine Ecosystems of the Red Sea (ICMERS-3), KAUST University, Saudi Arabia.
- Uba, K., **Hamdeno, M.**, Barth, A., and Alvera-Azcárate, A. (April 2024). Two extremes: Investigating the impact of the co-occurrence of medicanes and marine heatwaves in the Mediterranean Sea. **Oral presentation** at the European Geosciences

Union General Assembly 2024 (EGU 2024), Vienna, Austria. doi: 10.5194/egusphere-egu24-13779.

- **Hamdeno, M.**, Alvera-Azcárate, A., Krokos, G., and Hoteit, I. (April 2024). Marine heatwaves in the Red Sea: a study of their spatial characteristics, trends, and relationships to climate modes. **Poster presentation** at the European Geosciences Union General Assembly 2024 (EGU 2024), Vienna, Austria. doi: 10.5194/egusphere-egu24-13423.
- **Hamdeno, M.**, and Alvera-Azcárate, A. (May 2024). Comprehensive evaluation of marine and atmospheric heatwaves in the Mediterranean region. **Oral presentation** at the 55th International Liège Colloquium on Ocean Dynamics, Liège, Belgium, 27–31 May 2024.
- **Hamdeno, M.**, Uba, K., Barth, A., and Alvera-Azcárate, A. (2024). Investigating the interaction between Mediterranean extremes: A deep dive into Medicane Zorbas 2018. **Oral presentation** at the 43rd CIESM Congress – International Commission for the Scientific Exploration of the Mediterranean Sea, Palermo, Italy.
- **Hamdeno, M.**, and Alvera-Azcárate, A. (2025). The co-occurrences between marine and atmospheric heatwaves in the Mediterranean Sea. **Poster presentation** at the Living Planet Symposium 2025 (LPS 25), European Space Agency (ESA), in partnership with the European Commission and EUMETSAT.
- **Hamdeno, M.**, and Alvera-Azcárate, A. (2025). Dynamics and forcing mechanisms of marine heatwaves in the Mediterranean Sea. **Oral presentation** at the Mediterranean Geosciences Union Conference 2025 (MEDGU 2025). Paper ID: 850.